HEALTH PHYSICS

OFFICIAL JOURNAL OF THE HEALTH PHYSICS SOCIETY

Volume 5

KARL Z. MORGAN
Editor-in-Chief

W. S. SNYDER J. A. AUXIER
Editors

OFFICERS AND DIRECTORS OF THE HEALTH PHYSICS SOCIETY

President
JOHN S. LAUGHLIN

President-Elect
WALTER D. CLAUS

Treasurer
SAUL J. HARRIS

Most Recent Past President
ELDA E. ANDERSON ✠

Secretary
FRANK L. PASCHAL, JR.

Executive Secretary
RUSSELL F. COWING

Board of Directors
G. V. BEARD
L. J. CHERUBIN
F. P. COWAN
W. T. HAM
W. H. LANGHAM
K. Z. MORGAN
R. M. SIEVERT
G. W. C. TAIT
R. C. THORBURN

MEMBERS OF THE HONORARY EDITORIAL ADVISORY BOARD

Austria: J. J. ZAKOVSKY • *Belgium:* Z. M. BACQ · R. BOULENGER
Canada: F. D. SOWBY · H. E. JOHNS · G. C. BUTLER • *Denmark:* J. C. JACOBSEN · H. LEVI
France: H. P. JAMMET · L. BUGNARD · A. ALLISY · *Germany:* E. H. GRAUL · H. HOLTHUSEN
IAEA: M. SUZUKI · *India:* A. S. RAO · *Italy:* A. PERUSSIA · *Japan:* M. K. NAKAIDZUMI · S. SHIMIZU
Netherlands: W. J. OOSTERKAMP · A. H. W. ATEN, JR. • *Norway:* K. KOREN
Sweden: R. M. SIEVERT · L. CARLBOM · *Switzerland:* F. ALDER · G. JOYET · *Turkey:* P. CAMBEL
United Kingdom: W. G. MARLEY · W. BINKS · W. V. MAYNEORD · J. S. MITCHELL · E. E. POCHIN
United States: G. FAILLA · R. D. EVANS · C. L. DUNHAM · A. M. BRUES · P. S. HENSHAW · S. WARREN
J. C. BUGHER · H. A. BLAIR · L. B. SILVERMAN · L. D. MARINELLI · W. T. HAM · B. MOYER
H. M. PARKER · L. SILVERMAN · C. A. TOBIAS · C. R. WILLIAMS · S. BLOCK
Uruguay: F. LEBORGNE · *U.S.S.R.:* F. KROTKOV · *World Health Organization:* P. DOROLLE

PERGAMON PRESS NEW YORK OXFORD

HEALTH PHYSICS

The Official Journal of the Health Physics Society

EDITORS

Dr. K. Z. MORGAN (*Editor-in-Chief*), *Director, Health Physics Division, Oak Ridge National Laboratory, Oak Ridge, Tennessee, U.S.A.*

Dr. W. S. SNYDER, *Health Physics Division, Oak Ridge National Laboratory, Oak Ridge, Tennessee, U.S.A.*

Dr. J. A. AUXIER, *Health Physics Division, Oak Ridge National Laboratory, Oak Ridge, Tennessee, U.S.A.*

INSTRUCTIONS TO CONTRIBUTORS

Manuscripts should be submitted to Dr. K. Z. MORGAN, Health Physics Division, Oak Ridge National Laboratory, P.O. Box X, Oak Ridge, Tennessee. The author's institution is requested to pay a publication charge of $10.00 per page, which entitles the author to 50 free reprints.

Manuscripts submitted for publication in *Health Physics* can be accepted only on the condition that they have not been submitted elsewhere. Manuscripts must be typed, on one side of the paper only, with double or triple spacing and the original and one duplicate copy should be submitted. The figures should be glossy prints of approximately 8 × 10 inches or original line drawings with lettering which will be legible after reduction of the size of the figure. Attach the figures to separate sheets together with the figure number. Captions should be typed on a separate sheet and attached to the manuscript.

An abstract of 200 words or less must accompany the manuscript. It should give a precise account of the major results of the research as well as some indication of methods or applications when these are of interest. Avoid excessively general remarks.

Other considerations of style and form may be in accordance with generally accepted journalistic practices.

Pergamon Press are also publishers of the following journals:

JOURNAL OF NUCLEAR ENERGY (*including* THE SOVIET JOURNAL OF ATOMIC ENERGY*) PART A: REACTOR SCIENCE; PART B: REACTOR TECHNOLOGY; PART C: PLASMA PHYSICS—ACCELERATORS—THERMONUCLEAR RESEARCH
JOURNAL OF INORGANIC AND NUCLEAR CHEMISTRY
TETRAHEDRON (*The International Journal of Organic Chemistry*)
TETRAHEDRON LETTERS (*The International Organ for the Rapid Publication of Preliminary Communications in Organic Chemistry*)
TALANTA (*An International Journal of Analytical Chemistry*)
INTERNATIONAL JOURNAL OF APPLIED RADIATION AND ISOTOPES
BIOCHEMICAL PHARMACOLOGY
* BIOPHYSICS
* JOURNAL OF MICROBIOLOGY, EPIDEMIOLOGY AND IMMUNOBIOLOGY
* PROBLEMS OF HEMATOLOGY AND BLOOD TRANSFUSION
* PROBLEMS OF ONCOLOGY
* PROBLEMS OF VIROLOGY
* SECHENOV PHYSIOLOGICAL JOURNAL OF THE U.S.S.R.
* ELECTRIC TECHNOLOGY, U.S.S.R.
* RADIO ENGINEERING
* RADIO ENGINEERING AND ELECTRONICS
* TELECOMMUNICATIONS
* THE PHYSICS OF METALS AND METALLOGRAPHY
* THE ABSTRACTS JOURNAL OF METALLURGY
* APPLIED MATHEMATICS AND MECHANICS
CHEMICAL ENGINEERING SCIENCE
JOURNAL OF ATMOSPHERIC AND TERRESTRIAL PHYSICS
PLANETARY AND SPACE SCIENCE
GEOCHIMICA ET COSMOCHIMICA ACTA
BULLETIN GÉODÉSIQUE
ANNALS OF THE INTERNATIONAL GEOPHYSICAL YEAR
JOURNAL OF THE MECHANICS AND PHYSICS OF SOLIDS
INTERNATIONAL JOURNAL OF MECHANICAL SCIENCES
SPECTROCHIMICA ACTA
ACTA METALLURGICA (*for the Board of Governors of Acta Metallurgica*)
INTERNATIONAL JOURNAL OF THE PHYSICS AND CHEMISTRY OF SOLIDS
SOLID-STATE ELECTRONICS
RHEOLOGY ABSTRACTS
DEEP-SEA RESEARCH
JOURNAL OF NEUROCHEMISTRY
JOURNAL OF PSYCHOSOMATIC RESEARCH
JOURNAL OF CHILD PSYCHOLOGY AND PSYCHIATRY
JOURNAL OF INSECT PHYSIOLOGY
SMALL ANIMAL PRACTICE
JOURNAL OF AIR AND WATER POLLUTION
INTERNATIONAL ABSTRACTS OF BIOLOGICAL SCIENCES (*for Biological and Medical Abstracts Ltd.*)
VACUUM
OPERATIONAL RESEARCH QUARTERLY
ANNALS OF OCCUPATIONAL HYGIENE
ELECTROCHIMICA ACTA
COMPARATIVE BIOCHEMISTRY AND PHYSIOLOGY
HUMAN FACTORS

* *Translations of the Russian Journals published on behalf of the Pergamon Institute, a division of Pergamon International Corporation*

Leaflets giving further details and subscription rates of each of these journals are available on request

LIST OF CONTENTS

NUMBERS 1/2

Suggested radiation protection regulations. Draft of revision to Appendix B, Handbook 61 . . 1

E. B. WAGNER and G. S. HURST: A Geiger–Müeller γ-ray dosimeter with low neutron sensitivity . 20

G. L. BROWNELL, W. H. ELLETT, R. A. RYDIN and G. J. HINE: Large plastic scintillators for radioactivity measurement 27

P. S. HARRIS: Radiation dose estimation in the 1958 Los Alamos criticality accident . . . 37

M. L. RANDOLPH, H. G. JONES and D. L. PARRISH: Decay of polonium–beryllium fast neutron sources 45

E. L. RAY and S. E. HAMMOND: The use of an α-pulse-height analyzer in environmental monitoring 50

E. D. GUPTON, D. M. DAVIS and J. C. HART: Criticality accident application of the Oak Ridge National Laboratory badge dosimeter 57

A. BROIDO and J. D. TERESI: Analysis of the hazards associated with radioactive fallout material—I. Estimation of γ- and β-doses 63

D. A. GARDINER and K. E. COWSER: Optimization of radionuclide removal from low-level process wastes by the use of response surface methods 70

P. ZIGMAN and J. MACKIN: Early time decay of fission product mixtures—II. γ-Energy release and ionization rates following thermal neutron fission of U^{223} 79

J. G. KEREIAKES and M. S. MIRAGLIA: Relative biological effectiveness of Co^{60} γ-radiation for various responses in mice 85

W. J. BAIR, D. H. WILLARD and L. A. TEMPLE: The behavior of inhaled $Ru^{106}O_2$ particles . . 90

Note:

Comments on the revision to Appendix B, NBS Handbook 61 99

Health Physics Society Placement Column 100

NUMBERS 3/4

A. MORGAN and D. G. STANBURY: The contamination of rivers with fission products from fallout 101

R. L. FRENCH and M. B. WELLS: Calculations of weapons radiation penetration in air . . . 108

J. B. EGGEN, R. L. FRENCH and A. REETZ, JR.: Fast-neutron spectra and dose-rate calculations . 119

D. J. RASO: Transmission of scattered γ-rays through concrete and iron slabs 126

J. A. TWENTE and W. S. S. JEE: The determination of localized concentration of Pu^{239} in bone . 142

T. TAMURA ad D. G. JACOBS: Improving cesium selectivity of bentonites by heat treatment . . 149

H. K. SHAPAR: Significance of health physics evidence in the trial of a case of radiation personal injury 155

M. M. WEISS and W. W. MUMFORD: Microwave radiation hazards 160

W. HIGINBOTHAM, E. RAINEY and J. CHESTER: Ten-channel radiation monitor for pulsed accelerators 169

H. C. KINNE, JR.: The health physicist in nuclear warfare 173

G. S. HURST, R. H. RITCHIE, F. W. SANDERS, P. W. REINHARDT, J. A. AUXIER, E. B. WAGNER, A. D. CALLIHAN and K. Z. MORGAN: Dosimetric investigation of the Yugoslav radiation accident . . 179

D. R. NELSON, R. D. BIRKOFF, R. H. RITCHIE and H. H. HUBBELL, JR.: Measurement of electron flux in media bombarded by X-rays 203

W. D. MOSS, E. C. HYATT and H. F. SCHULTE: Particle size studies on plutonium aerosols . . 212

RYOSUKE YOKOTA, SABURO NAKAJIMA and EIJI SAKAI: High sensitivity silver-activated phosphate glass for the simultaneous measurement of thermal neutrons, γ- and/or β-rays 219

Notes:

KRISTIAN KOREN and ARNE BULL: Determination of radioiodine in milk 225

A. H. W. ATEN, JR., J. W. DALENBERG and W. C. M. BAKKUM: Concentration of uranium in sea fish 225

J. A. AUXIER, F. W. SANDERS and P. N. HENSLEY: A device for determining the orientation of persons exposed to neutron and/or γ-radiation 226

I. MICHELSON: Strontium-90 in the total diet 227

I. MICHELSON: Radium-226 in the total diet 229

News 231

Health Physics Society Placement Column 243

Obituary 244

AUTHOR INDEX

ATEN, A. H. W. JR. p. 225
AUXIER, J. A. pp. 179, 226
BAIR, W. J. p. 90
BAKKUM, W. C. M. p. 225
BIRKOFF, R. D. p. 203
BROIDO, A. p. 63
BROWNELL, G. L. p. 27
BULL, A. p. 225
CALLIHAN, A. D. p. 179
CHESTER, J. p. 169
COWSER, K. E. p. 70
DALENBURG, J. W. p. 225
DAVIS, D. M. p. 57
EGGEN, J. B. p. 119
ELLETT, W. H. p. 27
FRENCH, R. L. pp. 108, 119
GARDINER, D. A. p. 70
GUPTON, E. D. p. 57
HAMMOND, S. E. p. 50
HARRIS, P. S. p. 37
HART, J. C. p. 57
HENSLEY, P. N. p. 226
HIGINBOTHAM, W. p. 169
HINE, G. J. p. 27
HUBBLE, H. H., JR. p. 203
HURST, G. S. pp. 20, 179
HYATT, E. C. p. 212
JACOBS, D. G. p. 149
JEE, W. S. S. p. 142
JONES, H. G. p. 45
KEREIAKES, J. G. p. 85
KINNE, H. C., JR. p. 173
KOREN, K. p. 225
MACKIN, J. p. 79
MICHELSON, I. pp. 227, 229
MIRAGLIA, M. S. p. 85
MORGAN, A. p. 101
MORGAN, K. Z. p. 179
MOSS, W. D. p. 212
MUMFORD, W. W. p. 160
NAKAJIMA, S. p. 219
NELSON, D. R. p. 203
PARRISH, D. L. p. 45
RAINEY, E. p. 169
RANDOLPH, M. L. p. 45
RASO, D. J. p. 126
RAY, E. L. p. 50
REETZ, A., JR. p. 119
REINHARDT, P. W. p. 179
RITCHIE, R. H. pp. 179, 203
RYDIN, R. A. p. 27
SAKAI, E. p. 219
SANDERS, F. W. pp. 179, 226
SCHULTE, H. F. p. 212
SHAPAR, H. K. p. 155
SMITH, J. W. p. 200
STANBURY, D. G. p. 101
TAMURA, T. p. 149
TAYLOR, L. S. p. 1
TEMPLE, L. A. p. 90
TERESI, J. D. p. 63
TWENTE, J. A. p. 142
WAGNER, E. B. pp. 20, 179
WEISS, M. M. p. 160
WELLS, M. B. p. 108
WILLARD, D. H. p. 90
YOKOTA, R. p. 219
ZIGMAN, P. p. 79

Health Physics Pergamon Press 1961. Vol. 5, pp. 1–19. Printed in Northern Ireland

SUGGESTED RADIATION PROTECTION REGULATIONS*

DRAFT OF REVISION TO APPENDIX B, HANDBOOK 61†

PREFACE‡

HANDBOOK 61 on the Regulation of Radiation Exposure by Legislative Means was published in December 1955 as recommendations of the NCRP. At the time, the handbook represented a substantial departure from the type of recommendations the Committee had published in the past. However, such recommendations appeared to be needed, since various agencies at all levels of Government were actively seeking the advice of the NCRP in the development of radiation protection laws and codes. Appendix B of Handbook 61 contained a set of suggested regulations which the Committee felt could be used to provide a common framework for the regulatory control of radiation sources. The Committee did not intend Appendix B to be used as a model code.

In 1958 the Committee recognized that more and more regulations for radiation protection were being developed at all levels of Government and that all or parts of Appendix B were being used without change in these regulations. The NCRP decided to reactivate the subcommittee which had prepared Handbook 61 so that Appendix B could be revised into a more satisfactory model from both a regulatory and administrative point of view. This revision was being carried out by the reorganized subcommittee when the NCRP formally decided to withdraw from further activities or recommendations on methods of legislative and regulatory control of radiation. At the time when the NCRP made this decision, the reorganized Subcommittee No. 10 had already expended considerable effort on a revision of Appendix B of Handbook 61. This model regulatory code incorporates several improvements over the original form as published in Handbook 61. However, the revision had not reached the stage for final complete agreement by the Main Committee. Since it may be useful to others working on the formulation of regulatory codes, the NCRP is sponsoring the publication of this draft of the revision. Because of its decision to withdraw from the field, the NCRP does not make this in the form of an official recommendation.

The reorganized subcommittee and its advisors included individuals associated with the AEC, U.S. Department of Labor, U.S. Public Health Service, and several State agencies, in addition to a number of lawyers, radiologists and health physicists, prominent in the field. The suggested regulations for radiation protection given below are the result of the work of this subcommittee and its advisors.

It should be emphasized that while the members of this subcommittee as well as the Main Committee are drawn in part from various Federal and State agencies, this report is not to be construed as representing the official position of any of the agencies concerned. This report represents the views of the subcommittee at this particular stage of preparation with its members acting as individuals within their own areas of technical competence.

* Prepared by The National Committee on Radiation Protection and Measurements.

† National Bureau of Standards Handbook 61, *Regulation of Radiation Exposure by Legislative Means*. For sale by the Superintendent of Documents, Government Printing Office, Washington 25 D.C.

‡ Transmitted for the National Committee on Radiation Protection and Measurements by LAURISTON S. TAYLOR, Chairman.

1

The subcommittee working on this report included the following individuals:

Working Group	*Advisory Group*
W. A. McAdams, Chairman	W. H. Eells
P. Hodges	G. T. Frampton
J. Lieben	L. M. Hydeman
E. P. Pendergrass	M. Kleinfeld
J. A. Reynolds	L. Manning
L. Rogers	R. R. Newell
L. S. Taylor	F. A. Norton
J. G. Terrill, Jr.	M. Stein
	E. Dale Trout

Appendix A of Handbook 61 dealt with a Suggested State Radiation Protection Act. The committee believes that this phase of the protection problem is being adequately handled by other groups and individuals, and withdraws Appendix A from its current recommendations.

With the release of this document, the NCRP declares void its recommendations contained in Appendix A and Appendix B of Handbook 61 entitled "Regulation of Radiation Exposure by Legislative Means".

1. PURPOSE

These regulations state the requirements that shall be applied to sources of radiation to reduce, to an acceptable level, the risk that any person will be injured by radiation, and that shall be used to evaluate or control personnel exposure to radiation.

2. SCOPE AND APPLICATION

These regulations shall apply to the manufacture, use, storage, handling, transportation and disposal of all radiation machines and radioactive materials except as exempted by the provisions of Section 4. Nothing in these regulations shall be construed to limit the kind or amount of radiation that may be intentionally applied to a patient for diagnostic or therapeutic purposes by, or under the direction of, a licensed physician or dentist.*

3. DEFINITIONS

For the purposes of these regulations the following definitions shall apply:

Absorbed dose of any ionizing radiation is the energy imparted to matter by ionizing particles per unit mass of irradiated material at the place of interest. The unit of absorbed dose is the rad.

Agency is that governmental agency that is given the responsibility for administering these regulations.

Controlled area is a defined area in which the occupational exposure of personnel to radiation or to radioactive material is under the supervision of an individual in charge of radiation protection. (This implies that a controlled area is one that requires control of access, occupancy, and working conditions for radiation protection purposes.) The boundaries of a controlled area shall be determined with the advice of a Health Physicist.

Dose, as used in these regulations, means RBE dose. (See definitions of RBE and rem.)

Dose rate is the dose per unit time.

Health physicist is a person fitted by training and experience to perform radiation surveys and to oversee radiation monitoring. (If the ability of a Health Physicist is questioned, the Agency shall be the judge of his professional qualifications.)

Installation is a place containing more than one source of radiation.

Maximum permissible dose (MPD) is the dose of radiation that, in the light of present knowledge, is not expected to cause appreciable bodily injury to a person at any time during his lifetime. Appreciable bodily injury means any bodily injury or effect that competent medical authorities would regard as being deleterious to the health and well being of the individual.

Monitoring is the determination of the amount of radiation or radioactive material present in any location or of the dose received by a person.

Personnel monitoring is the determination of the radiation dose received by the person, during a specified period, by film badges, small ionization chambers, or other dosimeters.

* *Alternative wording:* ". . . . . licensed practitioners of the healing arts whose license privileges include the use of radiation sources."

rad is the unit of absorbed dose. It is 100 ergs per gram.

Radiation, as used in these regulations, is γ-rays and X-rays, α- and β-particles, high-speed electrons, neutrons, protons, and other nuclear particles; but not sound nor radio waves, nor visible, infrared, or ultraviolet light.

Radiation machine is any device that produces radiation when in operation.

Radioactive material is any material, solid, liquid, or gas, that emits radiation spontaneously.

Relative biological effectiveness (RBE) is a numerical factor which is used to compare the effectiveness of absorbed dose of radiation delivered in different ways. The standard of comparison is X- or γ-radiation having a linear energy transfer in water of 3 keV/μ. A list of RBE values for various kinds of radiation is given in Section 14, Table 1.

rem is the unit of RBE dose and is equal to the dose in rads multiplied by the appropriate RBE.

Source of radiation is a radiation machine or a quantity of radioactive material. *A sealed source* is a quantity of radioactive material enclosed to prevent the escape of any radioactive material.

Survey is a critical evaluation of the hazards and the risk of injury from a source of radiation.

User is a person or organization having administrative control over one or more source of radiation.

4. EXEMPTIONS

The following materials, machines and conditions are exempt from these regulations:

(a) Radioactive materials of an equivalent specific radioactivity not exceeding that of natural potassium (10^{-9} c/g of potassium).

(b) Quantities of radioactive materials not exceeding the amounts specified in Section 14, Table 2, provided that the user does not possess more than 10 such quantities, and also provided that the dose rate to the whole body at the point of nearest approach to such sources does not exceed 0.5 rem/year. The manufacture of sealed sources shall not be exempt.

(c) Radioactive material in combination with non-radioactive material in concentrations not exceeding the numerical values of Table 3, Column 2, expressed in μc/g, for solids and liquids, and the numerical values of Table 3, Column 3, expressed in μc/ml, for gases. (For example, 2×10^{-5} μc of antimony-124 per g of gasoline.)

(d) Domestic television receivers, provided that the dose rate at 5 cm from any outer surface is less than 0.5 mrem/hr.

(e) Other electrical equipment that produces radiation incidental to its operation for other purposes, provided that the dose rate to the whole body at the point of nearest approach to such equipment when any external shielding is removed does not exceed 0.5 rem/year. The production testing or factory servicing of such equipment shall not be exempt.

(f) Radiation machines which cannot be used in such manner as to produce radiation (for example, X-ray machines in transport or electrical equipment in storage).

(g) Radioactive material being transported across a state in conformance with regulations of any Federal agency having jurisdiction over safety in interstate transport.

(h) Other sources of radiation that the Agency finds should be exempted.

5. REGISTRATION

(a) The user shall register each source of radiation with the Agency within 30 days after receipt of the source, and once every 2 years thereafter as long as he continues to possess the source. When the user possesses more than one source, he may register his installation, instead of the several sources. The registration shall be submitted on a form provided by the Agency, and shall describe each source, its location and use, and the waste disposal practices, if any. The registration shall also give the name and address of the user, and the name, address and qualifications of the Health Physicist.

(b) The user shall notify the Agency in writing within 30 days of any changes with respect

to his radiation sources which may substantially increase the potential for personnel exposure.

(c) Acknowledgment of registration shall not imply the Agency's approval of the conditions described in the registration.

6. MAXIMUM PERMISSIBLE EXPOSURE LIMITS

The user shall control all sources of radiation in such a way as to provide reasonable assurance that no person will receive a dose of radiation in excess of any maximum permissible exposure limit specified in paragraphs (a) through (d) below.

(a) **External exposure—Occupational*

(1) Except as provided in part (2) below of this section, the maximum permissible dose (MPD) for persons within a controlled area shall be as listed in the following table:

Part of body	(A) Maximum dose permitted in any calendar year	(B) Maximum dose permitted in any calendar quarter
Whole body, head and trunk, major portion of the bone marrow, gonads, or lens of eye.	5 rems	3 rems
Skin of large body area.	30 rems	10 rems
Hands and forearms, feet and ankles.	75 rems	25 rems

(2) A dose to the whole body, head and trunk, etc., in addition to that listed in the table of part (1) above shall be permitted for a calendar year provided that:

(i) During any calendar quarter, the maximum dose of 3 rems, listed in column (B) of the table in part (1) above, is not exceeded, and

(ii) The user has determined the individual's previously accumulated occupational dose, and

(iii) The dose when added to the previously accumulated occupational dose, does not exceed the maximum permissible accumulated dose (MPAD) calculated according to the formula: MPAD = $5(N - 18)$ rems, where N is the individual's age in full years beyond age 18.

(b) *Internal exposure—Occupational*

For persons within a controlled area the radiation dose to the tissues of the body from radioactive materials within the body shall be controlled by limiting the average rates at which such materials are taken into the body. Where this intake results from breathing contaminated air, the concentration of the radionuclides in the air, averaged over any calendar quarter, shall not exceed the concentrations listed in Section 14, Table 3, Column 1. The values in this table are for a work week of 40 hr. For longer work weeks the values must be adjusted downward accordingly. Where this intake results from the occurrence of radioactive material in drinking water and foodstuffs, the permissible concentrations shall be

* The following alternative to paragraph (a) may be used if desired:

(a) *External exposure—Occupational*

For persons within a controlled area,

(1) The maximum permissible dose (MPD) to the whole body, head and trunk, major portion of the bone marrow, gonads, or lens of the eyes, accumulated at any age shall be 5 rems multiplied by the number of years beyond 18 [i.e. MPD = 5 $(N - 18)$ rems, where N is the age in full years and is greater than 18]; and the dose in any period of 13 consecutive weeks shall not exceed 3 rems.

(2) The maximum permissible dose to the skin of the whole body, accumulated at any age, shall be 30 rems/year; and the dose in any period of 13 consecutive weeks shall not exceed 10 rems.

(3) The maximum permissible dose to the hands and forearms, and the feet and ankles shall be 75 rems/year; and the dose in any 13 consecutive weeks shall not exceed 25 rems.

the same as in paragraph (d) below on "Internal exposure—Non-occupational".†

(c) *External exposure—Non-occupational*

For persons outside a controlled area, the maximum permissible dose to the whole body, due to sources within the controlled area or to radioactive materials escaping the controlled area, shall be 0.5 rem in any year. In meeting this requirement, the user may take reasonable advantage of operational factors such as the amount of time that the radiation is present or that the area is occupied by any person.

(d) *Internal exposure—Non-occupational*

For persons outside a controlled area, the radiation dose to tissues of the body from radioactive materials within the body shall be controlled by limiting the average rates at which such materials are taken into the body. Where this intake results from the occurrence of radioactive materials in the air, drinking water, or foodstuffs, the average concentrations of the radionuclides in the air, or drinking water, or foodstuffs, averaged over any calendar quarter, shall not exceed the concentrations listed in Section 14, Table 3, Columns 2 and 3.

(e) *Concurrent exposure*

When external exposure and internal exposure are concurrent the limits indicated above should be reduced appropriately. If external exposure occurs at a per cent and internal exposure occurs at b per cent of their respective separate limits, then the combined exposure is considered acceptable if $a + b$ does not exceed 100. The same principle applies if there is concurrent exposure to several radionuclides with or without concurrent external exposure.

7. SURVEYS AND MONITORING

(a) The user shall provide for surveys and monitoring sufficient to assure compliance with other sections of these regulations. Such surveys and monitoring shall be performed by a Health Physicist or under his direction.

(b) The user shall provide for the routine personnel monitoring for external exposure of all persons within a controlled area. However, on the advice of a Health Physicist, he may discontinue such personnel monitoring if:

(1) The dose rates at which any person is exposed are predictable, and

(2) The dose to all exposed persons is determined by some other reliable means, and

(3) There is reasonable assurance that an accident causing exposure in excess of the exposure limits specified in Section 6(a) will not occur.

8. RADIATION EXPOSURE RECORDS AND REPORTS

(a) The user shall keep individual exposure records for all persons entering a controlled area.

(1) The user shall preserve these records as long as the employee remains in his employment. When an employee terminates, the user shall send a copy of all the employee's exposure records to the Agency and shall provide the Agency and the employee with a summary of the records for each calendar year of employment. These records shall include the employee's Social Security number.

(2) When the individual entering a controlled area is not an employee of the user, the records obtained shall be preserved and reported according to procedures established by the Agency.

(b) The user shall keep records showing the levels of radiation outside of the controlled areas to which persons are, or may be, exposed as a result of sources under his control.

(c) The user shall record the details of any circumstances wherein any individual

† It should be noted that the occupational MPC values given here for water and food are 1/10 those recommended by the NCRP in Handbook 69. Since, in most situations, the water and food supply used by occupational workers is also available to other people, it may be reasonable in these cases to use a single set of values for concentration limits in food and water.

receives an exposure as a result of sources under his control, in excess of the applicable limits specified in Section 6.

(d) The user shall keep records showing the date, the amount, and kind of radioactive materials received by, or transported out of, a controlled area. He shall also keep records on the release of radioactive materials to the environs sufficient to demonstrate compliance with other sections of these regulations.

(e) All the records referred to in paragraphs (a) through (d) shall be made available to the Agency on request.

(f) When it is known or believed that any person may have received an external exposure in excess of the maximum permissible limits specified by the applicable portions of Section 6 or that any person may have been exposed to a concentration of radioactive material in air or water which, when averaged over a calendar quarter, was in excess of the limits specified in the applicable portions of Section 6, the user shall report to the Agency, within 7 days of the discovery, all of the facts relevant to the incident.

(g) Except as provided in Section 13 (b) (1), the user shall report to the Agency, within 24 hr, any release of radioactive material to the environs in a concentration, which, when averaged over a period of 24 hr, exceeds 500 times the permissible concentration listed in Column 2 or 3 of Table 3, or in total quantity released in any 24-hr period exceeding 1000 times the amount listed in Column 1 of Table 2.

(h) The loss or theft of any source of radiation shall be reported to the Agency within 24 hr after such loss or theft is discovered.

9. CONTROL OF EXPOSURE

(a) The user shall provide for the services of a Health Physicist and with his advice shall establish operating rules and procedures which will provide reasonable assurance that the other provisions of these regulations will be carried out.

(b) To meet the other provisions of these regulations the user shall provide, or have readily available, instruments adequate for the detection and measurement of radiation and radioactive material; and he shall further see that these instruments are maintained in proper calibration.

(c) Every employee and authorized visitor shall use such radiation safety devices as are furnished for his protection and shall carry out all radiation safety rules that concern or affect his conduct.

10. STORAGE OF RADIOACTIVE MATERIALS

(a) The user shall see that radioactive materials are kept in a manner that will provide reasonable assurance that, during routine access to a controlled area, no person will be exposed in excess of the limits set forth in Section 6. The user shall also take precautions to minimize exposure of personnel in the event of fire, earthquake, flood, windstorm, explosion or other emergency.

(b) The user shall see that vaults or rooms used for storing materials that may emit radioactive gases are ventilated in such a manner that the concentration of the gases in the air does not exceed the levels specified in the appropriate portions of Section 6.

(c) When there is a reasonable possibility that chemical, radiation, or other action might lead to leakage of radioactive material from a container, the user shall provide a secondary tray or catchment to the container adequate to retain the entire amount of radioactive material.

11. CONTROL OF RADIOACTIVE CONTAMINATION

(a) The user shall see that all work with radioactive materials is carried out under conditions which will minimize the possibility of spread of radioactive material that could result in the exposure of any person above any limit specified in Section 6 of these regulations.

(b) Where the nature of the work is such that a person or his clothing may become contaminated with radioactive material, both shall be monitored according to procedures established by the Health Physicist. Personal contamination shall be removed according to procedures established by the Health Physicist.

(c) Clothing or other material contaminated to a degree which could result in the exposure of any person above any limit specified in Section 6 should be retained inside the installation until it can be decontaminated or disposed of according to procedures established by the Health Physicist.

12. RADIATION LABELING

(a) The user shall indicate the presence of radiation by posting conspicuous signs or labels which bear appropriate wording (such as "caution—X-ray", "danger—radiation", "caution—radioactive material") to explain the nature of the hazard.

(b) All such radiation warning signs and labels shall bear the standard symbol. This symbol is shown below:

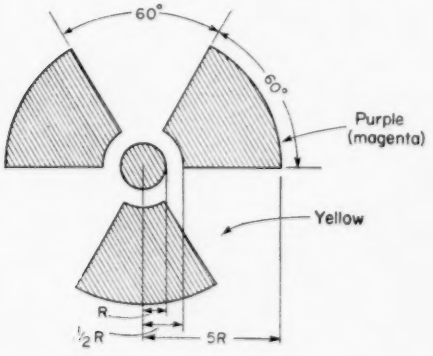

(c) The standard color specifications for these radiation warning signs and labels shall be a background of yellow with the distinctive symbol in purple (magenta).

(d) The use of this symbol for any other purpose is expressly prohibited. The symbol and the lettering used with it shall be as large as practical, consistent with size of the equipment or material. The lettering shall not be superimposed on the symbol.

(e) The user shall put such signs or labels on radiation machines and on all containers, source holders, manufactured products or other items containing a quantity of radioactive material greater than the amounts listed in Section 14, Table 2. The user is not required to label laboratory containers, such as beakers, flasks, and test-tubes, used transiently under operating rules established under Section 9(a).

(f) The user shall use such signs or labels to designate each controlled area. In addition to posting signs and labels, the user shall fence off, barricade, or otherwise restrict entrance to each controlled area that is readily accessible, but not normally occupied.

(g) The user shall remove all signs and labels bearing the radiation symbol when the hazard is no longer present.

13. DISPOSAL OF RADIOACTIVE WASTES

(a) No user shall release radioactive material into the air or water in such a manner to cause exposure of any person above the limits specified in Section 6. If several users are discharging radioactive waste to the same environs, they shall, upon being notified of the fact, co-operate in limiting the release and shall file with the Agency a statement of their agreed *pro rata* releases. If this is not done within a reasonable time, the Agency may assign quantity limits to them severally.

(b) For purposes of controlling the exposure of persons outside controlled areas each user shall control the release of radioactive material on the following basis:

(1) The average concentration of the radionuclide (or radionuclides) in air or

water at points of release from control of the user shall not exceed the limits specified in Section 6. However, with the approval of the Agency, the user may exceed these limits by taking advantage of the known environmental factors of occupancy, dilution, dispersion, etc., providing the average concentration of the radionuclide (or radionuclides) in air at points where it is commonly used by humans or in water at points of supply (exclusive of treatment, if any) prior to use by humans shall not exceed these limits.

(For any radionuclide where the effective half-life in the body is less than 60 days, the term "average" as used above shall mean the arithmetic mean of a series of determinations representative of plant operations and environmental conditions over any period of 13 consecutive weeks; for other radionuclides this arithmetic mean shall be taken over a period of any 12 consecutive months.)

(2) The total quantity of the radionuclide (or radionuclides) released in a period of any 24 consecutive hours, shall not exceed 100 times the quantities listed in Section 14, Table 2, Column 1, unless approval for the release of larger quantities is obtained from the Agency in advance.

(c) A user may dispose of radioactive waste by dumping or burial only in areas and by procedures approved by the Agency or by other agencies having jurisdiction over such matters.

(d) Nothing in these regulations shall be construed as permitting release of materials that would be unlawful for other reasons.

14. REFERENCE TABLES

The following tables are referred to in previous sections of these regulations:

Table 1. *RBE values**

Radiation	RBE
X-rays and γ-rays, of all energies, and electrons and β-rays above 0.03 MeV	1.0
Fast neutrons and protons up to 10 MeV	10
α-Particles	10
Heavy recoil nuclei	20

* The RBE values in this table are convenient approximations to relate dose in rads to dose in rems. The values will vary greatly with the biological effect being considered, the acuteness of the exposure and many other factors. The Health Physicist should evaluate these factors for each situation, and should adjust the values accordingly.

Table 2. Exempt quantities of radioisotopes

	Column 1 Unsealed sources (μc)	Column 2 Sealed sources (μc)		Column 1 Unsealed sources (μc)	Column 2 Sealed sources (μc)
Actinium 227	0.1	1	Palladium–rhodium 103	10	100
Americium 241	0.1	1	Phosphorus 32	10	100
Antimony 124	1	10	Platinum 191	10	100
Arsenic 73	10	100	193	10	100
74	10	100	Plutonium 239	0.1	1
76	10	100	Polonium 210	0.1	1
77	10	100	Potassium 42	10	100
Astatine 211	0.1	1	Praseodymium 143	10	100
Barium–lanthanum 140	1	10	Promethium 147	10	100
Beryllium 7	100	1000	Radium 226	0.1	1
Bromine 82	10	100	Rhenium 183	10	100
Cadmium–silver 109	10	100	186	10	100
Calcium 45	1	10	Rhodium 105	10	100
Carbon 14	1000	10,000	Rubidium 86	10	100
Cerium–praseodymium 144	1	10	Ruthenium 103	10	100
Cesium–barium 137	10	100	Ruthenium–rhodium 106	1	10
Chlorine 36	10	100	Samarium 151	1	10
Chromium 51	100	1000	153	10	100
Cobalt 58	10	100	Scandium 46	10	100
60	10	100	47	10	100
Copper 64	10	100	48	10	100
Curium 242	0.1	1	Silver 105	10	100
Europium 154	1	10	110	10	100
Fluorine 18	100	1000	111	10	100
Gallium 72	10	100	Sodium 22	10	100
Germanium 71	100	1000	24	10	100
Gold 196	10	100	Strontium 89	1	10
198	10	100	Strontium–yttrium 90	0.1	1.0
199	10	100	Sulfur 35	10	100
Holmium 166	10	100	Tantalum 182	10	100
Hydrogen (tritium) 3	1000	10,000	Technetium 96	1	10
Indium 114	1	10	99	1	10
Iodine 131	1	10	Tellurium 127	10	100
132	10	100	129	10	100
Iridium 190	10	100	Thallium 200	10	100
192	10	100	201	100	1000
Iron 55	10	100	202	10	100
59	1	10	204	10	100
Krypton 85	1000	10,000	Thorium nat.	100	1000
Lanthanum 140	10	100	Thorium–protoactinium 234	1	10
Lead 203	10	100	Thulium–ytterbium 170	1	10
210 + dtrs	0.1	1	Tin 113	10	100
Lutecium 177	10	100	Tungsten 181	10	100
Manganese 52	10	100	185	10	100
54	10	100	Uranium 233	0.1	1
56	10	100	natural	1000	10,000
Molybdenum 99	10	100	Vanadium 48	10	100
Nickel 59	10	100	Yttrium 91	1	10
63	10	100	Zinc 65	10	100
Niobium 95	10	100	Zirconium–niobium 95	10	100
Palladium–silver 109	10	100			

Table 3. Concentrations in water and air above natural background

Element (Atomic number)	Isotope*		Column 1 Air (μc/ml)	Column 2 Water (μc/ml)	Column 3 Air (μc/ml)
Actinium (89)	Ac 227	S	2×10^{-12}	2×10^{-6}	8×10^{-14}
		I	3×10^{-11}	3×10^{-4}	9×10^{-13}
	Ac 228	S	8×10^{-8}	9×10^{-5}	3×10^{-9}
		I	2×10^{-8}	9×10^{-5}	6×10^{-10}
Americium (95)	Am 241	S	6×10^{-12}	4×10^{-6}	2×10^{-13}
		I	1×10^{-10}	2×10^{-4}	4×10^{-12}
	Am 243	S	6×10^{-12}	4×10^{-6}	2×10^{-13}
		I	1×10^{-10}	3×10^{-5}	4×10^{-12}
Antimony (51)	Sb 122	S	2×10^{-7}	3×10^{-5}	6×10^{-9}
		I	1×10^{-7}	3×10^{-5}	5×10^{-9}
	Sb 124	S	2×10^{-7}	2×10^{-5}	5×10^{-9}
		I	2×10^{-8}	2×10^{-5}	7×10^{-10}
	Sb 125	S	5×10^{-7}	1×10^{-4}	2×10^{-8}
		I	3×10^{-8}	1×10^{-4}	9×10^{-10}
Argon† (18)	A 37	Sub	6×10^{-3}	—	1×10^{-4}
	A 41	Sub	2×10^{-6}	—	4×10^{-8}
Arsenic (33)	As 73	S	2×10^{-6}	5×10^{-4}	7×10^{-8}
		I	4×10^{-7}	5×10^{-4}	1×10^{-8}
	As 74	S	3×10^{-7}	5×10^{-5}	1×10^{-8}
		I	1×10^{-7}	5×10^{-5}	4×10^{-9}
	As 76	S	1×10^{-7}	2×10^{-5}	4×10^{-9}
		I	1×10^{-7}	2×10^{-5}	3×10^{-9}
	As 77	S	5×10^{-7}	8×10^{-5}	2×10^{-8}
		I	4×10^{-7}	8×10^{-5}	1×10^{-8}
Astatine (85)	At 211	S	7×10^{-9}	2×10^{-6}	2×10^{-10}
		I	3×10^{-8}	7×10^{-5}	1×10^{-9}
Barium (56)	Ba 131	S	1×10^{-6}	2×10^{-4}	4×10^{-8}
		I	4×10^{-7}	2×10^{-4}	1×10^{-8}
	Ba 140	S	1×10^{-7}	3×10^{-5}	4×10^{-9}
		I	4×10^{-8}	2×10^{-5}	1×10^{-9}
Berkelium (97)	Bk 249	S	9×10^{-10}	6×10^{-4}	3×10^{-11}
		I	1×10^{-7}	6×10^{-4}	4×10^{-9}
Beryllium (4)	Be 7	S	6×10^{-6}	2×10^{-3}	2×10^{-7}
		I	1×10^{-6}	2×10^{-3}	4×10^{-8}
Bismuth (83)	Bi 206	S	2×10^{-7}	4×10^{-5}	6×10^{-9}
		I	1×10^{-7}	4×10^{-5}	5×10^{-9}
	Bi 207	S	2×10^{-7}	6×10^{-5}	6×10^{-9}
		I	1×10^{-8}	6×10^{-5}	5×10^{-10}
	Bi 210	S	6×10^{-9}	4×10^{-5}	2×10^{-10}
		I	6×10^{-9}	4×10^{-5}	2×10^{-10}
	Bi 212	S	1×10^{-7}	4×10^{-4}	3×10^{-9}
		I	2×10^{-7}	4×10^{-4}	7×10^{-9}
Bromine (35)	Br 82	S	1×10^{-6}	3×10^{-4}	4×10^{-8}
		I	2×10^{-7}	4×10^{-5}	6×10^{-9}
Cadmium (48)	Cd 109	S	5×10^{-8}	2×10^{-4}	2×10^{-9}
		I	7×10^{-8}	2×10^{-4}	3×10^{-9}
	Cd 115m	S	4×10^{-8}	3×10^{-5}	1×10^{-9}
		I	4×10^{-8}	3×10^{-5}	1×10^{-9}

* Soluble (S); insoluble (I); submersion in a cloud of gaseous material (Sub).
† Noble gas—values given for submersion in an infinite cloud.

Table 3—(*contd.*)

Element (Atomic number)	Isotope*		Column 1 Air (μc/ml)	Column 2 Water (μc/ml)	Column 3 Air (μc/ml)
	Cd 115	S	2×10^{-7}	3×10^{-5}	8×10^{-9}
		I	2×10^{-7}	4×10^{-5}	6×10^{-9}
Calcium	Ca 45	S	3×10^{-8}	9×10^{-6}	1×10^{-9}
(20)		I	1×10^{-7}	2×10^{-4}	4×10^{-9}
	Ca 47	S	2×10^{-7}	5×10^{-5}	6×10^{-9}
		I	2×10^{-7}	3×10^{-5}	6×10^{-9}
Californium	Cf 249	S	2×10^{-12}	4×10^{-6}	5×10^{-14}
(98)		I	1×10^{-10}	2×10^{-5}	3×10^{-12}
	Cf 250	S	5×10^{-12}	1×10^{-5}	2×10^{-13}
		I	1×10^{-10}	3×10^{-5}	3×10^{-12}
	Cf 252	S	6×10^{-12}	7×10^{-6}	2×10^{-13}
		I	3×10^{-11}	7×10^{-6}	1×10^{-12}
Carbon	C 14	S	4×10^{-6}	8×10^{-4}	1×10^{-7}
(6)	(CO_2)	Sub	5×10^{-5}	—	1×10^{-6}
Cerium	Ce 141	S	4×10^{-7}	9×10^{-5}	2×10^{-8}
(58)		I	2×10^{-7}	9×10^{-5}	5×10^{-9}
	Ce 143	S	3×10^{-7}	4×10^{-5}	9×10^{-9}
		I	2×10^{-7}	4×10^{-5}	7×10^{-9}
	Ce 144	S	1×10^{-8}	1×10^{-5}	3×10^{-10}
		I	6×10^{-9}	1×10^{-5}	2×10^{-10}
Cesium	Cs 131	S	1×10^{-5}	2×10^{-3}	4×10^{-7}
(55)		I	3×10^{-6}	9×10^{-4}	1×10^{-7}
	Cs 134m	S	4×10^{-5}	6×10^{-3}	1×10^{-6}
		I	6×10^{-6}	1×10^{-3}	2×10^{-7}
	Cs 134	S	4×10^{-8}	9×10^{-6}	1×10^{-9}
		I	1×10^{-8}	4×10^{-5}	4×10^{-10}
	Cs 135	S	5×10^{-7}	1×10^{-4}	2×10^{-8}
		I	9×10^{-8}	2×10^{-4}	3×10^{-9}
	Cs 136	S	4×10^{-7}	9×10^{-5}	1×10^{-8}
		I	2×10^{-7}	6×10^{-5}	6×10^{-9}
	Cs 137	S	6×10^{-8}	2×10^{-5}	2×10^{-9}
		I	1×10^{-8}	4×10^{-5}	5×10^{-10}
Chlorine	Cl 36	S	4×10^{-7}	8×10^{-5}	1×10^{-8}
(17)		I	2×10^{-8}	6×10^{-5}	8×10^{-10}
	Cl 38	S	3×10^{-6}	4×10^{-4}	9×10^{-8}
		I	2×10^{-6}	4×10^{-4}	7×10^{-8}
Chromium	Cr 51	S	1×10^{-5}	2×10^{-3}	4×10^{-7}
(24)		I	2×10^{-6}	2×10^{-3}	8×10^{-8}
Cobalt	Co 57	S	3×10^{-6}	5×10^{-4}	1×10^{-7}
(27)		I	2×10^{-7}	4×10^{-4}	6×10^{-9}
	Co 58m	S	2×10^{-5}	3×10^{-3}	6×10^{-7}
		I	9×10^{-6}	2×10^{-3}	3×10^{-7}
	Co 58	S	8×10^{-7}	1×10^{-4}	3×10^{-8}
		I	5×10^{-8}	9×10^{-5}	2×10^{-9}
	Co 60	S	3×10^{-7}	5×10^{-5}	1×10^{-8}
		I	9×10^{-9}	3×10^{-5}	3×10^{-10}
Copper	Cu 64	S	2×10^{-6}	3×10^{-4}	7×10^{-8}
(29)		I	1×10^{-6}	2×10^{-4}	4×10^{-8}
Curium	Cm 242	S	1×10^{-10}	2×10^{-5}	4×10^{-12}
(96)		I	2×10^{-10}	3×10^{-5}	6×10^{-12}

Table 3—(*contd.*)

Element (Atomic number)	Isotope*		Column 1 Air (μc/ml)	Column 2 Water (μc/ml)	Column 3 Air (μc/ml)
	Cm 243	S	6×10^{-12}	5×10^{-6}	2×10^{-13}
		I	1×10^{-10}	2×10^{-5}	3×10^{-12}
	Cm 244	S	9×10^{-12}	7×10^{-6}	3×10^{-13}
		I	1×10^{-10}	3×10^{-5}	3×10^{-12}
	Cm 245	S	5×10^{-12}	4×10^{-6}	2×10^{-13}
		I	1×10^{-10}	3×10^{-5}	4×10^{-12}
	Cm 246	S	5×10^{-12}	4×10^{-6}	2×10^{-13}
		I	1×10^{-10}	3×10^{-5}	4×10^{-12}
Dysprosium (66)	Dy 165	S	3×10^{-6}	4×10^{-4}	9×10^{-8}
		I	2×10^{-6}	4×10^{-4}	7×10^{-8}
	Dy 166	S	2×10^{-7}	4×10^{-5}	8×10^{-9}
		I	2×10^{-7}	4×10^{-5}	7×10^{-9}
Erbium (68)	Er 169	S	6×10^{-7}	9×10^{-5}	2×10^{-8}
		I	4×10^{-7}	9×10^{-5}	1×10^{-8}
	Er 171	S	7×10^{-7}	1×10^{-4}	2×10^{-8}
		I	6×10^{-7}	1×10^{-4}	2×10^{-8}
Europium (63)	Eu 152 (TV/2 = 9.2 hr)	S	4×10^{-7}	6×10^{-5}	1×10^{-8}
		I	3×10^{-7}	6×10^{-5}	1×10^{-8}
	Eu 152 (TV/2 = 13 yr)	S	1×10^{-8}	8×10^{-5}	4×10^{-10}
		I	2×10^{-8}	8×10^{-5}	6×10^{-10}
	Eu 154	S	4×10^{-9}	2×10^{-5}	1×10^{-10}
		I	7×10^{-9}	2×10^{-5}	2×10^{-10}
	Eu 155	S	9×10^{-8}	2×10^{-4}	3×10^{-9}
		I	7×10^{-8}	2×10^{-4}	3×10^{-9}
Fluorine (9)	F 18	S	5×10^{-6}	8×10^{-4}	2×10^{-7}
		I	3×10^{-6}	5×10^{-4}	9×10^{-8}
Gadolinium (64)	Gd 153	S	2×10^{-7}	2×10^{-4}	8×10^{-9}
		I	9×10^{-8}	2×10^{-4}	3×10^{-9}
	Gd 159	S	5×10^{-7}	8×10^{-5}	2×10^{-8}
		I	4×10^{-7}	8×10^{-5}	1×10^{-8}
Gallium (31)	Ga 72	S	2×10^{-7}	4×10^{-5}	8×10^{-9}
		I	2×10^{-7}	4×10^{-5}	6×10^{-9}
Germanium (32)	Ge 71	S	1×10^{-5}	2×10^{-3}	4×10^{-7}
		I	6×10^{-6}	2×10^{-3}	2×10^{-7}
Gold (79)	Au 196	S	1×10^{-6}	2×10^{-4}	4×10^{-8}
		I	6×10^{-7}	1×10^{-4}	2×10^{-8}
	Au 198	S	3×10^{-7}	5×10^{-5}	1×10^{-8}
		I	2×10^{-7}	5×10^{-5}	8×10^{-9}
	Au 199	S	1×10^{-6}	2×10^{-4}	4×10^{-8}
		I	8×10^{-7}	2×10^{-4}	3×10^{-8}
Hafnium (72)	Hf 181	S	4×10^{-8}	7×10^{-5}	1×10^{-9}
		I	7×10^{-8}	7×10^{-5}	3×10^{-9}
Holmium (67)	Ho 166	S	2×10^{-7}	3×10^{-5}	7×10^{-9}
		I	2×10^{-7}	3×10^{-5}	6×10^{-9}
Hydrogen (1)	H 3	S	5×10^{-6}	3×10^{-3}	2×10^{-7}
		Sub	2×10^{-3}	—	4×10^{-5}
Indium (49)	In 113m	S	8×10^{-6}	1×10^{-3}	3×10^{-7}
		I	7×10^{-6}	1×10^{-3}	2×10^{-7}
	In 114m	S	1×10^{-7}	2×10^{-5}	4×10^{-9}
		I	2×10^{-8}	2×10^{-5}	7×10^{-10}

Table 3—(contd.)

Element (Atomic number)	Isotope*		Column 1 Air (μc/ml)	Column 2 Water (μc/ml)	Column 3 Air (μc/ml)
	In 115m	S	2×10^{-6}	4×10^{-4}	8×10^{-8}
		I	2×10^{-6}	4×10^{-4}	6×10^{-8}
	In 115	S	2×10^{-7}	9×10^{-5}	9×10^{-9}
		I	3×10^{-8}	9×10^{-5}	1×10^{-9}
Iodine (53)	I 126	S	8×10^{-9}	2×10^{-6}	3×10^{-10}
		I	3×10^{-7}	9×10^{-5}	1×10^{-8}
	I 129	S	2×10^{-9}	4×10^{-7}	6×10^{-11}
		I	7×10^{-8}	2×10^{-4}	2×10^{-9}
	I 131	S	9×10^{-9}	2×10^{-6}	3×10^{-10}
		I	3×10^{-7}	6×10^{-5}	1×10^{-8}
	I 132	S	2×10^{-7}	6×10^{-5}	8×10^{-9}
		I	9×10^{-7}	2×10^{-4}	3×10^{-8}
	I 133	S	3×10^{-8}	7×10^{-6}	1×10^{-9}
		I	2×10^{-7}	4×10^{-5}	7×10^{-9}
	I 134	S	5×10^{-7}	1×10^{-4}	2×10^{-8}
		I	3×10^{-6}	6×10^{-4}	1×10^{-7}
	I 135	S	1×10^{-7}	2×10^{-5}	4×10^{-9}
		I	4×10^{-7}	7×10^{-5}	1×10^{-8}
Iridium (77)	Ir 190	S	1×10^{-6}	2×10^{-4}	4×10^{-8}
		I	4×10^{-7}	2×10^{-4}	1×10^{-8}
	Ir 192	S	1×10^{-7}	4×10^{-5}	4×10^{-9}
		I	3×10^{-8}	4×10^{-5}	9×10^{-10}
	Ir 194	S	2×10^{-7}	3×10^{-5}	8×10^{-9}
		I	2×10^{-7}	3×10^{-5}	5×10^{-9}
Iron (26)	Fe 55	S	9×10^{-7}	8×10^{-4}	3×10^{-8}
		I	1×10^{-6}	2×10^{-3}	3×10^{-8}
	Fe 59	S	1×10^{-7}	6×10^{-5}	5×10^{-9}
		I	5×10^{-8}	5×10^{-5}	2×10^{-9}
Krypton† (36)	Kr 85m	Sub	6×10^{-6}	—	1×10^{-7}
	Kr 85	Sub	1×10^{-5}	—	3×10^{-7}
	Kr 87	Sub	1×10^{-6}	—	2×10^{-8}
Lanthanum (57)	La 140	S	2×10^{-7}	2×10^{-5}	5×10^{-9}
		I	1×10^{-7}	2×10^{-5}	4×10^{-9}
Lead (82)	Pb 203	S	3×10^{-6}	4×10^{-4}	9×10^{-8}
		I	2×10^{-6}	4×10^{-4}	6×10^{-8}
	Pb 210	S	1×10^{-10}	1×10^{-7}	4×10^{-12}
		I	2×10^{-10}	2×10^{-4}	8×10^{-12}
	Pb 212	S	2×10^{-8}	2×10^{-5}	6×10^{-10}
		I	2×10^{-8}	2×10^{-5}	7×10^{-10}
Lutecium (71)	Lu 177	S	6×10^{-7}	1×10^{-4}	2×10^{-8}
		I	5×10^{-7}	1×10^{-4}	2×10^{-8}
Manganese (25)	Mn 52	S	2×10^{-7}	3×10^{-5}	7×10^{-9}
		I	1×10^{-7}	3×10^{-5}	5×10^{-9}
	Mn 54	S	4×10^{-7}	1×10^{-4}	1×10^{-8}
		I	4×10^{-8}	1×10^{-4}	1×10^{-9}
	Mn 56	S	8×10^{-7}	1×10^{-4}	3×10^{-8}
		I	5×10^{-7}	1×10^{-4}	2×10^{-8}
Mercury (80)	Hg 197m	S	7×10^{-7}	2×10^{-4}	3×10^{-8}
		I	8×10^{-7}	2×10^{-4}	3×10^{-8}

Table 3—(*contd.*)

Element (Atomic number)	Isotope*		Column 1 Air (μc/ml)	Column 2 Water (μc/ml)	Column 3 Air (μc/ml)
	Hg 197	S	1×10^{-6}	3×10^{-4}	4×10^{-8}
		I	3×10^{-6}	5×10^{-4}	9×10^{-8}
	Hg 203	S	7×10^{-8}	2×10^{-5}	2×10^{-9}
		I	1×10^{-7}	1×10^{-4}	4×10^{-9}
Molybdenum (42)	Mo 99	S	7×10^{-7}	2×10^{-4}	3×10^{-8}
		I	2×10^{-7}	4×10^{-5}	7×10^{-9}
Neodymium (60)	Nd 144	S	8×10^{-11}	7×10^{-5}	3×10^{-12}
		I	3×10^{-10}	8×10^{-5}	1×10^{-11}
	Nd 147	S	4×10^{-7}	6×10^{-5}	1×10^{-8}
		I	2×10^{-7}	6×10^{-5}	8×10^{-9}
	Nd 149	S	2×10^{-6}	3×10^{-4}	6×10^{-8}
		I	1×10^{-6}	3×10^{-4}	5×10^{-8}
Neptunium (93)	Np 237	S	4×10^{-12}	3×10^{-6}	1×10^{-13}
		I	1×10^{-10}	3×10^{-5}	4×10^{-12}
	Np 239	S	8×10^{-7}	1×10^{-4}	3×10^{-8}
		I	7×10^{-7}	1×10^{-4}	2×10^{-8}
Nickel (28)	Ni 59	S	5×10^{-7}	2×10^{-4}	2×10^{-8}
		I	8×10^{-7}	2×10^{-3}	3×10^{-8}
	Ni 63	S	6×10^{-8}	3×10^{-5}	2×10^{-9}
		I	3×10^{-7}	7×10^{-4}	1×10^{-8}
	Ni 65	S	9×10^{-7}	1×10^{-4}	3×10^{-8}
		I	5×10^{-7}	1×10^{-4}	2×10^{-8}
Niobium (Columbium) (41)	Nb 93m	S	1×10^{-7}	4×10^{-4}	4×10^{-9}
		I	2×10^{-7}	4×10^{-4}	5×10^{-9}
	Nb 95	S	5×10^{-7}	1×10^{-4}	2×10^{-8}
		I	1×10^{-7}	1×10^{-4}	3×10^{-9}
	Nb 97	S	6×10^{-6}	9×10^{-4}	2×10^{-7}
		I	5×10^{-6}	9×10^{-4}	2×10^{-7}
Osmium (76)	Os 185	S	5×10^{-7}	7×10^{-5}	2×10^{-8}
		I	5×10^{-8}	7×10^{-5}	2×10^{-9}
	Os 191m	S	2×10^{-5}	3×10^{-3}	6×10^{-7}
		I	9×10^{-6}	2×10^{-3}	3×10^{-7}
	Os 191	S	1×10^{-6}	2×10^{-4}	4×10^{-8}
		I	4×10^{-7}	2×10^{-4}	1×10^{-8}
	Os 193	S	4×10^{-7}	6×10^{-5}	1×10^{-8}
		I	3×10^{-7}	5×10^{-5}	9×10^{-9}
Palladium (46)	Pd 103	S	1×10^{-6}	3×10^{-4}	5×10^{-8}
		I	7×10^{-7}	3×10^{-4}	3×10^{-8}
	Pd 109	S	6×10^{-7}	9×10^{-5}	2×10^{-8}
		I	4×10^{-7}	7×10^{-5}	1×10^{-8}
Phosphorus (15)	P 32	S	7×10^{-8}	2×10^{-5}	2×10^{-9}
		I	8×10^{-8}	2×10^{-5}	3×10^{-9}
Platinum (78)	Pt 191	S	8×10^{-7}	1×10^{-4}	3×10^{-8}
		I	6×10^{-7}	1×10^{-4}	2×10^{-8}
	Pt 193m	S	7×10^{-6}	1×10^{-3}	2×10^{-7}
		I	5×10^{-6}	1×10^{-3}	2×10^{-7}
	Pt 193	S	1×10^{-6}	9×10^{-4}	4×10^{-8}
		I	3×10^{-7}	2×10^{-3}	1×10^{-8}

Table 3—(contd.)

Element (Atomic number)	Isotope*		Column 1 Air (μc/ml)	Column 2 Water (μc/ml)	Column 3 Air (μc/ml)
	Pt 197m	S	6×10^{-6}	1×10^{-3}	2×10^{-7}
		I	5×10^{-6}	9×10^{-4}	2×10^{-7}
	Pt 197	S	8×10^{-7}	1×10^{-4}	3×10^{-8}
		I	6×10^{-7}	1×10^{-4}	2×10^{-8}
Plutonium (94)	Pu 238	S	2×10^{-12}	5×10^{-6}	7×10^{-14}
		I	3×10^{-11}	3×10^{-5}	1×10^{-12}
	Pu 239	S	2×10^{-12}	5×10^{-6}	6×10^{-14}
		I	4×10^{-11}	3×10^{-5}	1×10^{-12}
	Pu 240	S	2×10^{-12}	5×10^{-6}	6×10^{-14}
		I	4×10^{-11}	3×10^{-5}	1×10^{-12}
	Pu 241	S	9×10^{-11}	2×10^{-4}	3×10^{-12}
		I	4×10^{-8}	1×10^{-3}	1×10^{-9}
	Pu 242	S	2×10^{-12}	5×10^{-6}	6×10^{-14}
		I	4×10^{-11}	3×10^{-5}	1×10^{-12}
Polonium (84)	Po 210	S	5×10^{-10}	7×10^{-7}	2×10^{-11}
		I	2×10^{-10}	3×10^{-5}	7×10^{-12}
Potassium (19)	K 42	S	2×10^{-6}	3×10^{-4}	7×10^{-8}
		I	1×10^{-7}	2×10^{-5}	4×10^{-9}
Praseodymium (59)	Pr 142	S	2×10^{-7}	3×10^{-5}	7×10^{-9}
		I	2×10^{-7}	3×10^{-5}	5×10^{-9}
	Pr 143	S	3×10^{-7}	5×10^{-5}	1×10^{-8}
		I	2×10^{-7}	5×10^{-5}	6×10^{-9}
Promethium (61)	Pm 147	S	6×10^{-8}	2×10^{-4}	2×10^{-9}
		I	1×10^{-7}	2×10^{-4}	3×10^{-9}
	Pm 149	S	3×10^{-7}	4×10^{-5}	1×10^{-8}
		I	2×10^{-7}	4×10^{-5}	8×10^{-9}
Protoactinium (91)	Pa 230	S	2×10^{-9}	2×10^{-4}	6×10^{-11}
		I	8×10^{-10}	3×10^{-4}	3×10^{-11}
	Pa 231	S	1×10^{-12}	9×10^{-7}	4×10^{-14}
		I	1×10^{-10}	2×10^{-5}	4×10^{-12}
	Pa 233	S	6×10^{-7}	1×10^{-4}	2×10^{-8}
		I	2×10^{-7}	1×10^{-4}	6×10^{-9}
Radium (88)	Ra 223	S	2×10^{-9}	7×10^{-7}	6×10^{-11}
		I	2×10^{-10}	4×10^{-6}	8×10^{-12}
	Ra 224	S	5×10^{-9}	2×10^{-6}	2×10^{-10}
		I	7×10^{-10}	5×10^{-6}	2×10^{-11}
	Ra 226	S	3×10^{-11}	1×10^{-8}	1×10^{-12}
		I	2×10^{-7}	3×10^{-5}	6×10^{-9}
	Ra 228	S	7×10^{-11}	3×10^{-8}	2×10^{-12}
		I	4×10^{-11}	3×10^{-5}	1×10^{-12}
Radon (86)	Rn 220	S	3×10^{-7}	—	1×10^{-8}
		I	—	—	—
	Rn 222	S	3×10^{-8}	—	1×10^{-9}
Rhenium (75)	Re 183	S	3×10^{-6}	6×10^{-4}	9×10^{-8}
		I	2×10^{-7}	3×10^{-4}	5×10^{-9}
	Re 186	S	6×10^{-7}	9×10^{-5}	2×10^{-8}
		I	2×10^{-7}	5×10^{-5}	8×10^{-9}
	Re 187	S	9×10^{-6}	3×10^{-3}	3×10^{-7}
		I	5×10^{-7}	2×10^{-3}	2×10^{-8}

Table 3—(*contd.*)

Element (Atomic number)	Isotope*		Column 1 Air (μc/ml)	Column 2 Water (μc/ml)	Column 3 Air (μc/ml)
	Re 188	S	4×10^{-7}	6×10^{-5}	1×10^{-8}
		I	2×10^{-7}	3×10^{-5}	6×10^{-9}
Rhodium (45)	Rh 103m	S	8×10^{-5}	1×10^{-2}	3×10^{-6}
		I	6×10^{-5}	1×10^{-2}	2×10^{-6}
	Rh 105	S	8×10^{-7}	1×10^{-4}	3×10^{-8}
		I	5×10^{-7}	1×10^{-4}	2×10^{-8}
Rubidium (37)	Rb 86	S	3×10^{-7}	7×10^{-5}	1×10^{-8}
		I	7×10^{-8}	2×10^{-5}	2×10^{-9}
	Rb 87	S	5×10^{-7}	1×10^{-4}	2×10^{-8}
		I	7×10^{-8}	2×10^{-4}	2×10^{-9}
Ruthenium (44)	Ru 97	S	2×10^{-6}	4×10^{-4}	8×10^{-8}
		I	2×10^{-6}	3×10^{-4}	6×10^{-8}
	Ru 103	S	5×10^{-7}	8×10^{-5}	2×10^{-8}
		I	8×10^{-8}	8×10^{-5}	3×10^{-9}
	Ru 105	S	7×10^{-7}	1×10^{-4}	2×10^{-8}
		I	5×10^{-7}	1×10^{-4}	2×10^{-8}
	Ru 106	S	8×10^{-8}	1×10^{-5}	3×10^{-9}
		I	6×10^{-9}	1×10^{-5}	2×10^{-10}
Samarium (62)	Sm 147	S	7×10^{-11}	6×10^{-5}	2×10^{-12}
		I	3×10^{-10}	7×10^{-5}	9×10^{-12}
	Sm 151	S	6×10^{-8}	4×10^{-4}	2×10^{-9}
		I	1×10^{-7}	4×10^{-4}	5×10^{-9}
	Sm 153	S	5×10^{-7}	8×10^{-5}	2×10^{-8}
		I	4×10^{-7}	8×10^{-5}	1×10^{-8}
Scandium (21)	Sc 46	S	2×10^{-7}	4×10^{-5}	8×10^{-9}
		I	2×10^{-8}	4×10^{-5}	8×10^{-10}
	Sc 47	S	6×10^{-7}	9×10^{-5}	2×10^{-8}
		I	5×10^{-7}	9×10^{-5}	2×10^{-8}
	Sc 48	S	2×10^{-7}	3×10^{-5}	6×10^{-9}
		I	1×10^{-7}	3×10^{-5}	5×10^{-9}
Selenium (34)	Se 75	S	1×10^{-6}	3×10^{-14}	4×10^{-8}
		I	1×10^{-7}	3×10^{-4}	4×10^{-9}
Silicon (14)	Si 31	S	6×10^{-6}	9×10^{-4}	2×10^{-7}
		I	1×10^{-6}	2×10^{-14}	3×10^{-8}
Silver (47)	Ag 105	S	6×10^{-7}	1×10^{-4}	2×10^{-8}
		I	8×10^{-8}	1×10^{-4}	3×10^{-9}
	Ag 110m	S	2×10^{-7}	3×10^{-5}	7×10^{-9}
		I	1×10^{-8}	3×10^{-5}	3×10^{-10}
	Ag 111	S	3×10^{-7}	4×10^{-5}	1×10^{-8}
		I	2×10^{-7}	4×10^{-5}	8×10^{-9}
Sodium (11)	Na 22	S	2×10^{-7}	4×10^{-5}	6×10^{-9}
		I	9×10^{-9}	3×10^{-5}	3×10^{-10}
	Na 24	S	1×10^{-6}	2×10^{-4}	4×10^{-8}
		I	1×10^{-7}	3×10^{-5}	5×10^{-9}
Strontium (38)	Sr 85m	S	4×10^{-5}	7×10^{-3}	1×10^{-6}
		I	3×10^{-5}	7×10^{-3}	1×10^{-6}
	Sr 85	S	2×10^{-7}	1×10^{-4}	8×10^{-9}
		I	1×10^{-7}	2×10^{-4}	4×10^{-9}

Table 3—(contd.)

Element (Atomic number)	Isotope*		Column 1 Air (μc/ml)	Column 2 Water (μc/ml)	Column 3 Air (μc/ml)
	Sr 89	S	3×10^{-8}	1×10^{-5}	1×10^{-9}
		I	4×10^{-8}	3×10^{-5}	1×10^{-9}
	Sr 90	S	3×10^{-10}	1×10^{-7}	1×10^{-11}
		I	5×10^{-9}	4×10^{-5}	2×10^{-10}
	Sr 91	S	4×10^{-7}	7×10^{-5}	2×10^{-8}
		I	3×10^{-7}	5×10^{-5}	9×10^{-9}
	Sr 92	S	4×10^{-7}	7×10^{-5}	2×10^{-8}
		I	3×10^{-7}	6×10^{-5}	1×10^{-8}
Sulfur (16)	S 35	S	3×10^{-7}	6×10^{-5}	9×10^{-9}
		I	3×10^{-7}	3×10^{-4}	9×10^{-9}
Tantalum (73)	Ta 182	S	4×10^{-8}	4×10^{-5}	1×10^{-9}
		I	2×10^{-8}	4×10^{-5}	7×10^{-10}
Technetium (43)	Tc 96m	S	8×10^{-5}	1×10^{-2}	3×10^{-6}
		I	3×10^{-5}	1×10^{-2}	1×10^{-6}
	Tc 96	S	6×10^{-7}	1×10^{-4}	2×10^{-8}
		I	2×10^{-7}	5×10^{-5}	8×10^{-9}
	Tc 97m	S	2×10^{-6}	4×10^{-4}	8×10^{-8}
		I	2×10^{-7}	2×10^{-4}	5×10^{-9}
	Tc 97	S	1×10^{-5}	2×10^{-3}	4×10^{-7}
		I	3×10^{-7}	8×10^{-4}	1×10^{-8}
	Tc 99m	S	4×10^{-5}	6×10^{-3}	1×10^{-6}
		I	1×10^{-5}	3×10^{-3}	5×10^{-7}
	Tc 99	S	2×10^{-6}	3×10^{-4}	7×10^{-8}
		I	6×10^{-8}	2×10^{-4}	2×10^{-9}
Tellurium (52)	Te 125m	S	4×10^{-7}	2×10^{-4}	1×10^{-8}
		I	1×10^{-7}	1×10^{-4}	4×10^{-9}
	Te 127m	S	1×10^{-7}	6×10^{-5}	5×10^{-9}
		I	4×10^{-8}	5×10^{-5}	1×10^{-9}
	Te 127	S	2×10^{-6}	3×10^{-4}	6×10^{-8}
		I	9×10^{-7}	2×10^{-4}	3×10^{-8}
	Te 129m	S	8×10^{-8}	3×10^{-5}	3×10^{-9}
		I	3×10^{-8}	2×10^{-5}	1×10^{-9}
	Te 129	S	5×10^{-6}	8×10^{-4}	2×10^{-7}
		I	4×10^{-6}	8×10^{-4}	1×10^{-7}
	Te 131m	S	4×10^{-7}	6×10^{-5}	1×10^{-8}
		I	2×10^{-7}	4×10^{-5}	6×10^{-9}
	Te 132	S	2×10^{-7}	3×10^{-5}	7×10^{-9}
		I	1×10^{-7}	2×10^{-5}	4×10^{-9}
Terbium (65)	Tb 160	S	1×10^{-7}	4×10^{-5}	3×10^{-9}
		I	3×10^{-8}	4×10^{-5}	1×10^{-9}
Thallium (81)	Tl 200	S	3×10^{-6}	4×10^{-4}	9×10^{-8}
		I	1×10^{-6}	2×10^{-4}	4×10^{-8}
	Tl 201	S	2×10^{-6}	3×10^{-4}	7×10^{-8}
		I	9×10^{-7}	2×10^{-4}	3×10^{-8}
	Tl 202	S	8×10^{-7}	1×10^{-4}	3×10^{-8}
		I	2×10^{-7}	7×10^{-5}	8×10^{-9}
	Tl 204	S	6×10^{-7}	1×10^{-4}	2×10^{-8}
		I	3×10^{-8}	6×10^{-5}	9×10^{-10}

Table 3—(contd.)

Element (Atomic number)	Isotope*		Column 1 Air (μc/ml)	Column 2 Water (μc/ml)	Column 3 Air (μc/ml)
Thorium (90)	Th 227	S	3×10^{-10}	2×10^{-5}	1×10^{-11}
		I	2×10^{-10}	2×10^{-5}	6×10^{-12}
	Th 228	S	9×10^{-12}	7×10^{-6}	3×10^{-13}
		I	6×10^{-12}	1×10^{-5}	2×10^{-13}
	Th 230	S	2×10^{-12}	2×10^{-6}	8×10^{-14}
		I	1×10^{-11}	3×10^{-5}	3×10^{-13}
	Th 231	S	1×10^{-6}	2×10^{-4}	5×10^{-8}
		I	1×10^{-6}	2×10^{-4}	4×10^{-8}
	Th 232	S	2×10^{-12}	2×10^{-6}	7×10^{-14}
		I	1×10^{-11}	4×10^{-5}	4×10^{-13}
	Th 234	S	6×10^{-8}	2×10^{-5}	2×10^{-9}
		I	3×10^{-8}	2×10^{-5}	1×10^{-9}
	Th natural	S	2×10^{-12}	1×10^{-6}	6×10^{-14}
		I	4×10^{-12}	1×10^{-5}	1×10^{-13}
Thulium (69)	Tm 170	S	4×10^{-8}	5×10^{-5}	1×10^{-9}
		I	3×10^{-8}	5×10^{-5}	1×10^{-9}
	Tm 171	S	1×10^{-7}	5×10^{-4}	4×10^{-9}
		I	2×10^{-7}	5×10^{-4}	8×10^{-9}
Tin (50)	Sn 113	S	4×10^{-7}	9×10^{-5}	1×10^{-8}
		I	5×10^{-8}	8×10^{-5}	2×10^{-9}
	Sn 125	S	1×10^{-7}	2×10^{-5}	4×10^{-9}
		I	8×10^{-8}	2×10^{-5}	3×10^{-9}
Tungsten (Wolfram) (74)	W 181	S	2×10^{-6}	4×10^{-4}	8×10^{-8}
		I	1×10^{-7}	3×10^{-4}	4×10^{-9}
	W 185	S	8×10^{-7}	1×10^{-4}	3×10^{-8}
		I	1×10^{-7}	1×10^{-4}	4×10^{-9}
	W 187	S	4×10^{-7}	7×10^{-5}	2×10^{-8}
		I	3×10^{-7}	6×10^{-5}	1×10^{-8}
Uranium (92)	U 230	S	3×10^{-10}	5×10^{-6}	1×10^{-11}
		I	1×10^{-10}	5×10^{-6}	4×10^{-12}
	U 232	S	1×10^{-10}	3×10^{-5}	3×10^{-12}
		I	3×10^{-11}	3×10^{-5}	9×10^{-13}
	U 233	S	5×10^{-10}	3×10^{-5}	2×10^{-11}
		I	1×10^{-10}	3×10^{-5}	4×10^{-12}
	U 234	S	6×10^{-10}	3×10^{-5}	2×10^{-11}
		I	1×10^{-10}	3×10^{-5}	4×10^{-12}
	U 235	S	5×10^{-10}	3×10^{-5}	2×10^{-11}
		I	1×10^{-10}	3×10^{-5}	4×10^{-12}
	U 236	S	6×10^{-10}	3×10^{-5}	2×10^{-11}
		I	1×10^{-10}	3×10^{-5}	4×10^{-12}
	U 238	S	7×10^{-11}	4×10^{-5}	3×10^{-12}
		I	1×10^{-10}	4×10^{-5}	5×10^{-12}
	U natural	S	7×10^{-11}	2×10^{-5}	3×10^{-12}
		I	6×10^{-11}	2×10^{-5}	2×10^{-12}
Vanadium (23)	V 48	S	2×10^{-7}	3×10^{-5}	6×10^{-9}
		I	6×10^{-8}	3×10^{-5}	2×10^{-9}
Xenon (54)	Xe 131m	Sub	2×10^{-5}	—	4×10^{-7}
	Xe 133	Sub	1×10^{-5}	—	3×10^{-7}
	Xe 135	Sub	4×10^{-6}	—	1×10^{-7}

Table 3—(*contd.*)

Element (Atomic number)	Isotope*		Column 1 Air (μc/ml)	Column 2 Water (μc/ml)	Column 3 Air (μc/ml)
Ytterbium	Yb 175	S	7×10^{-7}	1×10^{-4}	2×10^{-8}
(70)		I	6×10^{-7}	1×10^{-4}	2×10^{-8}
Yttrium	Y 90	S	1×10^{-7}	2×10^{-5}	4×10^{-9}
(39)		I	1×10^{-7}	2×10^{-5}	3×10^{-9}
	Y 91m	S	2×10^{-5}	3×10^{-3}	8×10^{-7}
		I	2×10^{-5}	3×10^{-3}	6×10^{-7}
	Y 91	S	4×10^{-8}	3×10^{-5}	1×10^{-9}
		I	3×10^{-8}	3×10^{-5}	1×10^{-9}
	Y 92	S	4×10^{-7}	6×10^{-5}	1×10^{-8}
		I	3×10^{-7}	6×10^{-5}	1×10^{-8}
	Y 93	S	2×10^{-7}	3×10^{-5}	6×10^{-9}
		I	1×10^{-7}	3×10^{-5}	5×10^{-9}
Zinc	Zn 65	S	1×10^{-7}	1×10^{-4}	4×10^{-9}
(30)		I	6×10^{-8}	2×10^{-4}	2×10^{-9}
	Zn 69m	S	4×10^{-7}	7×10^{-5}	1×10^{-8}
		I	3×10^{-7}	6×10^{-5}	1×10^{-8}
	Zn 69	S	7×10^{-6}	2×10^{-3}	2×10^{-7}
		I	9×10^{-6}	2×10^{-3}	3×10^{-7}
Zirconium	Zr 93	S	1×10^{-7}	8×10^{-4}	4×10^{-9}
(40)		I	3×10^{-7}	8×10^{-4}	1×10^{-8}
	Zr 95	S	1×10^{-7}	6×10^{-5}	4×10^{-9}
		I	3×10^{-8}	6×10^{-5}	1×10^{-9}
	Zr 97	S	1×10^{-7}	2×10^{-5}	4×10^{-9}
		I	9×10^{-8}	2×10^{-5}	3×10^{-9}

Health Physics Pergamon Press 1961. Vol. 5, pp. 20–26. Printed in Northern Ireland

A GEIGER–MÜELLER γ-RAY DOSIMETER WITH LOW NEUTRON SENSITIVITY

E. B. WAGNER and G. S. HURST
Health Physics Division, Oak Ridge National Laboratory*
Oak Ridge, Tennessee

(*Received* 25 *March* 1960)

Abstract—It has been shown that a commercially available halogen type Geiger–Müeller counter when properly shielded with Sn and Pb provides a very practical and satisfactory device for measuring the dose due to γ-radiation in the presence of neutrons. The device measures the dose in roentgens with nearly uniform response for effective X-ray energies above about 200 keV and up to at least 1.25 MeV γ-energies. Calculations show that the fast neutron response is less than 0.15 per cent, and experiments indicate that it is less than 0.5 per cent. Experiments show that about 5×10^9 thermal neutrons per cm^2 give a response equivalent to 1 r of γ-radiation. When necessary, the thermal neutron response can be decreased by a factor of 300 by using a Li shield described in the text.

I. INTRODUCTION

IN MANY problems in radiation protection, radiobiology, physics and radiation shielding, it is desirable to measure the doses from coexistent neutron and γ-radiation separately. Proportional counters can be used to measure the neutron dose in mixed radiation fields.[1,2] When ionization instruments such as the C–CO_2 chamber are used to measure the γ-component of a mixed radiation field, the sensitivity of these devices to neutrons can lead to considerable error when the neutron to γ ratio is greater than 1. For instance, when a C–CO_2 chamber is used in a radiation field composed of fast neutrons and γ-rays of equal dose rates (measured in tissue rad hr^{-1}), the fast neutrons will contribute approximately 10 per cent of the indicated dose. The neutron response in general varies with the energy of the neutrons and the characteristics of the particular instrument. Recently a single ion detector with a low neutron response has been developed by AUXIER *et al.*[3] for measurements of γ-dose in the presence of high neutron fields. However, it and other counting methods[4,5] used for this purpose are more complex than the one described in this paper. In the present work we have shown that a small halogen type Geiger–Müeller counter can be arranged with suitable shields to provide an instrument that is (a) energy independent for X- or γ-radiation above about 200 keV, (b) insensitive to fast neutrons, and (c) insensitive to thermal neutrons.

2. γ-RAY RESPONSE OF THE COUNTER

The counter used is a Phillips no. 18509† micro G–M counter filled with neon, argon and a halogen quenching agent. The counter has a 0.48 cm inside diameter, and a 1.6 cm effective length. The cathode is made of stainless steel, and has a wall thickness of 90 mg cm^{-2}. As shown by Fig. 1, the unshielded counter has a high energy dependence for X-rays with an effective energy below 200 keV. The counter can be made to furnish readings of exposure dose in roentgens that are essentially independent of γ-ray energies down to 150 keV by shielding it with 0.053 in. of tin plus 0.010 in. of lead on the sides, and 0.022 in. of tin plus

* Operated by Union Carbide Corporation for the U.S. Atomic Energy Commission.

† Manufactured by N. V. Philips, Gloelampenfabrieken, Amsterdam, The Netherlands, and sold in the U.S.A. by Amperex Electronic Corporation, Hicksville, L.I., New York.

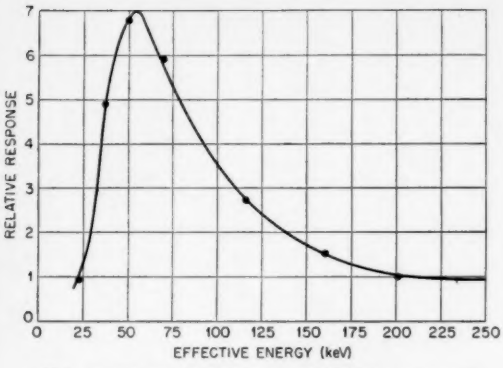

FIG. 1. Response of the unshielded counter as a function of γ-ray energy.

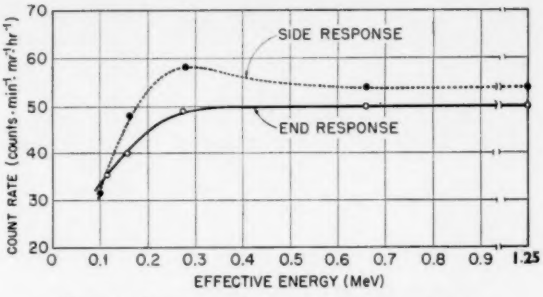

FIG. 2. Response of the shielded counter as a function of γ-ray energy. (Shield consists of 0.053 in. Sn and 0.010 in. Pb on sides and 0.022 in. Sn and 0.004 in. Pb on ends.)

0.004 in. of lead on the end (Fig. 2). The relative angular response of the counter to a Cs^{137} source is shown by Table 1. A drawing of the probe unit showing the arrangement discussed above together with a Li shield, which will be discussed later, is shown in Fig. 3.

The counter is capable of indicating γ-dose rates from 0.1 mr hr^{-1} to 300 r hr^{-1}. The

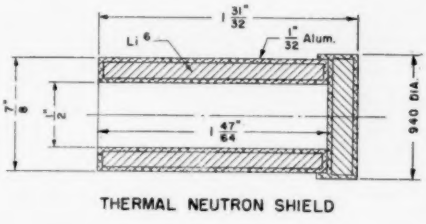

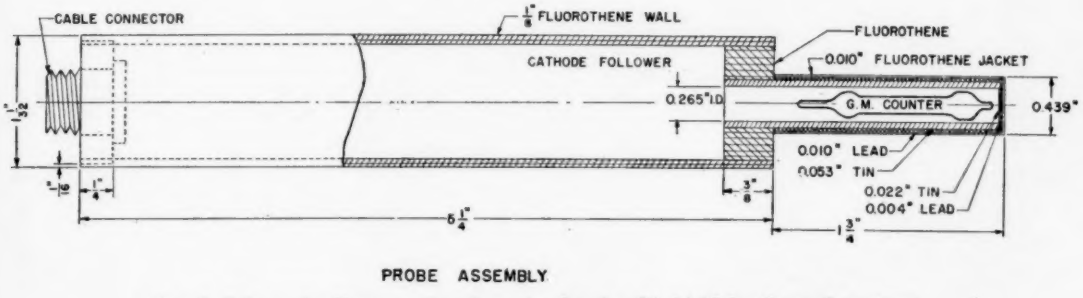

FIG. 3. Schematic diagram of probe unit, showing Li shield for thermal neutrons.

response as a pulse device is essentially linear from 0.1 mr hr^{-1} to 5 r hr^{-1} as shown by the curve in Fig. 4. As shown by Fig. 5 the response as a current device is approximately logarithmic from 2 r hr^{-1} to 100 r hr^{-1}; above 150 r hr^{-1} the curve begins to flatten.

3. FAST NEUTRON RESPONSE OF THE COUNTER

One expects that the response of the counter to fast neutrons would be less than the response of an ionization chamber having the same construction as the counter, for the same reasons as those given in the case of the single ionization detector.[3] That is, the counts produced per unit of energy absorbed by heavy recoils is much less than the counts produced per unit of energy absorbed from γ-radiation. Furthermore, it is well known that one tissue rad of neutrons will dissipate much less energy per gram in high atomic weight materials than will one tissue rad of γ-radiation. Therefore, it is expected that the

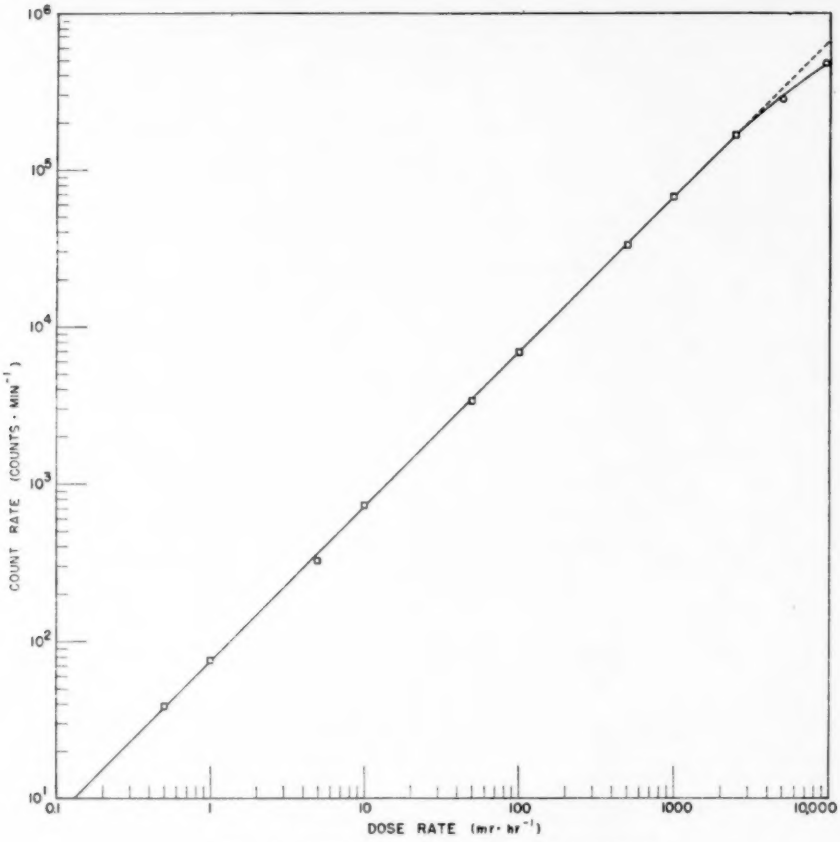

FIG. 4. Count rate as a function of γ-dose rate.

Table 1. *Relative angular response of G–M counter**

(Response determined with Cs^{137} source and with shielding around counter)

Angle (source in front of counter)	Counts min^{-1}/mr hr^{-1}	Relative response
0°	50.3	0.96
15°	47	0.90
30°	52.6	1.00
45°	55.2	1.05
60°	56.8	1.08
75°	54.4	1.03
90°	55.7	1.06

* Angle between the axis of the counter and the line drawn from source to center of counter.

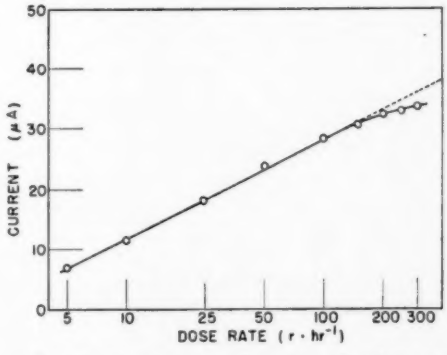

FIG. 5. Current as a function of γ-dose rate.

response of the counter for one rad of fast neutrons compared to its response to one rad of γ-radiation will be quite small. Nevertheless it is desirable to estimate the relative response of the counter to fast neutrons, particularly since inelastic scattering, in the high atomic weight materials making up the γ-energy correction shield, may contribute to the neutron response.

The relative neutron response, R_n, will be defined as the ratio,

$$\frac{\text{number of counts produced by one tissue rad of fast neutrons}}{\text{number of counts produced by one tissue rad of } \gamma\text{-radiation}}$$

For convenience of calculation, R_n for a specified neutron energy can be expressed as

$$R_n = \frac{N_n E_n C_n}{N_\gamma E_\gamma C_\gamma} + \frac{f N_n E_\gamma' C_\gamma'}{N_\gamma E_\gamma C_\gamma} \qquad (1)$$

where

N_n = number of neutrons cm^{-2} equivalent to one tissue rad

N_γ = number of photons cm^{-2} equivalent to one tissue rad

E_n = the amount of energy absorbed per g of the gas filling for 1 neutron cm^{-2}

E_γ = the amount of energy absorbed per g of the gas filling for 1 photon cm^{-2}

C_n = number of counts produced per rad of neutron absorption in the counter

C_γ = number of counts produced per rad of γ-absorption in the counter

fN_n = γ-ray flux due to inelastic collisions of neutrons. In this expression the prime denotes quantities which arise from inelastic collisions

In order to estimate E_γ, C_γ, E_γ', C_γ' and f appearing in equation (1), it is assumed that the counter is a spherical cavity whose diameter is 1 cm and that the gas inside the cavity is neon at a pressure of 15 cm Hg. The counter shell is assumed to be a mixture of 900 mg cm^{-2} tin and 280 mg cm^{-2} lead. This ignores the walls of the counter itself since the mass of the energy correction shield is much more than the mass of the counter wall. For estimating the quantities E_n and C_n, it is assumed that the shell, like the cavity, is composed of neon. This procedure should lead to an overestimate of the neutron response since the energy transferred to neon is greater than the energy transferred to the shell materials.

Neglecting pair production, the quantity E_γ may be evaluated from

$$E_\gamma(\text{MeV g}^{-1}) = \left(\sum_i \sigma_i N_i f_c + \sum_i \tau_i N_i f_{pe}\right) \times \frac{(dE/dx)_{\text{gas}}}{(dE/dx)_{\text{shell}}} \qquad (2)$$

where

N_i = number of atoms of type i in 1 g of the wall

σ_i = Compton scattering cross-section per atom

τ_i = photoelectric cross-section per atom

f_c = average energy transferred to an electron undergoing Compton scattering

f_{pe} = average energy transferred to an electron formed by the photo-electric process

dE/dx = stopping power for electrons in the specified medium

Following the procedure of HURST *et al.*[6] and using the cross-sections in DAVISSON and EVANS[7] and dE/dx values from Ref. 8 it is found that $E_\gamma = 0.042$ MeV g^{-1} for a photon energy of 1.0 MeV.

The quantity E_n for neon is evaluated at 5 MeV* from the following:

$$E_n(\text{MeV g}^{-1}) = 5 N_{ne} \sigma_s \frac{2Mm}{(M+m)^2} \qquad (3)$$

where N_{ne} is the number of neon atoms per g, σ_s is the neutron scattering cross-section for neon, $M = 20$ for neon, and $m = 1$. Thus, $E_n = 0.040$ MeV g^{-1}, taking $\sigma_s = 3 \times 10^{-24}$ cm^2.

The quantities C_n and C_γ are approximately equal to the reciprocal of the energy expended per traversal of recoil neon atoms and electrons, respectively; thus, $C_n = 2$ MeV^{-1} and $C_\gamma = 3000$ MeV^{-1}.

* The choice of this energy will be justified later.

For a thin spherical shell the additional γ-flux averaged over the volume inside the shell is just $3/2\, fN_n$ where f may now be interpreted as the fraction of neutrons producing γ-radiation by inelastic collisions. To obtain an upper limit for f we use the total non-elastic cross-section for lead and tin[9] to calculate the number of γ-rays. Thus,

$$f = \sum_i \sigma_i^{ne}\, n_i \qquad (4)$$

where σ_i^{ne} is the total non-elastic cross-section for atoms of type i, and n_i is the number of atoms of type i per cm^2. Using $\sigma^{ne} = 2$ barns for tin and $\sigma^{ne} = 3$ barns for lead, $f = 10^{-2}$.

We will further assume that all the inelastically produced γ-rays are 1.0 MeV;* then $E_\gamma' = E_\gamma$, and $C_\gamma' = C_\gamma$. Thus, equation (1) reduces to

$$R_n = \frac{N_n E_n C_n}{N_\gamma E_\gamma C_\gamma} + \frac{3fN_n}{2N_\gamma} \qquad (5)$$

The ratio N_n/N_γ is readily obtained from HURST *et al.*[6] using the tissue dose vs. energy curves for photons at 1.0 MeV and neutrons at 5.0 MeV. Thus, $N_n/N_\gamma = 0.03/0.28 = 0.11$.

The numerical values for the two terms in equation (5) are 0.07×10^{-3} and 1.5×10^{-3}, respectively. The recoil term is small compared to the inelastic term, and an upper limit to the neutron response at 5 MeV is 1.5×10^{-3}. By evaluating the second term in equation (5), it is seen that the contribution to the neutron response due to inelastic collisions in the γ-energy correction shield is a maximum at about 5.0 MeV neutron energy.

The assignment of a reasonably valid neutron response of the G–M counter by experimental methods is not possible at the present time due to the unavailability of a facility giving a radiation field with a sufficiently large neutron to γ ratio. However, by an intercomparison of the G–M counter with both the single ion detector and silver metaphosphate glass dosimeters, using Godiva II neutrons, it is possible to set an upper limit. The neutron response of the G–M counter is not believed to be greater than the glass dosimeter which was found to have less than 1 per cent neutron response using monoenergetic neutrons (0.6 to 1.5 MeV) from the ORNL Van de Graaff generator.[11] Recent studies in which the G–M counter was irradiated with monoenergetic neutrons in the energy range from 0.68 MeV to 4.2 MeV indicate that the response in this energy range is less than 0.5 per cent.

* This approximation is rather good for 3 MeV neutrons, where experimental data on inelastic γ-ray production in Sn is available.[10]

4. RESPONSE TO THERMAL NEUTRONS

The response of the counter to thermal neutrons was determined experimentally, making use of the water thermal column at the ORNL Graphite Reactor. This was accomplished by means of four separate exposures: (1) exposure of the bare probe unit (Fig. 3) during which the equivalent γ-reading due to reactor produced γ-radiation and the response of the counter to thermal neutrons were recorded; (2) exposure of the probe unit partially covered with the foils to determine the incident thermal flux; (3) exposure of the probe unit surrounded by a Li shield (see Fig. 3) during which the reactor γ-radiation was measured with a reduced incident thermal neutron flux; and (4) exposure of the probe unit with the Li shield but with Au foils inside the shield to measure the thermal neutron flux penetrating the shield.

From these exposures one may evaluate: (a) the effectiveness of the Li shield; (b) the neutron response of the counter; and (c) the reactor produced γ-dose rate d_γ (in r hr^{-1}) as follows:

$$\begin{aligned} D_1 &= d_\gamma + BN_1 \\ D_2 &= fd_\gamma + BN_2 \end{aligned} \qquad (6)$$

where D_1 and D_2 are the readings in r hr^{-1} obtained in exposures (1) and (3), respectively; B is the equivalent roentgen response per unit flux (n cm^{-2}); N_1 and N_2 are the neutron fluxes integrated for 1 hr (n cm^{-2} hr^{-1}) measured in exposures (2) and (4), respectively, and f is the transmission factor for γ-radiation through the Li shield. By exposure to Cs^{137} γ-radiation it was found that $f = 0.987$. The experimental values for D_1 and D_2 were 10.2 r hr^{-1} and 7.0 r hr^{-1}, respectively, when values of N_1 and N_2 were 1.5×10^{10} n cm^{-2} and

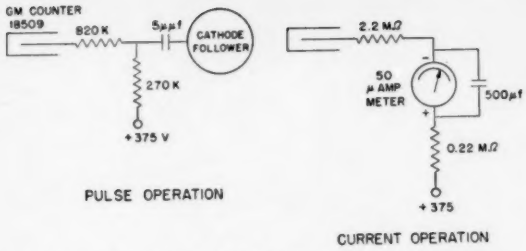

FIG. 6. Input circuits used for pulse and current modes of operation.

4.9×10^7 n cm^{-2}, respectively. Using these with the values of f quoted above, it was found that $B = 2.14 \times 10^{-10}$ r/n cm^{-2}, and $d_\gamma = 7.1$ r hr^{-1}. This value for the γ-dose agreed well with the value obtained with a C–CO_2 ionization chamber.[12] Thus it may be concluded that the thermal neutron response of the probe unit is quite low, requiring about 5×10^9 n cm^{-2} to produce the same response as 1 r of γ-radiation. Further, the thermal neutron response may be reduced by using the Li shield. With the Li shield, about 1.5×10^{12} n cm^{-2} would be required to produce the same response as 1 r of γ-radiation since N_1/N_2 is about 300.

5. CHARACTERISTICS OF THE COUNTERS AND ELECTRONICS CONSIDERATIONS

The selection of circuit parameters to use with the counter was based in part on data given by VAN DUUREN *et al.*[13], and by determining experimentally the optimum values for good balance between such factors as dead time, plateau slope, adequate quenching, and a high voltage compatible for both pulse and current operation of the counter. Fig. 6 shows the input circuitry that was used to obtain the pulse data. With this circuit the dead time of the counter is approximately 18 μsec, and the pulse amplitude is 25 V at the grid of the input cathode follower. Fig. 7 shows a typical curve of count rate as a function of high voltage (using a fixed γ-source) for the circuit as shown in Fig. 6. Although the counts vs. high voltage curve as shown in Fig. 7 is not ideal, with a regulated high voltage supply it is adequate since a 1 per cent change in high voltage results in less than a 1 per cent change in response. Fig. 6 shows the input circuitry that was used to obtain the current as

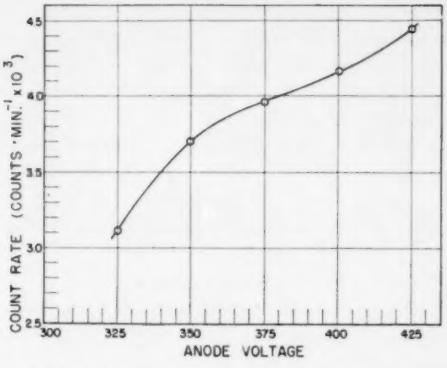

FIG. 7. Count rate as a function of counter voltage for fixed dose rate.

a function of dose rate (the data shown in Fig. 5). The high voltage required for both modes of operation is only 375 V.

Nine 18509 tubes were checked for variance of counting rate as a function of high voltage to ascertain their interchangeability in a particular circuit. The curves were very similar in shape, and, as can be seen in Table 2, six of the counters had a spread of only 5 per cent. This variation should present no problems as the readout circuitry could be designed with an adjustable sensitivity control allowing correct calibration for any particular counter. Although a limited number of counters have been used for only a few months' service, they have been very stable and dependable.

Table 2. Relative sensitivity of G–M counters
(All counters received the same γ intensity of ~15 mr/hr)

Counter no.	Counts min^{-1}/mr hr^{-1} with +375 V on anode	Relative response
1	273	1.01
2	253	0.94
3	265	0.98
4	272	1.01
5	286	1.06
6	270	1.00
7	287	1.06
8	269	1.00
9	262	0.97

The probe unit (7 in. long by 1 in. diameter) contains the G–M tube with its shielding and a cathode follower as shown by Fig. 3. Where the range covered by the pulse mode of operation is sufficient, the probe unit may be fed into a scalar by means of a cable of any desired length up to about 100 ft. A simple a.c. operated readout unit has been designed which allows either pulse or current mode of operation and has provisions for giving a direct readout of either dose rate or integrated dose for the pulse mode ranges. Further details of the complete electronic instrument will be reported separately at a later date.

Acknowledgments—The writers are grateful to J. A. HARTER, H. H. HUBBELL, JR., R. H. RITCHIE, J. A. AUXIER, R. E. ZEDLER, ADA CARTER, R. M. SIMMONS and P. W. REINHARDT, all of the Oak Ridge National Laboratory, for helpful suggestions and assistance.

REFERENCES

1. G. S. HURST, *Brit. J. Radiol.* **27,** 353 (1954).
2. E. B. WAGNER and G. S. HURST, *Rev. Sci. Instrum.* **29,** 153 (1958).
3. J. A. AUXIER, G. S. HURST and R. E. ZEDLER, *Health Phys.* **1,** 21 (1958).
4. R. S. CASWELL, *Radiology* **68,** 101 (1957).
5. M. SLATER, G. B. BUNYARD and M. L. RANDOLPH, *Rev. Sci. Instrum.* **29,** 601 (1958).
6. G. S. HURST, W. A. MILLS, F. P. CONTE and A. C. UPTON, *Rad. Res.* **4,** 49 (1956).
7. C. M. DAVISSON and R. D. EVANS, *Rev. Mod. Phys.* **24,** 79 (1952).
8. National Bureau of Standards Circular 577 (1956)
9. D. J. HUGHES and R. B. SCHWARTZ, *Neutron Cross Sections* (2nd Ed.). Brookhaven National Laboratory Report BNL-325 (1958).
10. V. E. SCHERRER, B. A. ALLISON and W. R. FAUST, *Phys. Rev.* **96,** 386 (1954).
11. Health Physics Annual Progress Report, ORNL-2806, p. 123 (1959).
12. T. V. BLOSSER. Private communication.
13. K. VAN DUUREN, A. J. M. JASPERS and J. HERMSEN, *Nucleonics* **17,** No. 6, 86 (1959).

Health Physics Pergamon Press 1961. Vol. 5, pp. 27–36. Printed in Northern Ireland

LARGE PLASTIC SCINTILLATORS FOR RADIOACTIVITY MEASUREMENT*

G. L. BROWNELL†‡, W. H. ELLETT†, R. A. RYDIN‡ and G. J. HINE§

(*Received* 28 *March* 1960; in revised form 28 June 1960)

Abstract—This study of counting systems utilizing large plastic scintillators includes an investigation of the component parts, the γ-ray spectra obtained from large scintillators, and the application of large scintillators to total-body and low-level sample counting. Properties of the component parts investigated were: (1) light production from plastic scintillators of different manufacture; (2) the influence of crystal size and shape on light collection efficiency; and (3) the photocathode response of 5-in. and 16-in. photomultiplier tubes. Experimental spectra taken with a 16-in. diameter by 8-in. thick cylinder of plastic are shown and the results for 0.662 MeV γ-rays compared to a calculated (Monte Carlo) pulse-height distribution. The application of large plastic scintillators to total-body counting is evaluated by comparing the response of an array of 16-in. by 8-in. plastic scintillators to a single 8-in. by 4-in. NaI detector. Spectra taken with an 18-in. by 18-in. plastic well counter are presented, and data is presented on the performance of this device as a low-level sample counter.

I. INTRODUCTION

LARGE plastic scintillators are useful for measuring low-level concentrations of radioactivity, i.e. micromicrocuries per gram. Such levels of radioactivity are encountered by health physicists in the monitoring of individuals exposed to small amounts of radioisotopes. These radioisotopes may result from uranium fission as in the case of Cs^{137} or from operation of high-energy machines as with Zn^{65}. The measurement of normally occurring levels of K^{40} is also of interest in certain medical and health physics problems. Furthermore, many medical and industrial radioisotope techniques can be carried out using micromicrocurie per gram levels of radioactivity if suitable instrumentation is available.

The ability to measure low levels of radioactivity depends on the absolute sensitivity of the detector, the background level, and the maximum sample size which can be used. The usual detecting systems are large NaI (Tl) crystals,[1] large-volume liquid or plastic scintillators,[2] and in some cases large, high pressure ionization chambers.[3]¶ Of these the NaI detectors have received the greatest use. Plastic scintillators offer both advantages and disadvantages for such measurements. Their primary advantage is availability in large dimensions. This permits large samples to be measured as well as providing high absolute sensitivity. The possibility of molding or machining plastic into complex shapes allows flexibility in the design of counters for specialized applications. The ease of handling plastic blocks, their chemical stability, and the lack of fire hazard gives them certain advantages with respect to large liquid scintillation counters. The disadvantage in the use of plastic scintillators arises primarily from the low atomic number of the plastic material. Almost no photoelectric interactions are recorded and the observed spectrum is due primarily to Compton interactions. However, the Compton distribution itself is often adequate for the identification of certain γ-ray lines even though the resolution is considerably inferior to that of sodium iodide.[5]

* This investigation was supported in part by a research grant C-2187 from the U.S. Public Health Service and by the June Rockwell Levy Foundation.

† Physics Research Laboratory, Massachusetts General Hospital, Boston, Massachusetts.

‡ Department of Nuclear Engineering, Massachusetts Institute of Technology, Cambridge, Massachusetts.

§ Radioisotopes Unit, Boston VA Hospital, Boston, Massachusetts.

¶ An excellent review of the three methods is given in the "Measurements of Body Radioactivity"[4].

In this paper, problems related to the use of large plastic scintillators for radioactivity measurement are discussed. Light output and collection are observed for a number of plastic materials, and the factors involved in light collection discussed. Calculations leading to theoretical spectra from plastic blocks are reported and resultant spectra compared to experiment. Finally, the possible application of large plastic scintillators to body counters and sample counters is discussed.

II. LIGHT PRODUCTION AND COLLECTION FROM PLASTIC SCINTILLATORS

Plastic scintillators consist of a polymer (usually polyvinyltoluene) containing a primary scintillator such as PPO* and a secondary wavelength shifter such as POPOP†. The density of these plastic blocks ranges from 1.02 to 1.04 gm/cm^3 and their refractive index from 1.5 to 1.6. Light production in four commercially prepared plastic scintillators‡ was compared by measuring the conversion electron spectrum from Ba^{137} ($E_\beta = 624$ keV). The scintillators in each case consisted of a 1-in. diameter cylinder 1 in. high. The scintillators were placed on a Dumont 6292 photomultiplier tube without any reflector and the resultant spectra analyzed with a 256-channel pulse-height analyzer. The relative pulse heights were obtained by comparing the resultant spectra, Table 1. The slight variation among scintillators may result in differences in the wavelength match between scintillator and photomultiplier tube. Two of the scintillators were retested with Teflon tape covering all surfaces except that exposed to the photocathode. The addition of this light-reflecting material increased the light output by amounts ranging from 25 to 50 per cent. This increase may be somewhat dependent upon surface finish of the scintillators since light collected by total internal reflection is unchanged. A 1 in. × 1 in. NaI (Tl) detector with an aluminum oxide reflector is included in Table 1. It is seen that its output is approximately four times that of the two plastic detectors with Teflon light reflectors. It is concluded that small samples of the plastic scintillators listed in Table 1 are quite similar in their light production.

Table 1. Relative response of 1 in. × 1 in. plastic scintillators to Ba^{137} conversion electrons

Scintillator*	Relative response
A (no reflector)	49
B (no reflector)	52
C (no reflector)	66
D (no reflector)	60
C (plus Teflon)	84
D (plus Teflon)	100
NaI (Tl)	400

* Sample designation is not correlated with the list of manufacturers in the text.

Light collection from plastic scintillators depends on the crystal size and geometry as well as the reflectivity of the walls. To measure the effect of scintillator size, various thicknesses of 1-in. diameter plastic samples were exposed to Ba^{137} conversion electrons. The pulse height and the resolution of the Ba^{137} electron line decreased with increasing height of the cylinder (Table 2). The maximum range of the 624-keV electrons in plastic is about 2.3 mm or somewhat more than $\frac{1}{16}$ in. Therefore all the light is produced in the top layer of the cylinders and the light has to pass through variable lengths of plastic to reach the photomultiplier. The drastic loss of pulse height and resolution, going from a $\frac{1}{16}$-in. to a 1-in. height cylinder cannot be explained by absorption of the fluorescent light in 1 in. of plastic material.§ It has to be assumed that a considerable fraction of the fluorescent light is permanently trapped within the plastic by internal reflection.

The effect of scintillator shape was investigated with $1\frac{3}{4}$-in. diameter × 2-in. samples of plastic scintillator material. By using a conical instead of a cylindrical shape the pulse height for the Ba^{137} electron line could be increased by more than 60 per cent with a corresponding

* 2:5-Diphenyloxazole.

† *p*-bis-12-(5-Phenyloxazolyl)1-benzene.

‡ Pilot B (Pilot Chemical Co., Waltham, Mass.).
NE-102 (Nuclear Enterprises Ltd., Winnipeg, Canada).
NATON-11 (Nash and Thompson Ltd., Surrey, England).
PVP-500 (Crystals, Inc., Westwood, N.J.).

§ The manufacturer reports a mean free path of over 18 in. for 1-in. diameter cylinders.

Table 2. Variation of pulse height and resolution of Ba^{137} *electron line with height of plastic scintillator*

Height of 1-in. diameter plastic scintillator (in.)	Relative pulse height	Resolution of 624-keV line (%)
$\frac{1}{16}$	100	18
$\frac{1}{4}$	81	21
1	45	29

improvement in line resolution, as compared to a right cylinder. The sides of the scintillator were machined to a 7° angle from the normal and the cone trunk placed with the broad end on the photomultiplier tube. Since the light is produced in a layer about 2 in. from the photocathode in the cylinder as in the conical-shaped piece, the light transmission has not been altered. Therefore the effect of the tilted sides can only be to increase the fraction of light that is channeled towards the photomultiplier tube and decrease the fraction that is trapped by total internal reflection. By using plastic scintillators of various sizes it could be demonstrated that a 5° angle seems to be about optimum (maximum pulse height) for both the Ba^{137} electron line and the Ba^{137} γ-rays. We have not investigated the effect of tapering on light collected from large cylinders.

III. PHOTOMULTIPLIER TUBES FOR LARGE PLASTIC SCINTILLATORS

If the scintillator were perfectly transparent to its own fluorescence and there were no light losses at the walls, it would be possible to obtain pulse-height information from a large scintillator with a single small photomultiplier tube. In actual practice, it is necessary to have the photocathode an appreciable fraction of the area of the scintillator.[6] The large photocathode area can be obtained either by using several small (3 in.–5 in.) photomultiplier tubes or by using a single large tube (12 in.–16 in.) having a diameter approximately equal to that of the scintillator. The single large tube provides a larger area, requires simpler electrical circuitry and is more economical. However, large tubes are not so highly developed for spectrometry as the smaller tubes and their performance limits the pulse-height resolution.

To investigate some of the factors which limit the resolution obtainable with large tubes the following series of tests were carried out. Photocathode response was measured by analyzing the pulse-height spectrum produced by a pulsed argon light which illuminated a small area on the photocathode.* Spectra were measured for fifty 0.5-in^2 areas on each of six 5-in. photomultiplier tubes (Dumont 6364) and for 170 areas on a single 16-in. photomultiplier tube (Dumont K 1328). Additional studies of pulse height and resolution as a function of area indicated that on a restricted area of the photocathode the pulse height was proportional to area over a range of from 0.005 to 0.5 in^2 and that the resolution was proportional to the inverse square root of the pulse height over the same range of areas. From the spectra obtained in these studies, equal pulse-height maps of the photocathode area were prepared. A typical response pattern for a 5-in. tube is shown in Fig. 1. The variation in response is nearly 5 to 1. The response patterns of all the 5-in. tubes tested were quite similar and all were related to the orientation of the dynode structure within the tube. The response pattern of the 16-in. tube is shown in Fig. 2. Here the variation in sensitivity is more irregular owing to variations in cathode thickness. However, superimposed on this pattern is a large gradient of sensitivity again related to the orientation of the first dynode. The dependence of the response pattern on first-

* The focusing and first dynode–cathode voltages were adjusted for optimum gain and resolution under the conditions of uniform photocathode illumination.

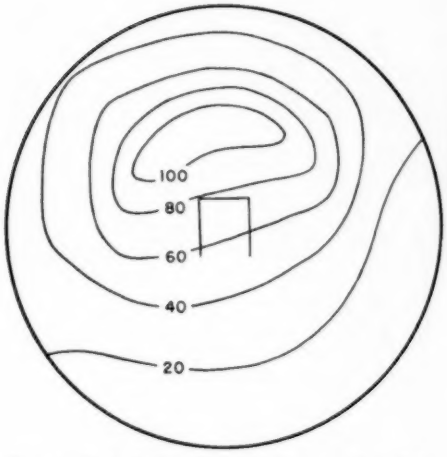

FIG. 1. Relative response pattern of a 5-in. photomultiplier tube. The contours delineate areas of equal sensitivity. The first dynode of the box-dynode structure is indicated.

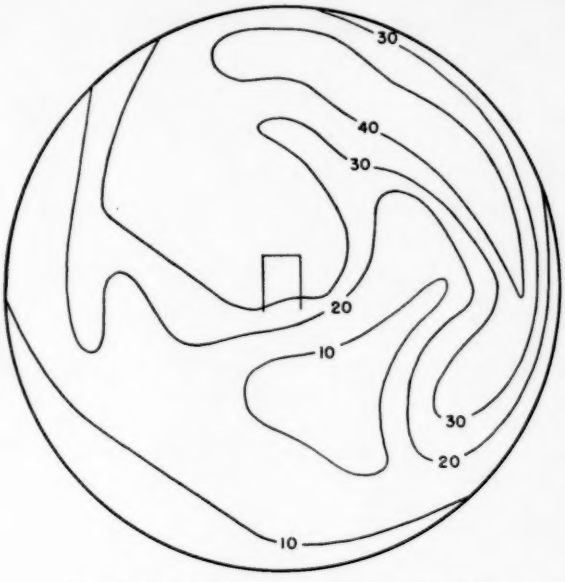

FIG. 2. Relative response pattern of a 16-in. photomultiplier tube.

dynode orientation indicates that some of the asymmetry shown in Figs. 1 and 2 is due to varying first-dynode multiplication and collection rather than photoelectron production.

An unexpected finding observed at certain points on the 16-in. photomultiplier tube face was the production of two distant Gaussian pulse distributions for constant intensity light pulses. Fig. 3 shows the spectra of pulses observed at a location 3 in. from the center of the tube face. At one position a clear double peak is observed indicating the existence of two quasistable electron trajectories between the photocathode and the first dynode. At a second position 2 in. away, these two peaks have merged to form a single broad peak. The existence of such unstable electron paths can have only a deleterious effect on the resolution of the system. It should be mentioned that the 16-in. photomultiplier tube was not designed for spectrometry. However, similar findings were observed to a lesser extent with the 5-in. photomultiplier tubes.

Nonuniform photocathode sensitivity and photoelectron collection reduces the resolution of photomultipliers by increasing the statistical uncertainty in the magnitude of the initial scintillation. Furthermore, if there exists a correlation between the position of the scintillation and photoelectron production in the photocathode material, the resolution will be decreased further by the nonuniformity, i.e. equal energy losses in the scintillator will produce different pulse, height distributions. HICKOK and DRAPER[7] have indicated that this effect is not important for large crystals. The large difference in index of refraction between NaI and glass results in a large number of internal light reflections within the NaI crystal.[8] The net result is fairly uniform light illumination. For plastic there is little change in refractive index and the light will have more of a tendency to be collected unevenly over the face of the photocathode.

IV. MONTE CARLO CALCULATIONS

The γ-ray spectra obtained from small blocks of plastic scintillator should be identical with the

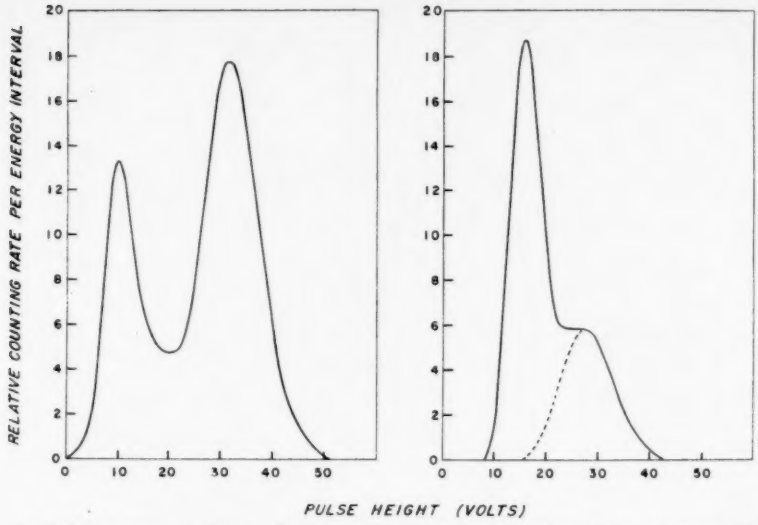

FIG. 3. Pulse spectra taken at two adjacent positions on the 16-in. photomultiplier tube of the photocathode. The presence of a double peak is clearly indicated at the first position. In each case photocathode illumination was confined to 0.5 in^2 area.

distribution of absorbed energy in a single Compton interaction. As the size of the plastic scintillator increases, the number of multiple Compton interactions will increase, producing a broadened distribution. Eventually the plastic scintillator will reach a size within which all the γ-ray energy will be absorbed. At this point a total absorption peak should be observed. However, decreased resolution with these larger blocks resulting from decreased light collection and increased light attenuation may prevent the total absorption peak from being observed. To investigate this problem and to determine the theoretical shape of spectra obtained with plastic blocks a study has been performed using Monte Carlo techniques to calculate energy absorption within plastic blocks of various sizes. The Monte Carlo program is similar to that developed by BERGER for sodium iodide crystals.[9,10] In this study 5000 histories of 0.662 MeV γ-rays incident on a 16-in. diameter $\times$ 8-in. thick plastic scintillator were traced with an IBM 704 computer. The results are approximate, as γ-rays of less than 50 keV energy were assumed to be totally absorbed. Actually, there will be some leakage of γ-rays of this energy near the surface of the scintillator.

The results of these calculations are shown in Fig. 4. The single interaction Compton distribution is shown in dashed lines for comparison. It is seen that the single interaction Compton distribution has been broadened considerably by multiple interactions, the calculated distribution extending to the full energy of 662 keV.

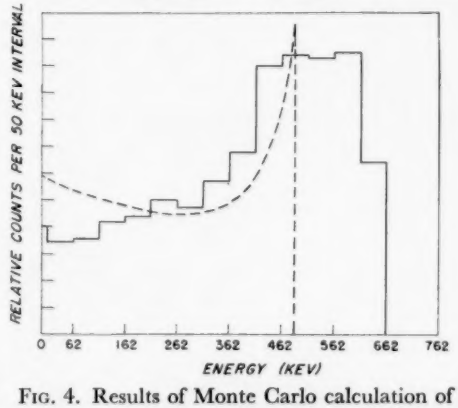

FIG. 4. Results of Monte Carlo calculation of the pulse spectra produced by 0.662 MeV γ-rays incident on the center of a 16-in. diameter $\times$ 8-in. high plastic scintillator. The single Compton pulse-height distribution for 0.662 MeV γ-rays is shown by the dotted line.

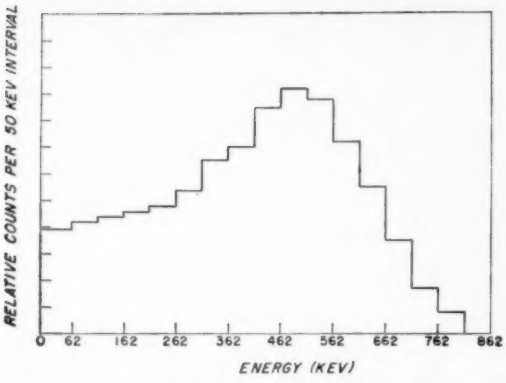

FIG. 5. Experimental pulse-height spectra of 0.662 MeV γ-rays obtained with a 16-in. diameter by 8-in. high plastic scintillator and a 16-in. photomultiplier tube. The area under this curve has been normalized to that of the calculated spectrum, Fig. 4.

Fig. 5 presents an experimental spectrum obtained with a 16-in. diameter $\times$ 8-in. thick plastic scintillator* and a 16-in. Dumont photomultiplier tube. A point source of cesium-137 was placed on the center of the front surface of the scintillator. The distribution is broadened considerably compared to that obtained theoretically by the statistics of photoelectron production and collection. However, the experimental spectrum agrees well with the calculated spectra and the peak lies near that of a single Compton interaction distribution. It is apparent that a plastic scintillator of considerably greater dimensions than used in this study would be required for total absorption. It is interesting to note, however, that even for this-size scintillator as many as ten or twelve Compton interactions were recorded for a single incident γ-ray. Of practical importance is the relatively small number of low-energy pulses in the spectra. This considerably simplifies the problem of obtaining high counting efficiency while discriminating against photomultiplier tube noise.[6]

* The plastic scintillator (Pilot B) was coated with a reflector consisting of aluminum oxide suspended in silica gel, under the direction of H. D. LEVINE of the Health and Safety Laboratory, New York Operations Office, USAEC, and loaned to us for these tests.

V. A LARGE-AREA DETECTOR FOR TOTAL BODY COUNTING

Experimental and theoretical studies have been carried out on the feasibility of using a multiple array of large plastic scintillators as detector units for total-body counting. Such a multiple assembly would combine some of the isotope identification characteristics of a large NaI crystal with the high counting efficiency of total-body liquid scintillation counters. The absolute γ-ray detection efficiency of a 16-in. diameter by 8-in. thick block of plastic scintillator and an 8-in. diameter by 4-in. thick NaI crystal as a function of energy are shown in Fig. 6. The calculations are for normally incident γ-rays. For the sodium iodide detector the fraction of detected events recorded in the photopeak is also plotted.[11] The detection efficiency

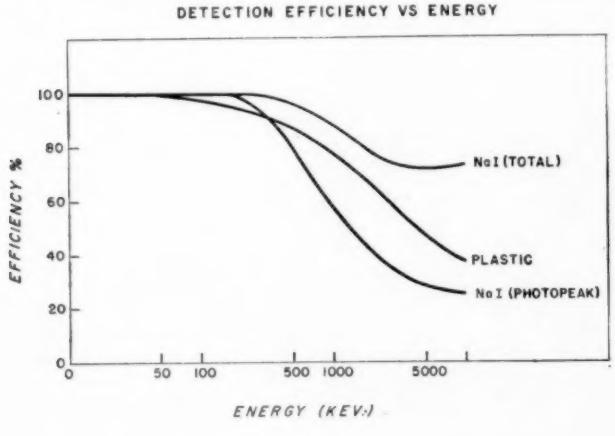

FIG. 6. Efficiencies for an 8-in. diameter by 4-in. thick NaI detector and a 16-in. diameter by 8-in. thick plastic scintillator.

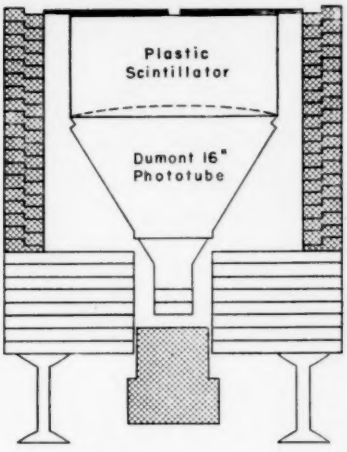

FIG. 7. Experimental arrangement for testing the large plastic scintillator with a 16-in. photomultiplier tube. An 8-in. iron top was added for background measurements.

of both detectors is high in the γ-energy range of interest in low-level counting.

Spectra of Co^{60}, Na^{22}, Cs^{137} and I^{131} were obtained experimentally with the 16-in. diameter by 8-in. thick block of plastic referred to earlier. The observations were made as shown in Fig. 7. Sources were positioned directly above and at the center of the scintillator. A $\frac{1}{4}$-in. layer of lead was placed above the scintillator to exclude low-energy background radiation in the room. Pulse-height spectra were measured for the 16-in. diameter $\times$ 8-in. high plastic scintillator with a 256-channel magnetic core analyzer. The experimental spectra are shown in Fig. 8. Although the resolution is inferior to that of a large NaI crystal, γ-rays of widely different energy can be clearly distinguished. The peak of each distribution does not correspond to the full energy of the γ-ray but more nearly to the energy of the Compton edge, as previously discussed.

A "half-resolution" for spectra obtained with liquid and plastic scintillators has been defined by BIRD and BURCH[12]. The "half-resolution" is the ratio of the energy interval between the peak of the distribution and the point on the high-energy side at which the intensity is decreased by one-half. With this scintillator the half resolution for cobalt-60 is approximately 21 per cent and increases to 34 per cent for cesium-137 and 50 per cent for iodine-131. Some of this resolution may result from nonuniformities in the 16-in. photomultiplier cathode surface, but the major portion undoubtedly

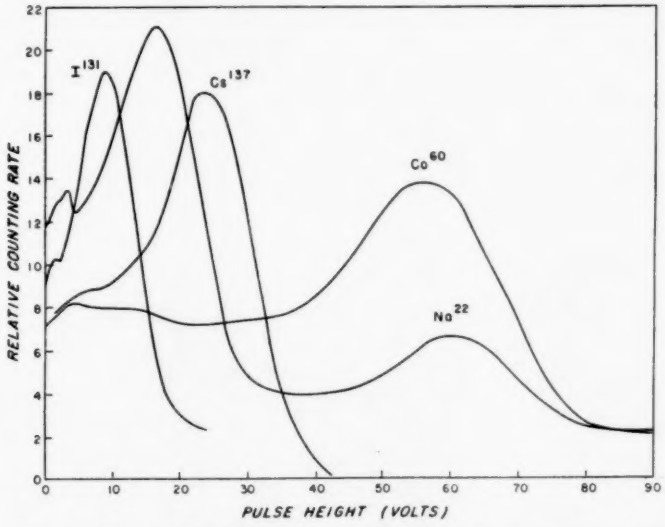

FIG. 8. Spectral distribution of pulses for various isotopes as measured with the arrangement shown in Fig. 7.

Table 3. Comparison between an 8 in. *diameter* × 4 in. *long* NaI *detector and eight* 16-in. *diameter* × 8-in. *high plastic detectors for the detection of normal body burdens of radioactivity*

(Counting time is that required for a 5 per cent standard error)

Isotope	Detector	Counting time (min)	Efficiency	Net count rate	Background count rate
Cs^{137} $E\gamma$ = 0.662 MeV	8-in. diameter × 4-in. long NaI	218	0.71 (photopeak)	41	143
0.84 γ/dis	Plastic array	11	0.83 (total)	1850	17,600
K^{40} $E\gamma$ = 1.46 MeV	8-in. diameter × 4-in. long NaI	50	0.47 (photopeak)	71	55
0.11 γ/dis	Plastic array	2.8	0.71 (total)	4600	29,600

results from multiple Compton interactions in the plastic which tend to broaden the single Compton distribution.

The sides of the shield shown in Fig. 7 consist of 3-in. thick lead rings. The top and bottom of the shield are 8 in. of iron lined with $\frac{1}{4}$ in. of lead on their inner surface. The $\frac{1}{4}$-in. lead layer serves to absorb the soft components of build-up radiation generated in the iron. The integral background counting rate of the 16-in. plastic scintillator in this assembly was 12,500 counts/min with a base line cutoff of approximately 50 keV. At 200 keV the integral background counting rate decreased to 5700 counts/min. The temporary shielding arranged for this test was minimal for low-level counting, and the background counting rates could probably be reduced further in a permanent installation.

A single large NaI detector used for total-body counting must be placed some distance from the subject (usually 50 cm) to minimize geometric errors in the measurements.[13] The large area and relatively low-cost of plastic scintillators suggest that by placing a multiple detector array as close to the subject as possible, the good geometry configuration of the liquid total-body counter could be approached. Based on the data of Figs. 6 and 8, we have compared the time required to measure total-body radioactivity using an array of eight 16-in. diameter by 8-in. thick plastic scintillators, with that required by a single 8-in. diameter by 4-in. thick NaI crystal. NaI crystals could, of course, also be used in a multiple array. However, it would require thirty-two 8-in. NaI detectors to have the same geometric efficiency as the plastic array.

In this comparison, it is assumed: that the body contains 0.123 μc potassium-40[14] and 6×10^{-3} μc cesium-137,[15] that an 8 in. × 4 in. NaI detector is used at 50 cm, and that the eight plastic scintillators are placed as close to the trunk as possible to give an estimated geometrical efficiency of 40 per cent. Background data for the NaI detector have been taken from MILLER[13] assuming a window width equal to 2 × resolution. Appropriate window settings were selected for the two isotopes. Table 3 presents the results of calculations of the time required for the determination of K^{40} and Cs^{137} levels in the body to an accuracy of 5 per cent. The counting times for the plastic scintillators are considerably less than those for the NaI detector, reflecting the greater geometrical efficiency. It is highly likely that the background values for the plastic scintillator could be reduced, as these values result from a single study. It would appear that arrays of large plastic detectors may have application in cases where a large number of routine measurements at or near background levels are desired.

VI. LARGE PLASTIC WELL COUNTERS

An 18-in. diameter by 18-in. plastic well counter* has been used in our laboratory to measure the radioactivity of γ-emitting isotopes.

* Nuclear Enterprises Ltd., Winnipeg, Canada.

Table 4. Comparison of NaI *and plastic well counters*

(Sample requirements assume 5 per cent standard error for a 50-min counting time)

	18 in × 18 in. Plastic	5½ in × 4 in. NaI
Sample size (cm^3)	2000	20
Resolution Cs^{137} $E\gamma = 0.662$ MeV (%)	60	12
Integral background (counts/min) 0.2–2.5 MeV	5000	400
Background in Cs^{137} window (counts/min)	2100	21
Required sample concentration ($\mu\mu c/cm^3$)	0.072	1.05
Required sample activity ($\mu\mu c$)	144	21

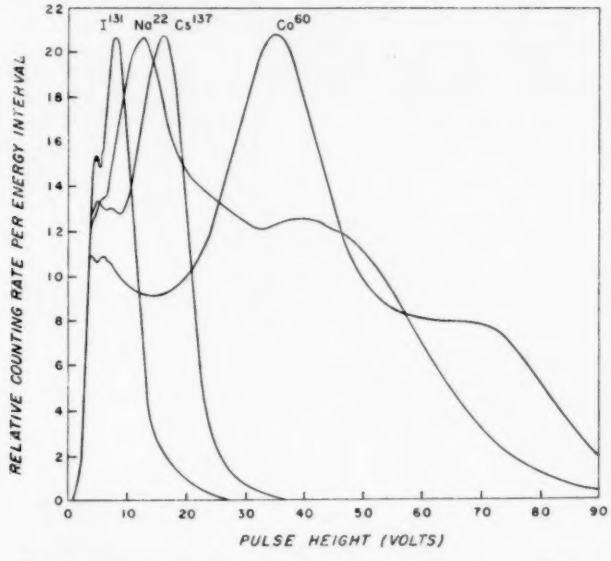

FIG. 9. Spectra obtained with the 18-in. diameter × 18-in. thick plastic well counter and four 5-in. photomultiplier tubes.

The well cavity is 5.6 in. in diameter and 12 in. deep. A 2-l. sample can be accommodated with nearly 4π geometry. Light is collected from the scintillator by pairs of 5-in. photomultiplier tubes located on the top and bottom of the scintillator which is packed in magnesium oxide. For pulse-height analysis, the output of the four photomultiplier tubes are summed in an addition circuit before amplification. A coincidence circuit between the top and bottom pairs of photomultiplier tubes reduces the effects of tube noise by inhibiting the recording of noncoincident pulses. Pulse-height spectra taken with this arrangement are shown in Fig. 9. The spectra are seen to be comparable to those obtained with the solid block of plastic and a single 16-in. photomultiplier tube. Resolution is adequate to allow single-channel pulse-height analysis. This is important, since the use of a window in low-level counting allows background reduction as well as isotope separation.

Table 4 shows a comparison of the sensitivity of this plastic scintillator with the sensitivity of a 5-in. diameter by 5½-in. sodium iodide well counter, assuming that a large amount of sample is available for both. Because of the

large size used in the plastic scintillator its sensitivity is approximately a factor of 14 greater than that of the sodium iodide although, of course, the resolution and absolute sensitivity are both poorer. As in the case of plastic scintillators for total-body counting, large plastic well counters would seem to be advantageous in cases where large numbers of low-level samples are to be measured in a relatively short time. They should find application in low-level tracer studies and in determining natural radioactivity for reactor site monitoring.

Acknowledgments—The authors would like to express their appreciation to Mr. MANFRED WACHTER for writing the IBM program for the Monte Carlo computations, and for many helpful discussions. Part of this work was performed at the Massachusetts Institute of Technology Computation Center, Cambridge, Massachusetts.

REFERENCES

1. C. E. MILLER and L. D. MARINELLI, *Science* **124,** 122 (1956).
2. E. C. ANDERSON, R. L. SCHUCH, J. D. PERRINGS and W. H. LANGHAM, *Nucleonics* **14,** No. 1, 23 (1956).
3. R. M. SIEVERT, *Ark. Fysik* **3,** 337 (1951).
4. Measurements of Body Radioactivity. *Brit. J. Radiol.* Suppl. No. 7 (1957).
5. G. L. BROWNELL, W. H. ELLETT and H. D. LEVINE, *Nucleonics* **16,** No. 2, 68, (1958).
6. M. A. VAN DILLA, R. S. SCHUCH and E. C. ANDERSON, *Nucleonics* **12,** No. 9, 22 (1954).
7. R. L. HICKOK and J. E. DRAPER, *Rev. Sci. Instrum.* **29,** 994 (1958).
8. W. J. VAN SCIVER, *Proceedings of the Large Crystal Spectrometry Symposium* (Edited by J. G. CARVER). O.T.S., U.S. Dept. Commerce, Washington D.C.
9. M. J. BERGER, *J. Res. Nat. Bur. Stand.* **55,** 343 (1955).
10. M. J. BERGER and J. DOGGETT, *Rev. Sci. Instrum.* **27,** 269 (1955).
11. W. F. MILLER, J. REYNOLDS and W. J. SNOW, *Rev. Sci. Instrum.* **28,** 717 (1957).
12. P. M. BIRD and P. R. J. BURCH, *Phys. in Medicine and Biology* **2,** 217 (1958).
13. C. E. MILLER, *Progress in Nuclear Energy* (Edited by J. C. BUGHER, J. COURSAGET and J. F. LOUTET) Series VII, Vol. 2, p. 87. Pergamon Press, New York (1959).
14. E. C. ANDERSON, *I.R.E. Trans.* **NS-3,** No. 4, 96 (1956).
15. E. C. ANDERSON, *Science* **128,** 882 (1958).

Health Physics Pergamon Press 1961. Vol. 5, pp. 37–44. Printed in Northern Ireland

RADIATION DOSE ESTIMATION IN THE 1958 LOS ALAMOS CRITICALITY ACCIDENT*

P. S. HARRIS
Los Alamos Scientific Laboratory, University of California
Los Alamos, New Mexico

(*Received* 24 *March* 1960)

Abstract—An accidental radiation excursion occurring during a Pu^{239} recovery operation resulted in significant exposure of three personnel, one exposure terminating in fatality. Radiation of the fatally exposed person was nonuniform, and it was possible only to estimate his average body dose and dose incident to specific body areas. His average fast neutron dose was estimated as about 900 rads, and γ-ray dose as 3000–4000 rads. The fast neutron doses incident to the head and upper abdomen were estimated as 2600 and 3000 rads, respectively, and the respective incident γ-ray doses as about 7800 and 9000 rads. A second operator received a neutron dose estimated at 2.6 rads, and his film badge showed a γ-dose of 118 rads. The third person's neutron and γ-doses were estimated as 1.4 and 31.5 rads, respectively. Most of the γ-ray dose to the nonfatality exposed operators was accumulated during subsequent trips near the source.

INTRODUCTION

On 30 December 1958, a radiation excursion occurred during a Pu^{239} recovery operation at the DP-site of the Los Alamos Scientific Laboratory. The criticality occurred when an operator started a stirrer in the process of extracting plutonium from an aqueous into an organic phase. Specific details of the operation and the accident are given elsewhere.[1] The excursion resulted in the highest accidental radiation exposure incurred to date in the atomic energy field. Although slight exposure was sustained by other personnel in the vicinity, this report is confined to the exposure of the three recovery process operators (CK, RD and JR), who were working in the operation at the time. The operator CK, who started the stirrer, received a supralethal dose of radiation; therefore, practically all the report is given over to considerations of the dose sustained by this individual.

There were a number of complications connected with evaluation of doses to personnel directly involved in the accident. These complications included geometrical and moderator characteristics of the source and movement of personnel in the vicinity of the source after the accident. Insofar as assessment of dose to the operator CK was concerned, standard dosimeter coverage was inadequate or absent.

PHYSICAL CHARACTERISTICS OF THE SOURCE

The excursion occurred in a 250-gal stainless steel tank containing approximately 150 gal of material. A schematic diagram of the tank is shown in Fig. 1. The critical reaction occurred in the upper organic layer, labeled solvent. The organic phase (consisting of a tributylphosphate–kerosene mixture) contained 3.27 kg of Pu^{239} in solution. The aqueous phase below contained only 40 g of plutonium, while the total solids ("heel", etc.) contained only 60 g. Apparently, when the stirrer was started, the material in the organic phase was brought into a critical configuration in the horizontal center of the tank slightly below the center of the organic layer. The geometric level of the critical reaction was determined by linear measurement of the long-lived induced γ-activity in a stainless steel baffle located inside the tank.

There was apparently enough heating by the reaction and dispersal by continued stirrer operation

* Work performed under the auspices of the U.S. Atomic Energy Commission.

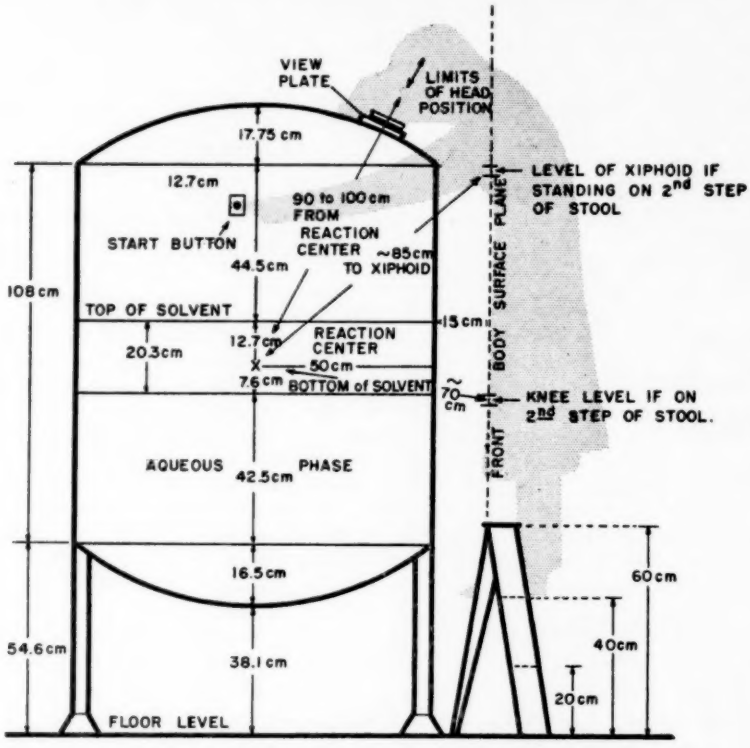

FIG. 1. Schematic diagram of solvent-treating tank and likely position of subject.

to prevent oscillation of the system, as occurred in the Oak Ridge accident.[2a] Thus the whole event consisted of a single, supercritical reaction. The total fissions was determined subsequently by standard radiochemical analysis and found to be $\sim 1.5 \times 10^{17}$. The pulse width, under these conditions, was probably less than 200 μsec. There was undoubtedly a considerable thermal shock created by the rapid temperature increase in the solution. The tank, in fact, was found to have moved $\frac{3}{8}$ in.

The general position of an operator in performing the standard operation is indicated by the posed photograph shown in Fig. 2. A number of operators were questioned, and demonstrated this standard technique. The schematic shown in Fig. 1 gives the most likely dimensions, distances and conditions that prevailed at the time of the accident. In no case during demonstration of the technique was the frontal plane of an operator's body found to be closer than 6 in. to the tank. Thus thermal shock could not be transmitted directly to the chest, abdomen, etc. From the dimensions shown in Fig. 1, it can be seen that the area of the xiphoid was actually closer to the essentially unmoderated critical reaction center than any other portion of the body. Also, the geometry was such that inverse square could materially change the dose (by a factor of 2 over the average body thickness of 30 cm) without any consideration of absorption. Finally, it can be seen that the moderator mass varied from essentially zero to greater than 70 cm of H_2O over the exposure profile. These conditions certainly made dose distribution of both neutrons and γ-rays very nonuniform as far as the operator CK was concerned. It was, therefore, only possible to consider average dose to the body and incident dose to specific areas.

NEUTRON DOSE

Neutron dose to the operator CK was of primary interest. This portion of his total exposure was due almost exclusively to fast rather than thermal neutrons. The incident neutron dose to various regions of the body

BLANK
PAGE

FIG. 2. Posed photograph of operator performing standard plutonium recovery process.

would be expected to vary with distance from the source and thickness of intervening moderator. Depth dose would be expected to vary also with respect to both geometry and absorption.

Several measurements were available from which the fast neutron component of CK's dose could be estimated. These included measurements of blood and total body Na^{24} activity, serum sodium specific activity, induced activity in materials in his pockets or clothing, and specific induced activities in selected tissues. The applicability of all such measurements to neutron dose estimation is predicated on the assumption that thermal neutrons did not cause an appreciable amount of the total activity measured. This assumption seems justified on the basis that thermal neutron fluxes were low or that activation cross-sections were small, or a combination of both.

If one accepts the above assumption, two uncertainties remain in the estimation of fast neutron dose from Na^{24} measurements. One is the estimation of the total amount of Na^{23} (fixed plus exchangeable) in the body. Surprisingly, this is not well known, although 105 g is the value given for the standard 70-kg man.[3] Total body activity measurements apply to total body sodium, whereas specific activity measurements of blood or serum sodium apply primarily to the exchangeable fraction. The second uncertainty is variation in induced Na^{24} activity per unit of neutron dose as a function of source spectrum change. It can be postulated that the activity per unit dose is a slowly changing function of spectrum. This assumption implies that the mass and moderating ability of the irradiated object are enough to wipe out any significant spectral effect.

An experiment was performed using a Los Alamos prompt critical assembly (Godiva II) as a fission neutron source to check the second uncertainty. Varying thicknesses of polyethylene moderator were interposed between the source and a point of measurement and neutron dose measured. Afterward, an 18-l. polyethylene jug filled with a 1.29% $NaHCO_3$ solution in water was positioned at the same point and the induced Na^{24} activity measured as a function of moderator thickness. Results of the measurements are shown in Table 1 and indicate that induced activity per unit of neutron dose is not a strong function of spectral degradation under these conditions. Induced Na^{24} measurements can be used, therefore, to estimate the average fast neutron dose to the exposed subjects.

Table 1. Effect of thickness of moderator on induced Na^{24} activity in $NaHCO_3$ water solution

(CH_2) thickness (in.)	Na^{24} activity (c/min per rad)
0	80
3	80
6	100
9	100

Estimation of average fast neutron dose

Total body sodium activities can be used to estimate average fast neutron dose by comparison with burro experiments carried out in connection with the Oak Ridge National Laboratory's Y-12 criticality accident.[2] In these experiments, a burro was exposed to 48 rads of fission neutrons and induced Na^{24} activity measurements carried out. Assuming sodium concentration in man is the same as that in the burro (comparison of blood concentrations indicate that this assumption is reasonable), the average total body fast neutron dose could be estimated from total body Na^{24} measurements using the following expression:

$$\text{Rad}_S \text{ (ave)} = \frac{\text{Act}_S}{\text{Act}_B} \times \text{Rad}_B$$

where Act_S = activity in the subject in μc/kg; Act_B = activity in the burro in μc/kg; Rad_B = dose to the burro; and Rad_S = the dose to the subject. The Na^{24} activity in the burro was found to be 0.236 μc/kg, following a total neutron dose of 48 rads. In a similar manner, the average fast neutron dose to the exposed subjects could be estimated from blood Na^{24} activity and specific activity of the serum sodium. The burro exposed to 48 rads had a blood Na^{24} activity of 0.29 mμc/ml and a

Table 2. Average total body fast neutron dose from body and blood Na^{24} *concentration and serum sodium specific activity*

Subject	Body Na^{24} (μc/kg)	Blood Na^{24} (mμc/ml)	Serum Na S.A. (mμc/mg)	Dose estimates		
				Body Na^{24} (rads)*	Blood Na^{24} (rads)†	Serum Na S.A. (rads)
CK	4.10	5.3	3.77	835	880	968
RD	0.014	0.016	0.01	2.8	2.6	2.6
JR	0.007	—	—	1.4	—	—

* Assuming total body sodium concentration in man and burro is the same.
† Assuming the blood sodium concentration in man and burro is the same.

serum sodium specific activity of 0.187 mμc/mg (assuming a 50 per cent hematocrit).

Average fast neutron doses, estimated from the various Na^{24} measurements, are shown in Table 2. Values for CK's average body dose ranged from 835 to 968 rads. RD's and JR's average neutron doses were estimated at 2.6 and 1.4 rads, respectively.

The average fast neutron dose to CK can be estimated also from the Godiva II experimental data (Table 1) using the Na^{24} values obtained for the 18-l. water phantom containing 1.29 per cent $NaHCO_3$. With 6–9 in. of moderator between the fission neutron source and the phantom, the induced Na^{24} activity was approximately 100 c/min per rad. Under this set of circumstances, the initial counting rate of the phantom was 5.58×10^3 c/min, with a dose of 57.1 rads. Calibration of the counting equipment indicated a sensitivity of 1.92×10^{-3} μc/c per min. Thus the total activity induced in the phantom was 10.7 μc. The sodium concentration in the phantom was 3.53 g/l., while the value given for man[3] is 1.5 g/kg, or 1.5 g/l. based on a density of unity. CK's total body Na^{24} activity was 293 μc, or 4.10 μc/kg. The induced Na^{24} activity of the phantom was 10.7 μc/18 kg = 0.595 μc/kg. From these values, CK's average neutron dose is estimated as

$$\frac{4.10}{0.595} \times \frac{3.53}{1.5} \times 57.1 = 926 \text{ rads}$$

which agrees satisfactorily with the doses estimated from total body and blood Na^{24} measurements and serum sodium specific activity. Since there was no unequivocal reason for assuming any one of the above estimates was more accurate than the others, CK's average total body fast neutron dose was assumed to be the average of all the estimates or ~900 rads. His tissue dose, however, definitely was not uniform and varied both with depth and with respect to moderator characteristics and geometry of the source.

Estimation of fast neutron dose incident to specific regions

Fast neutron doses incident to specific regions of CK's body were estimated using other measurements. A sample of hair (which has a high sulfur content) was obtained, and the P^{32} activity produced by the $S^{32}(n,p)P^{32}$ reaction was measured. This is a threshold reaction for neutrons with energies greater than 2.5–3 MeV. The cross-section for the fission neutron spectrum is 0.230 barn, which is about the same as the thermal neutron cross-section for the $P^{31}(n,\gamma)P^{32}$ reaction. Hair, however, contains less than 1 per cent as much phosphorus as sulfur, and thermal neutron production of P^{32} from P^{31} may be neglected. The sulfur concentration in CK's hair was found to be 45.6 mg/g, and the P^{32} activity was 27 dis/min per mg of sulfur. The fast neutron flux incident to the head was estimated from the relation

$$N = N^*/\lambda = \varphi \frac{\sigma f A}{W}$$

or

$$\varphi_S = \frac{N^* W}{\lambda \sigma f A}$$

where N^* = activity per g of hair (20.5 dis/sec per g); W = atomic weight of sulfur; λ = decay constant for P^{32} (5.65×10^{-7} sec^{-1}); σ = activation cross-section (0.230×10^{-24} cm^2 n^{-1}); f = fractional concentration of sulfur in hair (0.0456); A = Avogadro's number; and φ_S = total fast neutron flux seen by sulfur (n/cm^2). Thus

$$\varphi_S = \frac{20.5 \times 32}{5.65 \times 10^{-7} \times 0.230 \times 10^{-24}} \times \frac{1}{0.0456 \times 6.02 \times 10^{23}}$$

$$= 1.78 \times 10^{11} \text{ n/cm}^2$$

The flux-to-dose conversion factor for neutrons above the sulfur threshold is 3.63×10^{-9} rads/n per cm^2, giving a dose estimate of ~650 rads (above the sulfur threshold) incident to the region of CK's head. With the source as indicated in Fig. 1, the total neutron flux in the head direction was essentially an undegraded fission spectrum. Under these conditions, Godiva II measurements indicate that neutrons above the sulfur threshold deliver approximately 25 per cent of the total fission neutron dose. The total neutron dose incident to the head was, therefore, about 2600 rads. Extrapolation of measurements performed with the Godiva II assembly indicate that 1.5×10^{17} fissions should deliver a neutron dose of 3700 rads at a distance of approximately 100 cm from the source, the distance assumed in Fig. 1 as the most probable position of CK's head during performance of the stirrer operation. Although the two estimates differ appreciably, it is not surprising since the position of the head was not known. For this reason, the estimate from the P^{32} measurement was considered the more likely value.

Consideration of the distances and source characteristics shown in Fig. 1 suggests that the upper abdomen in the region of the xiphoid probably received the maximum incident neutron dose. Although other regions of the body were closer, the amount of moderator between the source and the body surface probably resulted in a considerably lower dose. A sample of CK's xiphoid cartilage was analyzed also for sulfur, phosphorus and P^{32}, and the results used to estimate incident fast neutron dose to this region of the body. The phosphorus-to-sulfur ratio was 0.028, and phosphorus capture of thermal neutrons could again be neglected. The P^{32} activity was 4.7 dis/sec per g, and the sulfur fraction by weight was 0.00926. The incident neutron flux (φ_S), calculated in the manner shown previously, was 2.05×10^{11} n/cm^2. Using the same conversion factors and assumptions used previously, the incident fast neutron dose to CK's upper abdominal area was estimated at about 3000 rads. Extrapolation of neutron dose data from the Godiva II assembly gave an estimate of ~5000 rads from 1.5×10^{17} fissions at the distance of the xiphoid (Fig. 1). The agreement between the two estimates is considered satisfactory when the uncertainty in CK's position, the increasing amount of moderator between source and surface, and differences in the two assemblies are considered. The increasing amount of moderator would tend to decrease the fraction of dose due to neutrons above the sulfur threshold.

Testicular tissue was analyzed also, but P^{32} activity was below the level of detection. Failure to detect P^{32} in the testicle supports the conclusion that moderation of the source spectrum by intervening water occurred with degradation of high energy neutrons below the sulfur threshold. It may be concluded also that a significant absorption of thermal neutrons occurred, since the phosphorus-to-sulfur ratio in the testicle was 0.11.

Metal buttons were removed from the coveralls worn by CK at the time of the accident and their induced activity measured. The radiation emitted was identified as the annihilation radiation from Cu^{64}. Unfortunately, the buttons (which varied in activity by a factor of ~1.7) were not labeled as to location as they were removed from the coveralls. The activity of the various buttons (corrected to time of accident) is shown in Table 3. Calibration of similar buttons taken from the same type of coverall was attempted during the Godiva II

Table 3. *Copper-64 activity of buttons from coveralls worn by CK (corrected to time of accident)* *

Activity (c/min)	Incident neutron dose (rads)
14,500	2500
13,500	2300
11,300	1900
11,100	1900
9800	1700
9480	1600
8730	1500
(Avg) 11,200	1900

* Position on coveralls not known.

experiments, designed to study effect of moderator on induced Na^{24} activity in the 18-l. water–$NaHCO_3$ phantom. The activity induced in the buttons resulted from thermal neutron capture. However, a free air measurement indicated that thermal neutrons from Godiva itself could be neglected. When the buttons were activated on the front of the phantom with 3, 6 and 9 in. of polyethylene moderator between the source and the buttons, the measurements indicated an essentially constant ratio of 0.17 rad/c per min. The incident neutron dose indicated by each button is shown in Table 3. These results show a variation of from 1500 to 2500 rads and are not inconsistent with the neutron dose considerations given previously.

γ-RAY DOSE

In many respects, estimation of CK's γ-ray exposure was more difficult than estimation of the neutron dose. γ-Doses to RD and JR were reasonably well known, since both were wearing film badges. No film badge results were available for CK, however, and the nature and geometry of the source were important in the estimation of his γ-dose by other means. The γ-to-neutron dose ratio would be expected to vary from point to point because of the moderating conditions. Three different components contributed to the total γ-ray dose. First was fission γ-rays; second capture γ-rays from hydrogen in the moderator; and third residual fission product γ-rays and induced activities in the tank and its contents. As far as CK was concerned, the third portion may be neglected. RD and JR (as will be seen later) received a major portion of their γ-ray exposure from residual fission products and associated activities.

Estimates of the γ-to-neutron dose ratio in the area occupied by CK may be made from the results of the Oak Ridge National Laboratory's mock-up experiment following the Y-12 accident.[2b] These experiments indicated a dose ratio of approximately 3. Although a value of 3 may apply roughly to the upper portion of CK's body, it certainly would not apply to the lower portion in the directions of large thicknesses of hydrogenous moderator. In the presence of significant amounts of hydrogenous moderator, the γ-to-neutron ratio increases rather rapidly due to hydrogen capture γ-rays.[4] Neglecting fission γ-rays, the capture γ-to-neutron dose ratio increases rapidly from 0.5 at 20 cm of water shielding to 5 at 50 cm, and 20 at 100 cm. Application of these observations to the distances and source conditions shown in Fig. 1 suggests that the incident γ-to-neutron dose ratio over CK's body may have varied from 3:1 at the head and xiphoid region to 10:1 at the feet. In the regions of high ratios, however, the neutron dose was very significantly decreased due to fast neutron moderation. Experiments indicate that the fast neutron dose relaxation length[5] is of the order of 10 cm in a water shield. Some build-up close to the source occurs, but one would estimate that the actual fast neutron incident dose to the lower portion of CK's body was only a few per cent of the unmoderated value in the region of the head and xiphoid shown by the sulfur measurements. Therefore, even though the γ-dose to the lower portions of the body may have been ten times as great as the neutron dose, the total dose to this area was undoubtedly only a fraction of that to the upper portions. From these considerations, an estimate of 3000–4000 rads as CK's average total body γ-ray dose seems reasonable.

Located in a rack 137 ft from the center of the criticality excursion were forty-six previously unexposed film badges. After the accident, these films showed an average γ-ray exposure of 670 ± 90 mr. Calculations showed that only

Table 4. Transmission data for Co^{60} γ-rays

Position	Dose rate (mr/hr) *	Transmission factor
Film badge rack	1.86	7.0×10^{-6}
JR's station	4.23	1.6×10^{-5}
RD's station	5.64	2.1×10^{-5}

* Ionization chamber readings from 20-c source placed near the solvent-treating tank.

about 4 per cent of the reading registered by these badges could have resulted from residual fission product γ-ray exposure, which certainly constituted a negligible fraction of CK's dose. An experiment was carried out to measure γ-ray transmission from the source to the film badge rack before the general geometric features of the area were disturbed (only the contents of the solvent-treating tank had been transferred). Using a Co^{60} source (approximately 20 c) placed at about 6 in. from the outer wall of the solvent tank at a level approximating the level of the reaction, γ-ray dose rates were measured at RD's and JR's positions and at the film badge rack. Measurements were made with Victoreen 0.025-r ionization chambers and γ-rate meters (Eberline Model E-112B), and agreement between the two methods was quite good. Results of these measurements are shown in Table 4. Calibration of the Co^{60} source gave a dose rate of 4.4 r/min at a distance of 1 ft, which is in good agreement with the rated source strength of 20 c.

Using a transmission factor of 7×10^{-6} and a reading of 670 mr at the film badge rack, extrapolation to a position 1 ft from a point source at the center of the solvent-treating tank gave a total γ-dose of 9.57×10^4 rads. Similar extrapolations from RD's and JR's stations could not be made, since their film badges showed readings of 118 and 31.5 r, respectively, most of which was from fission γ-ray exposure accumulated during subsequent trips near the source. That this was the case is indicated by the γ-ray transmission factors at their respective stations. These data indicate that RD's prompt γ-dose was approximately 3 times that measured at the film badge rack (or about 2 r), and JR's dose was about 2.3 times the dose at the rack (or approximately 1.5 r).

Extrapolation of the total γ-dose at 1 ft from a point source at the center of the fission excursion (assuming no moderator effect) to the dose incident to CK's head and xiphoid regions gives a value of ~10,000 r to the head and a slightly higher value to the upper abdominal area. Considering the nature of the data and the extrapolations involved, this is considered to be in reasonable agreement with the values of 7800 and 9000 rads derived from the incident neutron dose (estimated from the P^{32} measurements) and a γ-to-neutron dose ratio of 3 to 1. The source was not actually a point source and certainly some of the γ-exposure to the film badges might have been from γ-ray production not in the immediate vicinity of the tank. It is possible also that the observed γ-ray transmission factors, which varied greatly from point to point because of intervening equipment, etc., were low compared to what actually was the case.

Another estimate of γ-ray dose may be made strictly on theoretical grounds. Considering only fission γ-rays, the total prompt γ-energy release is variously quoted as from 7.5 to 12 MeV per fission. Using 7.5 MeV and 1.5×10^{17} fissions, the total γ-energy available was about 1.5×10^{12} ergs. At 100 cm, the energy flux would be 1.5×10^7 ergs/cm^2. For γ-rays of intermediate energy, an energy flux of 3000 ergs/cm^2 results in a dose of 1 rad. Based on these considerations, the total fission γ-dose in the region of CK's head would have been around 4500 rads and in the region of the xiphoid greater than 6000 rads. These estimates agree within a factor of 2 with the 3 to 1 ratio of γ-to-neutron dose, and in view of the complications this is perhaps as good as can be expected.

TOTAL DOSE (CK)

As stated previously, both the fast neutron and γ-ray doses to CK were completely nonuniform. It is possible, therefore, only to estimate his average total body dose and total incident dose to the head and upper abdominal regions. In many respects, the neutron dose estimates were more satisfactory than those of γ-dose. The most reliable estimates of incident γ-dose to the head and upper abdominal areas (where the effects of the water moderator

Table 5. Summary of estimates of CK's radiation exposure

Region and conditions	Fast neutron dose (rads)	γ-Dose (rads)	Total dose (rads)
Head (incident)	2600	7800	10,400
Upper abdomen (incident)	3000	9000	12,000
Total body (average)	900	3000–4000	3900–4900

were minimum) are perhaps those based on a fast neutron-to-γ dose ratio of $\frac{1}{3}$. Taking the various factors into consideration, what seems to be the most reasonable estimates of CK's radiation exposure are summarized in Table 5.

The relative biological effectiveness (RBE) of fission neutrons for production of lethality in mice is approximately 2.[6] The mouse, however, is thin compared to the neutron mean free path, and the neutron dose may be assumed to be uniform throughout and over the entire body. Since these were not the conditions of CK's exposure, it is virtually impossible to choose an appropriate RBE value for the fast neutron component of his dose. No attempt is made, therefore, to estimate his average total body exposure in rems. It seems advisable to say only that his average total body exposure was probably between 3900 and 4900 rads, of which about 900 rads was due to fission neutrons, and that a considerably greater portion of the dose was delivered to the upper half of the body than to the lower half.

Acknowledgments—The writer wishes to acknowledge the services of E. A. Bemis and D. H. Meyer of Group H-1 of the Los Alamos Scientific Laboratory in carrying out special studies done on the coverall buttons, and also J. N. P. Lawrence of Group H-6 for theoretical calculations of average total body exposure.

REFERENCES

1. H. C. Paxton, R. D. Baker, W. J. Maraman and R. Reider, *Los Alamos Scientific Laboratory Report LAMS*-2293. Los Alamos, New Mexico (1959).
2(a). *Accidental Radiation Excursion at the Y-12 Plant June* 16, 1958, U.S. Atomic Energy Commission Report Y-1234. Office of Technical Services, U.S. Department of Commerce, Washington, D.C. (1958).
2(b). G. S. Hurst, R. H. Ritchie and L. C. Emerson, *Health Phys.* **2,** 121 (1959).
3. Recommendations of the International Commission on Radiological Protection, *Brit. J. Radiol.* Suppl. 6 (1954).
4. B. T. Price, C. C. Horton and K. T. Spinney, Radiation shielding. International Series of Monographs on Nuclear Energy, Division 10, *Reactor Design Physics* Vol. 2, p. 287. Pergamon Press, New York (1957).
5. B. T. Price, C. C. Horton and K. T. Spinney, Radiation shielding. International Series of Monographs on Nuclear Energy, Division 10, *Reactor Design Physics* Vol. 2, p. 178. Pergamon Press, New York (1957).
6. J. B. Storer, P. S. Harris, J. E. Furchner and W. H. Langham, *Rad. Res.* **6,** 188 (1957).

Health Physics Pergamon Press 1961. Vol. 5, pp. 45–49. Printed in Northern Ireland

DECAY OF POLONIUM–BERYLLIUM FAST NEUTRON SOURCES

M. L. RANDOLPH, H. G. JONES and D. L. PARRISH*
Biology Division, Oak Ridge National Laboratory,† Oak Ridge, Tennessee

(*Received* 25 *April* 1960; *in revised form* 8 *June* 1960)

Abstract—The half-life for fast neutron emission of three Po–Be fast neutron sources has been measured by long counter detection methods and found to agree to within less than 2 per cent of the half-life of the α-emitter even, in one case, over a period of ten half-lives.

INTRODUCTION

For purposes requiring modest neutron fluxes, such as calibrations of detectors and some low-level studies, radiochemical sources offer maximum convenience, and Po–Be sources provide about the highest energy spectra and highest fluxes of such sources. Although it might be taken as axiomatic that the fast neutron emission of a Po–Be source should decay proportionately with the polonium isotope, there have been repeated warnings and vague hints that such is not necessarily the case.[1–4] Attempts to explain deviations from the expected output are generally based on presumed migration of the polonium or beryllium, or both, thus changing the distributions of the elements and the efficiency of neutron production per α-particle emitted. Such changes might be caused by the energy released in α-decay or by rough handling of a source. We present here the results of careful measurements of the neutron emission of three Po–Be sources conducted over several years.

EXPERIMENTAL METHODS

Our measurements involved two detectors, three sources and three locales. One detection system consisted of a standard long counter,[5] A-1-A preamplifier, and A-1 amplifier[6] with a 50- to 70-ft cable between amplifier and preamplifier. The counter was run at 2500 V with amplifier gain setting of 64 × 1 and discriminator at 12 V. The delay line was used. Typical measurements at these settings indicated sensitivity changes of less than ±2 per cent for a counter voltage change of ± 100 V or a discriminator change of ±6 V. Average pulse heights were about 56 V and noise became detectable at about 4 V. Circuits were run continuously and all vacuum tubes were checked at least every 3 months. From additivity studies, coincidence losses were estimated, and corrections were made in the few cases where necessary. The sensitivity per fast neutron was about 3×10^4 times that per γ-ray photon. The second detection system consisted of a long counter modified for flat response to 14 MeV after the suggestions of Graves and Davis[7]. The counter was desensitized by the use of low gas pressure and normal rather than enriched B in the counter tube. Both detection methods used the same electronics except for the 0.5 mc time constant rather than delay line. Operating conditions were: counter voltage, 1700 V, gain, 8 × 1, discriminator, 12 V, sensitivity constant to within ±1 per cent for a change of ±100 V on the counter and ±5 V on the discriminator, average pulse height, 52 V; and circuit noise became detectable at 4 V. The sensitivity per neutron was about 10^6 times that per γ-ray photon.

The Po–Be sources tested were: Po^{210}–Be, outside dimensions 1 × 1 in. cylinder, originally containing about 100 c of Po^{210} mixed with beryllium and encapsulated at Mound Laboratory in September, 1956; a 30-c Po^{210}–Be source, length and diameter about 1.8 cm encapsulated at Mound Laboratory in August, 1954; and a Po^{208}–Be source, outside dimensions 2 × 2 cm cylinder, originally containing about 2 c of Po^{208}, mixed with beryllium and encapsulated in March, 1953. The 100-c Po^{210}–Be source was mounted in a permanent facility, but the others were mobile. The Po^{208}–Be source has also served

* Present address: R.C.A. Service, Patrick AFB, Florida.

† Operated by Union Carbide Corporation for the United States Atomic Energy Commission.

as a standard for several radiobiological experiments,[8–11] and the 100-c Po^{210}–Be source has been used as a chronic fast neutron source for studies, some of which have been briefly summarized by UPTON[12]; and others will be reported.

The locales or scattering surroundings involved were: (1) a large, low scatter room ("hill") in which sources were placed on the axis of the detector at 100 cm from its foremost face; (2) a "cup" that bolted on to the detector holding the source reproducibly at about 7 cm from the foremost face; and (3) a high-scatter chamber ("pit") with 4-ft-thick concrete walls about 20 × 10 × 10 ft, inside of which sources were placed at 100 cm from the large detector or 145 cm from the small detector.

Logarithms of counting rates were subjected to statistical analysis by the method of least squares, without weighting of observations, to obtain the half-life values as well as the corresponding analyses of variance to test for linearity. Additional analyses provided comparisons of locales, two Po^{210}–Be sources, detectors, and half-lives for neutron emission vs. α-emission. Repeat determinations of counting rates performed on the same day are referred to as a set of observations and were treated as independent, although these usually included the same experimental variations in source positioning and neutron scattering.

As TEMPLETON[13] indicated, decay of Po^{208} samples is complicated by the presence of Po^{209} with a maximum half-life of roughly 200 years.[14] MARTIN *et al.*[15] found that the efficiencies of production of Po^{208} and Po^{209} and their decay constants are such that the ratio of their initial α-emission is 720:4. Since both polonium isotopes emit α's with about the same energy[16] and both have negligible γ-emissions,[17] the expected neutron emission, $E(t)$, at time t years after production of the isotope is:

$$E(t) = \frac{E(0)}{724}\left(720\, e^{-\lambda 208\, t} + 4\, e^{-\lambda 209\, t}\right) \qquad (1)$$

where λ is the usual disintegration constant for the designated isotope. We have thus corrected all the Po^{208} data given here, using 100 years as the half-life of Po^{209}.[14,15,18] A typical calculation (for 1000 to 2400 days after production of isotopes) indicates that omission of this consideration would yield a half-life about 20 days longer. Since our first measurements of this study were performed more than 2 years after production of the Po^{208}, it seems unlikely that short-lived contaminants (e.g. Po^{210}) can be of significance, although in principle equation (1) should include a term for Po^{210}.

Soon after fabrication of the Po^{208}–Be source, its neutron emission was calibrated versus the Los Alamos Ra–Be standard source no. E-665. The source was recalibrated 2154 days later against the National Bureau of Standards primary Ra–Be photoneutron standard source "NBS-1."[19] HUGHES's report[20] on intercomparisons of neutron standards indicated good agreement between the Los Alamos and NBS standards.

The sources have been handled with reasonable gentleness but without special precautions. The 100-c Po^{210}–Be source has been raised and lowered more than 1000 times in its facility; and the Po^{208}–Be source has been removed from its storage shield, handled, and returned more than 300 times.

RESULTS

The eight half-life values and their 95 per cent confidence intervals resulting from these measurements are given in Table 1, which also gives the duration and number of observations and number of sets of observations for each half-life value. For comparison, the half-lives for the two polonium isotopes and statistical estimates of our best values for the neutron decay are also given.

DISCUSSION

Each of the last four accurate, independent values reported for the half-life of Po^{210} is very near 138.4 days.[21–24] Our values for two Po^{210}–Be sources are less than 2 per cent greater than this value and neither difference is by itself statistically significant at the 5 per cent level. For the 100-c source, measurements extended over a period of ten half-lives and the emission decreased by a factor of 10^3. Statistically pooling the data for these two sources, we obtained an average about 0.7 per cent higher than the expected value.

Results of the statistical F-test indicate significant deviations from linearity (i.e. exponential decay) for the two cases of the large BF_3 detector in the pit and suggest deviations for several other cases. However, the F-test is primarily dependent on the ratio of the variances determined from the deviations of the means for various days from those predicted by a least-squares fit to the sum of the variances of individual measurements on various days from their daily means. Thus an indication of nonlinearity can also be interpreted as merely an indication that the variances from day to day in alignment and distance of the source, in amounts of neutron scattering from

Table 1. *Half-life values for fast neutron emission of* Po–Be *sources*

Source	Detector	Locale	Half-life point estimate and 95 per cent confidence interval* (days)	Duration of measurements (days)	Number of observations	Sets of observations
Po^{208}–Be, 1 c	Large	Pit	1024 ± 14	1852	89	40
	Large	Hill†	1018 ± 55	1420	11	5
	Large	Cup	1053 ± 8	1335	72	36
	Small	Pit	1024 ± 55	1192	30	26
	Small	Cup	1013 ± 14	1307	301	139
	L.A. and N.B.S.	—	1090 ± 100‡	2154	—	2
	Our best value§		1041 ± 6			
Po^{208}, best value for α-emission			1058 ± 1			
Po^{210}–Be, 20 c	Large	Pit	140.4 ± 2.2	216	33	8
Po^{210}–Be, 100 c	Large	Hill†	139.1 ± 0.7	1420	14	5
Average for Po^{210}–Be sources			139.2 ± 0.6			
Po^{210}, best value for α-emission			138.4 ± 0.1‡			

* Properly, the 95 per cent confidence intervals are not quite symmetric about the point estimates. Limits given here include the greater deviations from point estimates.

† Parallel measurements of the Po^{210}– and Po^{208}–Be sources were made on the same days throughout the hill measurements.

‡ Width of confidence interval uncertain.

§ Does not include the LA–NBS calibrations.

miscellaneous objects, and in amplifier gain or discriminator level produced greater variability than the variations in observed counting rates during a day, which for the strong sources and large detectors were very small. Because of this and because visual inspection of plots of the seven sets of data revealed only one questionably systematic departure from linearity, we doubt that the *F*-tests should be interpreted as proving nonlinearity in these data.*

The statistical analyses also show that the standard deviation for an individual measurement was less than 5 per cent for every case and less than 3 per cent for all but the exceptional case just mentioned. This result furnished support for statements made elsewhere[10,11] about the precision of our fast neutron dosimetry in biological experiments. An attempt was made to determine whether these deviations were primarily daily deviations or deviations of daily means from the least-squares fits. As might be expected, the daily deviations, perhaps half of which arise from counting statistics, accounted for about 80 per cent of the total deviation for the measurements with the source in the cup (the most reproducible positioning and least subject to neutron scattering) and accounted for only from 20 to 50 per cent of the total deviation at the pit locale (which, because of the high scattering, probably is the most sensitive to variations in positioning and surroundings).

We know of but three published values[13,14,25] for the half-life of Po^{208}. Confidence limits for these experiments all overlap, the latest and most precise being 2.93 ± 0.03 years (1070 ± 11 days). However, the preliminary value

* The exception was the case of the Po^{208} source with small detector in the pit, against which were four plots for the same source without apparent systematic deviation from linearity.

obtained by JORDAN at Mound Laboratory for the half life of Po^{208} by calorimetric measurements is 1058 days $\pm$ perhaps 1 day, and roughly 100 years for Po^{209}. His value is just at the lower limit of TEMPLETON's range. JORDAN's Po^{208} sample and the Po^{208} for our source came from the same production batch.

All six individual Po^{208}–Be neutron half-lives in Table 1 are within ± 5 per cent of JORDAN's value, and four of the 95 per cent confidence limits overlap his value. Two individual values and the statistical average of our values, however, are significantly lower than his value by statistical standards. Possible artifacts that may cause these deviations include overcorrection for Po^{209} contaminant, overestimation of the number of degrees of freedom since repeat measurements on a single day are not entirely independent values, and gradual drift in the sensitivity of the small detector. Drift of the large detector seems unlikely since the Po^{210}–Be values measured with this detector during the same time interval are if anything, too high.

If this sensitivity $S(t)$ of a detector has the exponential variation with time t,

$$S(t) = S(0)\, e^{-ct} \tag{2}$$

where c is a constant, the observed counting rate, $R(t)$ at time t, produced by a source with decay constant λ will be

$$R(t) = R(0)\, e^{-(c+\lambda)t} \tag{3}$$

An independent indication of the sensitivity of the small detector is available through the frequent simultaneous use of this detector and an associated particle counter to monitor the 14-MeV neutron output of a Cockcroft–Walton accelerator. The system has been partially described elsewhere.[10,11] Least-squares analysis of measurements, made on 87 days during the same 3-year period as these Po–Be source measurements were made, yield, the 95 per cent confidence interval for the natural logarithm of the ratio of doses indicated by the long counter and the α-counter, $\ln (L/\alpha)$, as

$$\ln (L/\alpha) = (0.013 \pm 0.018) - (3.9 \pm 3.8)10^{-5}t' \tag{4}$$

where t' is the number of days since 30 July, 1956. The linear fit of (L/α) vs. t' is very similar to the exponential fit given by equation (4). If this variation with time is real, exact and entirely attributable to the small detector, the half-life values can be corrected to about 1087 and 1075 days, respectively, both of which are larger than the expected value.

During its use, this small BF_3 detector, with a volume of about 10 ml, has given about 5×10^9 counts but has not yet suffered the catastrophic deterioration described by SOBERMAN *et al.*[26]

As TOCHILIN and ALVES pointed out, variations in the mechanical mixing of source preparations may yield slightly different neutron spectra.[27] Our measurements give no information on this subject nor have we observed marked asymmetry as has been suggested by other workers, who used different sources.[4,28]

CONCLUSIONS

The half-life for fast neutron emission from three Po–Be sources has been measured and agrees with the expected value for the α-emitter to within less than 2 per cent, even though one experiment was continued over a period of 10 half-lives. Partly because these experiments did not fulfill certain orthogonality requirements for the rigorous statistical analysis and partly because an independent check of one detector suggested a small drift in its sensitivity, the hints of nonlinear decay and the indicated statistical significance of the small differences between the half-life of the polonium isotopes and neutron emission of Po–Be sources cannot be regarded as proved.

Acknowledgments—We are especially grateful to Dr. A. W. KIMBALL for his helpful consultations on the interpretation of the statistical analyses and for performance of these analyses using an ORACLE code prepared by Dr. M. A. KASTENBAUM. The fast neutron sources have been made available to us through the courtesy of various other members of the Oak Ridge National Laboratory, including Mr. J. A. MARTIN, Dr. A. C. UPTON and Dr. G. S. HURST. Mr. K. C. JORDAN of Mound Laboratory generously made his preliminary data on the decay of Po^{208} available to us before its publication.

REFERENCES

1. H. L. ANDERSON and B. T. FELD, *Rev. Sci. Instrum.* **18,** 186 (1947).
2. D. J. HUGHES, *Pile Neutron Research* p. 72. Addison-Wesley, Cambridge, Mass. (1953).

3. K. J. McCallum, *Nucleonics* **5,** No. 7, 11 (1949).
4. H. M. Borella, S. C. Sigoloff and L. C. Logie, *A Direct Determination of the Gamma Emission from a* Po–Be *Source.* School of Aviation Medicine, USAF, Report No. 56–59 (1956).
5. A. O. Hanson and J. L. McKibben, *Phys. Rev.* **72,** 673 (1947).
6. F. I. Magee, P. R. Bell and W. H. Jordan, *Rev. Sci. Instrum.* **23,** 30 (1952).
7. E. R. Graves and R. W. Davis, *Phys. Rev.* **97,** 1205 (1955).
8. G. S. Hurst, W. A. Mills, F. P. Conte and A. C. Upton, *Rad. Res.* **4,** 49 (1956).
9. C. W. Sheppard, M. Slater, E. B. Darden, Jr., A. W. Kimball, G. J. Atta, C. W. Edington and W. K. Baker, *Rad. Res.* **6,** 173 (1957).
10. A. D. Conger, M. L. Randolph, C. W. Sheppard and H. J. Luippold, *Rad. Res.* **9,** 525 (1958).
11. C. W. Edington and M. L. Randolph, *Genetics* **43,** 712 (1958).
12. A. C. Upton, *J. Gerontol.* **12,** 306 (1957).
13. D. H. Templeton, *Phys. Rev.* **78,** 312 (1950).
14. E. L. Kelly and E. Segrè, *Phys. Rev.* **75,** 999 (1949).
15. J. A. Martin, R. S. Livingston, R. L. Murray and M. Rankin, *Nucleonics* **13,** No. 3, 28 (1955).
16. D. G. Karraker, A. Ghiorso and D. H. Templeton, *Alpha Decay Energies of Polonium Isotopes.* U.S. Atomic Energy Commission Unclassified Report UCRL-1091 (1951).
17. E. H. Dagget and G. R. Grove, *Phys. Rev.* **99,** 1 (1955).
18. K. C. Jordan, *The Half-life of* Po^{208} *by Calorimetry.* To be published.
19. R. S. Caswell, National Bureau of Standards Report Test No. G.2477a (1959).
20. D. J. Hughes, *Nucleonics* **12,** No. 12, 26 (1954).
21. W. H. Beamer and W. E. Easton, *J. Chem. Phys.* **17,** 1298 (1949).
22. D. C. Ginnings, A. F. Balls and D. T. Vier, *J. Res. Nat Bur. Stand.* **50,** 75 (1953).
23. M. L. Curtis, *Phys. Rev.* **92,** 1489 (1953).
24. J. F. Eichelberger, K. C. Jordan, S. R. Orr and J. R. Parks, *Phys. Rev.* **96,** 719 (1954).
25. D. H. Templeton, J. J. Howland and I. Perlman, *Phys. Rev.* **72,** 758 (1947).
26. R. K. Soberman, S. A. Korff, S. S. Friedland and H. S. Katzenstein, *Rev. Sci. Instrum.* **24,** 1058 (1953).
27. E. Tochilin and R. V. Alves, *Nucleonics* **16,** No. 11, 145 (1958).
28. L. F. Curtis and A. Carson, *Phys. Rev.* **76,** 1412 (1949).

Health Physics Pergamon Press 1961. Vol. 5, pp. 50–56. Printed in Northern Ireland

THE USE OF AN α-PULSE-HEIGHT ANALYZER IN ENVIRONMENTAL MONITORING*

E. L. RAY and S. E. HAMMOND

Health Physics Department, The Dow Chemical Company, Rocky Flats Plant
Denver, Colorado

(*Received* 5 *July* 1960)

Abstract—The use of a Frisch grid ion chamber and a 100-channel analyzer is described for identification and estimation of long-lived α-contamination in environmental samples. The preparation techniques are described for air, water and vegetation samples. Typical pulse-height graphs are presented for air and vegetation samples.

1. INTRODUCTION

SEVERAL α-emitters are present at the Rocky Flats Plant; identification and determination of these components by differential chemical analysis is feasible but expensive and time-consuming. An alternative is α-pulse-height analysis. After the initial capitalization, it becomes an economical means of determining component activities. It is also a versatile tool and lends itself to numerous applications in bioassay, production problems, and research and development. This technique has been used at other AEC installations.[1,2]

2. DISCUSSION

2.1. *Instrumentation*

An α-particle pulse-height analyzer is an instrument designed to determine the energy spectrum of α-emitting samples. A graph is usually plotted from the data showing counts vs. energy in MeV of the α-particles. The data can be presented in a variety of ways, depending upon the type of analyzer.

The H-100[3], an improved version of the original D. H. Wilkinson "kicksorter" and the LASL model-15 pulse-height analyzer, presents the data in terms of counts per channel. Each channel is read on a mechanical register. The H-100 is a 100-channel "slow" pulse-height analyzer consisting of a linear amplifier, coding and timing circuits, register read-out and d.c. power supplies (Fig. 1). The analyzer is used with a Frisch grid ionization chamber. The counting gas is a mixture of 10% methane and 90% argon. The chamber[4] produces a 1-mV pulse for an α-energy of 5 MeV (Fig. 2). The sample is placed such that all the ionization occurs in the region *G* between the cathode and the grid. The grid is held at an intermediate positive potential with respect to the cathode. The collector plate is polarized through the large resistor *R*. When ionization is produced in the region *G*, the electrons drift towards the grid, and the positive ions in the opposite direction. During this phase, no charge is produced on the collector plate because it is screened electrostatically by the grid from the induced effect of the electrons and the positive ions. The electrons pass through the grid into the region *H* with only a very small percentage of the electrons being captured by the grid. In this region the electrons begin to induce on the collector plate a charge which rises from zero to the full value as the electrons move through the distance from the grid to the collector plate. In the same time the voltage pulse rises and is thereafter uninfluenced by the positive ions left in the region *G*. The magnitude of the total charge collected in the chamber is proportional to the initial energy of the α-particle and independent of α-particle track position. The gridded chamber provides 2 per cent resolution at half height, enabling qualitative and quantitative interpretation of a sample, for example, a

* U.S. Atomic Energy Commission Contract AT(29-1)-1106.

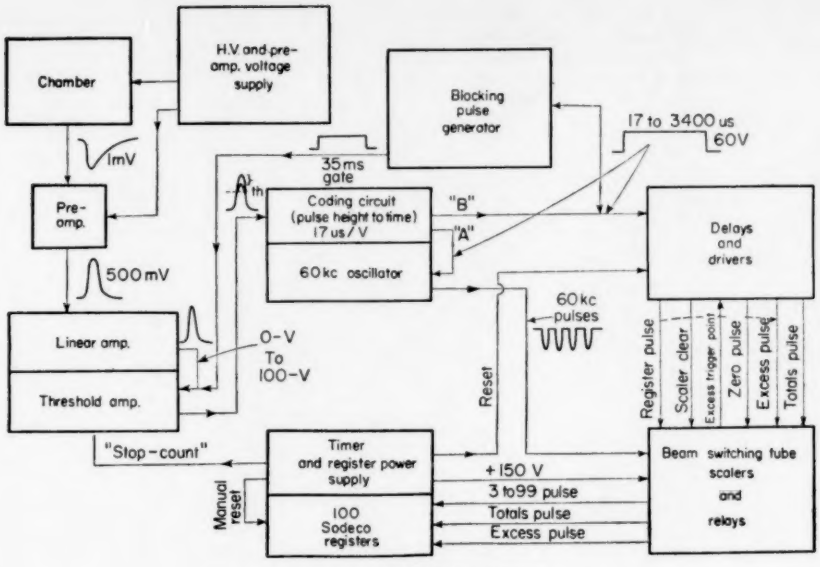

FIG. 1. H-100 block diagram.

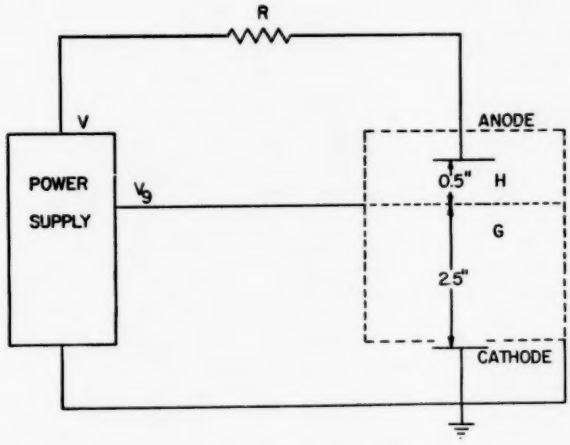

FIG. 2. Frisch grid chamber.

mixture of depleted uranium and plutonium (Fig. 3).

A new chamber is now being constructed to reduce the background contribution from the chamber walls and to decrease the likelihood of chamber-contamination resulting from flaking of active material from a sample disk.

The chamber consists of a sensitive-volume cage suspended in a large gas-tight container. Thus, any sample-flaking or any activity in the container walls is outside the sensitive volume. The mechanical problem of transporting the sample without poisoning the large volume of gas has been solved by incorporating an arm which rotates the sample through an arc from a gas lock into position in the sensitive volume.

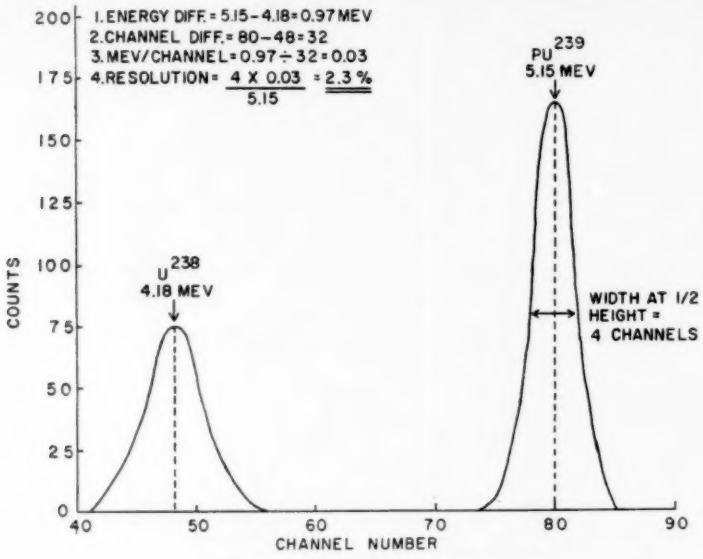

FIG. 3. Typical α-pulse-height graph.

An interlock is provided to avoid accidental opening of the interior volume to the outside atmosphere.

2.2. *Sample preparation*

Pulse-height analysis requires that the activity be plated as a thin source on a conducting medium. A thick source will degrade the energies of the α-particles through self-absorption, which will in turn "smear" the peaks and lower the resolution of the instrument. A non-conducting backing medium, such as filter paper, cannot be counted directly. This is because positive ions will accumulate on an insulated sample and build up a positive charge upon its surface. This raises the potential toward the anode and causes successive pulses of the same energy to be recorded in lower channels, or, in effect, destroys the resolution of the instrument. Fig. 4 shows a pulse-height analysis of a thick source.

Air samples are collected on Whatman 40 or HV-70 paper. Acid-leaching of HV-70 or acid digestion of Whatman 40 followed by evaporation of the acid solution on stainless steel disks provide a thin source and near-quantitative recoveries of the activity.

Water and vegetation samples can be analyzed by various solvent extraction or carrier techniques. We use a standard ether extraction procedure in which the digested inorganic salts present are dissolved in acidified aluminum nitrate solution and extracted with a small volume of diethylether. The ether layer is then transferred to a few milliliters of water, evaporated, and the resulting solution transferred to a counting disk. Over-all recoveries average 87 per cent for water and 60 per cent for vegetation samples.[6]

Soil samples are treated as above with adequate results for our purposes. Silica destruction and fusions could be incorporated into the procedure for a more rigorous treatment.

2.3. *Pulse-height analysis*

Precision of a quantitative determination by pulse-height analysis depends upon counting statistics; thus the practical consideration of how much time to spend on any one sample becomes the limiting factor. The advantage of the method is that no operator attention is required. Low-level samples can be run all night or over a weekend to achieve a high degree of precision.

In interpreting pulse-height analyses, the activity as related to the mass of each isotope must be considered. The α-energy of U^{235} which is the major isotopic constituent of enriched uranium is 4.58 MeV, yet, since the activity of U^{234} is much greater, a pulse-height analysis of enriched uranium will be seen as a single peak in the 4.76-MeV region (U^{234}).

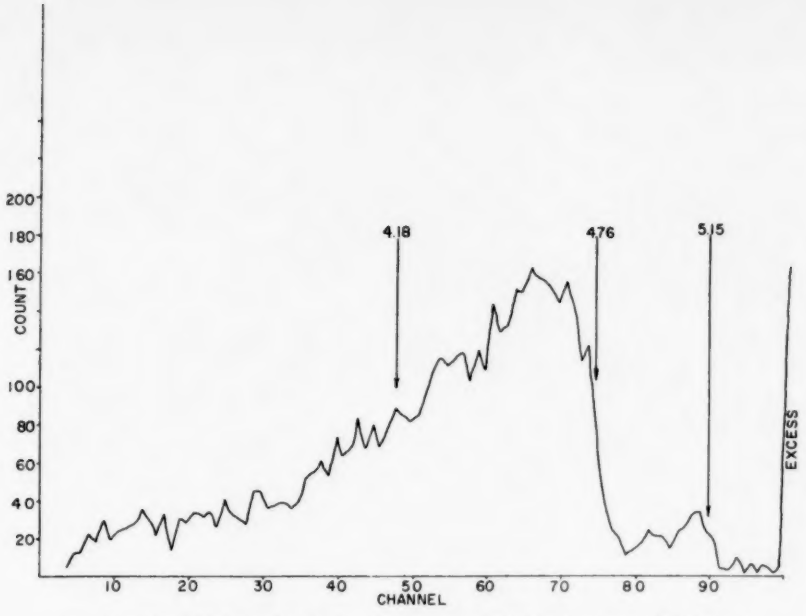

FIG. 4. Pulse-height analysis showing poor resolution due to a thick source.

Similarly, depleted uranium will appear as a single peak at 4.18 MeV (U^{238}) even though traces of the more active isotopes of normal uranium are present.

The pulse-height analysis of normal uranium shows peaks of equal heights for U^{234} and U^{238} (secular equilibrium). This presents a drawback in low-level contamination studies in that any contaminants present of the same order of magnitude as naturally occurring activity prevent an interpretation of the origin of observed uranium activity.

Fig. 5 is an example of a typical curve obtained from a sample of 10 dis/min counted for 5½ hr. Plutonium accounts for about 20 per cent of the total activity. In this case we are unable to say too much about the remainder. The difference in height of the two uranium peaks may be real or merely statistical. That is, this portion of the activity may be all natural uranium, some natural uranium with additional depleted and enriched uranium contamination, or nearly all a mixture of depleted and enriched uranium.

For extreme accuracy, the total contribution of each isotope is determined by comparing the areas under the respective curves. In most cases, however, a comparison of peak heights is sufficient for practical considerations.

Figs. 6 and 7 are analyses of samples of about the same activity (2 dis/min) counted for 61 hr and 18 hr, respectively. The better precision obtained from the longer counting time is readily apparent; however, the shorter time was adequate to give a measure of the activities present.

Two plots of the same air sample taken three days apart show that in the first determination a large number of counts in the excess channel were recorded (Fig. 8). These are due to radon daughter products which had mostly decayed out by the time of the second count (Fig. 9), while the long-lived α-count remained constant.

Channel width, in volts (V), is a function of the amplifier gain. Channel width in keV, then, is also a function of amplifier gain. Hence, the spectrum width per 100 channels may be varied by changing the gain according to the needs of the specific problem.

The qualitative detection of such isotopes is still possible except in the case of a very small

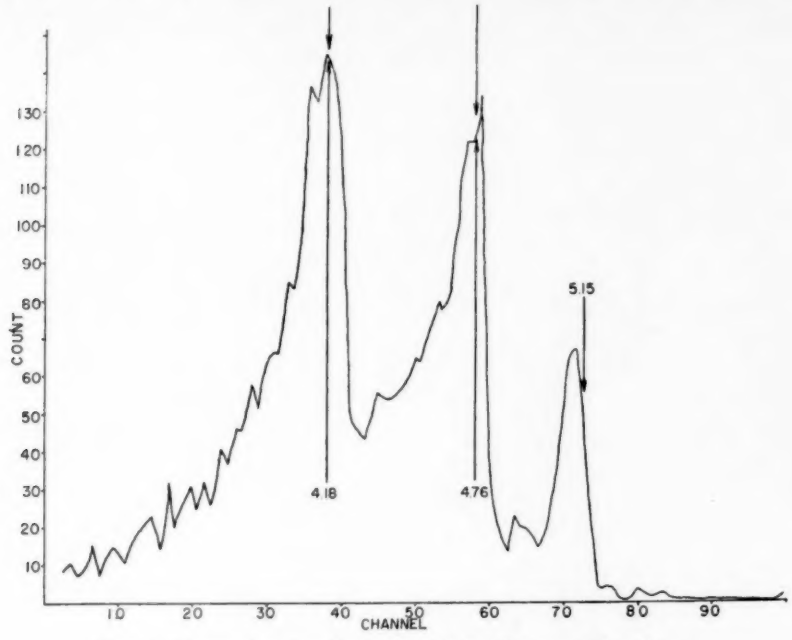

FIG. 5. Vegetation sample, 10 dis/min in 5½ hr counting time.

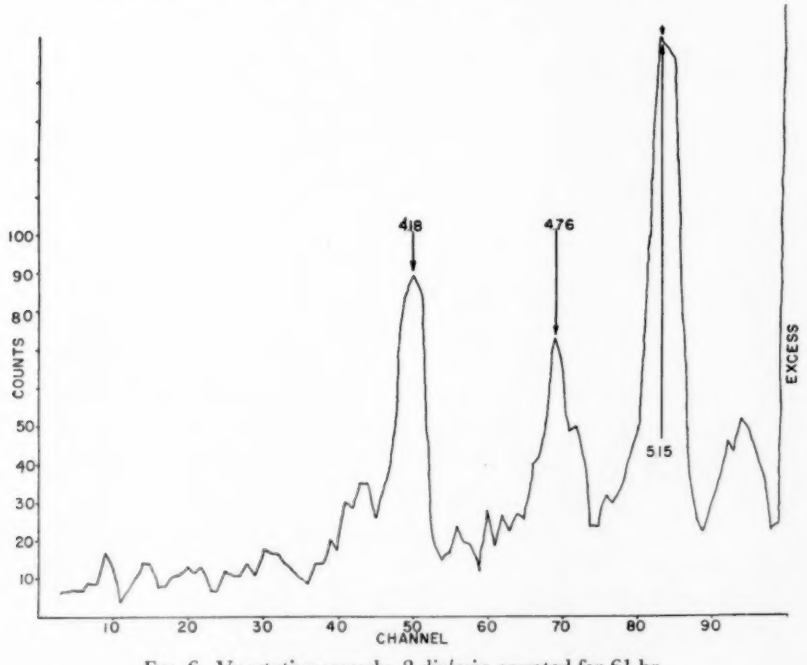

FIG. 6. Vegetation sample, 2 dis/min counted for 61 hr.

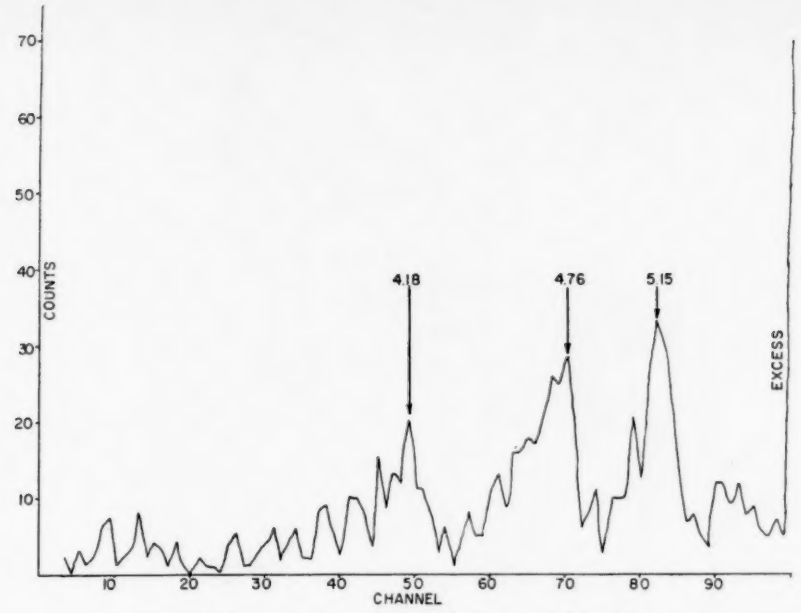

FIG. 7. Vegetation sample, 2 dis/min counted for 18 hr.

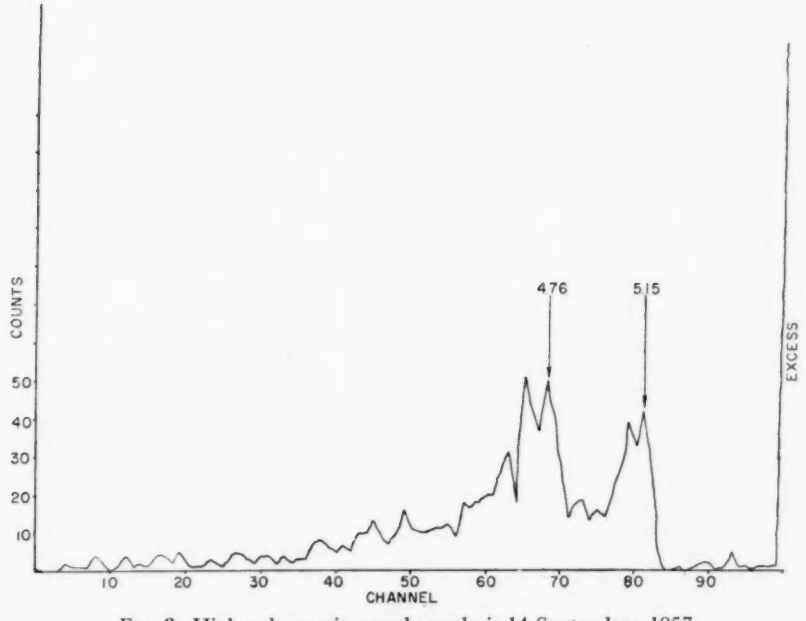

FIG. 8. High-volume air sample analysis 14 September, 1957.

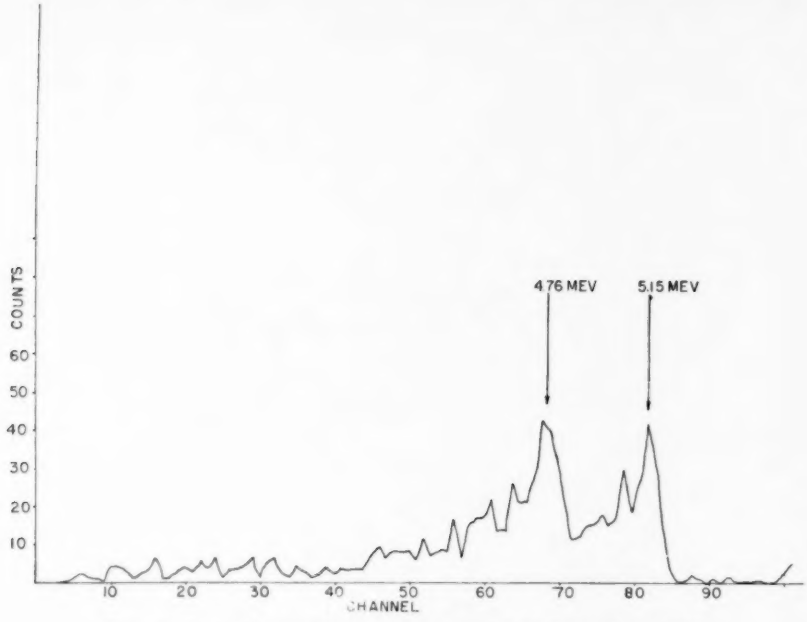

FIG. 9. Same air sample as Fig. 8 counted 17 September, 1957.

amount (activity-wise) of a lower energy α-count in the presence of a large amount of a slightly higher energy. In this case, the peak from the lower-energy α-count will be lost in the build-up of the other peak.

Another limitation in practice is that even slight changes in the pressure of the gas in the chamber will cause a shift of peak location. If this occurs while counting a sample, the effect will be to broaden the various peaks or decrease resolution.

CONCLUSIONS

Within the limitations mentioned above, α-pulse-height analysis provides a convenient method of identification and estimation of the α-emitters present in a sample. Its chief advantage lies in the minimal operator time required as compared with differential chemical analyses.

The method is extremely versatile. In addition to using it in environmental monitoring problems, it may be used as a tool in bioassay determinations, bioassay and analytical methods development, waste disposal problems, production development, and production control.

Acknowledgments—J. R. MANN, V. P. JOHNSON and W. H. TYREE of the Health Physics Electronics Group furnished technical advice on the instrument and prepared the drawings; S. HAMMONS, JR., of the Laboratory Group was responsible for collection of the analytical data used in this paper.

REFERENCES

1. E. L. GEIGER, *Health Phys.* **1,** 405 (1959).
2. E. B. EBERSOLE, A. HARBERTSON, J. K. FLYGARE, JR. and C. W. SILL, *Determination of Radium-226 and Thorium-230 in Mill Effluents.* Health and Safety Division of the Idaho Operations Office (1960).
3. J. R. MANN, 100-*Channel Pulse Height Analyzer Model H-100.* RFP-145 (1959).
4. H. L. MILLER, *Rev. Sci. Instrum.* **27,** 330 (1956).
5. H. I. Control Laboratory Routine Chemical Procedures, HW-20136 (1951).

Health Physics Pergamon Press 1961. Vol. 5, pp. 57–62. Printed in Northern Ireland

CRITICALITY ACCIDENT APPLICATION OF THE OAK RIDGE NATIONAL LABORATORY BADGE DOSIMETER

E. D. GUPTON, D. M. DAVIS and J. C. HART
Health Physics Division, Oak Ridge National Laboratory,* Oak Ridge, Tennessee

(*Received* 19 *January* 1960; *in revised form* 31 *March* 1960)

Abstract—Nuclear accidents have emphasized the need for a personnel meter with which the radiation dose may be determined accurately within a few hours. The badge-type dosimeter developed at ORNL fulfills this need. It contains an indium foil which permits the immediate segregation of anyone who may have had a medically significant dose of neutron radiation. A gold foil is used for thermal neutron measurement and sulfur is used for fast (>2.5 MeV) neutron measurement. To be meaningful the gold and sulfur measurements must be correlated with the Threshold Detector Units of the type reported by HURST. The film used in this badge is DuPont type 553 for β–γ measurement and Eastman Type A for neutron measurement. Provision is made in the badge for the incorporation of a chemical dosimeter and a silver phosphate glass dosimeter for the measurement of γ-radiation.

I. INTRODUCTION

RECENT nuclear accidents have emphasized the need for a personnel metering system which effectively and accurately determines, within a few hours, the neutron and γ-radiation dose received by persons in the vicinity of such accidents.

Although film dosimeters of various types have been used for many years, film dosimetry has some undesirable characteristics: the photographic emulsion is light sensitive, the response is photon energy dependent, and is relatively unstable under adverse circumstances. Fortunately, most of these objections have been minimized by the proper application of film dosimetry techniques. Energy dependence, which is probably the most difficult problem in film dosimetry, has been circumvented satisfactorily by using a system of filters properly arranged in a package or "badge" which contains a film packet.[1]

Most film dosimeter combinations include two packets of emulsions: one packet is used for β–γ dosimetry; the second for neutron dosimetry. Although β–γ dose estimates can be made over a wide range of several hundred rads, neutron dose estimates are limited to a maximum range of approximately 10 rads. Consequently neutron dose in excess of 10 rads must be determined by other methods.

In many cases the film dosimeter includes a security identification feature. This permits one device to serve two general functions—that of monitoring and that of security applications. This dual function is particularly advantageous in that it assures that the film dosimeter is worn by all personnel that are likely to be exposed to ionizing radiation.

The new ORNL Badge Dosimeter includes materials which permit measurement of moderate to high level neutron exposures and the immediate identification of those persons who may have received significant doses due to neutron and/or γ-radiation.

II. BADGE DESCRIPTION

Model I of the ORNL badge dosimeter introduced at ORNL in the spring of 1958 utilizes a case of butyrate plastic and, when fully assembled, weighs approximately 33 g. The over-all dimensions of the badge assembly are approximately $2\frac{1}{2}$ in. $\times$ $1\frac{3}{4}$ in. $\times$ $\frac{5}{16}$ in. This model provides a compartment for two dosimeter films and a slide arrangement for film containment. There are four filters in the front

* Operated by Union Carbide Corporation for the U.S. Atomic Energy Commission.

of the badge as follows: (1) A combination filter of 0.020 in. plastic, 0.015 in. cadmium, 0.005 in. gold, 0.015 in. cadmium and 0.012 in. plastic, in that order; (2) a combination filter consisting of 0.020 in. plastic, 0.040 in. aluminum and 0.012 in. plastic; (3) a third filter of 0.082 in. plastic; and (4) a "window" of 0.020 in. plastic. There are two filters in the back of the badge which include: (5) a combination filter of 0.052 in. plastic and 0.010 in. lead; and (6) a single filter of 0.062 in. plastic. A $\frac{1}{2}$-g rod of elemental sulfur and a $\frac{7}{16}$-in. diameter, 0.005-in. thick gold foil are in a cavity in the slide. An indium foil, $1\frac{1}{4}$ in. $\times$ $\frac{1}{4}$ in. $\times$ 0.015 in. thick and perforated with an identification number, is located in the front of the badge. The laminated security pack (see Fig. 1) completes the assembly.

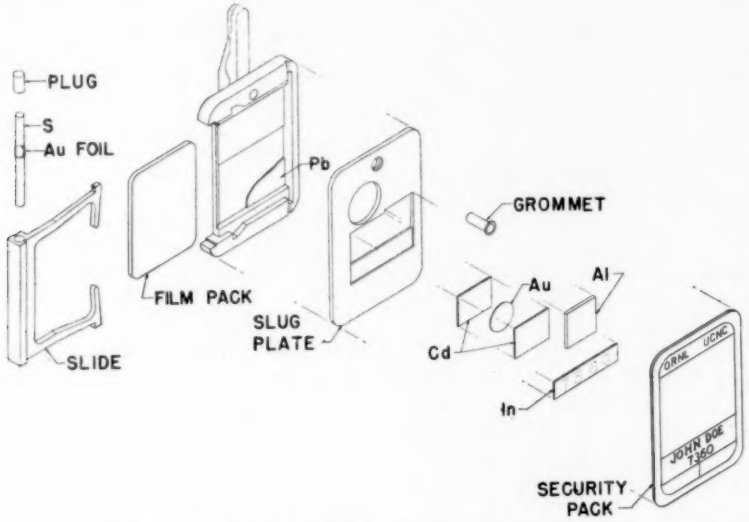

FIG. 1. Model I of the ORNL badge dosimeter (1958).

Model II of the ORNL badge dosimeter (Fig. 2) replaced Model I. It includes certain "convenience" features: (1) a tamper-proof insert with a magnetically operated latch, (2) a sulfur pellet rather than a sulfur rod, (3) provisions for chemical and silver phosphate glass dosimeters, (4) the capability of parts salvage for re-issue and (5) convenience features which allow increased efficiency in assembly.

III. DOSIMETRY APPLICATIONS

The four filters in the front of the badge and the two filters behind the film packets provide data to determine the β–γ dose.[2] DuPont packet 553 is used and is found to have a normal "hard" γ-dose range of 0.030–500 rads. Routine neutron dosimetry is accomplished through use of Eastman Type-*A* film which is found to have a maximum usable range of approximately 0.020–10 rads from 3 MeV neutrons.[3] The ability to interpret high level neutron exposures depends upon concurrent use of stationary Threshold Detector Units (TDU) developed by HURST *et al.*[4] The TDU provides an estimate of the neutron spectra in five energy regions. The thermal flux is determined by the difference in activation between two gold foils, one of which is surrounded by cadmium. The fast flux and energy distribution are determined by fission and activation analyses of Pu^{239}, Np^{237}, U^{238} and a S^{32} pellet which together provide measurements of the flux above 1 keV, 0.75 MeV, 1.5 MeV and 2.5 MeV, respectively. The total neutron dose is calculated from the flux determination.

Fig. 3 shows the fission cross-sections of Pu^{239}, Np^{237} and U^{238}, and the S^{32} (n, p) P^{32} cross-section. To avoid thermal neutron activation of the Pu^{239}, Np^{237} and U^{238}, a B^{10} "shield" (Fig. 4) is used. The B^{10} shield presents the same thickness to any incident neutron. The cavity is lined with 0.025 in. cadmium to capture neutrons which may be moderated by the boron.

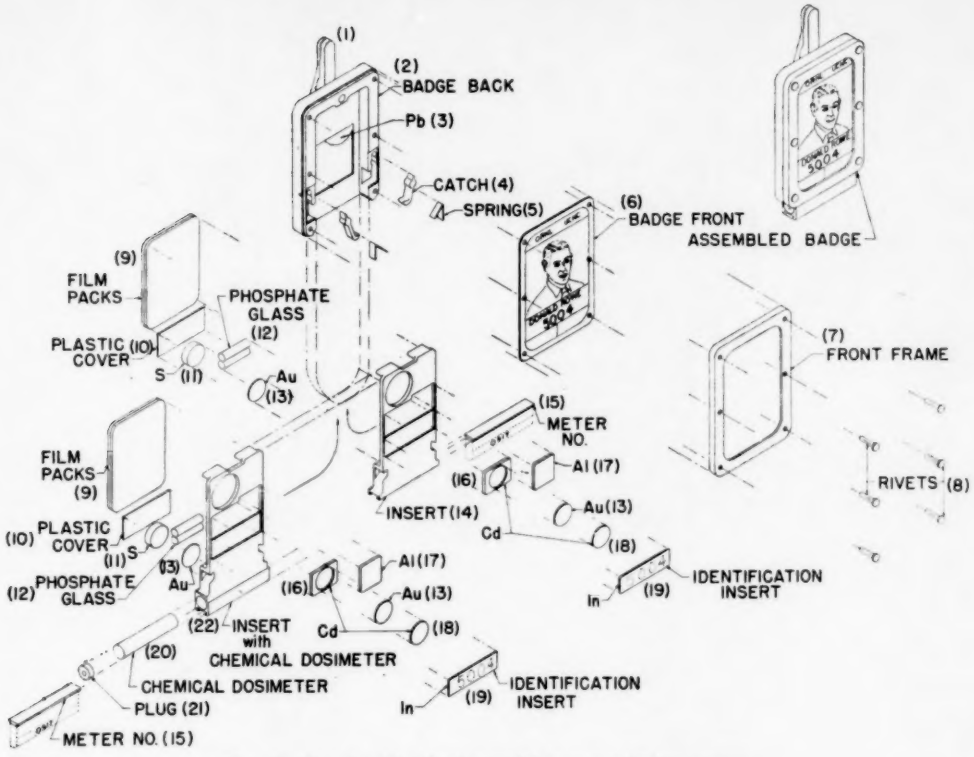

FIG. 2. New health physics multi-purpose badge meter.

TDU's, along with γ-radiation dosimeters, are located in fixed positions in areas where nuclear accidents are considered possible. They are placed so that the neutron and γ-environment of the accident may be reconstructed. The sulfur and gold components of the badge are activated by neutrons such that counting techniques permit determination of the thermal neutron exposure from the two gold foils, and high energy (greater than 2.5 MeV) neutron exposure from the sulfur. The counting procedures are performed with the same counters used with TDU analysis. Exposure to intermediate energy neutrons is determined by normalizing the data from the badge to that of the TDU located in the vicinity of the badge wearer, or by fitting the data from the badge to the spectrum at the point of exposure, if such is known.

IV. LIMITATIONS

The badge alone is not an absolute neutron dosimeter; however, the dose to the badge may be determined, and the badge is closely associated with the person on whom it is located. The interpreted dose will be a function of the relative orientation of the badge with respect to the source of radiation. In theory, the badge accompanies the person throughout the exposure interval and receives a dose proportional to that received by the person. Errors in dosimetry due to lack of knowledge of relative orientation during exposure of source, person and badge can be reduced by increasing the number of dosimeters on the person. However, there are administrative problems associated with wearing multiple badges. One proposed supplement to the badge and TDU system includes a belt which contains, in its structure, small detectors which would be located at 60 to 90° intervals about the midsection of the wearer. The belt affords information which would permit a more accurate determination of tissue doses. When used alone, the badge should be worn in the

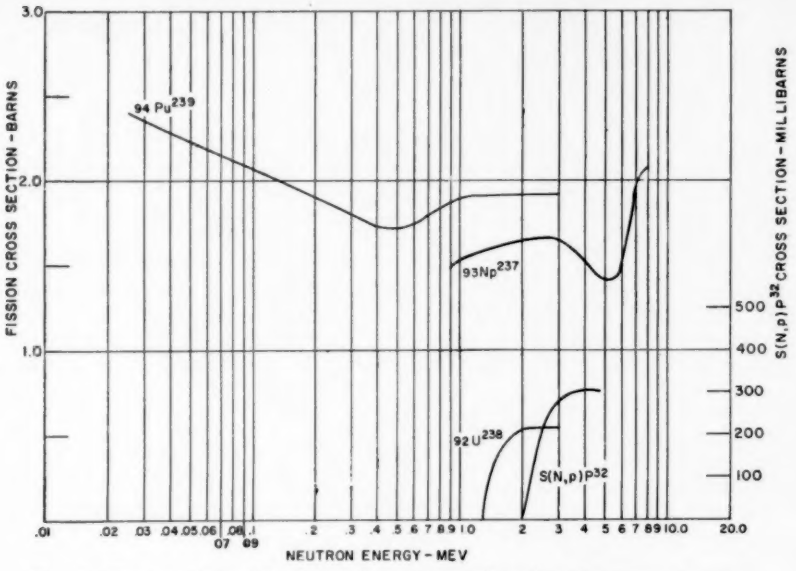

FIG. 3. Cross-section of threshold detector as a function of neutron energy.

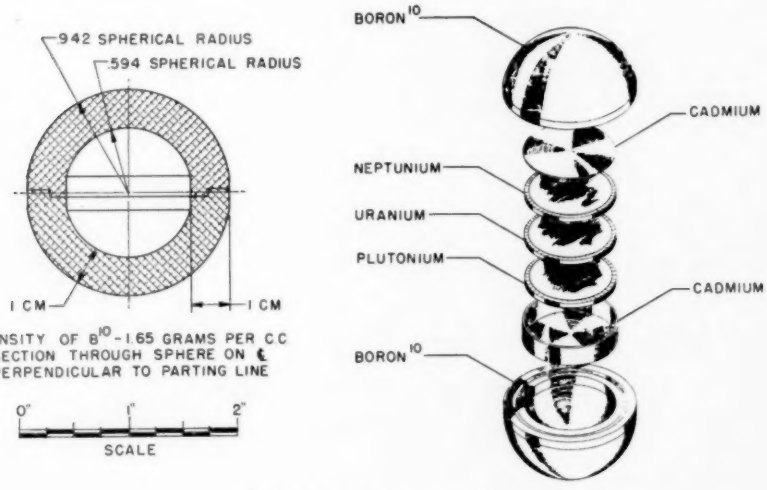

FIG. 4. Boron shield.

chest region because of the reduced attenuation by the thoracic cavity and because of proximity to the lens of the eye.

V. EMERGENCY PROCEDURE

Immediately following a nuclear incident, those persons who may have received a significant exposure to neutrons may be segregated easily by measuring the radiation of the activated indium foil in the badge. (Indium-115, which constitutes 96 per cent of that occurring naturally, has a thermal neutron activation cross-section of 145 barns. The resulting In^{116} has a half-life of 54 min.)[5] Experimental work

performed by ORNL Applied Health Physics Sections indicates that the badge containing approximately 0.4 g of indium will show a sizeable response on a G–M survey meter for at least 3 hr following a neutron exposure which includes 2 or more rads of thermal neutrons incident upon the body. Dose rate readings obtained from two commonly used survey-type instruments following neutron exposures are shown in Table 1.

Table 1. *Badge dose rate readings resulting from neutron exposures*

Neutron exposure	First Collision dose (rads)	Multiple* Collision Dose (rems)	Instrument reading at "contact" with badge in mr/hr (radium equivalent)			
			$H+1/2$ hr	$H+2$ hr	$H+3$ hr	$H+6$ hr
$10^{11} n_t/cm^2$	2 ± 0.2	200	150†	40†	20‡	3‡
100 rads n_f + $10^{11} n_t/cm^2$	102 ± 5	1200	220†	70†	20‡	5‡
$10^9 n_t/cm^2$	0.02 ± 0.002	2	12‡	3‡		

* Peak dose inside body.[6]

† Readings taken with ORNL Cutie Pie.

‡ Readings taken with Victoreen model 389C probe, shield closed; the shield open to shield closed reading ratio was 2 to 1.

Note: The counting rate, with the TDU counter, of the bare gold foil, 24 hr after exposure to $10^{11} n_t/cm^2$, is approximately 50,000 c/m.

Badges were exposed in the ORNL Graphite Reactor to obtain the exposures noted, which were determined from coincident exposure of foils and threshold detectors. The first collision rad doses were obtained from NBS Handbook 63.[6] The instrument readings were obtained with the indicated instruments at times subsequent to the mean time of exposure (H) in hours.

As soon as possible, badges of all persons who may have been involved are monitored with a portable G–M survey meter. Based upon counting rates and elapsed time since the incident, persons whose badge reading indicate an exposure greater than 25 rads are referred to the Medical Unit as "significant" exposure cases. Further analysis of the films, foils, etc., in the badge will be started immediately in order that some measure of the dose may be determined early. Normally, a film processing laboratory such as that maintained at ORNL can identify dosimetry films exposed in excess of 5 rads of γ-radiation at a rate of 500 or more per hour. Blood sodium activation analyses may be initiated by medical personnel at this time.

When fully developed and made available for such applications, γ-dosimeters (of the chemical or phosphate glass type) will be provided and used in the procedure for rapidly determining the highly exposed individuals.

VI. SUMMARY

The ORNL badge is a small, lightweight, durable, personal dosimeter. It weighs approximately 33 g, fully loaded, and the dimensions are approximately $2\frac{1}{2}$ in. $\times$ $1\frac{3}{4}$ in. $\times$ $\frac{5}{16}$ in.

The badge utilizes films for routine monitoring and films plus foils, phosphate glass and chemical dosimeters for high level (accidental) exposures. Indium and gold are used as indicators for exposures following neutron accidents. For neutron dosimetry, the badge must be supplemented with Threshold Detector Units. The combined dosimetry and security features of the badge minimize administrative problems.

REFERENCES

1. E. D. Gupton, *Radiology* **66,** 253 (1956).
2. Applied Health Physics Semi-Annual Report, July-December, 1956, Oak Ridge National Laboratory, CF 57-1-173.
3. J. S. Cheka, *Nucleonics* **12,** No. 6, 40 (1954).
4. G. S. Hurst, J. A. Harter, P. N. Hensley, W. A. Mills, M. Slater and P. W. Reinhardt, *Rev. Sci. Instrum.* **27,** 153 (1956).
5. *Neutron Cross Sections*, AECU-2040 (1952).
6. *Protection Against Neutron Radiation up to 30 Million Electron Volts*, NBS Handbook 63. U.S. Dept. of Commerce (1957).

Health Physics Pergamon Press 1961. Vol. 5, pp. 63–69. Printed in Northern Ireland

ANALYSIS OF THE HAZARDS ASSOCIATED WITH RADIOACTIVE FALLOUT MATERIAL—I
ESTIMATION OF γ- AND β-DOSES

A. BROIDO* and J. D. TERESI†
U.S. Naval Radiological Defense Laboratory
San Francisco, 24, California

(*Received* 26 *October* 1959; *in revised form* 21 *May* 1960)

Abstract—An estimate of the contact β-dose-rate and the γ-dose-rate both at the surface and within the body due to radioactive fallout contamination was made. The γ-dose-rate at external distances of from 0.01 to 30 cm from the contaminated body surface was estimated and correlated with the associated surface β-dose-rate. The surface-β-dose to an individual contaminated to the same extent per unit surface area as the surrounding field was compared to the γ-dose at 1 m above the surrounding area. For the case in which there is one photon of 1 MeV energy per disintegration the surface β- dose was found to be about forty times the γ-dose at 1 m above the infinitely large contaminated field.

INTRODUCTION

WHEN a person is exposed to radioactive fallout from a nuclear detonation, he will be contaminated with materials which emit both β- particles and γ-rays. An estimate of the contact β-dose-rate and the γ-dose-rate to the individual both at the surface and within the body appears necessary in evaluating total contamination hazards to personnel. An estimate of the γ-dose-rate at external distances of 0.01 to 30 cm from the body surface is also of importance in correlating measured γ-dose-rate with the associated surface β-dose-rate. Such estimates would permit assessing the contact β-dose to personnel on the basis of γ-ray surveys made at various distances from the surfaces of the body.

SURFACE β-DOSE-RATE AS A FUNCTION OF SPECIFIC ACTIVITY

The surface β-dose-rate may be estimated, both experimentally and theoretically, assuming a uniform distribution of contamination over a 1 cm^2 plane surface.

* Present address: California Forest and Range Experiment Station, P.O. Box 245, Berkeley 1, California.

† The opinions or assertions contained in this article are the private ones of the writer and are not to be considered as official or reflecting the views of the Navy Department or the Naval Service at large.

Experimental

An estimate of the surface β-dose-rate from a known concentration of fission product activity may be made on the basis of experimental results with the 14*d* radioisotope, P^{32} (average β-energy = 700 keV). Although P^{32} is not a fission product, its β-ray spectrum is usually regarded as a reasonable approximation of the spectrum from fresh mixed fission products.[1] In determining the surface dose-rate for a plane surface contaminated with P^{32} at a concentration of 1 μc/cm^2, LOW-BEER[2] obtained a value of 5.05 reps/hr. For a similar experiment, RAPER *et al.*[3] obtained 5.95 reps/hr. The average of these two values, 5.5 reps/hr probably represents a reasonable approximation of the dose-rate produced at a surface by 1 μc/cm^2 of fresh fission product contamination.

Theoretical

A theoretical calculation of the dose-rate from 1 μc/cm^2 of mixed β-contamination depends upon an estimation of the exact energy distribution of the β-radiation. The dose-rate is a function of the number of ion pairs per centimeter produced by each disintegration. The specific ionization, I, for β-radiation varies inversely with the square of the velocity of the β-particle (in terms of the velocity of light) and is quite well represented for electrons between 0.06 and 1.6 MeV by the simple relation

*Table 1. Velocity and specific ionization for electrons of various energies**

β-Energy E (MeV)	Velocity, v (fraction of the velocity of light, c)	Specific ionization, I (ion pairs/cm of air)
0.0001	0.0198	0
0.00015	0.024	7700(maximum)
0.01	0.195	1100
0.05	0.413	260
0.1	0.548	150
0.5	0.863	60
1.0	0.941	50
2.0	0.979	45
3.0	0.989	45
4.0	0.993	45
5.0	0.996	45

* Values taken from FRIEDLANDER and KENNEDY[5].

$I = 45/v^2$ ion pairs per cm of dry air at 20°C and 1 atm. At energies above 1.5 MeV ($3m_0c^2$), theory predicts that the ionization losses should rise very slowly, by only 60 per cent between 1.5 and 500 MeV (approximately in proportion to the logarithm of the energy).[4] The relationship between I, v and the energy of the electron is given in Table 1.

To obtain the actual ionization produced above a uniformly contaminated surface, a folding factor must be applied to account for the tortuous path of the β-particle. According to PARKER[6] the number of ion pairs per centimeter of linear path in air produced by fast β-particles is 75. From this number and the definitions of the microcurie and the roentgen equivalent physical, one may calculate

$$I_\beta = \frac{(75)\ (3.7 \times 10^4)\ (3600)}{2(2.083 \times 10^9)} A_d = 2.4\mathrm{A}_d \tag{1}$$

where

I_β = β-surface-dose-rate (reps/hr)

A_d = the activity of the fission-product contamination (μc/cm^2)

It may be seen that this value, calculated for fast β-particles, is appreciably less than the experimental value obtained with P^{32}. However, since P^{32} (and mixed fission products) contain a considerable proportion of low-energy β-particles, the total ionization produced is expected to be somewhat higher* than the value using 75 ion pairs/cm. To correspond to the experimental value of 5.5 reps/hr for 1 μc/cm^2, the specific ionization of the β-mixture would have to be about 170 ion pairs/cm of linear path. Such a value corresponds to the ionization which would be produced by monoenergetic β-radiation of about 0.2 MeV. As would be expected, this energy value is considerably lower than the average energy of the β-particles from either P^{32} or a fission mixture. In the production of surface ionization, the importance of the low-energy β-particles is increased considerably out of proportion to the number of such particles. If one considers the effect of low-energy β-particles in this way, it would seem that the experimental value for the surface dose-rate for fission-product β-contamination as obtained from the equation

$$I_\beta = 5.5A_d \tag{2}$$

is not unreasonable.

γ-DOSE-RATE ESTIMATES

Estimates are presented here of the internal, surface and external γ-dose-rate produced by radioactive substances deposited uniformly on a human body. Equations are presented in the form

$$I_\gamma = \mu_E k f(\mu) A E \tag{3}$$

where μ_E = Klein–Nishina energy absorption coefficient (3.5×10^{-5} cm^{-1} used in this report)

I_γ = dose-rate (r/hr)

k = a constant (1.44×10^{-5} r/MeV times 1.332×10^8 dis/hr per μc)

$f(\mu)$ depends upon the total linear absorption coefficient

A = the specific activity (μc/cm^2)

E = the γ-energy (MeV/photon)

Such an equation is strictly applicable only for

* If one takes the experimental spectrum of P^{32} and extrapolates to zero energy on a Fermi plot, one obtains a value slightly greater than 100 ion pairs/cm. However, the actual value would be greater than this calculated value because of degradation to lower β-energies by the finite mass of the source.

the case of a monoenergetic γ-emitter. However, except in a few special cases considered below, $\mu_E f(\mu)$ is constant within 10 per cent for γ-energies from 0.2 to 1.5 MeV. Thus, equation (3) may be rewritten in the form

$$I_\gamma = KAE \tag{4}$$

in which $K = \mu_E k f(\mu)$.

For atomic-bomb debris, an average γ-ray energy may be used as an approximation to the true γ-energy distribution of the radioactive mixture. Equation (4) may then be replaced by either of the following two equivalent equations:

$$I_\gamma = KA_\gamma \bar{E}_\gamma \tag{4a}$$

or

$$I_\gamma = KA_d \bar{E}_d \tag{4b}$$

where

$\bar{E}_\gamma$ = average γ-energy per photon
A_γ = γ specific activity
$\bar{E}_d$ = average γ-energy per radioactive disintegration
A_d = specific activity of mixed atomic-bomb debris

The universal equivalence of equations (4a) and (4b) must be maintained, for if N is defined $N = A_d/A_\gamma$, then $\bar{E}_\gamma = N\bar{E}_d$ by definition, and $A_\gamma E_\gamma = A_d \bar{E}_d$.

Dose-rates at the center of a contaminated body

The dose-rate at the center of the human body was estimated in two ways: by representing the human form first as a cylinder of water, and second as a rectangular block of water. Water is expected to be a reasonable simulant since the density of the human body is almost unity. The values obtained by these two methods agree within about 15 per cent of the average of the two values.

Dose-rate at center of cylinder of water 15 cm *in radius and* 200 cm *in height*

The dose-rate at the center of a cylinder of water of radius of 15 cm and length 200 cm, the surface of which is uniformly contaminated with a monoenergetic γ-emitter, may be obtained from TERESI and BROIDO[7]:

$$I_\gamma = \mu_E k\ AE \left\{ \int_0^{\phi_1} (e^{-\mu R \sec\phi})\, d\phi - \boldsymbol{Ei}(-\mu L) + \boldsymbol{Ei}\left[-\mu\sqrt{(L^2 + R^2)}\right] \right\} \tag{5}$$

where

$\mu_E k = (3.5 \times 10^{-5})(1.44 \times 10^{-5})(1.332 \times 10^8) = 6.7 \times 10^{-2}$
L = semi-length of the cylinder = 100 cm
R = radius of the cylinder = 15 cm
$\phi_1 = \tan^{-1} L/R = 81.5°$
μ = total linear absorption coefficient of water (7×10^{-2} cm^{-1} for a 1-MeV gamma)
$\phi = \tan^{-1} l/R$, where l is the distance along L
I_γ, A and E have been previously defined and $-\boldsymbol{Ei}(-w)$ is the actual mathematical notation for the exponential integral

$$\int_w^\infty \frac{e^{-y}}{y}\, dy$$

in which, for this case,

$y = \mu L \sec\psi$, where $\psi = \tan^{-1} r/L$ and r is the distance along R

Substituting numerical values, equation (5) reduces to

$$I_\gamma = 0.02AE \tag{6}$$

Dose-rate at the center of a 40 × 20 × 200 cm *rectangular block of water*

The center is irradiated by contamination uniformly distributed over two rectangles 200 × 40 cm, 10 cm from the center; two rectangles 200 × 20 cm, 20 cm from the center; and two rectangles 20 × 40 cm, 100 cm from the center. Because of their small size and their distance from the center, the last two rectangles (the top and bottom of the rectangular phantom) contribute a negligible amount to the total dose. To take advantage of established equations of radiation intensity from contaminated circular disks given in the literature,[8] the other four rectangles were converted to equivalent circles by using a method found suitable for rectangles having dimensions encountered here. This method involves the use of a harmonic mean

technique to obtain the radius of the equivalent circle represented as follows:

$$R = \frac{2ab}{a+b} \tag{7}$$

where

R = radius of equivalent circle
a = half the length of the rectangle
b = half the width of the rectangle

Thus, for the 40 × 200 cm rectangle,

$$R_1 = 33.4 \text{ cm}$$

and for the 20 × 200 cm rectangle,

$$R_2 = 18.2 \text{ cm}$$

Using the equations given by PARKER[6], the following expression for the dose-rate at the center of the rectangular block of water may be obtained:

$$I_\gamma = AE\left(2(3.35\times10^{-2})[\boldsymbol{Ei}\{-\mu_w\sqrt{(h_1{}^2 + R_1{}^2)}\} - \boldsymbol{Ei}(-\mu_w h_1)] + 2(3.35\times10^{-2}) \times [\boldsymbol{Ei}(-\mu_w\sqrt{(h_2{}^2 + R_2{}^2)} - \boldsymbol{Ei}(\mu_w h_2)]\right) \tag{8}$$

where h_1 and h_2 are the perpendicular distances from sides to center. Substituting numerical values,

$$I_\gamma = 0.027AE \tag{9}$$

Dose-rates at various distances from the surface of the body

For the determination of the γ-dose-rate at the surface and at various distances from the surface, the technique described above is used. In the second case, the absorbing medium is air and the absorption coefficient of air (8×10^{-5} cm^{-1} for a 1-MeV gamma) is substituted for the absorption coefficient of water. The equations break down where $h = 0$; therefore the surface dose must be approximated by assuming a reasonably small value for h. Since the non-sensitive, outer, cornified layer of human skin is approximately 0.1 mm thick, this distance was chosen for the approximation to the surface dose. For this distance, the calculation was made using μ for both air and for water. The latter value gives an estimate of the dose to the sensitive papillary layer of the skin. The calculation may be illustrated for a height 0.01 cm above the front or back surface ($R_1 = 33.4$ cm) as follows:

$$I_\gamma = 3.35\times10^{-2}AE\,[\boldsymbol{Ei}\{-\mu_a\sqrt{(h^2 + R^2)}\} - \boldsymbol{Ei}(-\mu_w h)] \tag{10}$$

Substituting numerical values, $I_\gamma = 0.27AE$, in which $0.27 = K$ of equation (4). The contribution from the opposite and adjacent sides was found to be negligible (<5 per cent). Values of K for an internal distance of 0.01 cm and seven external distances ranging from 0.01 to 100 cm from the two sizes of rectangles comprising the phantom were calculated and are tabulated in Table 2.

Table 2. Values of K as a function of distance from a rectangular phantom

$R_1 = 33.4$ cm (rectangle = 40 × 200 cm)		$R_2 = 18.2$ cm (rectangle = 20 × 200 cm)	
h (cm)	K	h (cm)	K
−0.01 cm*	0.22	—	0.22
0.01	0.27	0.01	0.25
0.1	0.19	0.1	0.17
5	0.064	5	0.044
15	0.029	15	0.015
20	0.022	20	0.010
30	0.013	30	0.0051
100	0.0017	100	0.00055

* 0.01 cm within surface.

γ-Ray doses from contaminated circular areas of various sizes

The estimates given in the previous paragraph are based on the assumption that the contamination is distributed uniformly over the surface of the body. In the practical case the activity will most probably not be uniformly distributed, but rather will concentrate in certain collecting regions such as the neckline and the beltline. Consequently, it is of interest to calculate how such nonuniform distribution

will influence a survey measurement of a contaminated individual. For an estimation of this effect a survey distance of 15 cm (approximately 6 in. from the body) was assumed, and the contamination was assumed to be localized in circular areas of various restricted sizes. In Table 3 are values of K (as previously defined) for contaminated circles of radius ranging from 2 to 10 cm. Also shown are the two equivalent circles representing uniform contamination over an entire side or front surface of the rectangular phantom.

As can be seen in Table 3, a change in radius from 2 cm to the radius representing the large side of the rectangular phantom (33.4 cm) changes the dose-rate by a factor of 100 (0.3×10^{-3} to 29×10^{-3} r/hr for unit specific activity and for 1 MeV).

Dose-rates from a large contaminated field

Routine measurements of fallout dose-rates are made at a height of 1 m above the surface of the contaminated area, using an instrument which measures only γ-radiation. It is of interest to estimate such a dose-rate in terms of the concentration of active material on the area. This estimate may then be used to show the relation between doses from body contamination and from extended contaminated areas (infinite field) occupied by contaminated personnel. The dose-rate at 1 m above a large homogeneously contaminated plane is given by

$$I_\gamma = 3.35 \times 10^{-2} AE[-\boldsymbol{Ei}(-\mu_a h)] \quad (11)$$

In this case, the value for K changes approximately 40 per cent in going from 0.2 to 1.5 MeV

Table 3. Values of K for contaminated circular areas of various sizes

Radius (cm)	$K \times 10^3$
2	0.3
4	1.1
6	2.9
10	5.7
18.2	15
33.4	29

Table 4. Values of K as a function of γ-energy for the case of contamination distributed over an infinite field

E_γ (MeV)	K at surface of individual	K at center of individual
0.2	0.11	0.019
0.5	0.13	0.031
1	0.14	0.050
1.5	0.15	0.069

γ-energy. The values are listed on Table 4 for various energies.

Values given in column 2 of Table 4 are related to the dose-rate on the surface of the contaminated individual. In calculating the dose-rate within the body due to radiation emanating from a contaminated field, one may assume exponential absorption following the equation

$$I_\gamma = I_s e^{-\mu d} \quad (12)$$

where

I_s is the surface dose
μ is the absorption coefficient of water
d is the distance from the surface of the body to the center

Values of K for γ-radiation of various energies representing the dose at the center of a cylindrical body 15 cm in radius are given in column 3 of Table 4.

INTERRELATIONSHIPS

It is of interest to compare the γ-dose-rates to which an individual would be exposed from surface and field contamination. Also of interest is the comparison of the β- and γ-dose-rates* associated with body surface contamination. Since it is extremely difficult to measure the surface β-dose directly, it is of particular interest to be able to estimate the surface β-dose from γ-dose measurements.

Relative importance of surface and field γ-dose-rate

As may be seen from comparison of the values of K given above, the value of the surface dose-rate due to contamination of the individual is

* In this paper we are considering only the β- and γ-dose rates, not the relative hazards (see BROIDO[9]).

comparable with the dose-rate from an infinitely contaminated field (in fact, for equal specific activities, it is somewhat higher than this dose-rate). Within the body it may be seen that, except for the softest γ-rays, the dose-rate is appreciably higher as a result of radiation from a large contaminated field than from contamination of the entire surface of the body with activity at the same concentration. The value of the dose-rate from body contamination becomes even less important for the realistic situation in which personnel are not uniformly contaminated over the body surface. For example, if half the total body surface is contaminated (a reasonable maximum), the dose to the center from body contamination would represent only 15–35 per cent of the total γ-dose to the center. In most cases, the contamination will be distributed over relatively small areas of the body surface so that the total body γ-dose from body contamination is expected to be small compared with the dose from the large contaminated field.

Estimation of surface β-dose-rate from γ-measurement

For this purpose it is necessary to know the value of N, the number of β-disintegrations per γ-photon emitted. For the calculations presented here, N will be assumed to be unity. A common estimate[8] of N for several-day-old fission-bomb debris is approximately 2. For these cases the ratio of β–γ dose calculated below should be doubled.

(a) *Surface β-dose from γ-dose* 1 m *above large field.* If one assumes that an individual caught in a contaminating event is contaminated to the same extent as the surrounding field (that is, that the contamination per square centimeter on the individual is identical with that in the general field), the routine γ-survey data may be used to estimate the surface β-dose to which such an individual will be exposed. Assuming $N = 1$ and $E_\gamma = 1$ MeV, one may calculate that

$$\frac{I_\beta}{I_\gamma^\infty} = \frac{5.5A}{0.14A} \simeq 40 \qquad (13)$$

Thus the β-dose at the surface of the contaminated individual would be approximately forty times the γ-dose measured 1 m above the infinitely large contaminated field.

(b) *β–γ dose on the front surface of a contaminated individual.* Making the same assumptions as in the paragraph directly above, one may calculate the ratio of β–γ surface dose due to contamination on the front (or back) surface of an individual to be

$$\frac{I_\beta}{I_\gamma} = \frac{5.5A}{0.27A} \simeq 20 \qquad (14)$$

Comparison of β-dose with total γ-dose. From the ratios given above, it is seen that an individual, uniformly contaminated in an extended contaminated field, who receives a surface γ-dose from the field of D_γ^∞, will receive, also, a surface γ-dose from the material deposited on his body of about $2D_\gamma^\infty$. The total γ-dose at the surface of the body, then, during his stay in the contaminated field, will be three times the integrated γ-reading obtained at 3 ft from the contaminated plane. Under these conditions, the beta surface dose is expected to be only about thirteen times the total surface γ-dose. It must be pointed out, however, that for the 1 MeV gamma, the dose to the center of the body from body contamination is only about half the dose to the center from a large contaminated field. Consequently, the effective γ-dose to uniformly contaminated personnel in a contaminated field would be approximately 1.5 D_γ^∞. The γ-contribution of body surface contamination would decrease even further for the expected case of only partial body contamination.

REFERENCES

1. F. S. Goulding and G. Cowper, *Hazard due to Beta Radiation from Fission Products Deposited on the Ground After an Atomic Explosion.* CREL-529, Atomic Energy of Canada Limited (1953).
2. B. V. A. Low-Beer, *Radiology* **47,** 213 (1940).
3. J. R. Raper, R. E. Zirkle and K. K. Barnes, *Biological Effects of External Beta Radiation* (Edited by R. E. Zirkle) Chap. 1. McGraw-Hill, New York (1951).
4. R. D. Evans, *Advances in Biological and Medical Physics* (Edited by J. H. Lawrence and J. G. Hamilton) Vol. 1, pp. 151–221. Academic Press, New York (1948).
5. G. Friedlander and J. W. Kennedy, *Introduction to Radiochemistry.* John Wiley, New York (1949).

6. H. M. PARKER, *Advances in Biological and Medical Physics* (Edited by J. H. LAWRENCE and J. G. HAMILTON) Vol. 1, pp. 223–285. Academic Press, New York (1948).
7. J. D. TERESI and A. BROIDO, *Estimation of the Gamma Dose Associated with Radioactive Fallout Material.* TM 18, U.S. Naval Radiological Defense Laboratory (1954).
8. *The Effects of Atomic Weapons* (Revised Edition). U.S. Government Printing Office, Washington, D.C. (1950).
9. A. BROIDO, *Nucleonics* **13,** No. 3, 82 (1955).

Health Physics Pergamon Press 1961. Vol. 5, pp. 70–78. Printed in Northern Ireland

OPTIMIZATION OF RADIONUCLIDE REMOVAL FROM LOW-LEVEL PROCESS WASTES BY THE USE OF RESPONSE SURFACE METHODS

D. A. GARDINER and K. E. COWSER
Mathematics Panel and Health Physics Division, Oak Ridge National Laboratory*
Oak Ridge, Tennessee

(*Received* 21 *June* 1960)

Abstract—The principles of response surface methodology, and in particular the method of the path of steepest ascent, have been employed in an attempt to discover those combinations of: (a) dose of Grundite clay, (b) particle size of clay, (c) excess soda ash and (d) proportion of stoichiometric requirement for lime, which will remove the greatest amounts of Cs^{137} and Sr^{90} from ORNL process wastes.

The method of steepest ascent is a relatively new statistical technique which is applicable to experimentation in which the variables are measureable on a continuous scale. As such it is particularly useful for optimizing chemical processes and in fact found its first application in the chemical industry.[1] This paper describes a successful application of the technique to the optimization of radionuclide removals by a chemical process.

Laboratory experiments performed to date in accordance with these principles have led to combinations of the treatment variables which remove up to 95 per cent of the Cs^{137} and 96 per cent of the Sr^{90}. The largest removal of Cs^{137} occurred at 600 p.p.m. clay of 200-mesh, 470 p.p.m. of excess soda ash and 1.4 times the stoichiometric amount of lime. The removal of Sr^{90} was largest at 360 p.p.m. clay of 200-mesh, 520 p.p.m. excess soda ash and 2.5 times the stoichiometric amount of lime.

INTRODUCTION

At the Oak Ridge National Laboratory, a waste treatment plant for the processing of low-level wastes in large volume has been in operation since 1957. The plant has been successful in substantially reducing the amount of radioactivity contained in the waste material discharged into the surrounding area.[2] In an effort to improve the process further, an exploratory program of laboratory experimentation was conducted, the object of which was to locate the optimum point of operation for the waste treatment plant. This paper is an account of the experimental program.

1. THE WASTE TREATMENT VARIABLES

At ORNL the waste treatment plant is designed to process wastes by a lime-soda softening principle. To the radioactive wastes are added lime and soda ash for the purpose of removing Sr^{90}, and, for removing Cs^{137}, certain amounts of clay are added to facilitate precipitation.

The variables in the experimental program were accordingly:

(i) lime added, as a proportion of the stoichiometric requirement;
(ii) excess soda ash (in p.p.m.);
(iii) p.p.m. of clay per dose;
(iv) particle size of clay added.

The plant will also accommodate the addition of doses of calcium chloride to the influent and can be operated by recycling sludge through the system. In a previous series of experiments, however, calcium chloride dose and recycled sludge appeared to exert little influence on the removal of Sr^{90} and Cs^{137}. Therefore, these were not included as variables in the experimental program now being described.

* Operated by Union Carbide Corporation for the United States Atomic Energy Commission.

2. REMOVAL OF RADIONUCLIDES AS A RESPONSE SURFACE

The efficiency of the waste treatment plant may be measured by the percentage of radionuclides removed from the waste. The per cent removal of Sr^{90} and the per cent removal of Cs^{137} are two measures of the efficiency of the waste treatment process. Obviously, each measure is a function of the four treatment variables listed in Section 1. Let y_s stand for the percentage of strontium removed by the process and y_c stand for the percentage of cesium removed. Also let x_1 be a proportion of the p.p.m. of lime required to combine with the carbon dioxide carbonate hardness and magnesium hardness (i.e. stoichiometric requirement), x_2 be p.p.m. of excess soda ash, x_3 the p.p.m. of clay added and x_4 the particle size of the clay, measured by the size of mesh through which the clay can pass. The efficiency of the treatment process may be expressed then, as

$$\left.\begin{aligned} y_s &= f_s(x_1, x_2, x_3, x_4) \\ y_c &= f_c(x_1, x_2, x_3, x_4) \end{aligned}\right\} \qquad (2.1)$$

The forms of f_s and f_c are, of course, unknown. But equations (2.1) describe two response surfaces, one for Sr^{90} and one for Cs^{137}. The response, y_s, for example, might be plotted over the four-dimensional "plane" (hyperplane is a better word) of x_1, x_2, x_3 and x_4 and thus would describe a surface representing the per cent removal of strontium.

Responses over four-dimensional hyperplanes cannot be plotted conveniently on a plane, of course, but if there were only two independent variables, x_1 and x_2, for example, the response could be plotted as contours of equal response as in Fig. 1. In Fig. 1, the shape of the contour lines would be determined by the function, $f(x_1, x_2)$, if it were known.

Knowledge of the forms of f_s and f_c would be very desirable, but it is not necessary. The purpose of the experimental program was to find the point of highest response on the surface in terms of the variables x_1, x_2, x_3, x_4. An approximation to the functions f_s and f_c might very well suffice.

3. LINEAR APPROXIMATIONS TO THE RESPONSE SURFACES

The techniques employed in locating the points of optimum efficiency were very aptly

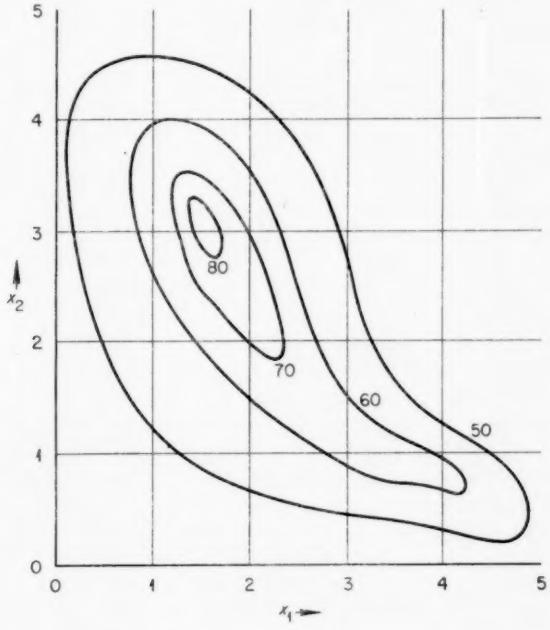

FIG. 1. Two-factor response surface.

described by Box and Wilson[1] in 1951. Basic to the application of the techniques is the ability to expand the unknown function in a Taylor series expansion. The expansion may be written

$$f = b_0 + \sum_{i=1}^{4} b_i x_i + \sum_{i,j=1}^{4} b_{ij} x_i x_j + \sum_{i,j,k=1}^{4} b_{ijk} x_i x_j x_k + \cdots \qquad (3.1)$$

Equation (3.1) is an infinite series, of course, but various approximations to the function f may be obtained by truncating the series at different points. The simplest (and often the crudest) approximation is obtained by dropping all terms involving the x's in quadratic terms and higher. The result is a linear approximation,

$$f = b_0 + \sum_{i=1}^{4} b_i x_i \qquad (3.2)$$

which represents a first approximation to the surface and is actually a five-dimensional hyperplane approximating the surface.

4. THE PATHS OF STEEPEST ASCENT

In general, equation (3.2) is a better approximation if the ranges of the x_i are small. (This is analogous to straight line interpolation in a table of logarithms, for example.) So, in a sufficiently small region of the space of the variables x_1, x_2, x_3 and x_4, equation (3.2) may be taken as an adequate approximation to the response surface.

If the coefficients b_i were known (or adequately estimated) it is easy to show that the direction in which to move in the space of x_1, x_2, x_3 and x_4, to obtain the greatest change in the response, f, is determined by the coefficients b_i. As a simple illustration, suppose that x_1, x_2, x_3 and x_4 were all measured in the same units. Then the step in the space of the four variables which would give the greatest increase in f for an increase of b_1 units in x_1 would require an increase of b_2 units in x_2, an increase of b_3 units in x_3, and an increase of b_4 units in x_4. The path described by this step is appropriately called the "path of steepest ascent".

Of course, if one should follow the path of steepest ascent beyond the boundaries of the region for which equation (3.2) was considered adequate, a new equation [of the same form as (3.2)] would be necessary and a new path of steepest ascent determined. Thus it is seen that experimentation carried along these lines is of a sequential nature and the exact length of the experimental program cannot be known in advance.

5. THE METHOD OF STEEPEST ASCENT APPLIED TO THE REMOVAL OF RADIONUCLIDES FROM PROCESS WASTES

An experimental program to improve the efficiency of the ORNL waste treatment plant was carried out using the principles described in Sections 2, 3 and 4. Two sequences of the application of the method were performed before the program was stopped. At the end of the program removals of 95 per cent of Cs^{137} and 96 per cent of Sr^{90} had been demonstrated, using actual process wastes as raw material.

The experiments were performed in a laboratory and so, strictly speaking, improvement of the efficiency of the plant has not been demonstrated. But certainly a good deal has been learned about the process and hopes for more efficient operation of the plant have been encouraged.

5.1. *The first simplex experiment*

Basic to the application of the method of steepest ascent is a knowledge of, or estimates of, the b_i of equation (3.2). These may be efficiently obtained through the use of a factorial type of experiment described by Box[3]. Five combinations of the four treatment variables (five points in a four-dimensional space) are chosen so that the combinations, if looked at as points in a geometrical figure, would describe a simplex.*

The first simplex experiment is shown in Table 1. Each row in Table 1 corresponds to a single "run" with treatment combinations as shown. The Cs^{137} and Sr^{90} removals for the runs are given in the last two columns in units of per cent removed.

Five beakers, containing 1 l. of process waste were treated with lime, soda ash and clay as given in Table 1. The beakers were placed in a mixing apparatus and simultaneously subjected to rapid mixing for 1 min and 34 sec at 288 rev/min. Then the contents were mixed for 34 min at 81 rev/min and allowed to settle for 2 hr and 22 min. Afterwards the supernate

* A simplex in three dimensions would require four points and would form a tetrahedron; in two dimensions a simplex has three points arranged in a triangle. In more than three dimensions the analogous figure is called simply a simplex.

Table 1. *First simplex experiment*

x_1 Lime* (proportion of stoichiometric requirement)	x_2 Excess soda ash (p.p.m.)	x_3 Clay dose (p.p.m.)	x_4 Particle size (mesh)	y_s Sr^{90} removed (%)	y_c Cs^{137} removed (%)
1.0	0	50	20–60	46	46
1.0	0	50	100–140	47	67
1.0	0	200	60–100	51	88
$\frac{1}{3}$	0	100	60–100	29	71
$\frac{1}{2}$	375	100	60–100	75	72

* The levels of lime shown here were inadvertently changed from those originally chosen. Hence the design is not orthogonal as was intended.

was filtered and samples of the filtrate were sent to the laboratory for analysis.

From the results of the analyses, estimates of equation (3.2) were obtained by the method of least squares. They were

$$y_s = 15.5 + 28.5x_1 + 0.11x_2 + 0.03x_3 + 0.01x_4 \qquad (5.1)\dagger$$

$$y_c = 31 - 6.0x_1 + 0.005x_2 + 0.209x_3 + 0.265x_4$$

From previous experimentation the standard deviation of strontium removal was believed to be 2.8 per cent and of cesium removal, 3.7 per cent. Using these standard deviations, the standard errors of the coefficients were calculated and are displayed with their coefficients in the table below.

i	Strontium-90		Cesium-137	
	b_i	Standard error	b_i	Standard error
1	28.5*	4.85	−6.0	6.44
2	0.11*	0.009	0.005	0.012
3	0.03	0.023	0.209*	0.030
4	0.01	0.050	0.265*	0.066

* Significantly different from zero at a very small probability level.

It is interesting to note from the table that, of the four coefficients, only the coefficients of x_1 (lime) and x_2 (soda ash) are significantly larger than their standard errors for the strontium equation. Just the opposite is true for the cesium equation. The only coefficients larger than their standard errors are those for x_3 (clay dose) and x_4 (particle size). This natural division of the four treatment variables into two groups was utilized for mapping a composite path of "steepest ascent" for the two responses.

† In dealing with the x_4 variable, the mid-point of the mesh size range was used as the measurement of particle size.

5.2. *The first path of steepest ascent*

Although the following procedure would not in general be recommended, it was decided to let the Sr^{90} equation in (5.1) determine the direction of the exploratory path in the plane of the x_1 and x_2 variables and to let the Cs^{137} equation determine the direction in the plane of the x_3 and x_4 variables.

From the strontium equation in (5.1) we may write

$$28.5x_1 + 0.11x_2 = \text{constant} \qquad (5.2)$$

which describes the estimated contours of equal strontium removal in the plane of x_1 and x_2. The path we are calculating should go through the center of the experimental region, which was at $x_1 = 1/2$ and $x_2 = 75$ p.p.m. Also the variables should be placed on an equal footing. The simplex design which yielded equation (5.1) treated one-sixth of a unit in x_1 as equivalent to 75 p.p.m. in x_2. Thus equation (5.2) is changed to read

$$(1/6)(28.5)\left(\frac{x_2 - 1/2}{1/6}\right) + (75)(0.11)\left(\frac{x_2 - 75}{75}\right) = \text{constant}$$

or

$$4.75\left(\frac{x_1 - 1/2}{1/6}\right) + 8.25\left(\frac{x_2 - 75}{75}\right) = \text{constant} \qquad (5.3)$$

The path of greatest increase in Sr^{90} over the plane of x_1, x_2 may be obtained from (5.3) by interchanging

the numerical coefficients, reversing the sign of one and equating the constant to zero. The results will be the equation of a line perpendicular to the contours of (5.2) and passing through $x_1 = 1/2$ and $x_2 = 75$. Thus we obtain

$$8.25\left(\frac{x_1 - 1/2}{1/6}\right) - 4.75\left(\frac{x_2 - 75}{75}\right) = 0$$

or

$$x_1 = 0.404 + 0.00128x_2 \qquad (5.4)$$

From equation (5.4) we determine that the path of steepest ascent [obtained by increasing x_2 because the coefficient of x_2 in (5.1) is positive] has $x_1 = 1/2$ for $x_2 = 75$, $x_1 = 0.79$* for $x_2 = 300$ and $x_1 = 1.0$ for $x_2 = 455$. These values of x_1 and x_2 appear in Table 2.

Similarly, the contours in the plane of x_3 and x_4, as determined from the Cs^{137} equation in (5.1), are expressed by

$$0.209x_3 + 0.265x_4 = \text{constant} \qquad (5.5)$$

The center of the design region was at $x_3 = 100$ p.p.m. and $x_4 = 80$-mesh, and 50 p.p.m. x_3 was equivalent to 40 units mesh. Thus, the perpendicular to equation (5.5) passing through the center of the design region is given by

$$(40)(0.265)\left(\frac{x_3 - 100}{50}\right) - (50)(0.209)\left(\frac{x_4 - 80}{40}\right) = 0$$

or

$$x_3 = 1.415 + 1.232x_4 \qquad (5.6)$$

Thus, from (5.6), mesh size of 155 calls for 193 p.p.m. clay, mesh size of 185 requires 229 p.p.m. clay and mesh size of 250 calls for 309 p.p.m. clay, along the path of steepest ascent through the plane of x_3 and x_4.

The experiments performed along the "composite" path are shown in Table 2 along with the measured responses at the points. There are nine experiments in all, arranged so that they occur at three distinct points along the line of equation (5.4) and at three distinct points along the line of equation (5.6).

That this phase of the program was successful may be seen by noting that within the groups of three experiments in Table 2, the Sr^{90} removals have increased from about 35 per cent to 85 per cent showing the effect of changing lime and soda ash, and over the three groups of three experiments, Cs^{137} removals have increased from about 90 per cent to 95 per cent, showing the effect of changing clay dose and particle size.

It was deemed inadvisable to extend these paths any further, however, because the last point in the x_1, x_2 plane was well beyond the region of the first simplex design, as was the last point in the x_3, x_4 plane. Instead, it was decided to re-estimate the paths of steepest ascent by performing another series of experiments in a new region of the treatment variable space.

5.3. *The second simplex experiment*

A new series of levels of the four treatment variables was chosen and another designed experiment was

* For convenience this was rounded to 0.80.

Table 2. Experiments along the first (composite) path of steepest ascent

x_1 Lime (proportion of stoichiometric requirement)	x_2 Excess soda ash (p.p.m.)	x_3 Clay dose (p.p.m.)	x_4 Particle size (mesh)	Responses	
				Sr^{90} (%)	Cs^{137} (%)
$\frac{1}{2}$	75	193	140–170	32	91
0.80	300	193	140–170	77	87
1.00	455	193	140–170	85	87
$\frac{1}{2}$	75	230	170–200	39	88
0.80	300	230	170–200	76	93
1.00	455	230	170–200	85	91
$\frac{1}{2}$	75	310	230–270	40	94
0.80	300	310	230–270	81	94
1.00	455	310	230–270	84	96

performed in a manner similar to the first simplex design. The second design was also of the simplex pattern and is shown, with the measured responses in Table 3. This time the design was completely replicated and so there are two responses given for each of the five points.

Table 3. Second simplex experiment

x_1 Lime (proportion of stoichiometric requirement)	x_2 Excess soda ash (p.p.m.)	x_3 Clay dose (p.p.m.)	x_4 Particle size (mesh)	Responses Sr^{90} (%)	Responses Cs^{137} (%)
$\frac{1}{2}$	460	300	170–200	81	82
				82	81
$\frac{1}{2}$	460	450	170–200	81	88
				81	88
2	460	375	170–200	93	87
				93	87
1	600	375	170–200	89	85
				89	81
1	495	375	230–270	89	92
				90	91

From Table 3 it may be noted that further improvements have been obtained in strontium removal, the range being between 81 and 93 per cent. The cesium removals, however, were disappointingly low and in fact were lower than some of the removals experienced along the first path of steepest ascent. This was puzzling until the linear approximations to the response surfaces were calculated. Then it was revealed that large levels of excess soda ash apparently had a detrimental effect on cesium removal. This had not been suspected before.

The equations calculated from the results of the second simplex experiment turned out to be

$$y_s = 55.8 + 8.04x_1 + 0.028x_2 - 0.0043x_3 + 0.055x_4 \quad (5.7)$$

$$y_c = 56.6 + 1.47x_1 - 0.0182x_2 + 0.0424x_3 + 0.0107x_4$$

The standard errors of the coefficients were computed from a five degree of freedom estimate of the standard deviation for Sr^{90} of 0.226 per cent and a similar estimate of the standard deviation for Cs^{137} of 1.492 per cent (calculated from the difference between replicates in the second simplex). These are shown below with their coefficients and the ratios, t, of the coefficients to the standard errors.

Student's t for five degrees of freedom (5 per cent level) is 2.571. Thus all the coefficients in the strontium equation, except that of x_3, are significantly different from zero. In the cesium equation only the

i	Strontium-90 b_i	Strontium-90 Standard error	Strontium-90 t	Cesium-137 b_i	Cesium-137 Standard error	Cesium-137 t
1	8.04	0.185	43.5	1.47	1.223	1.2
2	0.028	0.002	14.0	−0.0182	0.012	−1.5
3	−0.0043	0.002	2.2	0.0424	0.014	3.0
4	0.055	0.004	13.8	0.0107	0.026	0.4

Table 4. Calculation of second paths of steepest ascent

	Lime x_1	Excess soda ash x_2	Clay dose x_3	Response	
				Sr^{90}	Cs^{137}
Center of simplex	1.0	495	375		
Equivalent units	$\frac{1}{2}$	35	75		
Path for Sr^{90}					
b_i	8.04	0.028	−0.0043		
$b_i \times (\text{unit})^2$	2.01	34.3	−24.2		
Change per $\frac{1}{2}$ unit change in x_1	$\frac{1}{2}$	8.5	−6.0		
Path	1.0	495.0	375	86	92
	1.5	503.5	369	93	92
	2.0	512.0	363	95	94
	2.5	520.5	357	96	92
Path for Cs^{137}					
b_i	1.47	−0.0182	0.0424		
$b_i \times (\text{unit})^2$	0.368	−22.3	238.5		
Change per 80 units change in x_3	0.123	−7.48	80		
Path	1.00	495	375	86	92
	1.12	487.5	455	90	94
	1.23	481	525	90	94
	1.35	474	605	92	95

coefficient of x_3 is significant at the 5 per cent level.

But the interesting feature of equation (5.7) is the negative coefficient for x_2 in the cesium equation. Although it is only one and one half times its standard error (which would be significant at about the 20 per cent level), the effect on y_c when x_2 varies between 460 and 600 is considerable. This is what led us to believe that high levels of excess soda ash (x_2) are undesirable for removing radioactive cesium.

5.4. *The second paths of steepest ascent*

In order to improve further on the radionuclide removal, the paths of steepest ascent were recalculated from the information contained in equations (5.7). This time, since the strontium equation was sufficiently different from the cesium equation a separate path was calculated for each element. Also, since particle size was difficult to control and since its measurement by mesh size at best is very inexact, the particle size of clay was held to those particles which would pass through a screen of 200-mesh but not one of 230-mesh. This reduced the number of treatment variables to three.

The calculation of the second paths is shown in Table 4. This table illustrates a systematic short cut calculation of the paths which is based on the three-dimensional analog of the calculation shown in Section 5.2 of this paper. The first point on each path is the same and hence the table shows responses for seven additional experiments, not eight.

Since it would be inadvisable not to do so, both Sr^{90} and Cs^{137} removals were measured on each path. It may be noted that the points along the path calculated for Sr^{90} show increases in removal of Sr^{90} from 86 per cent to 96 per cent. The Cs^{137} removals on this path started at 92 per cent, rose to 94 per cent and fell back to 92 per cent, ostensibly no change.

Along the path calculated for Cs^{137}, the Sr^{90} removal increased from 86 per cent to only 92 per cent, while the Cs^{137} removals increased from 92 per cent to 95 per cent.

It may be noted also that the levels of excess soda ash along the paths are no greater than 503 p.p.m. This is approximately equal to the central level of x_2 used in the second simplex experiment, at which point the better Cs^{137} removals were experienced. So, refraining from the use of excess soda ash at very high levels brought cesium removals back to an encouragingly high percentage.

6. SUMMARY

In Fig. 2, which is a graphic history of the entire experimental program with respect to strontium removal, and in Fig. 3, which is the same with respect to cesium removal, the success of the program may be seen quite clearly. In

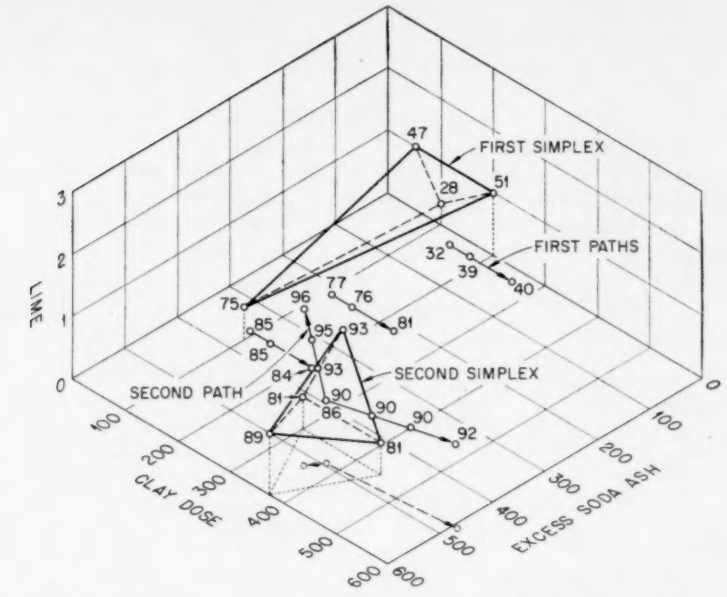

FIG. 2. Experimental points showing the per cent of strontium removal.

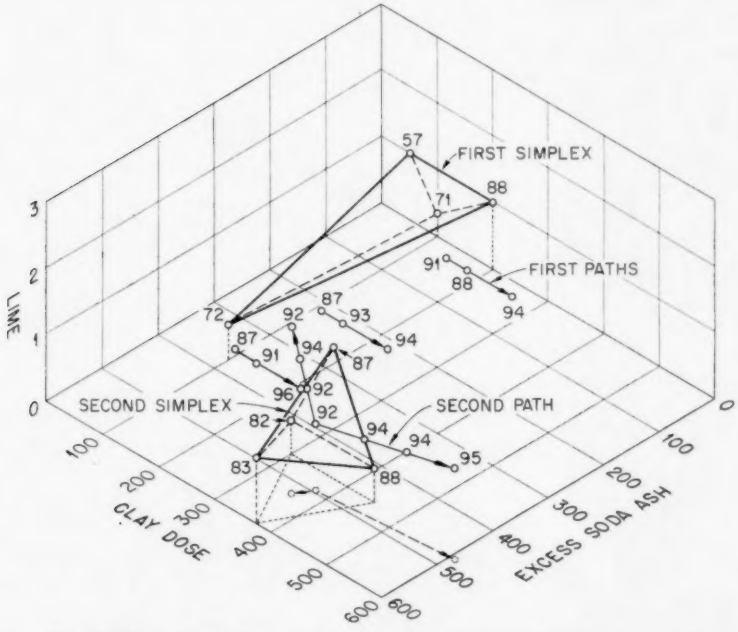

FIG. 3. Experimental points showing the per cent of cesium removal.

order to make these pictures possible, the variation in x_4, particle size of clay, has been ignored; thus the responses are shown in a three-dimensional plot.

In both figures, the positions of the experimental points are indicated by the circles placed in their proper locations according to the levels of lime, excess soda ash and clay dose used The numbers at the points are the per cent removals observed at those combinations of the treatment variables. Both figures are identical with respect to the positions of the points, the forms of the tetrahedra, and the directions of the paths of steepest ascent. The numbers in Fig. 2 are Sr^{90} per cent removals; those in Fig. 3 are Cs^{137} per cent removals.

The label "First Paths" refers to the three parallel arrows pointing in the direction of higher clay dose, one is at excess soda ash of 75 p.p.m. and 1/2 lime, another at 300 p.p.m. soda ash and 0.80 lime and the third is at 455 p.p.m. excess soda ash and 1.0 lime. These three arrows were referred to as the "composite path" in Section 5.2.

There are two arrows emanating from the second simplex because two paths of steepest ascent were calculated from the results of this design. Their directions over the plane of clay dose and excess soda ash, may be seen from their projections on that plane. In Fig. 2 the arrow labeled "Second Path" represents the path of steepest ascent calculated from Sr^{90} responses. It shows the increase from 86 per cent to 96 per cent removal as per Table 4. The other arrow in Fig. 2 shows the Sr^{90} per cent removals observed along the path calculated from Cs^{137} responses.

This labeling is reversed in Fig. 3. The path of steepest ascent calculated from the Cs^{137} per cent removals is now labeled "Second Path". Here cesium removal increased from 92 per cent to 95 per cent as noted before. The other arrow represents the path of steepest ascent for the Sr^{90} response, and shows relatively stable cesium removal.

7. CONTINUATION OF THE PROGRAM

No further experimentation in the laboratory is planned. More improvement might possibly be demonstrated by additional laboratory experiments, but the purpose of the program was to increase the efficiency of the waste treatment plant. The point of greatest strontium removal found in the laboratory program would appear to be a logical place to begin.

It is too much to hope that the point of optimum operation for the waste treatment plant would be the same as the point of optimum operation for a laboratory experiment. But, logically, the neighborhoods of the two optima should be the same. Using additional statistical tools, the authors believe that they now will be able to move the experimentation into the treatment plant and thereby accomplish the objectives of the program.

REFERENCES

1. G. E. P. Box and K. B. Wilson, *J. R. Statist. Soc.* (B) **13,** 1 (1951).
2. K. E. Cowser, H. J. Wyrick and D. A. Gardiner, *Low-Level Waste Water Treatment.* Health Physics Division Annual Progress Report, Oak Ridge National Laboratory, (ORNL-2806) p. 1 (1959).
3. G. E. P. Box, *Biometrika* **39,** 49 (1952).

Health Physics Pergamon Press 1961. Vol. 5, pp. 79–84. Printed in Northern Ireland

EARLY TIME DECAY OF FISSION PRODUCT MIXTURES—II

γ-ENERGY RELEASE AND IONIZATION RATES FOLLOWING THERMAL NEUTRON FISSION OF U^{235}

P. ZIGMAN* and J. MACKIN*
Analytical and Standards Branch, U.S. Naval Radiological Defense Laboratory
San Francisco 24, California

(*Received* 1 *August* 1960)

Abstract—Photon spectra at various times from 1 sec to 5 hr after instantaneous thermal neutron fission of U^{235} are listed. From these are computed total γ-ray energy release rates and theoretical air ionization rates 3 ft above an infinite plane uniformly contaminated with fission products. Equations which provide a good fit to the rate curves within the estimated accuracy of the data are (t in sec): $\Gamma(t) = 2.78t^{-1.23} - 2.41t^{-1.45}$ MeV/sec per fission and $I(t) = [1.41t^{-1.23} - 1.23t^{-1.45}]\ 10^{-8}$ r/hr per fission/ft^2. Comparisons of integrated doses calculated from the photon spectra with doses derived from the familiar $t^{-1.2}$ function show substantial differences for times after fission less than 1000 sec.

INTRODUCTION

An extensive number of articles have appeared in the literature concerning γ-ray energy release rates following instantaneous thermal neutron fission of U^{235}. It is intended here to summarize the more pertinent information on this subject, to present calculations from and certain revisions to reported early-time γ-decay values, and, finally, to compare such revised values with those computed from the familiar and widely quoted $t^{-1.2}$ expression.

γ-Energy release rates have been both measured experimentally and estimated by computation. The computational method has been used by Miller[1] and others[2–4] to obtain total γ-energy release rates by summing the photon energy release of the individual fission product radionuclides present at different post-fission times. The energy release of the individual products are calculated from their fission yields, disintegration rates, and decay characteristics. Information of this sort is not available for many of the initial fission products. Consequently, accurate summations of γ-energy release are presently restricted to post-fission times greater than about 1 hr, although Perkins and King[5] have approximated total photon emission and energy release back to 100 sec by estimating unknown half-lives and γ-ray abundances.

Experimental measurements of γ-energy release appear to be limited to the early work of Borst[6] and Sugarman *et al.*,[7] and to the more precise determinations first reported by Zobel and Love[8] and Peelle *et al.*[9] in 1956, and later, in revised form, by Maienschein[10]. These latter investigators[8–10] used Compton and pair spectrometers to determine the γ-abundances in the decay of fission product mixtures following short exposure of U^{235} in the Graphite Reactor at Oak Ridge National Laboratory or in the neutron flux at the Lid Tank Shielding Facility at that laboratory. The experimental equipment used in the Oak Ridge measurements did not permit observation of photons below 280 keV. γ-Ray spectral decay was determined at early times after fission, between 1.25 and 1600 sec.

Combination of the early-time Oak Ridge experimental data with computed values, which apply at relatively long times after fission,

* Present Address: Fuels and Materials Department, Atomics International, P.O. Box 309, Canoga Park, California.

should provide a description of energy release rates from 1 sec to many years. Such a combination was carried out by LaRiviere[11] who used the spectra reported by Zobel and Love in 1956 for early times and Miller's computations for later times. In order to effect a smooth transition between the two sets of data LaRiviere increased the experimental values by about 20 per cent. Following this, he used conversion factors reported by Miller and Loeb[12] to derive the theoretical ionization rate (r/hr) over an infinite plane uniformly contaminated with fission products. The latter estimates, useful in fallout analysis, are expressed in terms of roentgens per hour per fission per square foot at a height of 3 ft above the plane.

In a similar manner, Knabe and Putnam[13] combined the revised Oak Ridge experimental data[10] with the computations of Perkins and King. It was found that a smooth transition between the experimental data and the computations could be accomplished by extrapolation of the former from 1600 to 10^4 sec. Inasmuch as the experimental measurements did not include photon abundances below 280 keV, such abundances were introduced on the basis of comparisons of the extrapolated experimental curves with the compiled data.

Recent experiments[14] at this laboratory have permitted estimates of the photons below 280 keV. Such estimates provide an experimental basis for calculation of the energy release rates, MeV/sec, of photons below 280 keV. Also, as such photons are not included in the original Oak Ridge data and consequently do not appear in LaRiviere's computations of ionization rates vs. time after fission, recomputations of γ-release rates and ionization rates were in order. The need for such recomputations is emphasized by the 1958 revision of the Oak Ridge spectra.

This paper reports revised γ-decay values for post-fission times of 1.0 sec to about 4.8 hr. Two primary calculations are included, viz. (a) MeV/sec vs. time and (b) r/hr vs. time. In addition, the dosages (in roentgens) for various times of entry into an environment of deposited fission products and for different periods of exposure are computed. Comparisons are made with the energy emission and ionization rates at different times and with the dosage accumulations which could be predicted on the basis of the well-known Way–Wigner $t^{-1.2}$ decay of the composite fission product mixture.[15]

COMPUTATIONAL METHODS

Two sources of data have been used in these computations. One was estimates of photon release rates in the energy range 0.02–0.4 MeV based on recent decay rate measurements at this laboratory.[14] Large uncertainties in these estimates have a small effect on total energy release rates since this group contributes less than 10 per cent of the total energy release rates at the times considered. The other, and primary, source of information was the Knabe and Putnam summary of the Oak Ridge experimental work. Their summary includes the measured γ-ray release rates in eleven energy groups within the energy range 0.4–5.5 MeV as a function of time after an instantaneous fission event.

The combined data from the two sources are presented in Table 1. In this table the group designations are per Knabe and Putnam; with the exception of Group I, group energy ranges are also those employed by these authors.

Derivation of the total MeV/sec per fission, $\Gamma(t)$, emitted at a given time, t, was accomplished through a simple summation process. The following expression was used:

$$\Gamma(t) \cong \sum_{i=\mathrm{I}}^{\mathrm{VII}F} \varepsilon_i P_i(t) \qquad (1)$$

where $P_i(t)$ = number of photons per fission emitted per second within the ith energy group at time t

ε_i = geometric mean energy of the ith energy group (MeV/photon)

The derived summations are depicted graphically in Fig. 1.

Calculations of r/hr per fission/ft^2, i.e. ionization rate, $I(t)$, as a function of time after fission was made in a similar manner by substitution of the air absorption parameter,[12] μ_i, (r/hr) (p/sec)$^{-1}$ (ft^2)$^{-1}$, in equation (1), to obtain

$$I(t) \cong \sum_{i=\mathrm{I}}^{\mathrm{VII}F} \mu_i P_i(t) \qquad (2)$$

In this expression the air absorption parameter describes the theoretical air absorption, as a function of source photon energy, 3 ft above a uniformly contaminated infinite plane. This parameter essentially considers the linear air absorption coefficient per photon and photon scattering (i.e. build-up factor)[16].

Table 1. Photons per second per fission as a function of energy group and time after fission

Energy Group Number →	PHOTONS PER SECOND PER FISSION												
	I	II	III	IV	V	VI	VII A	VII B	VII C	VII D	VII E	VII F	TOTAL
Energy Range (MEV) →	0.02-0.4	0.4-0.9	0.9-1.35	1.35-1.8	1.8-2.2	2.2-2.6	2.6-3.0	3.0-3.5	3.5-4.0	4.0-4.5	4.5-5.0	5.0-5.5	0.02-5.5
Geometric Mean Energy (MEV)→	0.089	0.60	1.10	1.56	1.99	2.39	2.79	3.24	3.74	4.25	4.74	5.24	
Time After Fission (Seconds)													
1.0	1.6×10^{-1}	1.2×10^{-1}	7.2×10^{-2}	3.4×10^{-2}	2.5×10^{-2}	8.5×10^{-3}	7.5×10^{-3}	6.3×10^{-3}	4.6×10^{-3}	3.7×10^{-3}	2.1×10^{-3}	9.1×10^{-4}	4.5×10^{-1}
1.5	1.3	9.6×10^{-2}	5.3	2.7	1.8	8.2	6.5	5.5	4.0	2.7	1.5	6.0	3.5
2.0	1.0	8.1	4.1	2.3	1.4	7.6	5.8	4.8	3.6	2.1	1.2	5.6	2.9
3.0	7.3×10^{-2}	6.1	2.9	1.7	1.1	6.7	4.8	3.9	2.9	1.5	8.7×10^{-4}	4.2	2.1
4.0	5.5	5.0	2.3	1.4	8.5×10^{-3}	5.8	4.0	3.4	2.4	1.2	6.8	3.4	1.7
6.0	3.8	3.7	1.6	1.0	6.0	4.6	3.2	2.6	1.8	8.7×10^{-4}	4.8	2.4	1.2
9.0	2.4	2.6	1.1	7.1×10^{-3}	4.2	3.2	2.3	1.8	1.3	6.1	3.4	1.7	8.3×10^{-2}
1.3×10	1.7	1.9	7.6×10^{-3}	5.2	3.0	2.4	1.7	1.3	9.9×10^{-4}	4.4	2.4	1.2	5.9
1.9	1.1	1.3	5.3	3.7	2.2	1.7	1.2	9.4×10^{-4}	7.0	3.2	1.7	8.4×10^{-5}	4.1
2.8	8.8×10^{-3}	8.6×10^{-3}	3.8	2.6	1.5	1.1	8.2×10^{-4}	6.1	4.6	2.1	1.1	5.4	2.9
4.1	5.0	5.9	2.7	1.8	1.0	8.0×10^{-4}	5.8	4.2	3.1	1.5	7.5×10^{-5}	3.6	1.9
6.0	3.3	3.9	1.9	1.2	6.7×10^{-4}	5.2	3.7	2.7	2.0	1.0	4.7	2.3	1.3
8.8	2.1	2.6	1.3	8.5×10^{-4}	4.4	3.5	2.4	1.7	1.2	6.7×10^{-5}	2.9	1.4	8.3×10^{-3}
1.29×10^{2}	1.3	1.7	9.6×10^{-4}	5.7	2.9	2.3	1.5	1.0	7.6×10^{-5}	4.3	1.8	8.3×10^{-6}	5.6
1.89	8.5×10^{-4}	1.2	6.9	3.8	1.9	1.5	9.0×10^{-5}	6.0×10^{-5}	4.5	2.5	1.0	4.4	3.7
2.77	5.6	7.7×10^{-4}	4.8	2.5	1.3	1.0	5.3	3.5	2.7	1.5	5.2×10^{-6}	2.3	2.4
4.06	3.8	5.2	3.4	1.7	8.0×10^{-5}	7.0×10^{-5}	3.3	2.1	1.6	8.2×10^{-6}	2.8	1.2	1.7
5.95	2.9	3.4	2.3	1.1	5.2	4.2	1.8	1.2	8.7×10^{-6}	3.8	1.3	4.6×10^{-7}	1.1
8.70	2.3	2.3	1.5	7.0×10^{-5}	3.4	2.8	1.2	6.8×10^{-6}	5.0	1.7	5.4×10^{-7}	1.8	7.8×10^{-4}
1.28×10^{3}	1.7	1.5	9.2×10^{-5}	4.6	2.2	1.7	6.0×10^{-6}	3.7	2.7	6.2×10^{-7}	2.0	4.9×10^{-8}	5.2
1.87	1.2	1.0	5.8	3.1	1.3	1.1	3.4	2.0	1.4	2.1	6.4×10^{-8}	1.1	3.5
2.75	8.3×10^{-5}	6.6×10^{-5}	3.0	1.8	8.2×10^{-6}	6.8×10^{-6}	1.7	9.8×10^{-7}	7.1×10^{-7}	4.5×10^{-8}	1.3	1.0×10^{-9}	2.2
4.03	4.9	4.5	1.7	1.3	5.0	4.0	8.3×10^{-7}	4.7	3.4	6.0×10^{-9}	2.0×10^{-9}	- -	1.4
5.90	3.0	2.9	8.9×10^{-6}	7.6×10^{-6}	3.2	2.5	3.4	1.9	1.4	- -	- -	- -	8.2×10^{-5}
8.64	1.7	1.9	4.7	4.9	2.1	1.4	1.3	7.8×10^{-8}	5.7×10^{-8}	- -	- -	- -	5.1
1.27×10^{4}	1.1	1.2	2.4	2.7	1.3	6.8×10^{-7}	4.8×10^{-8}	2.8	2.1	- -	- -	- -	3.1
1.74	7.8×10^{-6}	8.8×10^{-6}	1.6	1.7	9.6×10^{-7}	4.2	2.5	1.4	1.0	- -	- -	- -	2.1

6—(20 pp.)

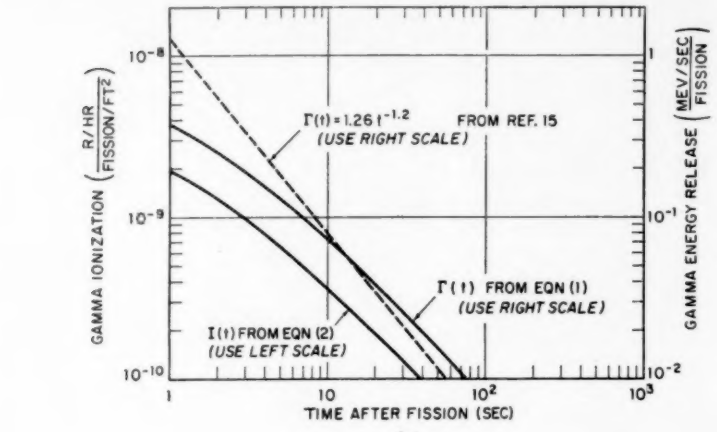
GAMMA IONIZATION (R/HR / FISSION/FT²)
GAMMA ENERGY RELEASE (MEV/SEC / FISSION)
Γ(t) = 1.26 t^-1.2 FROM REF. 15
(USE RIGHT SCALE)
Γ(t) FROM EQN (1)
(USE RIGHT SCALE)
I(t) FROM EQN (2)
(USE LEFT SCALE)
TIME AFTER FISSION (SEC)

(a)

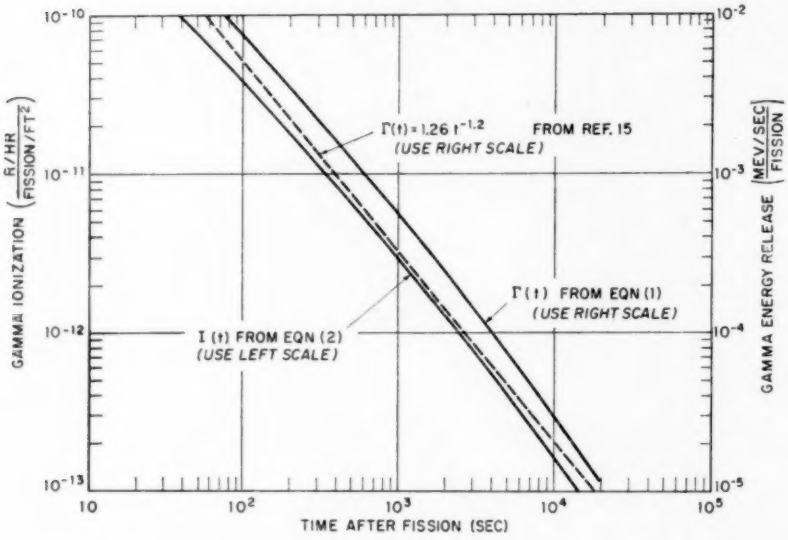
GAMMA IONIZATION (R/HR / FISSION/FT²)
GAMMA ENERGY RELEASE (MEV/SEC / FISSION)
Γ(t) = 1.26 t^-1.2 FROM REF. 15
(USE RIGHT SCALE)
Γ(t) FROM EQN (1)
(USE RIGHT SCALE)
I (t) FROM EQN (2)
(USE LEFT SCALE)
TIME AFTER FISSION (SEC)

(b)

FIG. 1 (a) and (b). Energy release and ionization rates as a function of time after fission.

The derived values from equation (2) are calculated for a contamination density of one fission per square foot. The resulting ionization values are presented in Fig. 1(a) and (b).

CONCLUSIONS

The data in Table 1 and Fig. 1(a) and (b) provide a reasonably complete and accurate summary of the number and energy release rates of the delayed γ-rays following thermal neutron fission of U^{235} to times after fission of approximately 5 hr. Energy release rates calculated from Table 1 do not agree, neither in absolute value nor in rate of change, with the WAY–WIGNER "rule of thumb" expression for energy release, $\Gamma(t) = 1.26t^{-1.2}$ MeV/sec per fission. As shown in Fig. 1(a), the experimental curves at times less than 10 sec yield lower values for energy release per fission and a slower rate of decay. It should be noted

that WAY–WIGNER did not expect the $t^{-1.2}$ function to hold for $t < 10$ sec;[15] as described below, a significant fraction of total dose is contributed prior to 10 sec. After approximately 100 sec, however, the rates of decay for both energy release and ionization rates are described fairly well by the $t^{-1.2}$ function. This makes possible the following expression for energy emission decay from 1 sec after fission:

$$\Gamma(t) = 2.78t^{-1.23} - 2.41t^{-1.45} \text{ MeV/sec per fission} \quad (3)$$

The corresponding expression for ionization rate is:

$$I(t) = [1.41t^{-1.23} - 1.23t^{-1.45}]10^{-8} \text{ r/hr per fission/ft}^2 \quad (4)$$

In each expression t is in seconds and the negative term adjusts for early time departure of decay rate from an approximate $t^{-1.2}$ dependence. Expressions (3) and (4) yield values largely within 5 to 10 per cent of the decay data presented in Fig. 1 (the greatest deviations are less than ± 20 per cent, values which are probably still within the accuracy of the Fig. 1 data). For times greater than that covered by Fig. 1, i.e. 10^4 sec, and extending to approximately 10^6 sec, γ-ionization values calculated through equation (4) are within 20 per cent of those resulting from the summations of MILLER and LOEB. In regard to total energy release, integration of equation (3) over the time period 1 to 10^8 sec yields 6.6 MeV/fission. This is identical with the value obtained by KNABE and PUTNAM by numerical integration.

Numerical integrations of Table 1 data were carried out to estimate theoretical ionization dose accumulated from exposure to an environment of deposited fission products.* Dosages 3 ft above an infinite plane uniformly contaminated by fission products (one fission/ft^2) were calculated in a manner similar to that used by MILLER and LOEB for initial exposure times of 1 hr post-fission. Accumulations from exposures beginning at post-fission times of 1,

* Equation (4) may be integrated (t in hours) to yield values which in most cases are within 5 to 10 per cent of those obtained by numerical integration.

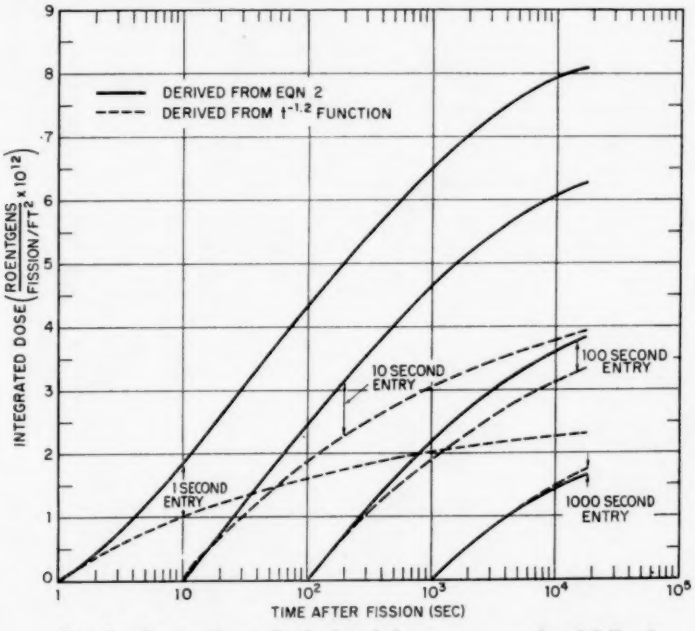

FIG. 2. Comparison of calculated dosages accumulated following four different entry times.

10, 100 and 1000 sec were derived and are presented in Fig. 2. These dosages were then compared to the dosages which would accumulate if the 1-, 10-, 100- and 1000-sec ionization rates decayed according to the $t^{-1.2}$ function. These latter integrations are also shown in Fig. 2.

It is evident from Fig. 2 that substantial differences exist between integrated doses calculated on the basis of the spectral data and calculated according to $t^{-1.2}$ decay. These differences are large for very early entry times and become progressively smaller (depending on duration of exposure) with increasing time of entry. Over the times considered, the integrated doses are substantially the same when calculated from initial times of approximately 1000 sec. Consequently, provided the initial ionization rate is known, it is possible to predict, with reasonable accuracy, dosage by the $t^{-1.2}$ expression for times of initial exposure in the order of 1000 sec. Alternatively, by use of equation (4), it is possible to integrate from earlier times of entry as short as 1 sec.

REFERENCES

1. C. F. Miller, *Gamma Decay of Fission Products from the Slow-Neutron Fission of* U^{235}. U.S. Naval Radiological Defense Laboratory Report USNRDL-TR-187 (1957).
2. P. J. Dolan, *Gamma Spectra of Uranium-235 Fission Products at Various Times After Fission.* AFSWP-524 (1959).
3. J. F. Scoles, *Calculated Gamma Ray Spectra from* U^{235} *Fission Products.* U.S. Air Force Nuclear Aircraft Research Facility, NARF-28-37T FZK-9-132 (1958).
4. A. T. Nelms and J. W. Cooper, *Health Phys.* **1,** 427 (1959); NBS Report 5853 (1958).
5. J. F. Perkins and R. W. King, *Nuclear Sci. & Engng.* **3,** 726 (1958).
6. L. B. Borst, *National Nuclear Energy Series. Radiochemical Studies: The Fission Products* (Edited by C. D. Coryell and N. Sugarman) Book 1, Paper 34. McGraw-Hill, New York (1951).
7. N. Sugarman, S. Katcoff, B, Finkle, N. Elliott and J. D. Knight, *National Nuclear Energy Series. Radiochemical Studies: The Fission Products* (Edited by C. D. Coryell and N. Sugarman) Book 1, Paper 37. McGraw-Hill, New York (1951).
8. W. Zobel and T. A. Love, *Proceedings of the Shielding Symposium held at the U.S. Naval Radiological Defense Laboratory, October,* 1956, Vol. 1. USNRDL-R and L-29 (1957).
9. R. Peelle, W. Zobel and T. A. Love, *Proceedings of the Shielding Symposium held at U.S. Naval Radiological Defense Laboratory, October,* 1956, Vol. 1. USNRDL-R and L-29 (1957).
10. F. C. Maienschein, R. W. Peelle, W. Zobel and T. A. Love, Gamma Rays Associated with Fission. *Proceedings of the Second International Conference on the Peaceful Uses of Atomic Energy, Geneva,* A/CONF., 15/P/670. United Nations, New York (1958).
11. P. D. LaRiviere, *Early-Time Gamma Ray Properties of* U^{235} *Gross Fission Products.* U.S. Naval Radiological Defense Laboratory Report USNRDL-TM-89 (1958).
12. C. F. Miller and P. Loeb, *Ionization Rate and Photon Pulse Decay of Fission Products from the Slow-Neutron Fission of* U^{235}. U.S. Naval Radiological Defense Laboratory Report, USNRDL-TR-247 (1958).
13. W. E. Knabe and G. E. Putnam, *The Activity of the Fission Products of* U^{235}. APEX-448 (1958).
14. J. L. Mackin, P. E. Zigman, P. O. Strom and M. J. Nuckolls, *Early Time Decay of Fission Product Mixtures—I. Scintillation Counter Measurements Following Thermal Neutron Fission of* U^{235}. U.S. Naval Radiological Defense Laboratory Report USNRDL-TR-359 (1960).
15. K. Way and E. P. Wigner, *Phys. Rev.* **73,** 1318 (1948); **70,** 115 (1946).
16. L. D. Gates, Jr. and C. Eisenhauer, *Spectral Distribution of Gamma Rays Propagated in Air.* AFSWP Report No. 502A (1954).

Health Physics Pergamon Press 1961. Vol. 5, pp. 85–89. Printed in Northern Ireland

RELATIVE BIOLOGICAL EFFECTIVENESS OF Co^{60} γ-RADIATION FOR VARIOUS RESPONSES IN MICE*

J. G. KEREIAKES† and M. S. MIRAGLIA

(*Received* 21 *December* 1959; *in revised form* 9 *September* 1960)

Abstract—The biological effectiveness of cobalt-60 γ-irradiation relative to 250 kVp X-irradiation for six different responses in CF_1 mice was found to be: 30-day lethality, 0.79 $\pm$ 0.06; mean survival time, 0.79 $\pm$ 0.04; body weight loss, 0.80 $\pm$ 0.04; intestinal weight loss, 1.00; splenic weight loss, 1.00 $\pm$ 0.06; and testicular weight loss, 0.63 $\pm$ 0.06. The RBE for intestinal weight loss varied with the level of the effect resulting in an average RBE determined for this response. Possible considerations for the observed differences in RBE are discussed.

ZIRKLE[1] and BOAG[2] have published excellent review articles on the relative biological effectiveness (RBE) of various ionizing radiations. Early experiments with mammals relied mainly on lethality as a biologic end-point. Since the radiosensitivity of certain organs and portions of the body varies considerably, it seemed advisable that a number of responses other than lethality be studied. Such studies would indicate the role of the specific organ or portion of the body in the over-all observed effect. These values for relative biological effectiveness would help facilitate decisions of permissible exposure of other mammals, including humans, to various ionizing radiations.

The experiments reported here evaluate the relative biological effectiveness of cobalt-60 γ-irradiation and 250 kVp X-irradiation for the following responses in CF_1 mice: 30-day lethality; mean survival time; body weight loss; intestinal, splenic and testicular weight loss.

MATERIALS AND METHODS

The cobalt-60 γ-rays and 250 kVp X-rays used have approximate linear energy transfer (LET) values of 0.3 keV/μ and 3.0 keV/μ, respectively.

X-rays were delivered by a General Electric Maxitron Unit operated at 250 kVp, 15 mA, 4.75 mm Be inherent filtration, 1 mm Al + 0.5 mm Cu added filtration, HVL 1.1 mm Cu, and tube target-sample distance of 50 cm. γ-Rays (1.17 and 1.33 MeV energy) were supplied by a 1000 c cobalt-60 unit. HVL of radiation is 12 mm Pb and tube target-sample distance of 47 cm was used. Dose rates of 81 rads/min and 63 rads/min, measured with a 100 r Victoreen ionization chamber placed in a paraffin phantom located at the center of the lucite cage (6 in. diameter), were found for the X-rays and Co^{60} γ-rays, respectively. The roentgen dose was converted to rads by assuming that 1 r is equivalent to 0.96 rad for X-rays and 0.98 rad for Co^{60} γ-rays. The 6 mm thick lucite cage cover was more than sufficient to provide electronic equilibrium for the γ-dose measurements.

Adult female and male (used only for the testicular weight loss study) CF_1 mice, weighing 21–23 g, were used. The mice were acclimatized to laboratory conditions for at least 2 weeks prior to use. Prior to and following irradiation exposure, the mice were fed water and Purina Laboratory Chow *ad libitum*. The mice were irradiated ten at a time in a shallow lucite cage. Radiation exposure was unilateral to dorsal surface in all cases.

The biological responses measured must be of a type which respond more or less quantitatively with dose in order that RBE values can be determined. The responses in the present study have been described previously by other investigators and been found to give quantitative dose–response curves which could be transformed to the linear relationship

$$Y = a + bX$$

where Y and X are indices of response and dose,

* Work carried out at the U.S. Army Medical Research Laboratory, Fort Knox, Kentucky.

† Presently, Assistant Professor of Radiology, Department of Radiology, University of Cincinnati College of Medicine, Cincinnati 29, Ohio.

respectively. The biological responses measured included 30-day mortality, mean survival time, whole body weight loss, intestinal weight loss, splenic weight loss and testicular weight loss.

The mice for the mortality study were exposed to graded doses, 400–800 rads, of both radiations, deaths noted every 24 hr, and 30-day mortality recorded. Mean survival time shows a quantitative dose–response relation in the dose range of about 500–1200 rads. Therefore, mean survival times were calculated for the 500–800 rad dose range for the mice used in the mortality study.

Body weight loss in irradiated animals is well established and shows a quantitative relationship with dose.[3] Mice were weighed and exposed to graded doses, 400–800 rads, of both radiations. Four days following exposure the mice were weighed again and weight loss determined.

The weight of the small intestine decreases significantly following irradiation exposure and the degree of weight loss appears to be quantitative with dose.[4,5] Mice were exposed to graded doses, 200–900 rads, of both radiations. Forty-eight hours following exposure, the irradiated mice and a non-irradiated control group were sacrificed. The small intestine from the pyloric juncture to the ileocecal valve was carefully dissected free. The intestine was opened along its entire length, washed free of contents, and excess water squeezed out by stripping down tissue with fingers and by gently blotting. The intestine was then placed in an individual pre-weighed planchet, dried in an oven at 90°C for 24 hr, planchet re-weighed, and intestine dry weight determined.

The spleen weights of irradiated animals decrease appreciably with increasing dose and show a quantitative dose–response relationship.[6,7] Groups of mice were exposed to graded doses, 200–700 rads, of both radiations. Four days following exposure, the irradiated mice and a non-irradiated control group were sacrificed, spleens dissected out and wet weights determined immediately.

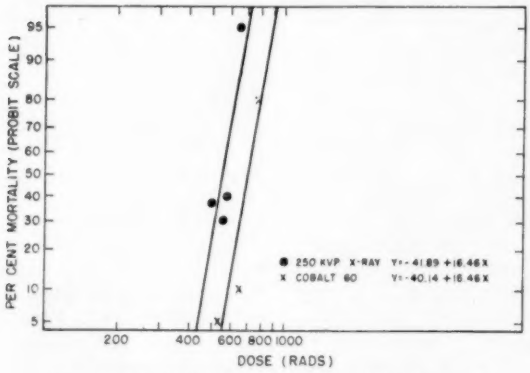

FIG. 1. Mortality in mice exposed to doses of Co^{60} γ-radiation and 250 kVp X-radiation (twenty mice per point).

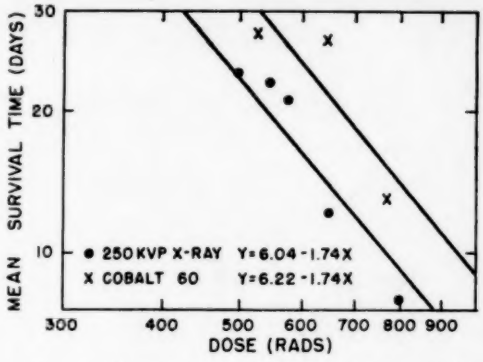

FIG. 2. Mean survival time in mice exposed to doses of Co^{60} γ-radiation and 250 kVp X-radiation (twenty mice per point).

The degree of testicular weight loss is quantitative with respect to dose for a certain dose range.[8,9] Groups of mice were exposed to graded doses, 75–425 rads, of both radiations. Four weeks following exposure, the irradiated mice and a non-irradiated control group were sacrificed, testes dissected out, and wet weights determined.

RESULTS

The mortality, mean survival time, and body weight loss data for both Co^{60} γ-radiation and 250 kVp X-radiation are given in Figs. 1 through 3. To facilitate analysis, probit transformation of dose-mortality data was performed and plotted against log dose. The mean survival time decreased logarithmically with increasing log dose. A linear relationship was found between body weight loss (per cent of control) and dose. For these responses, analysis of the data revealed no significant differences in slopes of the Co^{60} and X-ray regression equations. The regression lines were then adjusted to have a common slope, and the equations recalculated. The RBE of Co^{60} γ-rays in terms of 250 kVp X-rays was determined from the adjusted equations.

Changes in intestine, spleen, and testes weight for both radiations are given in Figs. 4 through 6. The mean organ weights are

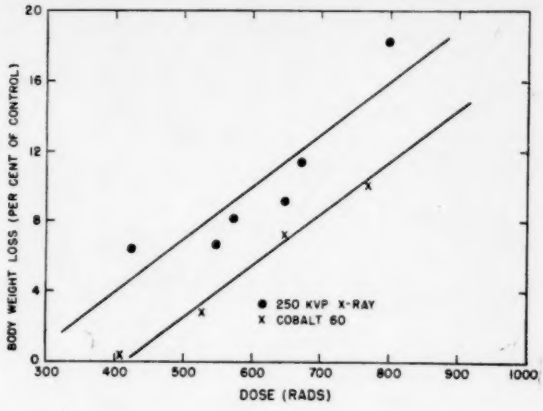

FIG. 3. Body weight loss in mice exposed to doses of Co^{60} γ-radiation and 250 kVp X-radiation (twenty mice per point). ●—$Y = -8.26 + 0.03X$; ×—$Y = -12.50 + 0.03X$.

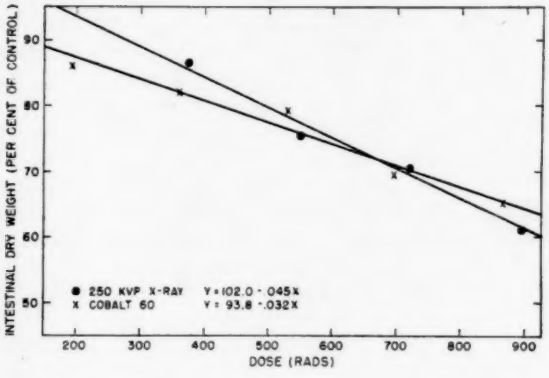

FIG. 4. Intestinal dry weight in mice exposed to doses of Co^{60} γ-radiation and 250 kVp X-radiation (twenty mice per point).

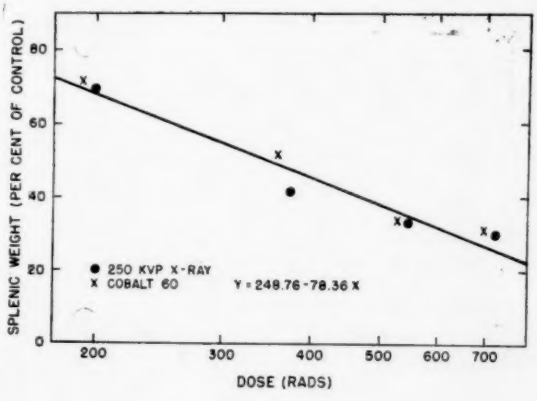

FIG. 5. Splenic weight in mice exposed to doses of Co^{60} γ-radiation and 250 kVp X-radiation (twenty mice per point).

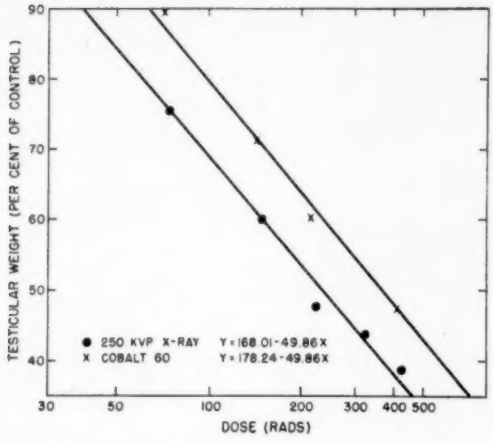

FIG. 6. Testicular weight in mice exposed to doses of Co^{60} γ-radiation and 250 kVp X-radiation (twenty mice per point).

expressed as per cent of control values. Testes and spleen weights show a linear response with log dose, whereas the intestinal weights show a linear response with increasing linear dose. Analysis of the intestinal weight loss equations showed that the slopes differed significantly and that the RBE varied with the level of the effect. By integrating the areas under the regression lines and obtaining the ratio, an average RBE was determined. Analysis of the regression equations for the splenic weight loss showed that they did not differ significantly and that a single equation adequately represented the data for both types of radiation. Since the slopes of the regression lines for testicular weight loss did not differ significantly, the lines were adjusted to have a common slope constant. The RBE was then determined from the adjusted equations.

Table 1. *Relative biological effectiveness of cobalt-60 γ-radiation for various responses in CF_1 mice*

Response	RBE (relative to 250 kVp X-radiation)
30-day mortality	0.79 ± 0.06
Mean survival time	0.79 ± 0.04
Body weight loss	0.80 ± 0.04
Intestinal weight loss	1.00
Splenic weight loss	1.00 ± 0.06
Testicular weight loss	0.63 ± 0.06

The RBE values for Co^{60} γ-radiation relative to 250 kVp X-radiation for the six responses are summarized in Table 1. The range of values is from 1.00 for intestinal and splenic weight loss, to about 0.80 for the three total body responses (mortality, mean survival time, and body weight loss), to 0.63 for testicular weight loss.

DISCUSSION

The biological effectiveness of Co^{60} γ-radiation relative to 250 kVp X-radiation was found to be different for the various responses measured in CF_1 mice. The different effectiveness may be ascribed in part to changing linear energy transfer (this is approximately 0.3 keV/u and 3 keV/u for Co^{60} γ-rays and 250 kVp X-rays, respectively) and thus a difference in dose deposition to tissue and bone. X-rays are considered to deliver a slightly higher dose to the bone marrow than the more energetic γ-rays, according to the data of SPIERS[10]. WOODARD[11] studied the loss of alkaline phosphatase in mouse bone following exposure to X-rays of 100, 180, 1000 and 22,000 kV peak energies. Based on incident dose, a relative effectiveness of 0.96, 1.00, 0.76 and 0.88 were found for the respective qualities. However, based on absorbed energy, it was felt that the RBE values were unity. The above could possibly explain, in part, the lesser effectiveness of Co^{60} γ-rays for the three total body responses (mortality, mean survival time, and body weight loss), but would not explain the lesser effectiveness of Co^{60} γ-rays for testicular weight loss.

No differences were observed in the RBE value for mortality and mean survival time, indicating that these two radiations qualitatively produce the same mode of damage. The organ weight loss studies show the following trend. The intestine, spleen and testes weight loss determinations were made at 2, 4 and 28 days, respectively. The greater the latent period (time interval following irradiation exposure at which response is measured), the less effective Co^{60} γ-rays appeared to be than 250 kVp X-rays. The postulations of BLAIR,[12,13]

recently discussed by STORER *et al.*,[14] may be applicable here. It has been suggested by BLAIR that two types of radiation damage occur—reparable and irreparable. Results from fractionated dose experiments performed using various radiations indicate that the higher the linear energy transfer of the radiation the greater is the extent of the irreparable damage. This is sometimes interpreted in terms of recovery rates; that is, a slower recovery rate for the higher linear energy radiation. The intestinal and splenic weight loss responses, because of their short latent period, measure primarily early damage.

Certain critical evaluations of the RBE values should be mentioned. The intestine and spleen values suffer from so-called "abscopal effect",[15] whereas the testes appear to be minimally affected by this phenomenon.[16–18] These considerations of the role of the abscopal effect on the RBE values warrant further study, particularly for partial-body radiation exposure conditions.

SUMMARY

The relative effectiveness of cobalt-60 γ-rays to 250 kVp X-rays for various biological responses in CF_1 mice was found to be: 30-day mortality, 0.79 ± 0.06; mean survival time, 0.79 ± 0.04; body weight loss, 0.80 ± 0.04; intestinal weight loss, 1.00; splenic weight loss, 1.00 ± 0.06; and testicular weight loss, 0.63 ± 0.06. The RBE for intestinal weight loss varied with the level of the effect resulting in an average RBE determined for this response. Possible considerations for the observed differences in RBE are discussed.

REFERENCES

1. R. E. ZIRKLE, *Radiation Biology* (Edited by A. HOLLAENDER) Vol. 1, Pt. 1, p. 315. McGraw-Hill, New York (1954).
2. J. W. BOAG, *The Relative Biological Efficiency of Different Ionizing Radiations.* National Bureau of Standards Report 2946, Washington, D.C. (1953).
3. D. E. SMITH and E. B. TYREE, *Amer. J. Physiol.* **177,** 251 (1954).
4. R. A. CONARD, *Proc. Soc. Exp. Biol., N.Y.* **82,** 333 (1953).
5. R. A. CONARD, *Proc. Soc. Exp. Biol., N.Y.* **86,** 664 (1954).
6. R. E. CARTER, P. S. HARRIS and J. T. BRENNAN, *The Effects of Acute Doses of X-irradiation on the Splenic and Thymic Weights of CF_1 Female Mice.* Los Alamos Scientific Laboratory Report LA–1075. Los Alamos, New Mexico (1950).
7. R. F. KALLMAN and H. I. KOHN, *Rad. Res.* **3,** 77 (1955).
8. A. B. ESCHENBRENNER and E. MILLER, *Arch. Path. (Lab. Med.)* **50,** 736 (1950).
9. H. I. KOHN and R. F. KALLMAN, *Brit. J. Radiol.* **27,** 586 (1954).
10. F. W. SPIERS, *Brit. J. Radiol.* **22,** 521 (1949).
11. H. G. WOODARD, *Rad. Res.* **3,** 359 (1955).
12. H. A. BLAIR, *A Formulation of the Injury, Life Span, Dose Relations for Ionizing Radiation—I. Application to the Mouse.* University of Rochester Report UR–206. Rochester, New York (1952).
13. H. A. BLAIR, *A Formulation of the Injury, Life Span, Dose Relations for Ionizing Radiation—II. Application to the Guinea Pig, Rat and Dog.* University of Rochester Report UR–207. Rochester, New York (1952).
14. J. B. STORER, P. S. HARRIS, J. E. FURCHNER and W. H. LANGHAM, *Rad. Res.* **6,** 188 (1957).
15. R. H. MOLE, *Brit. J. Radiol.* **26,** 234 (1953).
16. A. RAVENTOS, *Rad. Res.* **1,** 381 (1954).
17. H. I. KOHN, *Rad. Res.* **3,** 153 (1955).
18. R. F. KALLMAN and H. I. KOHN, *Rad. Res.* **3,** 77 (1955).

Health Physics Pergamon Press 1961. Vol. 5, pp. 90–98. Printed in Northern Ireland

THE BEHAVIOR OF INHALED $Ru^{106}O_2$ PARTICLES*

W. J. BAIR, D. H. WILLARD and L. A. TEMPLE
Biology Operation, Hanford Laboratories, General Electric Company, Richland, Washington

(*Received* 6 *July* 1960)

Abstract—About 24 per cent of total inhaled $Ru^{106}O_2$ was deposited in lungs of mice. Lung retention of deposited Ru^{106} was studied with a whole-body monitor. Radiochemical assay of tissues from mice killed at intervals up to 70 weeks after exposure confirmed retention in pulmonary tissues. Of three exponential components of the lung clearance curve the longest biological half-life was 230 days for about 2 per cent of the total lung deposition. Translocation to other tissues was also observed. Several tissues including ovaries and adrenal glands attained greater concentrations, though smaller quantities, than the lungs. The total dose to lung over the 70-week period was estimated to be 4600 rads per μc of total Ru^{106} deposited. An $MPC_{(air)}$ for $Ru^{106}O_2$ of 1.3×10^{-8} μc per cm^3 air for a 40-hr week was derived by assuming lung to be the critical organ and by extrapolating the data from mouse to man on the basis of differences in weight alone, ignoring differences in anatomy and physiology.

INTRODUCTION

BIOLOGICAL data are required for evaluating the hazard of inhaled radioactive particles and establishing maximum permissible limits. For this, it is necessary to know the fraction of inhaled material deposited, its subsequent behavior and its effect on the host.

Of the many fission products that need to be studied, Ru^{106} was chosen because it often occurs as the relatively insoluble dioxide, a characteristic which should favor prolonged retention in the pulmonary tissues. Ru^{106} is a β-emitter (maximum energy = 0.04 MeV) with a half-life of 1 year. The daughter of Ru^{106}, Rh^{106}, is also a β-emitter (maximum energy = 3.5 MeV) with a half-life of 30 sec. The energy released in the $Ru^{106} \rightarrow Rh^{106} \rightarrow Pd^{106}$ (stable) chain is therefore largely attributed to Rh^{106}. However, because of the short half-life of Rh^{106},[1] the biological distribution of the released energy will be determined by the physiological behavior of the parent Ru^{106}.

In this study female mice were exposed to aerosols of $Ru^{106}O_2$ and its physiological behavior determined over a period of 70 weeks. The results provide some basis for evaluating the hazards associated with the inhalation of relatively insoluble radioactive ruthenium compounds.

METHODS

Exposure to ruthenium oxide particle aerosols

The techniques used for exposing mice to air containing $Ru^{106}O_2$ particles are described in detail in a separate report.[2] Mice were individually placed head first into 50-ml conical centrifuge tubes with the bottom $\frac{1}{2}$ in. cut off to give a $\frac{3}{8}$-in. opening. The tubes, plugged with cellulose tissue and stoppered, were inserted into ports drilled into the side of a vertical exposure chamber constructed of a 16-in. length of 8-in. (o.d.) lucite tubing. The exposure chamber held eighty-four tubes in seven rows of twelve each. The aerosol was admitted at the top and exhausted at the bottom through an electrostatic precipitator to prevent contamination of the room air. The aerosol concentration varied approximately 25 per cent from the top to the bottom of the chamber. During all inhalation experiments aerosol samples were collected on millipore filters (type AA)† and the particles characterized and sized by electron microscopic examination.

Three methods were used to obtain $Ru^{106}O_2$ aerosols. (1) An aerosol of ruthenium acetate solution containing approximately 3 mc Ru^{106} per mg ruthenium acetate was produced with a jet-type aerosol generator.[2] The aerosol passed through an oven where it

* Work performed under Contract No. AT(45-1)-1350 between the Atomic Energy Commission and General Electric Company.

† Millipore Filter Corporation.

was heated to 700°C converting the ruthenium acetate to ruthenium oxide. Less than 10 per cent of the particles thus produced were soluble in water and the particle diameter ranged from 0.01 to 3 μ, the majority being 0.2 to 0.5 μ. The fog containing ruthenium oxide was passed into a lucite exposure chamber designed to expose only the nose of the mouse. (2) A suspension of ruthenium oxide particles prepared by oxidation of ruthenium trichloride (1.8 mc Ru^{106} per mg stable ruthenium per ml) with NaOH and H_2O_2, and suspended in 0.1 per cent Pluronics,* was placed in a small scale aerosol generator.[2] Dispersal of the particles in a fog was effected by forcing air at 20 lb/in^2 through an orifice (no. 80 size hole) in the side of a twelve-gage spinal tap needle sealed at the end and inserted into the suspension to a level placing the orifice just above the surface of the suspension. The fog containing ruthenium oxide was then passed into the mouse exposure chamber. The particle size ranged from 0.01 to 3.6 μ in diameter. The mean size was 0.33 μ and the median size was 0.2 μ. (3) Ruthenium oxide particles prepared by oxidation of ruthenium trichloride were washed, resuspended in 95% ethanol and added to finely powdered NaCl which was then dried, and reground to break up the clumps. The NaCl containing the ruthenium oxide particles was placed in gelatine capsules (no. 4) and, by means of a specially modified air pistol, dispersed into the mouse exposure chamber. [2] The particle size ranged from 0.05 to 5 μ. The mean size was approximately 1 μ.

After inhalation exposures the head region of each mouse was washed with soap and water to remove externally deposited Ru^{106} before monitoring.

Whole-body monitoring

Total-body burdens of Ru^{106} were obtained by encasing the live mouse in a plastic tube and placing the tube in a scintillation counter designed to monitor either the whole mouse or any increment along the length of the mouse.[3]

Tissue analysis

For determination of the tissue content of Ru^{106}, groups of mice were killed by cervical dislocation at intervals after exposure. Tissues were removed, minced and placed on stainless steel plates. Nitric acid was added and the samples were dried under infrared lamps. The stainless steel plates were counted with an end-window Geiger–Mueller tube.

* Polypropylene glycol-ethylene oxide polymer—Wyandotte Chemical Corporation.

RESULTS

Deposition and distribution following inhalation

In order to determine the amount of Ru^{106} retained and its distribution with time after inhalation, mice in groups of from ten to sixty were killed immediately after exposure. The respiratory and gastrointestinal tracts were removed for Ru^{106} assay. To obtain an estimate of the fraction that was deposited it was assumed that mice inhaled 25 ml air per minute.[4–6] The concentration of Ru^{106} in the air was determined from millipore filter samples of measured volumes of air drawn during the exposure. The deposition and distribution of Ru^{106} is shown in Table 1 and is given as the per cent of the estimated total $Ru^{106}O_2$ inhaled, which varied from one-half to three microcuries. The exposures were from 15 min to 2 hr duration. The percentage in the gastrointestinal tract was greater following long exposures and, conversely, the percentage present in the upper respiratory tract, which included the trachea and skinned head, was greater immediately following the short exposure. This seems to indicate temporary retention of deposited material in the upper respiratory tract with subsequent movement almost entirely to the gastrointestinal tract because the fraction in the lung was independent of the exposure time. The average fraction deposited in lungs was about 24 per cent for seven experiments, although in one experiment only 15 per cent and in another as much as 38 per cent was deposited in the lungs. However, the agreement between experiments was surprisingly good considering the necessity for assuming a minute volume. The uniformity of pulmonary deposition in the several experiments also indicates little or no effect of the suspending agent, Pluronics, used in method (2) for obtaining a RuO_2 aerosol. In two experiments half of the mice were not killed until 24 hr after exposure. The percentage of inhaled Ru^{106} present in lung at that time was 10–14 per cent, or about half that present immediately after exposure.

Retention

The retention of Ru^{106} in mice was studied in two ways. One group of fifty mice was

Table 1. *Deposition and distribution of inhaled* $Ru^{106}O_2$
(Percentage of total $Ru^{106}O_2$ inhaled)

Experiment	1	2	3	4	5	6	7
Duration of exposure	15 min (dust)	15 min	1 hr	1 hr	2 hr	2 hr	2 hr
Number of mice and strain	25 LAF_1	11 LAF_1	14 LAF_1	60 LAF_1	32 LAF_1	10 BAF_1	10 BAF_1
Per cent deposited in upper respiratory tract (trachea and skinned head) and subsequently swallowed	—	50	28	—	—	—	—
Per cent immediately present in GI tract	23	17	34	13	42	56	66
Per cent immediately present in lung	22	26	23	24	22	16	38
Per cent present in lung after 24 hr	—	—	—	14	10	—	—

Experiment no. 1. A capsule containing 25 μc $Ru^{106}O_2$ dust was fired into a 7-l. chamber, particle size range = 0.05–5 μ.

Experiments nos. 2, 3, 5, 6 and 7. $Ru^{106}O_2$ fog produced by aspirating a suspension, (5×10^{-3} μc/cm^3), particle size range = 0.01–4 μ, mean = 0.33 μ, median = 0.2 μ.

Experiment no. 4. $Ru^{106}O_2$ fog produced by combustion of ruthenium acetate aerosol, (1×10^{-4} μc/cm^3) particle size range = 0.01–4 μ, mean = 0.14 μ, median = 0.06 μ.

assayed with the whole-body monitor at weekly intervals for 8 weeks after exposure. The low body burden at that time, less than 0.02 μc, prevented further accurate monitoring. From fifteen to twenty mice from other groups were serially sacrificed at times up to about 500 days (70 weeks) after exposure and the total content of Ru^{106} in all tissues determined. The whole-body retention of Ru^{106} determined by both methods is shown in Fig. 1. Averages of individual whole-body burdens in per cent of the total quantity deposited are plotted logarithmically against time in days. The data were corrected for decay, and thus represent the biological retention of Ru^{106}. Both sets of data were fitted with straight lines by the method of least squares analysis. For whole-body monitoring from 7 to 56 days, $Y = 100t^{-0.93}$, and for the tissue assay method from 4 to 420 days, $Y = 86t^{-0.96}$, where Y is the percentage of the original dose that was present at any time t, in days, after administration. The retention of many radioisotopes has been observed by other investigators to follow a straight-line relation when plotted logarithmically[7–9] and indicates that a progressively decreasing fraction of the deposited material is retained per unit of time.

Shown also in Fig. 1 are the data for lung burdens obtained by assay of dissected tissue and are expressed as a percentage of the total Ru^{106} deposited. For lung, $Y = 60t^{-0.97}$ and is similar to that for the whole body. Pulmonary clearance is discussed further in a subsequent section.

Translocation

To determine the translocation of Ru^{106} from the lung to other tissues and the turnover from those tissues, mice were killed at various times up to 70 weeks after exposure by method (2). The distribution of Ru^{106} in these tissues is shown in Fig. 2 and is expressed as the percentage of the total Ru^{106} originally deposited. A

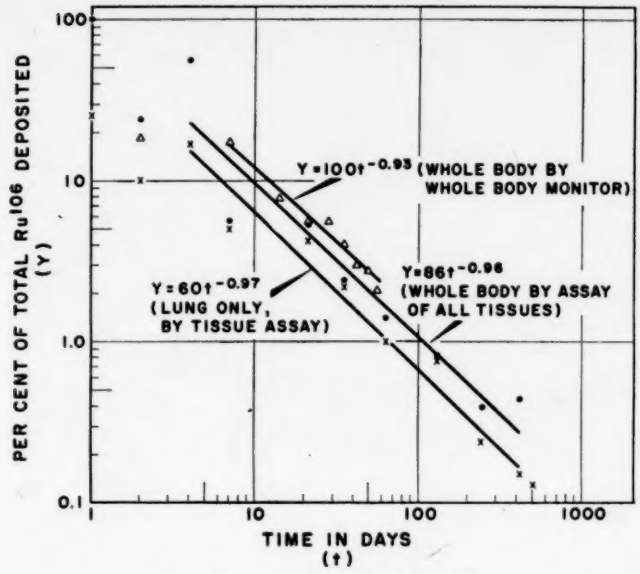

FIG. 1. Retention of Ru^{106} in mice.

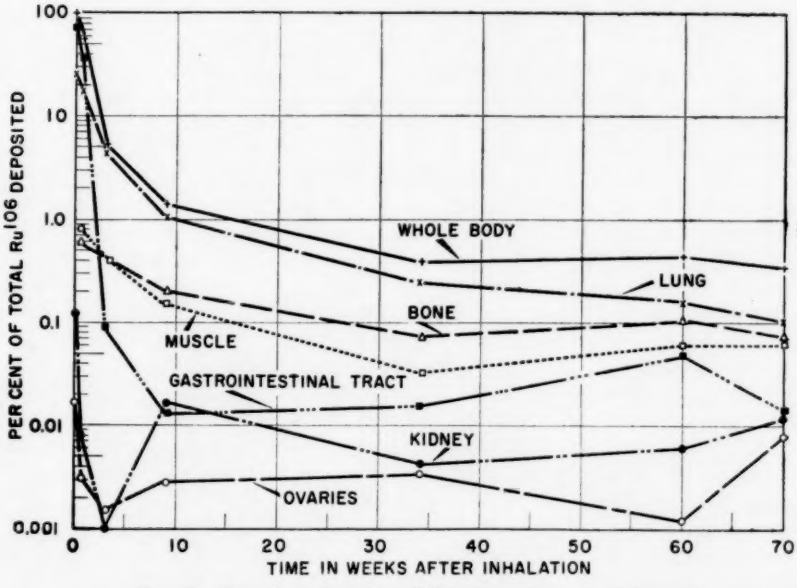

FIG. 2. Translocation of $Ru^{106}O_2$ (based on total deposition).

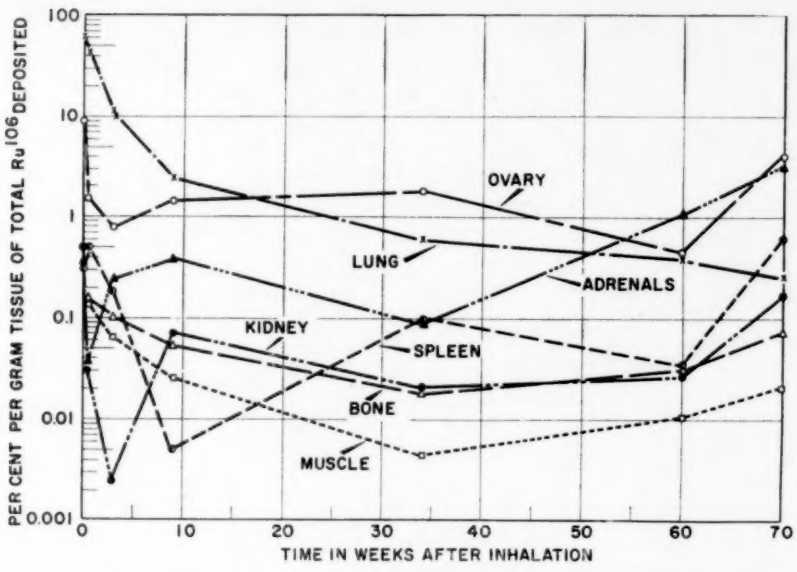

FIG. 3. Translocation of $Ru^{106}O_2$ (based on concentration in tissues).

semi-logarithmic plot is used for graphic purposes only. For the first few days after exposure the largest percentage of deposited Ru^{106} was in the gastrointestinal tract and somewhat less in lung and trachea. Small percentages appeared in other tissues including muscle, bone, kidney and ovary. Other tissues including spleen and liver contained even less and are not included in the figure. The immediate appearance of about 1 per cent of deposited Ru^{106} in these tissues, somewhat distant from the areas of deposition, suggests the presence of some soluble ruthenium compounds mixed with the oxides.

Throughout the remainder of the experiment, the lung contained the largest fraction of the deposited Ru^{106}, but decreased in total content while other tissues remained about the same or showed slightly increased Ru^{106} content. The lung contained about 0.1 per cent of the original total dose after 70 weeks when the whole-body burden was about 0.4 per cent. Although ruthenium is not generally considered a bone-seeking element, the build-up of Ru^{106} in bone in these experiments was greater than in any other tissues, accounting for about one-fourth of the total body content after 70 weeks. The muscle content was two-thirds that of bone.

For purposes of hazard evaluation the concentration rather than total quantity in a particular tissue is usually more important because the absorbed dose of radiation is dependent upon the radioactivity per gram of tissue. In Fig. 3 the concentration of Ru^{106} for several tissues at various times after exposure is expressed as per cent per gram of tissue of the total-body deposited Ru^{106}. The selective translocation of Ru^{106} from lung to other tissues is more apparent than is indicated in Fig. 2. Although quantitatively it was shown in Fig. 2 that a large proportion of Ru^{106} was translocated to bone and muscle, relative to the weight of tissue larger proportions were translocated to ovaries, adrenals, spleen and kidney.

It was interesting that, despite the consistently high concentration in ovary and adrenals, autoradiograms of these tissues have shown nothing. However, since the autoradiograms were prepared from only a few sections it was possible to have missed the Ru^{106}.

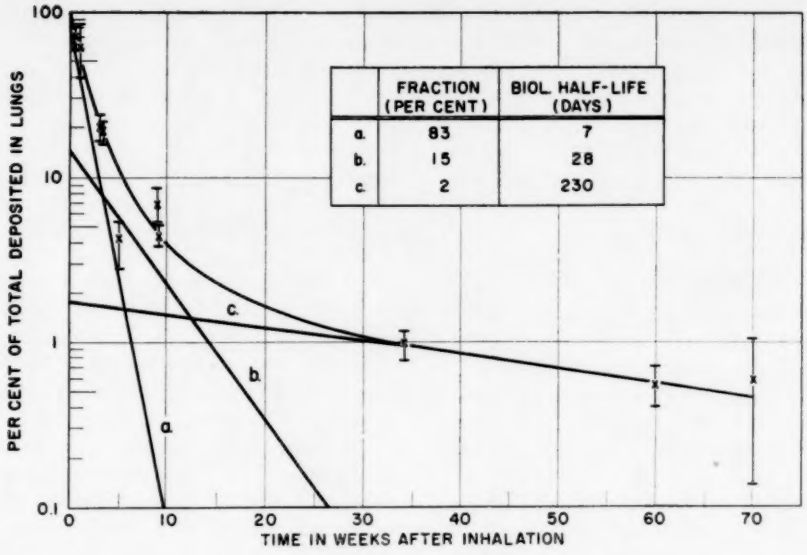

FIG. 4. Pulmonary retention of $Ru^{106}O_2$.

Lung clearance

The clearance of Ru^{106} from lung is of particular interest because it was the tissue containing the largest quantity throughout the experimental period. The lung clearance of Ru^{106} was determined from the assay of lung tissue removed from mice killed at intervals after being exposed by method (2). The data in Fig. 4 are expressed as the percentage of the total Ru^{106} originally deposited in lung and are corrected for the radioactive decay of Ru^{106}. Each point represents the mean value for from twelve to twenty mice and the standard deviations are shown. The clearance curve was resolved into three exponential components each having a different slope corresponding to the half-life of a particular fraction of the deposited material. The equation for clearance is of the form, $p = Ae^{-at} + Be^{-bt} + Ce^{-ct}$, where p is the percentage of the total material originally deposited in the lung that is present at a given time t. In this study $p = 83$ per cent $e^{-0.1t} +$ 15 per cent $e^{-0.024} + 2$ per cent $e^{-0.003t}$. Biological half-lives for each of these fractions were 7, 28 and 230 days, respectively. The effective half-lives were 7, 26 and 140 days.

DISCUSSION

Deposition and distribution

The International Commission on Radiological Protection assumed for man that 25 per cent of the quantity of an inhaled substance that is not readily soluble is exhaled, 50 per cent is deposited in the upper respiratory passages and swallowed, and 25 per cent is deposited in lungs, half of which is present 24 hr later.[10] These values compare favorably with experimental data observed in the present study. Although this is of interest, it does not necessarily validate the ICRP assumptions for man since a firm basis for the extrapolation of respiratory physiological data from mouse to man has not been established. The 24 per cent deposition in lungs of particles with a mean size 0.14 and 0.33 μ observed in this study is within the range of theoretical and experimental data summarized by HULTQVIST[11]. The total respiratory tract retention of particles between 0.1 and about 0.6 μ in diameter was between 20 and 40 per cent. The agreement of our mouse data with both experimental and theoretical data of others may only be fortuitous,

especially since it was necessary to assume a value for the mean minute volume. Also, many factors which were not controlled in these experiments are known to alter deposition of particles. These include respiratory frequency and tidal volume as was recently pointed out by STANNARD and MORROW.[12] Therefore, the deposition in Table 1 may serve only as a point of reference for these studies.

Retention and translocation

The whole-body turnover of Ru^{106} after inhalation was somewhat different than reported earlier after intratracheal injection where the percentage of the original dose at a given time after administration was expressed by two power-function equations[13]. The initial portion of the curve, 3–59 days, was expressed by $110t^{-0.4}$ and the latter portion, 59–427 days, by $1700t^{-1.0}$. Ru^{106} showed a higher retention during the earlier time after intratracheal administration than inhalation. In this study the slopes of the inhalation curves given by the exponents were about 1. This is in agreement with the second phase of the intratracheal experiment. Despite the demonstrated translocation of a fraction of the deposited Ru^{106} the turnover of Ru^{106} from lung proceeded at about the same rate as from the whole body. This lends credence to the idea of using whole-body monitoring techniques for determining pulmonary clearance in humans exposed to $Ru^{106}O_2$.

The translocation of Ru^{106} after deposition in the respiratory and gastrointestinal tract by inhalation was similar to that following intratracheal administration with the exception that retention was reduced by 10 per cent.[13] In both studies high concentrations were found in the ovaries. Higher concentrations of Ru^{106} also appeared in kidney and spleen but they represented only small fractions of the total amount deposited. In general, the distribution of Ru^{106} translocated from lung did not differ appreciably from that reported by others for intravenous, intraperitoneal, intragastric and intratracheal administration of $Ru^{106}Cl$ in rats.[14] Therefore, it is reasonable to assume that translocation of Ru^{106} from lung to other tissues proceeded largely as a result of slow solubilization of RuO_2 retained in lung and probably in the associated lymphatic tissues. Absorption of ruthenium from the gastrointestinal tract is considered negligible since THOMPSON *et al.*[14] found, at most, only a few per cent absorbed in rats after ingestion of compounds more soluble than RuO_2.

Because the lung contained the major portion of Ru^{106} throughout the duration of the experiment, both in total quantity and in concentration, it was the lung that received the greatest total radiation dose. An estimate of this dose is of interest in explaining possible pathology being studied in a parallel experiment. This estimate may be obtained from the lung-clearance data with the necessary assumption that the Ru^{106} is uniformly distributed throughout the lung tissue.* Using the equation of LOEVINGER *et al.*[15] and the exponentials for the clearance of Ru^{106}, the total dose to lung over the 70-week period was about 4600 rads/μc deposited in lung by inhalation. For the mice in this experiment depositing 0.1–0.5 μc, the total dose was 460–2300 rads. The estimated minimal dose at which an occasional lung cancer could be expected is about 1000 rads.[16] Lung-cancer was not detected by gross inspection of the mice in this experiment.

Maximum permissible limits

The clearance data can be used to derive a maximum permissible concentration of $Ru^{106}O_2$ in air by making several assumptions. In effect, one extrapolates from mouse to man and from a single exposure situation to one where exposure might be daily or continuous. The lung is assumed the critical organ and the Ru^{106} is assumed uniformly distributed throughout lung tissue. Extrapolation from mouse to man is based on differences in organ weight and ignores differences in physiology.

To extend the results obtained from lung-clearance studies following a single day's inhalation to the condition of daily administration, certain mathematical manipulations can be used. In general, these amount to finding the summation of an infinite number of daily

* Although autoradiograms show non-uniform distribution of Ru^{106} in lungs and other tissues.

doses and calling the result the dose at equilibrium. Specifically, if q_0 is the number of microcuries deposited in the lungs by 1 day's inhalation, and q is the number of microcuries that remain after some time, t, then the percentage of that originally deposited which is present at t is

$$p = 100\,\frac{q}{q_0} \tag{1}$$

If the doses are repeated daily, the sum of the daily percentages present becomes

$$P = p_1 + p_2 + \ldots + p_n$$

$$P = \sum_1^n p \tag{2}$$

Assuming daily doses are the same as continuous doses, then from the calculus

$$P = \int_0^t p\,dt \tag{3}$$

since each incremented p in equation (2) varies with time.

Experimentally, it was found that

$$p = Ae^{-at} + Be^{-bt} + Ce^{-ct} \tag{4}$$

Upon substituting this value for p in equation (3) and integrating between the limits shown

$$P = \frac{A}{a}(1 - e^{-at}) + \frac{B}{b}(1 - e^{-bt}) + \frac{C}{c}(1 - e^{-ct}) \tag{5}$$

From the experimental data the longest effective half-life observed for inhaled Ru^{106} is 140 days, which is small compared with 50 years, the duration assumed for continuous exposures.[10] Therefore, it is sufficiently accurate, for purposes of permissible limit estimations, to integrate equation (3) between zero and infinity. This gives the equilibrium value for P:

$$P_{eq} = \frac{A}{a} + \frac{B}{b} + \frac{C}{c} \tag{6}$$

This is the number of microcuries of Ru^{106} that should be present in the lung after deposition of 100 μc daily has occurred sufficiently long to reach the point when the rates of deposition and clearance are equal. On substituting experimental data for the right-hand members of equation (6) one obtains the number of microcuries that results:

$$P_{eq} = \frac{83}{0.099} + \frac{15}{0.0267} + \frac{2}{0.0049}$$
$$= 838 + 561 + 408 = 1807\ \mu c \tag{7}$$

For any number of microcuries deposited daily, q, other than 100, the equilibrium quantity present will be

$$Q_{eq} = \frac{P_{eq}}{100} \cdot q = 18.1\,q \tag{8}$$

The value for the maximum permissible lung burden at equilibrium, Q_{eq}, for $Ru^{106}O_2$ is given as 0.6 μc by the ICRP.[10] From equation (8), the corresponding maximum daily deposited amount is

$$q = \frac{0.6}{18.1} = 0.033\ \mu c \tag{9}$$

The quantity daily deposited is some fraction, f, of the quantity daily inhaled. Taking $f = 0.25$,[10] the permissible daily inhaled amount is

$$I = \frac{0.033}{0.25} = 0.13\ \mu c \tag{10}$$

This results from daily inhaling a volume of air containing M μc/cm^3. Taking 10^7 cm^3 as the volume of air inhaled by the standard man,[10] the permissible air concentration is

$$1.3 \times 10^{-8}\ \mu c/cm^3 \tag{11}$$

This value is not markedly different from estimates derived in studies of intratracheally administered $Ru^{106}O_2$.[18] The $MPC_{(air)}$ for a 40-hr week recommended by Committee II on Permissible Dose for Internal Radiation, ICRP[10], as well as the NCRP[17] for insoluble Ru^{106} is $6 \times 10^{-9}\mu c/cm^3$.

It is hoped that a more satisfactory basis for determining the maximum permissible concentration in air will be forthcoming with the completion of toxicity experiments on several species of animals.

SUMMARY

(1) The pulmonary deposition of inhaled $Ru^{106}O_2$ particles in mice was about 25 per cent of the total inhaled and was comparable to data published by others for particles of similar size.

(2) The clearance of Ru^{106} following inhalation of $Ru^{106}O_2$ determined by whole-body counting techniques approximated the value obtained for pulmonary turnover by serial sacrifice techniques. The rates were not in disagreement with earlier published data for intratracheal administration.

(3) Distribution of the small fraction of Ru^{106} translocated from lung was not markedly different from data published by others after administration of soluble forms.

(4) About 2 per cent of Ru^{106} deposited in lung was retained with a biological half-life of 230 days. The total dose to lung tissue per microcurie of Ru^{106} deposited in lung was about 4600 rads. Extrapolation of the data to man on a basis of difference in organ weight only, and assuming lung to be the critical organ, an $MPC_{(air)}$ for $Ru^{106}O_2$ of $1.3 \times 10^{-8} \mu c/cm^3$ for a 40-hr week was derived.

Acknowledgments—We are grateful to M. G. Brown for assisting in performing the experiments, to B. J. McClanahan and A. C. Case of the Biological Analyses Operation for radiochemical assays, and to W. L. Nicholson and A. D. Wiggins of the Operations Research and Synthesis Operation for advice during the planning phase of the experiment and for statistical analysis of the data. We are also indebted to Major J. L. Terry (USAF-VC), temporarily assigned to Hanford Biology Operation, who performed one of the experiments presented. We particularly wish to thank Dr. H. A. Kornberg for encouragement and for help in formulating equations for maximum permissible limits.

REFERENCES

1. L. R. Boyd, Ru^{106}–Rh^{106} *Activity*. Document HW-28924 (1958).
2. D. H. Willard, W. J. Bair and L. A. Temple, *Techniques for Exposure of Mice to Aerosols of Radioactive Particles*. Document HW-52368 (1958).
3. D. A. Campbell and L. D. Test, *Operation and Maintenance of Mouse Counter*. Document HW-39837 (1955).
4. The Committee on the Handbook of Biological Data, AERO Medical Laboratory, Wright Air Development Center, *Handbook of Biological Data*, WADC Technical Report 56-273, ASTIA, AD-110501 (1956).
5. A. C. Guyton, *Amer. J. Physiol.* **150,** 70 (1947).
6. W. J. Bair. Unpublished data.
7. D. Anthony, K. Lathrop and R. Finkle, *Radiotoxicity of Injected Sr^{89} for Rats, Mice and Rabbits —II. Metabolism and Organ Distribution*. Document MDDC-1363 (1946).
8. M. N. Swift, C. L. Prosser and E. S. Mika, *Effects of Sr^{89} and X-radiation on Goats*. Document CH-3888 (1948).
9. G. Sacher, *The Excretion, Retention, Distribution and Clinical Effects of Strontium^{89} in the Dog*—II. *Statistical Analysis of Excretion and Retention of Strontium^{89} for Individual Dogs*. Document CH-3866 (1946).
10. Report of Committee II on Permissible Dose for Internal Radiation, International Commission on Radiological Protection, (1959). *Health Phys.* **3,** 15, 16, 33, 153 (1960).
11. B. Hultqvist, *Kgl. Svenska Vetenskapsakademiens Handlingar, Fjarde Serien* **6,** No. 3, 1 (1956).
12. J. N. Stannard and P. E. Morrow, Retention of sub-micron aerosols in the human respiratory tract. *The Shorter-Term Biological Hazards of Fallout Field Symposium* (Edited by G. M. Dunning and V. A. Hilcken). United States Atomic Energy Commission (1956).
13. D. H. Willard, L. A. Temple and W. J. Bair, *Turnover and Tissue Distribution of Radioruthenium Oxide in the Lungs of Mice*. Document HW-52286 (1957.)
14. R. C. Thompson, M. H. Weeks, O. L. Hollis, J. E. Ballou and W. D. Oakley, *Amer. J. Roentgenol.* **79,** 1026 (1958).
15. R. Loevinger, J. G. Holt and G. J. Hine, *Radiation Dosimetry* (Edited by G. J. Hine and G. L. Brownell) Chap. 17. Academic Press, New York (1956).
16. Members of the Subcommittee on Inhalation Hazards of the Pathological Effects of Atomic Radiation Committee, National Academy of Sciences, Effects of inhaled radioactive particles, Draft III, April (1959).
17. *Maximum Permissible Body Burdens and Maximum Permissible Concentrations of Radionuclides in Air and in Water for Occupational Exposure*, U.S. Department of Commerce—National Bureau of Standards Handbook 69 (1959).
18. W. J. Bair, *Calculation of Maximum Permissible Concentration in Air, MPC_{Air} for Ru^{106} Particles*. Document HW-52287 (1957).

Health Physics Pergamon Press 1961. Vol. 5, pp. 99–100. Printed in Northern Ireland

NOTE

Comments on the Revision to Appendix B, NBS Handbook 61

(Prepared by Health Physics Society Committee on Radiation Regulation)

THE Committee on Radiation Regulation of the Health Physics Society has reviewed the revised "Suggested Radiation Protection Regulations" drafted by the NCRP Subcommittee 10, and published in this issue of *Health Physics* (Vol. 5, p. 1). The Committee feels that a number of improvements have been made over the earlier version of the "model code" as originally published in Appendix B of NBS Handbook 61. During its review, however, the Committee noted several points that might prove undesirable if the sections involved were enacted, as now written, into State Radiation Safety Codes. These points are discussed below.

The term "Health Physicist" has been substituted in the revised Model Code for the term "Qualified Expert" used in the original version of Appendix B. Through the activities and efforts of the Health Physics Society, and as a result of the certification program of the American Board of Health Physics, health physics is becoming more generally recognized as a scientific speciality practiced by persons with *extensive* training and experience and with *high* professional qualifications. Section 9(a) of the Model Code requires all users to provide for the services of a Health Physicist without distinction as to the need for such service. There are many "users" whose radiation installation consists of only one X-ray machine or perhaps only microcurie amounts of tracer material which may require only a trivial amount of health physics supervision. In such cases, the user himself can be sufficiently informed to provide the safety controls for the operating procedures involved. The services of the Health Physicist should be reserved for those hazard-control problems which require his special training and professional experience. In any case, the number of available Health Physicists, especially those that shall have been certified, is likely to be limited for some years to come. If radiation protection regulations are adopted using the term "Health Physicist" as in the Model Code, by necessity the term would have to be interpreted loosely (as implied by the definition given in Section 3) to include hundreds of persons whose knowledge of radiation hazard control may be adequate for limited or for special radiation programs but who would hardly qualify as professional Health Physicists. This could prove a serious detriment to the Profession and to its continued development.

The term "Qualified Expert" as used originally in HB 61 is subject to similar objection. Perhaps a more suitable term to use is "Qualified Person" or "Qualified Individual" as in the New Jersey Code. The principle to be established is that a person should be available who is qualified to cope with the specific radiation safety problems presented by the radiation installation and its operation. He need not necessarily be a professional Health Physicist, unless the problems are such that one is really required. If the term "Qualified Person" or "Qualified Individual" is used, the definition in Section 3 might include a parenthetical statement such as the following: (In judging the ability of the "Qualified Individual", the Agency may be guided by the requirements for certification of Health Physicists by the American Board of Health Physics, of Radiological Physicists by the American Board of Radiology, etc.)

Sections 7 and 8 contain the requirements for personnel monitoring in controlled areas and the keeping of monitoring records. It would seem more desirable to base monitoring requirements on the probability of exposure than on the definition of controlled area. In certain radiation installations such as hospitals and teaching institutions, it would be impractical and unnecessary to monitor all persons who enter for short periods of time a controlled area as defined in Section 3. It does seem sensible, however, to require personnel monitoring under conditions of possible exposure above certain reasonable levels. Perhaps one way for permitting more flexibility in applying the monitoring requirements is to reword Section 7(b) and Section 8(a) as follows:

7 (b). The user shall provide for routine personnel monitoring for external exposure of all persons within a controlled area under such circumstances that they receive or are likely to receive a dose in excess of (10, 25, etc.) per cent of the appropriate limits specified in Section 6(a). However, on the advice of a Qualified Person (Individual), personnel monitoring shall not be required providing:

(1) The dose rates at which any person is exposed are predictable, *or* the dose to all exposed persons is determined by some other reliable means, and

(2) There is reasonable assurance that an accident

causing exposure in excess of the exposure limits specified in Section 6(a) will not occur.

8 (a). The user shall keep individual exposure records for each person *for whom personnel monitoring is required.*

It has been pointed out to the Committee that Section 2 does not exempt from the monitoring and record-keeping requirements the personnel monitoring of patients receiving doses of radiation strictly for purposes of medical diagnosis and therapy. Undoubtedly, this interpretation was not intended by the NCRP Subcommittee No. 10 for the Model Code the purpose of which is to regulate occupational and not medical exposure. In order to avoid the technicality resulting from a literal interpretation requiring monitoring of all persons *including patients*, consideration should be given to adding a statement to Sections 7(b) and 8(a) to the effect that, "the requirements of this part shall not apply to the radiation intentionally applied to patients for diagnostic or therapeutic purposes by, or under the direction of, a licensed physician or dentist".

Section 13(b) (2) sets limits on the total quantity of radioactive wastes that may be released in 24 hr. It is not clear whether these limits apply to the discharge of activity into the atmosphere or to the release into sanitary sewage systems, or both. In any case, the proposed limits may be unnecessarily restrictive for certain installations which could otherwise safely dispose of considerably greater quantities by taking advantage of dilution techniques to assure allowable concentrations of radionuclides in uncontrolled areas. It would seem that the AEC approach used in 10 CFR 20.303 is more successful in achieving the degree of flexibility required to meet the varying needs of individual users. The AEC also exempts from its disposal limits excreta from patients undergoing medical diagnosis or therapy with radioactive materials. It would not be practical to apply the requirements of the Model Code, as written in Section 13, to the release of radioactive excreta from patients.

The Committee on Radiation Regulation of the Health Physics Society offers the comments above for the consideration of agencies who may choose to use the Model Code as a basis for drafting their own radiation regulations, or for persons who may be in the position to advise in the drafting of such codes. The Committee welcomes suggestions from anyone wishing to comment on radiation regulations in general, or upon the activities of the Committee.*

* Comments may be sent to the Committee Chairman, Robert O. Gorson, Department of Radiology, Jefferson Medical College Hospital, Philadelphia 7, Pa.

HEALTH PHYSICS SOCIETY
PLACEMENT COLUMN

Orders for ads to be sent prepaid to the Placement Committee at the address below. Ads will appear in the next issue following receipt.

1-Time Charges:

Position wanted: $0.25 per word ($4.00 minimum)
Position offered: $1.00 per word ($15.00 minimum)

Replies to employer or to
Mr. Joseph A. Lenhard,
Chairman Placement Committee H.P. Society,
Research and Development Divison, USAEC
P.O.B. E, Oak Ridge, Tenn.

POSITIONS OFFERED

HEALTH PHYSICIST

Immediate opening for a professional health physicist to perform both routine and non-routine radiation protection activities associated with the operation of a 5 MW research reactor, hot cells, and radioisotope laboratories. B.S. or M.S. with 6 to 18 months health physics experience required. Graduate of AEC Radiological Physics Fellowship program preferred. Resume should be submitted to:

Dr. Edward L. Alexander
Manager, Radiological Sciences
Columbia University
c/o Industrial Reactor Laboratories, Inc.
Plainsboro, New Jersey

CALIFORNIA
seeks
HEALTH PHYSICISTS
for
DEPARTMENT OF PUBLIC HEALTH
in Berkeley

Investigates radiological health hazards and sources of ionizing radiation. Directs health physics training programs.
Qualifications: College degree in Physical or Life Sciences including courses in nuclear or health physics or radiation biology.
For Senior: Five years of professional experience, two years of which must have included responsibility for a major program in radiological health.
Salary: $9,384–$11,400.
For Associate: Three years of professional experience in health physics.
Salary: $8,112–$9,852.

Send Resume by May 5, 1961, to

C. S. WARNER
ENGINEERING PERSONNEL SERVICES
CALIFORNIA STATE PERSONNEL BOARD
801 CAPITOL AVENUE
SACRAMENTO 14, CALIFORNIA

Health Physics Pergamon Press 1961. Vol. 5, pp. 101–107. Printed in Northern Ireland

THE CONTAMINATION OF RIVERS WITH FISSION PRODUCTS FROM FALLOUT

A. MORGAN and D. G. STANBURY
Health Physics Division, Atomic Energy Research Establishment, Harwell, Berks.

(*Received* 15 *December* 1959)

Abstract—The concentrations of some fission products in rain water falling on the catchment areas of three Thames tributaries are compared with the concentrations in river water over monthly periods. The fission products selected were Sr^{89}, Sr^{90}, Cs^{137} and Ce^{144}.

A comparison of the concentrations in corresponding samples of rain and river water showed that natural decontamination factors were smallest for Sr^{90} and greatest for Ce^{144}. The Sr^{90} concentrations in river water appear to depend to some extent on the permeability of the sub-soil in the catchment area, which suggests that surface run-off is an important source of contamination. The amount of Sr^{90} leaving each catchment area in the river is compared with the amount deposited. Normally less than 1 per cent leaves in the river, but in periods of heavy rain and high flow rates this may be considerably increased due to desorption from the soil and enhanced run-off.

The effect on the Sr^{90} concentration in river water of (a) increased testing of nuclear weapons and (b) a reactor accident are discussed briefly.

INTRODUCTION

In recent years increasing attention has been paid to the possible contamination of drinking water supplies with radioactive materials. The measurements of Stewart *et al.*[1] in the United Kingdom and of Kahn and Reynolds[2] in the United States, have shown that water from rivers and lakes contains detectable amounts of Sr^{90} and Cs^{137}, which are potentially the most hazardous of the long-lived fission products. These fission products, derived from the testing of atomic and thermonuclear weapons, are normally washed out of the lower atmosphere by rain after a hold-up period in the stratosphere, during which time the shorter-lived nuclides decay. In the U.K. at the present time, drinking water from rivers and lakes provides only a small fraction of the total dietary intake of Sr^{90} and Cs^{137}. However, it is important to know how the concentration of these nuclides will be affected by a sudden increase in deposition, whether from nuclear weapon testing or from a reactor accident.

The object of this experiment was to compare the depositions of some of the longer-lived fission products occurring in fallout on three catchment areas, with the amounts leaving in the rivers, in order to obtain information on their retention and on the natural decontamination processes involved. By making measurements on rivers flowing off different geological formations, it was hoped to discover whether the nature of the sub-soil had any effect on the decontamination process.

METHODS

The rivers selected were the Windrush, Ock and Pang, which are all tributaries of the River Thames. The geological formations in the three catchment areas are shown in Fig. 1. The Windrush and Ock flow mainly off limestone and clay, respectively, while a considerable portion of the Pang catchment area is chalk.

One-gallon grab samples were collected three times weekly from each river and bulked in large Polythene containers. No attempt was made to weight the volume of the sample according to the flow rate. A continuous record of the Windrush flow rate at the confluence with the Thames was made available by the Thames Conservancy Board, who also calibrated headwater piles in the Ock and Pang, enabling periodic measurements of their flow rates to be made.

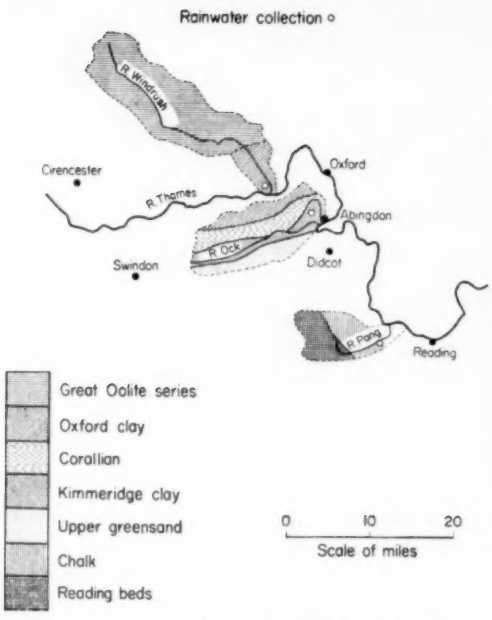

FIG. 1. Map showing geological formations in three catchment areas.

The results of flow-rate measurements on the three rivers, together with local rainfall data covering the same period, are shown in Fig. 2. The permeabilities of the different sub-soils are reflected in the variation of flow rate with rainfall, the Ock being highly sensitive, while the Pang is relatively unaffected.

Monthly rain-water samples were collected in two Polythene rain gauges at a single station in each catchment area. The positions of these stations are shown in Fig. 1. The rain gauges, containing solutions of carriers and a little nitric acid were placed in position on the first day of each month and replaced on the first day of the following month. Mean monthly rainfall figures for the three catchment areas were supplied by the Meteorological Office and this information, together with the measured concentrations of the various nuclides in the rain-water samples, enabled the monthly depositions on each catchment area to be calculated.

Analysis of samples

The methods used in the radiochemical analysis of rain-water and river-water samples for Sr^{89}, Sr^{90}, Cs^{137} and Ce^{144} were based on those described by OSMOND *et al.*[3] Calcium was removed from the strontium by the fuming nitric acid method of WILLARD and GOODSPEED[4] and standard radiochemical procedures were used for the subsequent purification of the strontium, caesium and cerium.

The volume of river water (60 l.) used in each determination was such that the natural strontium content had to be taken into account when estimating the true recovery of strontium carrier. The natural strontium content of calcium carbonate samples precipitated from water taken from each of the three rivers was measured by flame photometry. The values obtained were 2.7, 3.7 and 2.1 mg strontium per g calcium in samples of carbonate from the Windrush, Ock and Pang, respectively, and it was assumed that these values were constant for all samples from the same river.

All activity measurements were made with end-window Geiger counters calibrated with sources prepared from standard solutions of Sr^{89}, Sr^{90}–Y^{90}, Cs^{137} and Ce^{144}–Pr^{144} obtained from the Isotope Division, AERE, Harwell. Even with samples of 60 l. the activities of sources prepared from river water were small and the counters were invariably used in anti-coincidence arrays which gave backgrounds of from 1 to 1.5 counts/min.

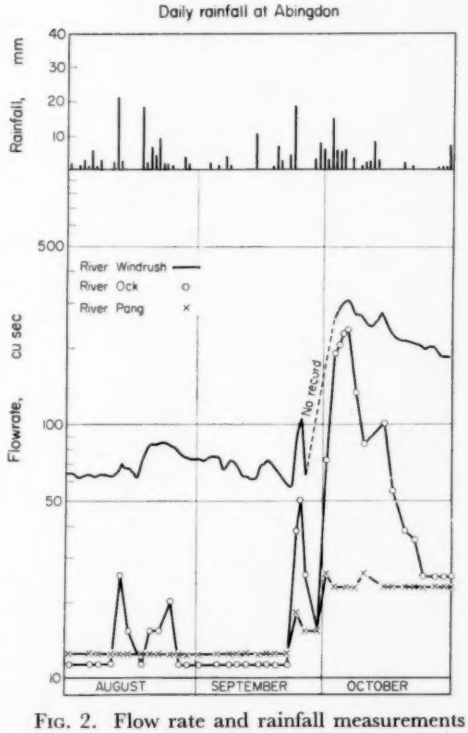

FIG. 2. Flow rate and rainfall measurements August–October 1958.

Table 1. *Concentrations of nuclides in rain water*

Catchment area	Month (1958)	Rainfall (cm)	Sr^{89}*	Sr^{90}	Cs^{137} ($\mu\mu c/l.$)	Ce^{144}*	Sr^{89}/Sr^{90}*
Windrush	August	7.6	104	5.0	5.9	49	21
Ock	August	7.9	87	4.8	5.1	47	18
Pang	August	11.2	70	3.2	4.1	36	22
Windrush	September	9.4	103	3.8	5.6	84	27
Ock	September	7.9	112	4.2	6.7	92	27
Pang	September	9.7	117	3.9	5.7	86	30
Windrush	October	7.1	101	3.5	4.4	57	29
Ock	October	7.9	114	3.9	5.0	74	29
Pang	October	7.6	112	3.9	5.6	70	29

* All Sr^{89} and Ce^{144} activities are corrected to the fifteenth day of the month in which the sample was collected.

In an attempt to detect and identify γ-emitting fission products other than Cs^{137} and Ce^{144}, the γ-spectra of some rain-water and river-water samples were measured. These samples were acidified, concentrated to a volume of 1 l. and poured into a container of 6 in. diameter and 4 in. deep, fabricated in Polythene. The container had a 2-in. deep recess in the underside, so that it fitted closely over a 3-in. diameter NaI (Tl) crystal. The crystal was operated in conjunction with a photomultiplier and multichannel pulse-height analyser.

RESULTS AND DISCUSSIONS

The rainfall data from the Meteorological Office and the results of the analyses for Sr^{89}, Sr^{90}, Cs^{137} and Ce^{144} in the various rain-water samples are given in Table 1. The concentrations of the same nuclides and also of calcium in the river-water samples are given in Table 2.

Rain water may find its way into streams and rivers by a number of routes. It may fall directly into the river or reach the river indirectly by surface run-off within the drainage area, particularly during periods of heavy rain. In dry spells, much of the flow is normally derived by seepage from the ground water reservoir. The high concentration of fission products found in surface soil by GUSTAFSON *et al.*[5] suggests that radioactive material is quickly removed from rain water percolating down through the soil by adsorptive or exchange

Table 2. *Concentrations of nuclides and calcium in river water*

River	Month (1958)	Calcium (g/l.)	Sr^{89}*	Sr^{90}	Cs^{137} ($\mu\mu c/l.$)	Ce^{144}*	Sr^{89}/Sr^{90}*
Windrush	August	0.086	1.50	0.23	0.02	0.14	6.5
Ock	August	0.092	1.95	0.32	0.35	0.14	6.1
Pang	August	0.085	1.14	0.13	0.09	0.33	8.8
Windrush	September	0.078	1.41	0.15	—	0.10	9.4
Ock	September	0.104	2.86	0.21	0.05	0.15	13.6
Pang	September	0.085	0.94	0.08	0.11	0.23	11.8
Windrush	October	0.102	1.86	0.29	0.06	0.09	6.4
Ock	October	0.138	3.13	0.53	0.04	0.55	5.9
Pang	October	0.099	0.45	0.18	0.06	0.14	2.5

* All Sr^{89} and Ce^{144} activities are corrected to the fifteenth day of the month in which the sample was collected.

Table 3. *Results on grab samples from the river Ock*

Date of Collection	Flow rate (ft^3/sec)	Calcium (g/l.)	Sr^{89}	Sr^{90}	Cs^{137} ($\mu\mu c$/l.)	Ce^{144}	Sr^{89}/Sr^{90}
6/10/58	234	0.107	7.39	0.83	0.07	0.73	8.9
6/11/58	202	0.118	8.88	0.74	0.08	1.21	12.0

processes. Consequently the concentration of fission products in rain water reaching rivers indirectly, will inevitably be depleted. This is confirmed by the measurements of STEWART *et al.*[1] who have shown that the concentrations of Sr^{90} and Cs^{137} in water from rivers and lakes is normally ten times less than in rain water and a hundred times less in water from deep wells.

Importance of surface run-off

If ground water is completely free of fission products, then surface run-off is likely to be the main source of contamination where rivers are concerned. This is confirmed by the fact that in each month the Sr^{89} and Sr^{90} concentrations are greatest in the Ock and least in the Pang. This effect is attributed to the different geological characteristics of the catchment areas. The Ock and lower reaches of the Windrush flow through impervious clay soil where the surface run-off of rain water may be considerable. On the other hand, a large proportion of the Pang catchment area is chalk, through which rain water will percolate and lose its activity before finding its way into the river or ground water reservoir. Additional evidence for the importance of run-off is shown by the analysis of grab samples from the River Ock, collected during or shortly after periods of heavy rain. The results for two samples are given in Table 3 and they show higher concentrations of Sr^{89}, Sr^{90} and Ce^{144} than in any of the monthly samples, despite the fact that the volume flow was about ten times higher than normal.

Hold-up times

A comparison of Sr^{89}/Sr^{90} ratios in radiostrontium from rain water and river water samples gives some measure of hold-up times as the Sr^{89} has a short half-life compared with that of Sr^{90}. Similar values for this ratio in rain and river water would be consistent with short hold-up times. During the course of the experiment, the Sr^{89}/Sr^{90} ratio in rain water increased, so that accurate estimates of hold-up times cannot be made, but it is clear from the low values for river water radiostrontium that it is at least a month older than that in rain. The fact that the Sr^{90} concentration in river water increases after heavy rain, as shown in Table 3, while the Sr^{89}/Sr^{90} ratio is still less than half that in rain water, suggests that under these conditions, desorption of Sr^{90} from the ground may be increased. Desorbed radiostrontium would have a depressed Sr^{89}/Sr^{90} ratio, which would reduce the high ratio which might be expected in river water, if all the activity was derived from surface run-off and rain falling directly into the river. This would account for the low values for this ratio found in the October samples when flow-rates were abnormally high and the Ock overflowed its banks in many places. The calcium contents of the October river-water samples are higher than in either of the other 2 months, and as this calcium must have been dissolved from the soil, it is likely that some of the radiostrontium will be derived from that source also. Both EDEN[6] and STEPANOV[7] have shown that the adsorption of radiostrontium on river mud is a reversible process and it is likely that the same will apply to soil.

Retention of Sr^{90} *within catchment areas*

Flow measurements made on the three rivers during August, September and October enable estimates to be made of the Sr^{90} leaving each catchment area in the river. These figures are given in Table 4 and are compared with the monthly depositions calculated from the rainfall data and catchment areas. The catchment areas above the sampling points, are estimated

Table 4. Comparison of Sr^{90} deposited on the catchment areas with that leaving in the rivers

River	Month	Sr^{90} deposited on catchment area (mc/month) (*a*)	Sr^{90} leaving catchment area (mc/month) (*b*)	$\frac{b}{a} \times 100$ (%)
Windrush	August	137	1.24	0.9
Ock	August	99	0.337	0.3
Pang	August	55	0.126	0.2
Windrush	September	129	0.819	0.6
Ock	September	88	0.244	0.3
Pang	September	58	0.080	0.1
Windrush	October	91	5.07	5.6
Ock	October	80	3.32	4.2
Pang	October	45	0.32	0.7

to be 363, 264 and 155 km^2 for the Windrush, Ock and Pang, respectively. It can be seen that under normal conditions, more than 99 per cent of the deposited Sr^{90} is retained in herbage and soil and does not leave the catchment area. After heavy rain when flow rates are abnormally high, as much as 6 per cent of the deposited Sr^{90} may appear to leave the catchment area. Although some of this will be due to enhanced run-off, it is likely that under such circumstances, a considerable contribution will be due to Sr^{90} desorbed from the soil.

Natural decontamination factors

A comparison of the concentrations of the selected fission products in corresponding rain- and river-water samples for each month shows that the difference is greatest in the case of Ce^{144}. The range and median values for the natural decontamination factors (concentration in rain water/concentration in river water) for the various nuclides are given in Table 5.

For the shorter-lived nuclides, hold-up times will enhance their decontamination factors and this accounts to some extent for the different values for Sr^{89} and Sr^{90}. However, the fact that the value for Ce^{144} (half-life 285 days) is considerably greater than that for Sr^{89} (half-life 51 days), confirms the conclusion that natural processes are more effective at removing Ce^{144} from rain water than is the case with the other nuclides considered. These results are in agreement with the work of EDEN[6] who has shown that both Cs^{137} and Ce^{144} are more strongly adsorbed than radiostrontium on river mud. That this selective removal of Ce^{144} continues in the river is shown by the analysis of suspended material filtered from the October river-water samples. In the case of Ce^{144}, the activity associated with the suspended matter from 1 l. of the original sample is approximately equal to that in solution in 1 l. For both Sr^{90} and Cs^{137}, however, the activity on the solids is an order of magnitude less than that in solution.

Table 5. Decontamination factors for various nuclides (all rivers)

Nuclide	Decontamination factor	
	Range	Median
Sr^{89}	36–250	61
Sr^{90}	7–50	22
Cs^{137}	15–130	63
Ce^{144}	110–840	370

The γ-spectrum of a concentrated river-water sample shown in Fig. 3, displays clearly the presence of radioruthenium (probably $Ru^{103} + Ru^{106}$) and $Zr^{95} + Nb^{95}$. Comparing the spectra from various samples shows that the concentrations of these nuclides in flood water from the Ock are greater than in any monthly

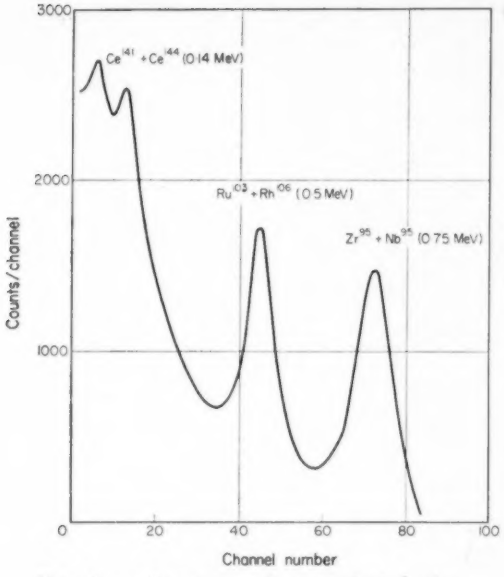

FIG. 3. γ-Spectrum of concentrated river-water sample.

sample from that river and the lowest concentrations are found in monthly samples from the Windrush and Pang.

Effect of increased Sr^{90} *deposition*

In estimating hazards resulting from the ingestion of radioactive nuclides, the International Commission on Radiological Protection[8] have derived maximum permissible drinking water concentrations $(MPC)_w$ for occupationally exposed persons. The $(MPC)_w$ for Sr^{90} is two orders of magnitude smaller than for any of the other nuclides considered in this paper, and this fact together with the relatively small decontamination factor for Sr^{90} combine to make the hazard from the other fission products small in comparison. Consequently further discussion will be restricted to this nuclide. In deriving $(MPC)_w$ values, it is assumed that intake of the nuclide considered is from drinking water only. At the present time, however, only a few per cent of the total Sr^{90} in human diet is normally derived from drinking water, so current concentrations cannot be compared directly with the $(MPC)_w$.

There are two situations which could lead to an increase in Sr^{90} concentration in rivers: firstly, an increase in fallout from weapon testing with widespread dissemination of fission products over comparatively long periods of time; secondly, where deposition is of short duration and restricted to a limited area, such as might be the case after a reactor accident.

Continuous widespread deposition resulting in an enhanced concentration of fission products in rain water would lead to an immediate increase in the Sr^{90} concentration in river water due to surface run-off. As the Sr^{90} accumulated in surface soil would also increase under these circumstances, it is likely that there would be more desorption from soil, but this would be a much slower process and its effect on the Sr^{90} concentration in river water would not be apparent immediately. If it is assumed that the Sr^{90} measured in the river-water samples is due exclusively to run-off, and is not held up for considerable periods within catchment areas, then the data in Tables 2 and 4, may be used to calculate approximately the depositions required to give a certain concentration in river water. As the work of VAUGHN *et al.*[9] suggests that the passage of river water through purification and filtration plant does not reduce the Sr^{90} concentration by more than a factor 2, this consideration may be neglected. As the contamination of vegetation and milk with Sr^{90} is dependent on the rate of deposition rather than the cumulative total in the soil, the contamination of foodstuffs would also increase under such conditions and drinking water would still provide only a small fraction of the total dietary intake.

In the case of a reactor accident giving rise to a heavy deposition of both short- and long-lived nuclides, the amounts reaching rivers will depend to a great extent on the solubility of the debris and on the weather conditions prevailing at the time. Adsorptive processes, hold-up times and dilution all play a part in reducing the concentration in river water, giving a large intrinsic safety factor which is not readily calculable.

Acknowledgments—The authors are indebted to the Thames Conservancy Board for advice on the choice

of rivers and for assistance in making flow-rate measurements; also to Dr. G. E. HARRISON of the Medical Research Council Radiobiological Unit, for permission to publish determinations of natural strontium.

REFERENCES

1. N. G. STEWART, R. N. CROOKS, R. G. D. OSMOND, M. J. OWERS and C. HEALY, *Preliminary Survey of Radiostrontium and Radiocaesium in Drinking Water in the United Kingdom.* Unclassified Report A.E.R.E. HP/R 2795 (1959).
2. B. KAHN and S. A. REYNOLDS *J. Amer. Wat. Wks. Ass.* 613 (1958).
3. R. G. OSMOND, M. J. OWERS, C. HEALY and A. P. MEAD, *The Determination of Radioactivity Due to Caesium, Strontium, Barium and Cerium in Waters and Filters.* Unclassified Report AERE-R2899 (1959).
4. H. H. WILLARD and E. W. GOODSPEED, *Industr. Engng. Chem. (Anal.)* **8,** 414 (1936).
5. P. F. GUSTAFSON, L. D. MARINELLI and S. S. BRAR, *Science* **127,** 1240 (1958).
6. G. E. EDEN, Personal communication; *Water Pollution Research,* 1958. H.M. Stationery Office, London (1958).
7. B. A. STEPANOV, *Gigiena i Sanitorriya* **11,** 3 (1957).
8. *Report of ICRP Committee II on Permissible Dose for Internal Radiation* (1959). Pergamon Press, London (1959); *Health Phys.* **3,** 1–233 (1960).
9. J. C. VAUGHN, R. W. SCHMIT, A. TENNY and A. SHOR, *J. Amer. Wat. Wks. Ass.* **50,** 581 (1958).

Health Physics Pergamon Press 1961. Vol. 5, pp. 108–118. Printed in Northern Ireland

CALCULATIONS OF WEAPONS RADIATION PENETRATION IN AIR*

R. L. FRENCH and M. B. WELLS
Convair, A Division of General Dynamics Corporation, Fort Worth, Texas

(*Received* 14 *June* 1960)

Abstract—The spatial, angular and energy distributions of the initial radiation from a nuclear weapon were calculated on a theoretical basis. The radiation components considered were fission neutrons and prompt fission, fission product and air-capture γ-rays. The principal simplifying assumptions employed in the theoretical model were neglect of (1) self-attenuation in the nuclear weapon; (2) blast effect on air density; and, (3) ground effects. Comparisons were made with measured data which clearly demonstrate that the spatial, angular and energy distributions of the initial radiations from a nuclear weapon are calculable.

1. INTRODUCTION

RADIATION dose received from the initial radiation of a nuclear weapon, like that from any other source, may be reduced by appropriate shielding. However, the design of efficient shielding, or the evaluation of the shielding effectiveness of existing structures, requires a detailed knowledge of the spatial, energy and angular distributions of the radiation. RITCHIE and HURST[1] have recently reported measured weapons radiation data of this type for "nominal bombs" (10–20 kilotons) and discussed their application in determining the radiation exposure to survivors of Hiroshima and Nagasaki, Japan.

In addition to the usual total γ-dose neutron dose and neutron fluxes as a function of distance in air from a burst, RITCHIE and HURST reported measured angular distributions of neutron flux, neutron dose and γ-dose. The data, expressed on a per kiloton basis, are limited to a range of from 400 to 2200 yd. Although the data are the most detailed published in open literature to date, the energy and angular distributions are somewhat sketchy; energy distributions are given for neutrons only and angular distributions are available for only one or two separation distances.

Calculated data would be invaluable to supplement the measured data and to provide details not easily obtained by experimental techniques. Thus, calculations of the initial radiation environment from a nuclear weapon have been performed and evaluated by comparison with the measured data. The methods of calculation were adapted from techniques used for Aircraft Nuclear Propulsion shielding applications. The methods and their evaluation are described in this paper.

2. THEORETICAL MODEL

The nuclear weapon was considered as a point isotropic source of radiation in an infinite medium of air. A source strength of 1.42×10^{23} uranium-235 fissions per kiloton was assumed. The radiation from the point source, called primary radiation, was assumed to consist of prompt fission γ-rays, fission product decay γ-rays and fission neutrons. Secondary γ-rays from neutron capture and inelastic scatter in the weapon were assumed negligible. In addition to the primary radiation, secondary γ-rays from neutron capture in nitrogen-14 in the surrounding air were calculated. The model, which includes both single and multiple scattering of radiation in air, is depicted in Fig. 1.

The first step in the calculation was to establish the intensity and energy spectra of the γ- and neutron radiation leaving the point isotropic source. GAMBLE[2] has measured the

* Work supported by Research and Development Division, Ordnance and Tank Automotive Command (Detroit Arsenal), U.S. Army.

energy spectrum of prompt γ-rays from U^{235} fission. The results show that most of the γ-rays are given off in the energy range of 0.25–7.0 MeV. For convenience of calculation, this range was divided into the five energy groups indicated in Table 1 and the source strength for each group was determined from GAMBLE's data.

The prompt fission γ-rays are emitted while the nuclear weapon is still essentially intact. As a result, these γ-rays are likely to suffer an appreciable decrease in intensity and modification in spectrum in penetrating to the exterior of the weapon. Because of a lack of information on the configuration and composition it was necessary to neglect self-attenuation in the weapon.

The limitation from neglecting self-attenuation does not apply to the second primary γ-component, fission product decay γ-rays, since they are given off a finite time after fission. Recent measurements[3] of fission product γ-rays show that essentially all of the γ-rays are given off within the first 200 sec, with 50 per cent being given off within the first 18 sec. During the first 200 sec the spectral shape does not change appreciably.

To obtain a source term for the fission product decay γ-rays, the measured spectrum was integrated over energy and time to 200 sec to obtain a total source strength of 3.37 photons per fission. These were divided among the same energy groups used for the prompt fission gamma calculation and are also shown in Table 1.

Although the fission product γ-rays are unaffected by self-attenuation, the source is dispersed and displaced as the fireball expands and rises. This effect should not cause the radiation environment at large distances to differ appreciably from that obtained from a stationary point source. A third effect, and one which is likely to be most significant for high-yield weapons, is the hydrodynamic effect. The blast wave from the burst causes the density of the air surrounding the weapon to undergo a sharp reduction during the time in which many of the fission product γ-rays are given off. As a result, air attenuation to nearby positions is reduced and the dose from fission product γ-rays increases.

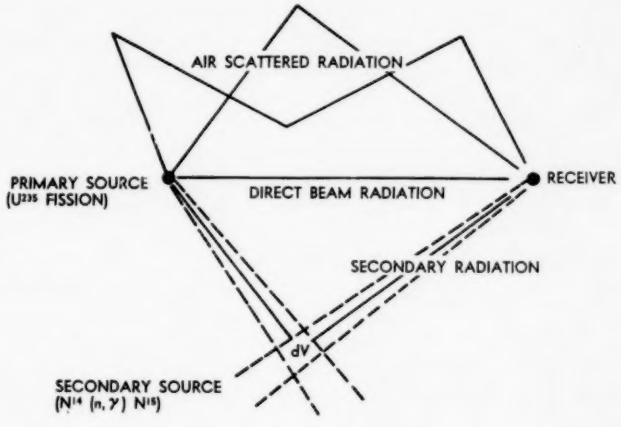

FIG. 1. Theoretical model for radiation sources and transfer mechanisms.

Table 1. U^{235} *fission* γ*-spectra*

Energy interval (MeV)	Source strength (photons per fission)	
	Prompt fission	Fission product
0.25–0.75	2.7612	1.3977
0.75–1.50	2.3741	1.1971
1.5–3.0	1.1806	0.5452
3.0–5.0	0.2903	0.1853
5.0–7.0	0.0498	0.0447
Total	6.6560	3.3700

This effect was not considered in the calculations.

To establish a neutron source term, it was assumed that all the fission neutrons escaped the weapon except for those necessary to sustain the chain reaction. Assuming an average of 2.5 neutrons per fission, the source term is 1.5 neutrons per fission. The neutron spectrum was represented by the analytic formula:

$$N(E) = 0.453 \exp(E/0.965) \sinh \sqrt{(2.29E)}$$

which is a fit to the thermal fission spectrum as given by CRANBERG *et al.*[4]

The angular and energy distributions of the direct-beam and air-scattered primary γ- and neutron fluxes at several separation distances were computed by a Monte Carlo procedure which is described in the next section.

The air-capture γ-rays were computed by dividing the air in all space about the burst into volume elements and determining the number of captures, S, in nitrogen-14 for each volume element from the equation

$$S = \phi \sigma N$$

where ϕ is the thermal neutron flux at the position of the volume element as determined from data in RITCHIE and HURST[1], N is the number of N^{14} atoms in the volume element, and σ is the capture cross-section of N^{14}. The nitrogen-14 capture γ-spectrum reported by BARTHOLOMEW and CAMPION[5], consists of a number of discrete lines between 3 and 11 MeV. For convenience they were represented by an average energy of 5.5 MeV in calculating the direct beam attenuation from the volume element to the receiver. Air-scattering data for 6-MeV γ-rays from the Monte Carlo calculations described in the next section were applied to account for build-up of the air-capture γ-rays in penetrating to the receiver positions.

3. MONTE CARLO CALCULATIONS

Angular distributions of the number flux and dose and of the energy spectra were obtained for both neutrons and γ-rays from a recently developed Monte Carlo procedure.[6] The procedure allows the use of either a monoenergetic point isotropic source or one with a known energy distribution. The Monte Carlo method is used to generate particle histories from which the collision density is obtained. The method of statistical estimation is used to determine, from the collision density, the particle flux and dose rate at five spherical boundaries concentric about the source.

The Monte Carlo technique[7] used to obtain the data in this paper includes statistical estimation, importance sampling, and systematic sampling. The use of these techniques allows one to obtain results with an acceptable variance at large penetration distances. All particles were forced to undergo only scattering collisions, and the biasing so introduced was removed by the use of particle "weights".[8] In the γ-ray problems, all photons were forced to undergo Compton scattering collisions; in the neutron problems, when inelastic scattering was energetically possible, a choice was made at random to determine the mode of scattering. Neutron and photon histories were terminated when the energy of the particle was degraded to 0.1 MeV for γ-rays and 0.2 MeV for neutrons.

The scattering angles and scattered energies for Compton scattering of γ-rays were chosen from the Klein–Nishina scattering formula by the use of a rejection technique developed by KAHN[9]. The total cross-sections and the Compton scattering cross-sections for air as a function of energy were computed from the microscopic cross-sections for oxygen and nitrogen as given by DAVISON and EVANS[10].

The neutron cross-sections for air were computed from the cross-sections for nitrogen and oxygen as given by LUSTIG *et al.*[11,12] The elastic scattering probabilities for nitrogen and oxygen were computed from the Legendre expansions given by LUSTIG *et al.*[11,12] for neutron energies above 0.25 MeV. Below 0.25 MeV, the elastic scattering probabilities were taken as isotropic in the center-of-mass system. The scattering probabilities for inelastic scattering by both nitrogen and oxygen were taken as isotropic in the center-of-mass system. Deduction of the inelastic scattering cross-sections for excitation of the various energy levels in nitrogen and oxygen required use of the inelastic scattering cross-section measurements reported by HUGHES and SCHWARTZ[13], CONNER[14], and THOMPSON and RISSER[15], and the inelastic cross-sections given by LUSTIG *et al.*[11,12] Neutrons were

allowed to lose energy at each collision, the amount of the loss depending on the collision nucleus, scattering angle and mode of scattering.

The Monte Carlo results for the air-scattered fluxes were obtained for eighteen equal angular intervals and ten energy intervals between the maximum source energy and the minimum energy at which particle histories were terminated. The unscattered particle flux at the receiver was computed for each problem; for the neutron calculation, which used a continuous source spectrum, the unscattered flux was stored in the computer as a function of the ten energy groups used in storing the scattered flux.

Since oxygen and nitrogen make up over 99 per cent of the volume of air, only these two elements were considered in the air scattering calculations. It is assumed that 78 per cent of the atoms per cubic centimeter of air are nitrogen atoms and that the remaining 22 per cent are oxygen atoms. The number of atoms per cubic centimeter in air at sea level air density (0.1293×10^{-2} g/cm^3) was taken as 5.37×10^{19}. All problems were run at sea-level air density. Since the air density at the site of the weapon tests differed from that used in the calculations, the transformation given by ZERBY[16] was applied to the calculated values to obtain results for the correct air density.

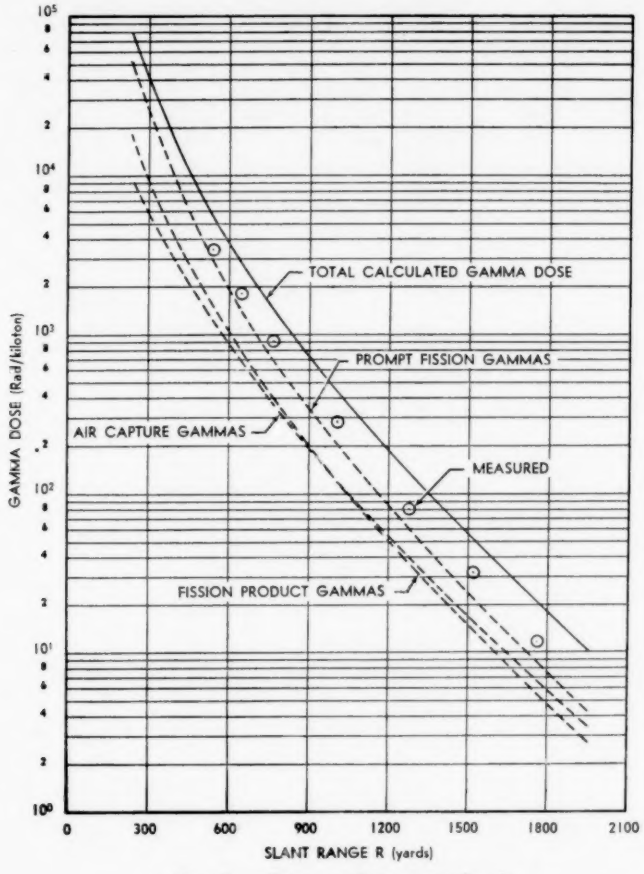

FIG. 2. γ-Dose vs. slant range in air.

γ-Ray problems were run for monoenergetic point isotropic sources of 0.5, 1, 2, 4 and 6 MeV and penetration distances of 180, 650, 1000, 1250 and 1500 yd. These energies represent the mid-points of the energy groups used for defining the γ-spectra at the source. Neutron-scattering data for a point isotropic fission source was obtained for the same penetration distances. In all problems a source strength of unity was used.

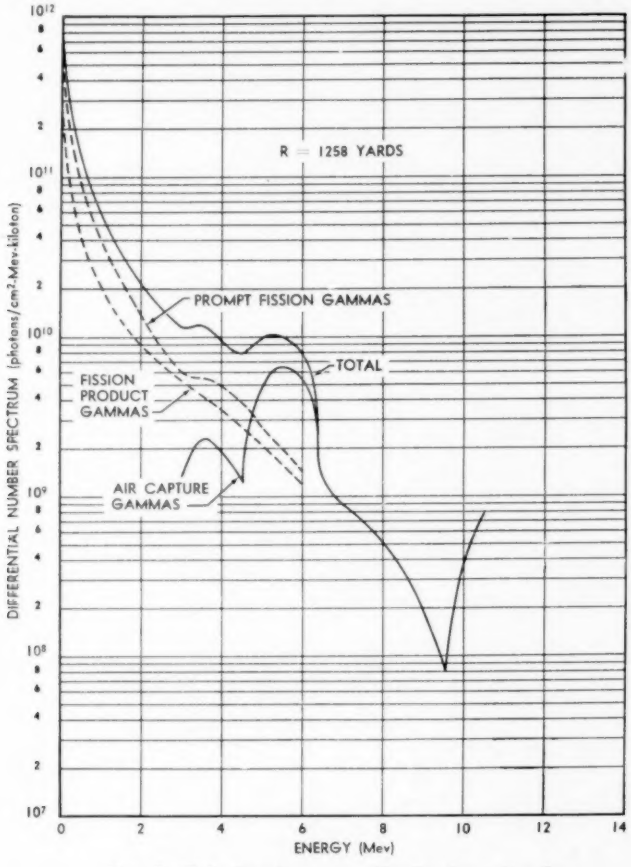

FIG. 3. Calculated energy distribution of γ-flux.

4. COMPARISON OF RESULTS

To facilitate comparison, the calculated and measured data[1] were reduced to a common form, absolute dose or flux per kiloton. Fig. 2 shows the comparison of the measured γ-dose vs. distance with the calculated components of the γ-dose. If all three calculated components are added at face value the total is approximately 70 per cent higher than the measured dose; whereas, if the prompt fission γ-rays are omitted from the total, the result is approximately equal to the measured dose. If it is assumed that the air-capture and fission product doses are reasonably correct and that the ground effect is unimportant, the data suggest that self-attenuation in the weapon reduces the prompt fission γ-dose to negligible proportions. The excellent slope agreement of the measured and calculated data indicates that the air-scattering parameters were correct.

Although no measured γ-ray energy spectra have been reported, spectral data are important

for shield penetration calculations. The calculated spectrum shown in Fig. 3 is for a distance of 1258 yd and is not significantly different from that calculated for other separation distances. Of particular interest is the prominence of the air-capture γ-rays at energies greater than 3 or 4 MeV. The air-capture γ-rays, because of their higher energy, are much more penetrating than the fission product and prompt fission γ-rays. Since the nitrogen-14 capture γ-spectrum[5] consists of a number of discrete lines, the photons were summed in 1 MeV energy intervals to form the continuum shown in Fig. 3. The air-scattered air-capture γ-rays are not included in this spectrum because a rough preliminary calculation indicated they were unimportant compared to the other γ-rays.

The agreement between the measured and calculated angular distributions of the γ-dose (Fig. 4) is best for angles less than 60°. The discrepancy at higher angles (which is not particularly significant in terms of total dose) could be caused by neglecting collimator wall scattering and capture γ-rays from the collimator materials in the calculations.

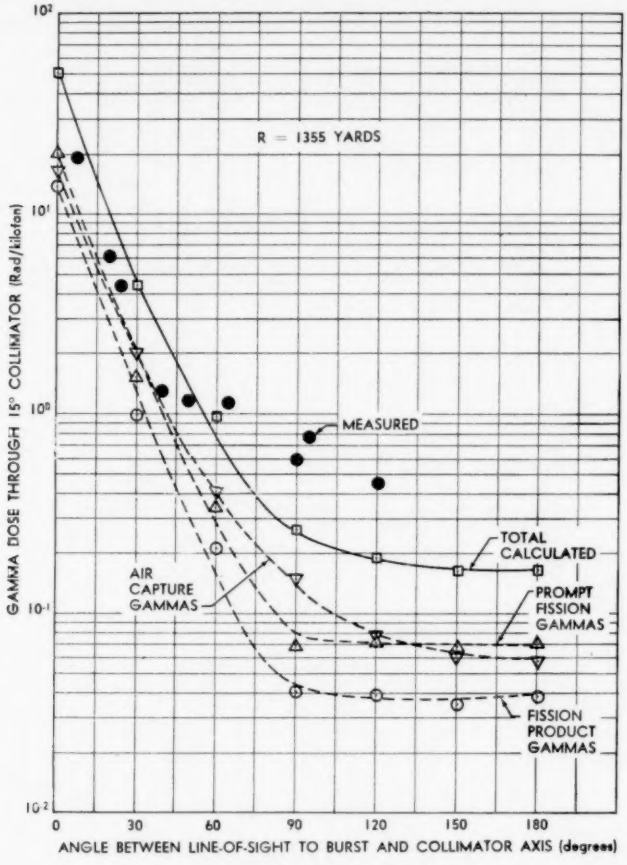

FIG. 4. Angular distribution of γ-dose.

The slope of the calculated neutron dose, shown in Fig. 5, is also in good agreement with the measured data over most of the five decades of attenuation. However, at the extreme distance (1500–2000 yd) the calculated dose has

started to diverge from the measured dose. It is believed that the calculated dose is too low at these distances because it does not reflect the increased statistical importance of the more penetrating high-energy neutrons. These observations also apply to the calculated neutron fluxes shown in the figure since they were used to compute the dose.

The neutron spectrum is essentially constant as indicated by the approximately parallel flux curves in Fig. 5. The calculated and measured neutron spectra at one particular range, 1258 yd, are compared in Table 2.

In Figs. 6 through 8, the measured and calculated angular distributions of the neutron flux are compared. The scatter in the measured points is caused partially by the collimators being placed at different angles of rotation about the source–receiver axis (see Figs. 6, 7 and 8 in Ritchie and Hurst[1]). The measured data shown represent an average of the data for collimators aimed above the horizon; for these collimators, the intensity did not vary with the angle of rotation by more than approximately 25 per cent. It is suspected that ground effects and scattering from the walls of the collimators used in the measurements contribute to the discrepancy in magnitude between the measured

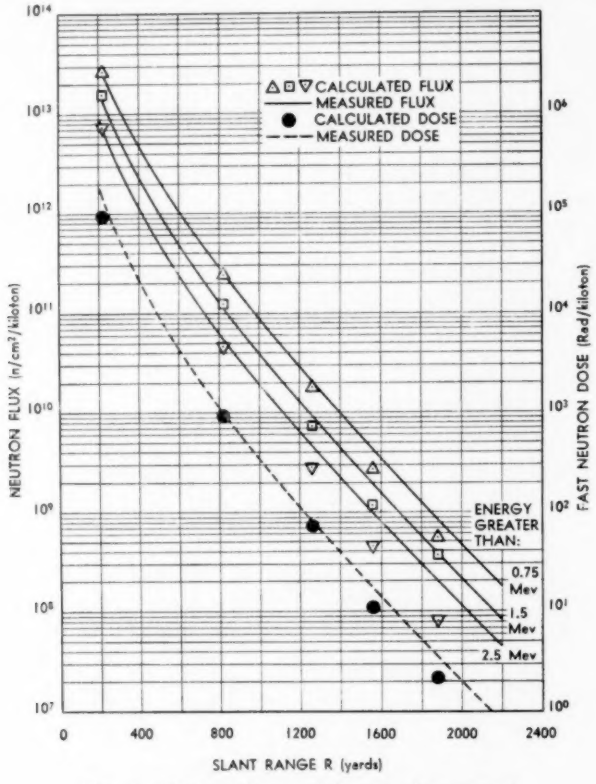

Fig. 5. Neutron dose and flux vs. slant range.

Table 2. Neutron spectra at 1258 yd

Energy group (MeV)	Neutron flux (neutrons/cm² per kiloton)	
	Measured	Calculated
0.75–1.5	1.2×10^{10}	1.0×10^{10}
1.5–2.5	5.0×10^{9}	4.6×10^{9}
>2.5	4.5×10^{9}	2.8×10^{9}

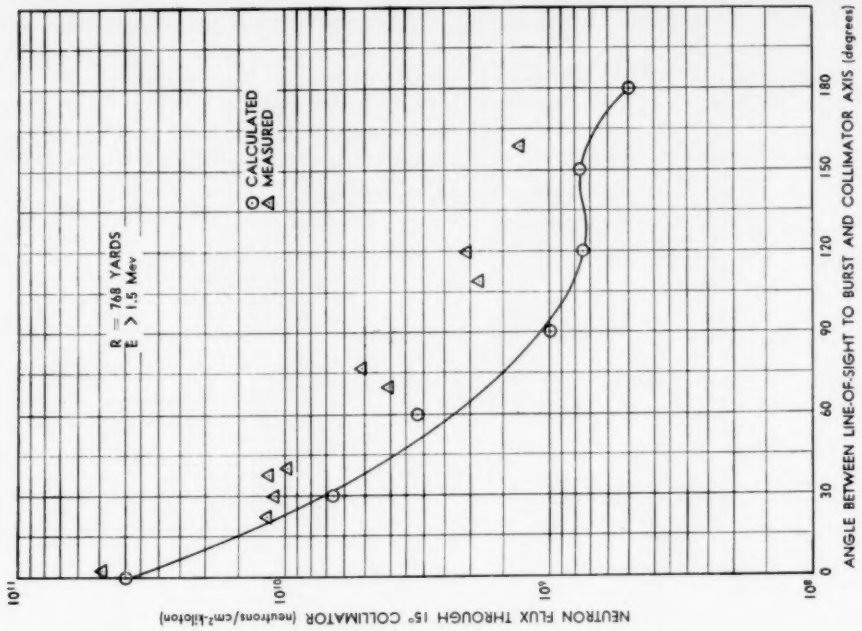
R = 768 YARDS
E > 1.5 Mev
CALCULATED
MEASURED
NEUTRON FLUX THROUGH 15° COLLIMATOR (neutrons/cm²-kiloton)
ANGLE BETWEEN LINE-OF-SIGHT TO BURST AND COLLIMATOR AXIS (degrees)

FIG. 7. Angular distribution of neutron flux.

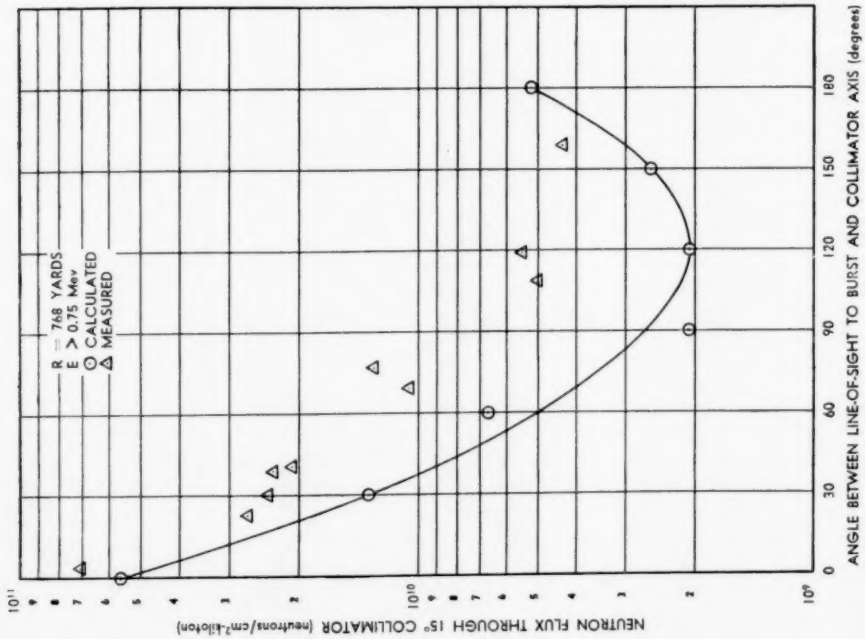
R = 768 YARDS
E > 0.75 Mev
CALCULATED
MEASURED
NEUTRON FLUX THROUGH 15° COLLIMATOR (neutrons/cm²-kiloton)
ANGLE BETWEEN LINE-OF-SIGHT TO BURST AND COLLIMATOR AXIS (degrees)

FIG. 6. Angular distribution of neutron flux.

and calculated data. The discrepancy caused by wall scattering should increase with collimator angle—as is the case.

The comparisons of the angular distributions of the fast-neutron dose at 1355 yd, shown in Fig. 9, indicate a similar discrepancy. If one integrates the measured dose distribution over a 4π solid angle the resultant dose is more than a factor of 2 greater than the total measured dose indicated in Fig. 5. However, because of the ground, it is doubtful that as much dose is actually received from the lower 2π as from the upper 2π solid angle.

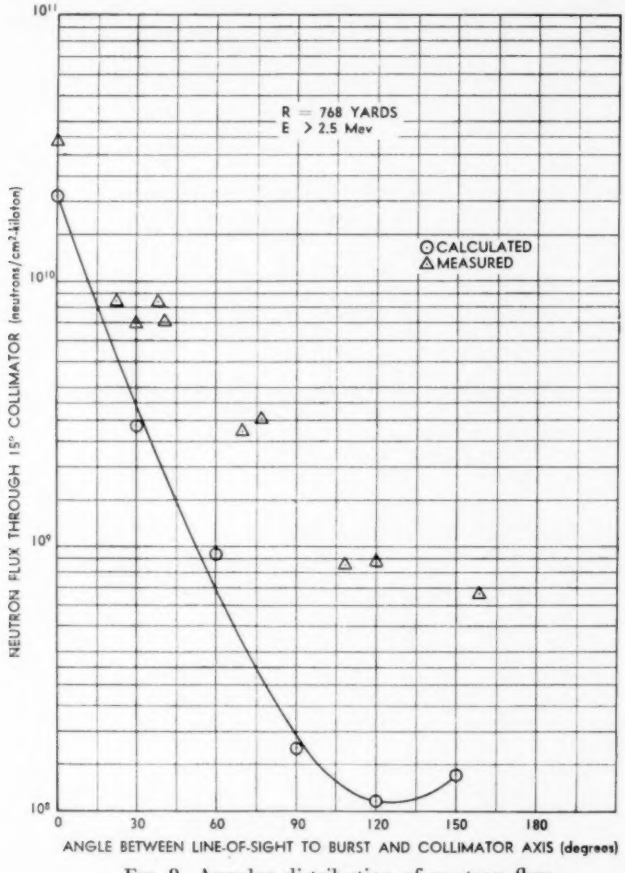

FIG. 8. Angular distribution of neutron flux.

5. CONCLUSIONS

The measured weapon radiation data reported by RITCHIE and HURST have been closely reproduced by calculations which are based on first principles of radiation physics. The calculated spatial distribution of the γ- and neutron doses and neutron fluxes are generally well within 70 per cent of the corresponding measured data. Similar agreement was obtained for the neutron energy distribution. The angular distribution data for neutrons agree rather well in shape but differ by more than a factor of two in magnitude in some cases. This discrepancy is believed to be caused, at least partially, by scattering from the walls of the collimators used for the measurements.

The assumptions employed in the present calculations are such that the agreement

observed above is probably fortuitous to some extent. The calculations have demonstrated, however, that the spatial, energy and angular distributions of the initial radiation from nuclear weapons are calculable.

It should be noted that many of the more pertinent assumptions could be avoided by applying data on nuclear weapon compositions and configurations.

Ground and hydrodynamic effects could be calculated by existing, or extensions of existing, Monte Carlo procedures. Such procedures for calculating the scattering of neutrons and γ-rays in a two-medium geometry such as air and

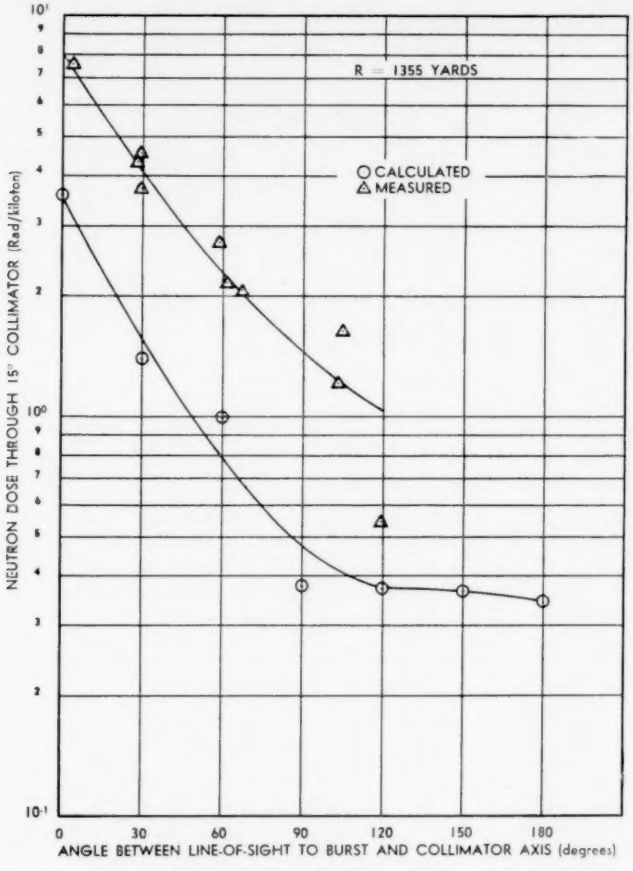

FIG. 9. Angular distribution of fast-neutron dose.

state-of-the-art shielding procedures. In particular, self-attenuation in the nuclear weapon should be calculable to within 25 per cent with the reactor shield penetration methods described by FRENCH and EGGEN[17,18]. Secondary γ-rays from thermal-neutron capture in the weapon could also be estimated. Calculations of these effects were not attempted in the present analysis because of the security classification of ground have been developed by WELLS[19,20], but their application has been limited to rather small separation distances.

Acknowledgments—The authors wish to acknowledge the assistance of L. M. BOSTICK, W. B. SELF and B. R. UZZELL, Convair–Fort Worth, in formulating and performing the various calculations. The suggestions of R. H. RITCHIE and G. S. HURST, Oak Ridge

National Laboratory, were invaluable in interpretation of the data.

REFERENCES

1. R. H. Ritchie and G. S. Hurst, *Health Phys.* **1,** 390 (1959).
2. R. L. Gamble, *Prompt Fission Gamma Rays from Uranium*-235. Ph.D Thesis presented to The University of Texas (1955).
3. *Neutron Physics Division, Annual Progress Report for Period ending* 1 *September* 1958. Oak Ridge National Laboratories Report ORNL-2609 (February 1958).
4. L. Cranberg, G. Frye, N. Nerson and L. Rosen, *Phys. Rev.* **103,** 662 (1956).
5. G. A. Bartholomew and P. J. Campion, *Canad. J. Phys.* **35,** 1347 (1957).
6. M. B. Wells, *Monte Carlo Calculations of Fast Neutron Energy Spectra.* Convair–Fort Worth Report FZM-1267 (1958).
7. H. Kahn, *Nucleonics* **6,** No. 5, 27 (1950).
8. E. D. Cashwell and C. J. Everett, *A Practical Manual on The Monte Carlo Method for Random Walk Problems.* Los Alamos Scientific Laboratory Report LA-2120 (1957).
9. H. Kahn, *Applications of Monte Carlo.* Rand Corporation Report RM-1237-AEC; Revised 27 April (1956).
10. C. M. Davison and R. D. Evans, *Rev. Mod. Phys.* **24,** 82 (1952).
11. H. Lustig, H. Goldstein and M. H. Kalos, *The Neutron Cross Sections of Nitrogen.* Nuclear Development Corporation of America Report NDA 86-1 (1957).
12. H. Lustig, H. Goldstein and M. H. Kalos, *An Interim Report on The Neutron Cross Sections of Oxygen.* Nuclear Development Corporation of America Report NDA 086-2 (1958).
13. D. J. Hughes and R. B. Schwartz, *Neutron Cross Sections.* Brookhaven National Laboratory Report BNL-325 (2nd Ed.) (1958).
14. J. P. Conner, *Phys. Rev.* **89,** 712 (1953).
15. L. C. Thompson and J. R. Risser, *Phys. Rev.* **94,** 941 (1954).
16. C. D. Zerby, *Radiation Flux Transformation as a Function of Density of an Infinite Medium with an Anisotropic Point Source.* Oak Ridge National Laboratory Report ORNL-2100 (1956).
17. R. L. French, *Nucleonics,* **18,** No. 3, 114 (1960).
18. R. L. French and J. B. Eggen, *Nucleonics,* **18,** No. 3, 117 (1960).
19. M. B. Wells, *Air and Concrete Scattering of Neutrons.* Convair–Fort Worth Report MR-N-197 (1958).
20. M. B. Wells, *Air and Concrete Scattering of Gamma Rays.* Convair–Fort Worth Report MR-N-229 (1959).

Health Physics Pergamon Press 1961. Vol. 5, pp. 119–125. Printed in Northern Ireland

FAST-NEUTRON SPECTRA AND DOSE-RATE CALCULATIONS*

J. B. EGGEN, R. L. FRENCH and A. REETZ, Jr.
Convair, A Division of General Dynamics Corporation, Fort Worth, Texas

(*Received* 26 *May* 1960)

Abstract—This article describes a method and its application for calculating fast-neutron spectra and dose rates about the Lid Tank Facility source plate, the Bulk Shielding Reactor and the Aircraft Shield Test Reactor. The method may be applied to any reactor whose shield is composed largely of hydrogenous materials. Dose rates and spectra calculated by the method are useful in shield design and in the analysis of experiments performed in reactor radiation fields.

The method is based upon fast-neutron differential energy spectra and dose rates calculated by the Nuclear Development Corporation of America for a point isotropic fission source in infinite media. These data represent a moments method solution of the Boltzmann transport equation for water and hydrocarbons. By representing a reactor core as an array of point isotropic sources and assuming that any material along the line-of-sight between a point source and a point detector may be represented by an equivalent thickness of water or hydrocarbon, the fast-neutron attenuation through any material may be determined by use of the results for these reference materials. The equivalent thickness of non-hydrogenous material is determined from the ratio of the effective removal cross-sections.

Results from dose-rate calculations by this method agree with measured BSR and LTSF pure water centerline data within 10 per cent. Calculated and measured spectra for the BSR and the ASTR compare favorably, although the ASTR calculation involves penetration of considerable amounts of non-hydrogenous materials.

INTRODUCTION

REACTOR shields are usually characterized by the presence of relatively large thicknesses of hydrogenous materials, which serve to control the leakage of fast neutrons. Although the reactor core, the moderator, the reflector and the γ-shielding contribute to the total fast-neutron attenuation, the total fast-neutron attenuation depends primarily upon the amount and type of hydrogenous shield material. This dependence has facilitated the development of a convenient and accurate means of calculating the fast-neutron leakage from reactors which are composed largely of hydrogenous materials.

The method of calculating the leakage is based upon fast-neutron differential energy spectra and dose rates calculated by the Nuclear Development Corporation of America (NDA) for a point isotropic fission source in infinite hydrogenous media. These data form the basic attenuation kernels required by the method. Non-hydrogenous materials are handled by a "substitution" concept based upon use of conventional removal cross-sections. Besides giving details of the method, comparisons of measured and calculated fast-neutron spectra and dose rates are presented for the Lid Tank Facility Source Plate, the Bulk Shielding Reactor and the Aircraft Shield Test Reactor.

DIFFERENTIAL ENERGY SPECTRA AND DOSE RATES

The fast-neutron dose rates and fluxes upon which the method is based were obtained by NDA through a moments method solution of the Boltzmann transport equation. A point isotropic fission source in water and in various

* Paper presented at the Annual Meeting of the Health Physics Society, 18–20 June 1959, Gatlinburg, Tennessee.

hydrocarbons was assumed.[1,2] The results of these calculations are summarized by KRUMBEIN[3]. Fast-neutron dose rates [$4\pi r^2 D(r)$ in units of mrep-cm^2/hr per source neutron] and fluxes [$4\pi r^2 N_0(r,E)$ in units of neutrons-cm^2/sec-MeV per source neutron] at selected energy levels are given for penetration depths of up to 120 g/cm^2.

For use in machine calculations, the following fourth-order exponential function of the penetration distance r was fitted to the data:

$$f(r) = \exp\,(a_0 + a_1 r + a_2 r^2 + a_3 r^3 + a_4 r^4) \quad (1)$$

where $f(r)$ = fast neutron dose rate in (mrep-cm^2/hr per source neutron)

r = source to detector separation distance (cm)

$a_0, \ldots, a_4$ = curve fit coefficients for data of KRUMBEIN[3]

Numerical values of the curve fit coefficients for transformer oil ($\sim CH_{1.7}$) and water are given in Table 1.

EQUIVALENT THICKNESS CONCEPT

Equation (1) may be applied directly in situations in which the radiation penetrates only water, hydrocarbons or other hydrogenous media. In most applications attenuation in the reactor core, as well as attenuation through γ-shielding or other non-hydrogenous materials, must be considered.

The effect of adding non-hydrogenous materials to hydrogenous media has been measured at the Lid Tank Facility at Oak Ridge.[4] It was found that the difference in attenuation caused by this new material could be expressed as a linear exponential function of the form $\exp\,(-\sum_R x)$, in which x is the penetration distance and $\sum_R$ is a quantity defined as the effective removal cross-section for that material. If it is assumed that any material along the line-of-sight between a point source and a point detector may be represented by an appropriate thickness of hydrogenous material as determined from its removal cross-section, then equation (1) can be applied. In applying the equation, it is assumed that only those materials on the source–detector line-of-sight will affect the results.

The equivalent thickness of any material along the source–detector line is determined by

$$r_{eq} = r_1 \frac{\sum_{R_i}}{\sum_{R_H}} \quad (2)$$

where r_{eq} = equivalent thickness of reference material;

r_i = actual thickness of ith material

$\sum_{R_i}$ = macroscopic removal cross-section of ith material

$\sum_{R_H}$ = macroscopic removal cross-section of reference material

After the total equivalent thickness of the reference material has been determined for all materials between the source and the detector, the fast-neutron spectra or dose rate per source neutron may be computed with equation (1). The results must be divided by $4\pi R^2$ where R is the physical distance between the source and receiver.

In applying the measured removal cross-sections[4] to equivalent thickness calculations, the relaxation length of fast neutrons is assumed to vary only slightly over the regions of interest and to be independent of energy. Because of the manner in which the cross-sections were determined, these assumptions should be most valid for configurations in which a material is backed by at least two relaxation lengths of hydrogenous material.

The assumption, which is made in this treatment, that boundary effects are negligible is probably least valid at the outside surface of a shield because comparatively little back scattering can occur from the air and surrounding media. Therefore, the use of data from an infinite hydrogenous medium should give dose rates which are too high.

The error due to neglecting a shield–air interface has been investigated[6] both experimentally and theoretically for one particular case: a PoBe neutron source with a water–air interface. For penetration of 21.6 cm of water the measured dose rate at the water–air interface was about 6 per cent lower than the measured dose rate at an equivalent distance in an essentially infinite water medium. Corresponding Monte Carlo calculations of neutron scattering in

Table 1. *Curve fit coefficients for equation* (1)

Transformer oil

Coef.	Neutron energy (MeV)						Dose rates
	0.33	1.1	2.44	5.63	8.1	12.08	
a_0	2.7197983 (0	1.9369870 (0	1.0336775 (0	−1.1373997 (0	−3.0318300 (0	−6.0568689 (0	−3.3916481 (0
a_1	−1.5883773 (−1	−1.5820624 (−1	−1.4621828 (−1	−1.0780009 (−1	−1.0867268 (−1	−8.7875862 (−2	−1.8015555 (−1
a_2	3.3538742 (−4	3.8295193 (−4	2.8517901 (−4	−2.5944872 (−5	1.3522865 (−4	1.8163875 (−4	8.7061189 (−4
a_3	−2.6010935 (−7	−7.3824731 (−7	−4.6226478 (−7	6.6461826 (−7	−3.3266906 (−7	−1.0742880 (−6	−3.7988699 (−6
a_4	−1.2625825 (−9	−9.6893160 (−11	−2.6158498 (−10	−1.7016865 (−9	2.1940849 (−10	1.8847789 (−9	6.0764465 (−9

Water

Coef.	Neutron energy (MeV)					Dose rates
	0.33	1.1	2.7	6.0	10.9	
a_0	4.4278213 (−2	−3.8542819 (−1	−1.2959495 (0	−3.9356776 (0	−7.6711270 (0	−4.4903805 (0
a_1	−1.6003212 (−1	−1.7213709 (−1	−1.5102476 (−1	−9.3893228 (−2	−8.3242431 (−2	−1.2389745 (−1
a_2	5.2038283 (−4	6.7921312 (−4	4.2219285 (−4	−7.2001421 (−5	−1.0043848 (−5	4.8581976 (−5
a_3	−1.9842901 (−6	−2.6764352 (−6	−1.3864949 (−6	4.5267700 (−7	−1.4879333 (−8	9.0842082 (−7
a_4	3.0346595 (−9	3.9382489 (−9	1.6871662 (−9	−8.5161234 (−10	1.1956180 (−10	−2.9845335 (−9

water indicated that about 7 per cent of the total dose at this distance in an infinite water medium is due to back-scattered neutrons.

TREATMENT OF DISTRIBUTED SOURCES

To arrive at an accurate expression of the flux from a distributed fission source an integration must be made over the source volume. In the integration, which must be made because of the source self-shielding, the distributed source is represented by an equivalent array of point isotropic fission sources. Each point source corresponds in strength and position to an elemental volume of the reactor core. Results are calculated separately for each point source and then summed over all points. For complex geometries, a machine program which utilizes a generalized geometry procedure is used to compute intercepted distances in materials between source and detector points.

The minimum number of points required to represent a given source depends on the core size, composition and the position for which results are to be calculated. For a source such as the ORNL Bulk Shielding Reactor, 132 uniformly spaced points were found to suffice for all positions external to the core. The relative strength for each source point may be determined from either measured or calculated power distribution data. The absolute source strengths are adjusted to give the total fission rate which corresponds to the desired power level.

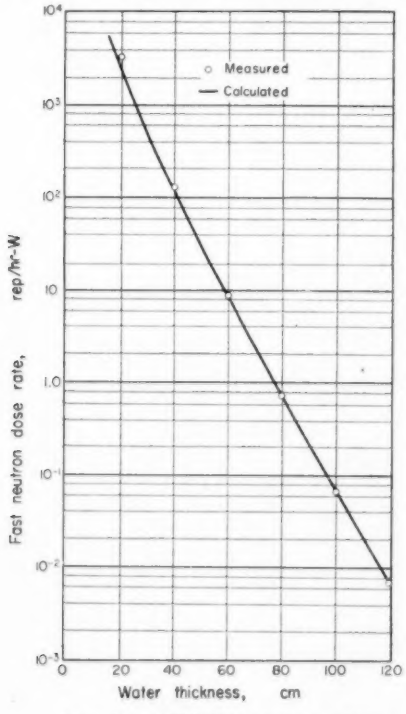

FIG. 1. LTSF dose rates in water.

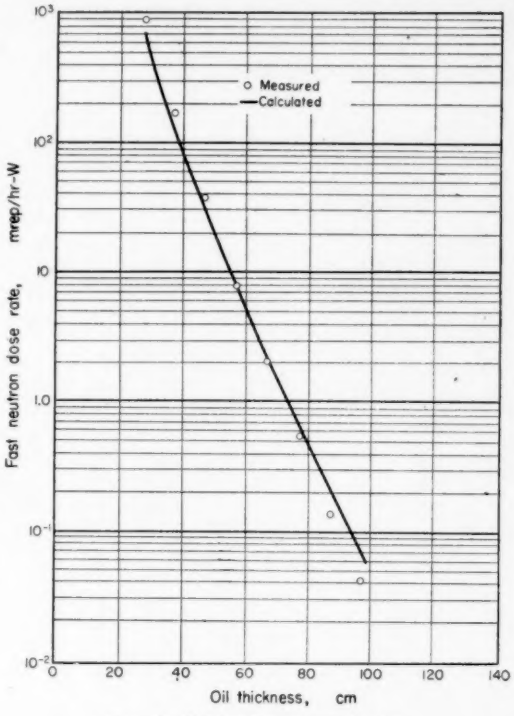

FIG. 2. LTSF dose rates in oil.

COMPARISON OF MEASURED AND CALCULATED DOSE RATES

Fig. 1 shows the fast-neutron dose rate as a function of water thickness for the Lid Tank Shielding Facility.* The measurements[8] were

* The Lid Tank Shielding Facility source plate (SP-2) is a circular enriched U^{235} converter plate which covers a hole through the Oak Ridge National Laboratory Reactor Shield. The facility itself is a large H_2O tank (11 ft × 7 ft 5 in. × 7 ft).

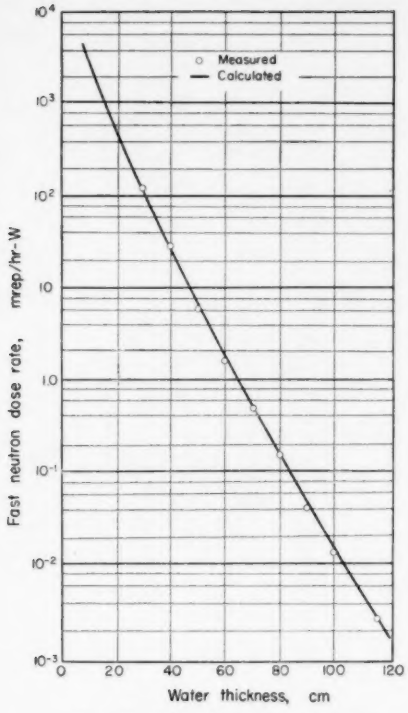

FIG. 3. BSR dose rates in water.

made in water along a line perpendicular to the center of a 21 per cent enriched uranium fission source plate. Water was used as the reference material in making the calculations.

Fig. 2 shows the fast-neutron dose rate as a function of oil thickness for the Lid Tank Shielding Facility. The measurements[8] were made in oil along a line perpendicular to the center of the source plate. A hydrocarbon having 1.7 hydrogen atoms per carbon atom was used as the reference material[2] in the calculations.

Fig. 3 shows the fast neutron dose rates in water along the center line of the Bulk Shielding Reactor.* The calculated values were obtained with water as the reference material.[1]

In each comparison, the predicted dose rates are in good agreement with the measured data. For the dose rates in water, the measured dose rates are, on the average, within 10 per cent of those calculated; whereas, for oil, the average difference is approximately 25 per cent with a maximum difference of approximately 40 per cent.

COMPARISON OF MEASURED AND CALCULATED SPECTRA

Fig. 4 shows that the calculated spectrum compares favorably with the measured spectrum[8,9] of the fast-neutron leakage from the Bulk Shielding Reactor, although the measurements were made with a collimated proton recoil counter, whereas the calculations were performed for a point 4π detector. A complete set of fast-neutron energy spectra, as well as γ-ray spectra, for the BSR center line has been calculated by the method and reported in another publication.[7]

Many applications of the technique described here for calculating dose rates and spectra have involved penetration of considerable amounts

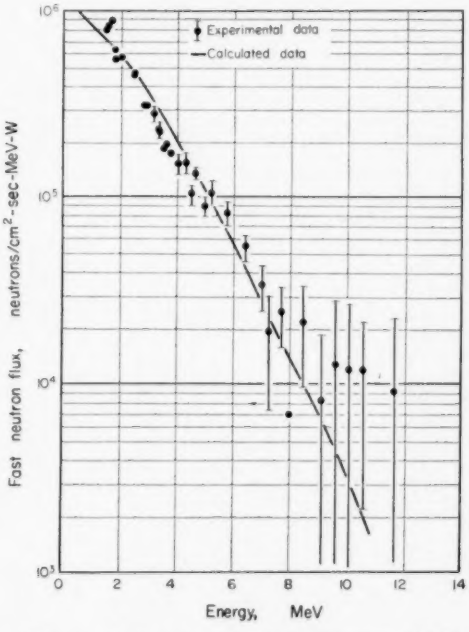

FIG. 4. Fast-neutron leakage spectrum of the bulk shielding reactor.

* The Bulk Shielding Reactor is an enriched U^{235}, H_2O moderated and reflected, swimming pool type, research reactor located at the Oak Ridge National Laboratory, Oak Ridge, Tennessee.

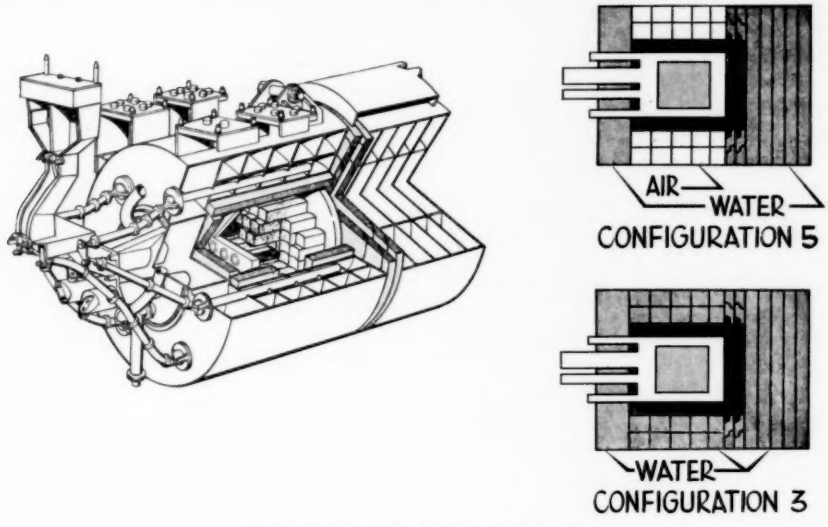

FIG. 5. Aircraft shield test reactor.

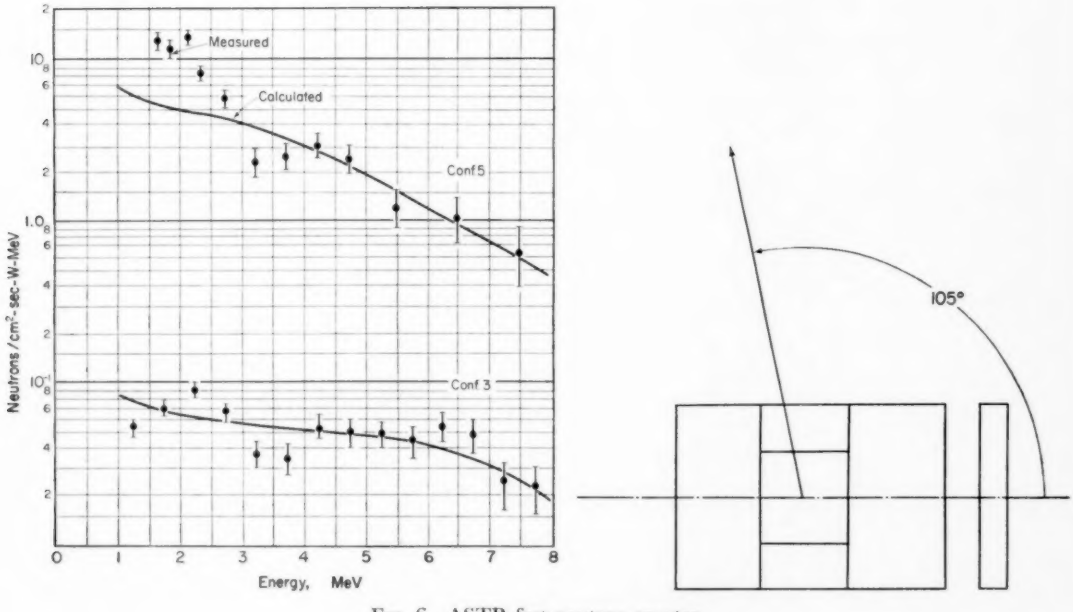

FIG. 6. ASTR fast-neutron spectra.

of non-hydrogenous materials. An example of the application to a complicated configuration is the calculation of dose rates and spectra from the Aircraft Shield Test Reactor,* shown in Fig. 5.

Fig. 6 shows measured and calculated fast-neutron spectra for two different shielding configurations of the Aircraft Shield Test Reactor. The measured spectra were obtained with nuclear emulsion plates. Good over-all agreement in magnitude and gross shape is noted, even though the spectrum changes considerably between the two configurations.

CONCLUSIONS

The differential energy spectra and dose-rate data from moments method solutions for point fission sources in infinite hydrogenous media have provided a useful and versatile method for calculating fast-neutron spectra and dose rates. Combined with the effective removal cross-section concept for treating layers of non-hydrogenous materials, the method is one of the best presently available for practical applications.

For the cases illustrated, the calculated and measured dose rates and spectra generally agree within 25 per cent. Although the agreement between calculated and measured dose rates for complex shields is not always as good as for the simple shields discussed here, the calculated dose rates rarely differ from the measurements by more than a factor of 2.

* The Aircraft Shield Test Reactor is an enriched U^{235}, H_2O moderated and reflected, portable research reactor with variable lead and water shielding, located at Convair, Fort Worth, Texas.

REFERENCES

1. R. ARONSON, J. CERTAINE, H. GOLDSTEIN and S. PREISER, *Penetration of Neutrons from a Point Isotropic Fission Source in Water.* Nuclear Development Corporation Report NYO-6267 (1954).
2. J. CERTAINE, H. GOLDSTEIN, M. KALOS and P. S. MITTELMAN, *Penetration of Neutrons from a Point Fission Source Through Carbon and Hydrocarbons.* Nuclear Development Corporation Report NDA 12-18 (1956).
3. A. D. KRUMBEIN, *Summary of NDA Unclassified Results of Moments Method Calculations for the Penetration of Neutrons Through Various Materials.* Nuclear Development Corporation Report NDA 92-2 (1957).
4. G. T. CHAPMAN and C. L. STORRS, *Effective Neutron Removal Cross Sections for Shielding.* Oak Ridge National Laboratory Report AECD-3978 (1955).
5. E. P. BLIZARD, Nuclear radiation shielding. *Nuclear Engineering Handbook* (Ed. by H. ETHERINGTON) Sec. 7-3. McGraw-Hill, New York (1958).
6. R. L. KLOSTER, *Analysis of the Moments Method Experiment.* Convair–Fort Worth Report FZK-9-138 (1959).
7. R. L. FRENCH and J. B. EGGEN, *Nucleonics* **18,** 117 (1960).
8. *Applied Nuclear Physics Division, Annual Report for Period Ending* 10 *September* 1956. Oak Ridge National Laboratory Report 2081 (1956).
9. H. GOLDSTEIN, *The Attenuation of Gamma Rays and Neutrons in Reactor Shields.* U.S. Government Printing Office, Washington, D.C. (1957).

Health Physics Pergamon Press 1961. Vol. 5, pp. 126–141. Printed in Northern Ireland

TRANSMISSION OF SCATTERED γ-RAYS THROUGH CONCRETE AND IRON SLABS*

D. J. RASO
Technical Operations Incorporated, Burlington, Massachusetts

(*Received* 27 *June* 1960)

Abstract—The penetration of γ-rays undergoing one or more scatterings in concrete and iron of various slab thicknesses (3.75–60.0 g/cm^2) has been investigated by the Monte Carlo technique. Radiation with energy of 350, 660 and 1250 keV and also the γ-ray spectra produced by the products (omitting volatile materials) of U^{235} fission at 1.12 and 23.8 hr after fission[1] were assumed to be incident on the medium at angles of $\cos\theta_0 = 0, 0.25, 0.50, 0.75$ and 1.0. The case histories of 5000 photons were followed on the IBM 704 digital computer. The information obtained included:

(1) Number and energy transmitted.
(2) The energy distribution of the transmitted radiation integrated over all directions.
(3) The angular distribution integrated over all energies.
(4) The angular distribution of the transmitted energy.
(5) The angular distribution of the transmitted "dose".

These computed quantities refer to transmitted current and an approximation is given for determining flux density. Comparisons are made with other theories and an experiment performed at USNRDL.

INTRODUCTION

THE attenuation of X-rays and γ-rays is ordinarily represented by an attenuation coefficient, which depends on the material and energy appearing in the exponential relation: $N/N_0 = e^{-\mu x}$ where N represents the intensity or number of photons transmitted, N_0 the intensity or number incident on the absorber, μ the total attenuation coefficient (probability of an interaction per unit thickness), and x the thickness of the absorber. This expression is valid only for relatively thin absorbers, and is derived on the assumption that the geometry of the arrangement of radiating source, absorber and detector is "good".

The essential feature of a "good" geometry experiment is that no scattered radiation can reach the detector. A well-defined incident beam and a detector sensitive to radiation from a single direction must be used. For any given aperture of the defining slits there exists a maximum thickness of the absorber (for a given energy of the photon) beyond which the likelihood of detecting scattered photons cannot be ignored.[2] In "poor" geometries, the aperture of the slits is increased, or the absorber thickness is increased, or a combination of both; some of the photons that are scattered find their way to the detector. Therefore, one finds a lower apparent attenuation coefficient than would be detected in "good" geometry.

On the other hand, "poor" geometries are of extreme importance because of the role they have in actual shielding problems. The use of walls for shielding personnel from radioactive contamination on the ground due to fallout is a prime example of "poor" geometry. For these geometries the above relationship is no longer valid and must be corrected to include the effect of scattered photons which have not only been deflected from their initial directions but have also been degraded in energy.

Three methods are most widely used in investigating the penetration and diffusion of

* This work was supported by the National Bureau of Standards and U.S. Naval Radiological Defense Laboratory.

scattered γ-rays in matter: (1) moment method; (2) successive scatterings; and (3) Monte Carlo method. A full description of these methods is not necessary since they are well developed elsewhere. The first method[3,4] has geometry limitations and cannot be used to solve the transport equation except in an infinite homogeneous medium. The second method[5] which takes into account finite boundary conditions, was utilized by PEEBLES. The calculation performed considers only three orders of scatterings, and does not take into account backscattered photons, important at low photon energies and thick slabs. The most effective means of handling γ-ray penetration problems in relatively thin slabs is the Monte Carlo method.

A number of reports are available which investigate the transmission of γ-rays in finite slabs by the Monte Carlo method.[6–9] The present report is expanded considerably to include: (1) more initial energies and mixed spectra; (2) five angles of incidence; and (3) information about the angular and energy distribution of the transmitted radiation in terms of both current and flux. A large quantity of data has been produced by this calculation, making it necessary to present results here in the form of illustrations. The detailed results of energy spectra and angular distributions of the transmitted radiation are presented in fifty-one tables of a separate report[10] which may be obtained upon request.

INFORMATION OBTAINED BY THE PROBLEM

The transmission of scattered photons through a medium contained between two infinite parallel planes a finite distance apart is investigated by the Monte Carlo method. In Fig. 1, a trajectory of a photon which is incident on the medium with energy E_0 and obliquity θ_0 is shown. The probability that a photon will be transmitted through the medium after undergoing one or more scatterings with an energy between E and $E + dE$ and an emergent angle between θ and $\theta + d\theta$ is $2\pi T(E, \theta; E_0, \theta_0) \sin\theta\, d\theta\, dE$. The factor $T(E, \theta; E_0, \theta_0)$ is the differential transmission (probability per unit solid angle per unit energy transmitted). The

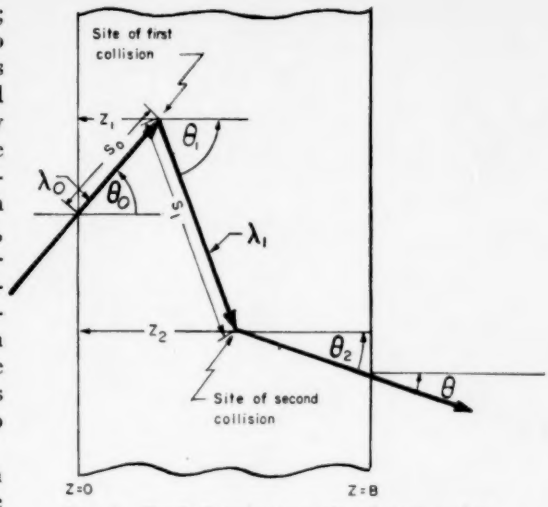

FIG. 1. Typical trajectory of a photon undergoing scatterings in a medium. Definition of obliquity angles.

quantities determined in this report are in the form of both partial integrals and total integrals over $T(E, \theta; E_0, \theta_0)$, as follows:

Transmitted scattered energy spectrum of number

$$\alpha_1(E_0, \theta_0; \Delta E) = \int_{\frac{i}{20}}^{\frac{i+1}{20}E_0} dE \int_0^{\pi/2} 2\pi T(E, \theta; E_0, \theta_0) \sin\theta\, d\theta \quad (1)$$

where $i = 0, 1, \ldots\ldots\ldots\ldots, 19$.

Transmitted scattered angular distribution of number

$$\beta_m(E_0, \theta_0; \Delta\theta) = \int_{\frac{\pi m}{36}}^{\frac{\pi(m+1)}{36}} 2\pi \sin\theta\, d\theta \int_{E_{\min}}^{E_0} T(E, \theta; E_0, \theta_0)\, dE \quad (2)$$

where $m = 0, 1, \ldots\ldots\ldots\ldots, 17$ and $E_{\min}$ = cut-off energy.

Transmitted scattered angular distribution of energy

$$\gamma_m(E_0, \theta_0; \Delta\theta) = \int_{\frac{\pi m}{36}}^{\frac{\pi(m+1)}{36}} 2\pi \sin\theta\, d\theta \int_{E_{\min}}^{E_0} \frac{E}{E_0} T(E, \theta; E_0, \theta_0)\, dE \quad (3)$$

Transmitted scattered angular distribution of "dose"

$$\delta_m(E_0, \theta_0;\ \Delta\theta) = \int_{\frac{\pi m}{36}}^{\frac{\pi(m+1)}{36}} 2\pi \sin\theta\, d\theta \times \int_{E_{\min}}^{E_0} E\mu_a(E)\, T(E, \theta;\ E_0, \theta_0)\, dE \tag{4}$$

where $\mu_a(E)$ is the energy absorption coefficient for air.

Scattered number transmitted

$$T_n = \sum_{i=0}^{i=19} \alpha_i(E_0, \theta_0;\ \Delta E) = \sum_{m=0}^{m=17} \beta_m(E_0, \theta_0;\ \Delta\theta) \tag{5}$$

Scattered energy transmitted

$$T_E = \sum_{m=0}^{m=17} \gamma_m(E_0, \theta_0;\ \Delta\theta) \tag{6}$$

Equations (1–6) apply to monoenergetic sources of energy E_0 but can be used as well for mixed spectra. A mixed spectrum is treated as a number of different monoenergetic sources each having its own spectral density at a given time. The spectral densities at a given time after fission (1.12 hr and 23.8 hr for the present report) were taken from Table 4 of reference 1. The upper limit in equations (2), (3) and (4) is replaced by the maximum energy of the source spectrum. Equation (3) is normalized by dividing by the mean γ-ray source energy, $\Sigma_l E_l K(t_i, E_l)$/total number of histories, where $K(t_i, E_l)$ is the spectral density at time t_i with energy E_l.

Except for equation (4), the above quantities refer to transmitted scattered *current*, i.e. flow per unit area and unit time across the exit face of the slab. The method used to convert to transmitted fluxes, i.e. flow per unit time through a unit area perpendicular to the direction of the transmitted scattered photons, is given in reference 10, as well as a method for obtaining the physical dose from equation (4).

METHOD OF CALCULATIONS

A beam of γ-rays is incident at various angles on an absorbing medium (concrete and iron) contained between two infinite parallel planes a finite distance apart. The trajectory of each photon (Fig. 1) is determined, by random sampling, from the known probability for a given event—collision, absorption, energy degradation, scattering through an angle, etc. (Pair production was not introduced, because the absorption coefficient for pair production in the energy ranges considered is negligible.) The random choice for an event which depends on the previous interaction is determined according to the physical laws governing scatterings.

Each collision in the medium is considered to be a Compton interaction; photoelectric absorption is taken into account by the introduction of a statistical weight factor (analytically calculated). The photon history is terminated when: (1) the photon passes through the medium without making a collision (unscattered passage); (2) the photon energy in the medium after multiple scattering is below a cut-off energy, 25 keV for concrete and 50 keV for iron (the cut-off energy is chosen low enough that photoelectric absorption reduces the photon flux to an insignificant amount below the cut-off);[11] (3) the photon after multiple collisions is back-scattered out of the medium, $Z < 0$, contributing to albedo; or (4) the photon passes through the boundary ($Z \geq B$) after undergoing multiple scattering in the medium (Fig. 1). The important parameters of the transmitted scattered photons are summed up in order to estimate the transmission of scattered photons.

The computer time to sample 5000 photon histories for the five cases (one source energy, five angles of incidence) varied, depending upon the slab thickness (approximately 10 min for slabs of 3.75 g/cm^2 and 50 min for slabs of 60 g/cm^2).

RESULTS

Scattered number and energy transmitted

The scattered number T_N and scattered energy T_E transmitted [as defined by equations (5) and (6), respectively, and the corresponding equations for mixed spectra] for the materials, concrete and iron, different source energies, angles of incidence and slab thicknesses are given in Tables 1–10. The results are normalized

Table 1. *Transmission after scatterings by concrete (effective* $Z = 13.4$, *composition by weight as given in Ref.* 17)
Based on 5000 photon histories per source energy of 0.35 MeV, cut-off energy = 0.025 MeV.

Scattered number transmitted, T_n

Cos θ_0	B (g/cm^2)				
	3.75	7.5	15	30	60
0	0.3230	0.2320	0.1250	0.0297	0.0010
0.25	0.3810	0.3780	0.2320	0.0572	0.0029
0.50	0.2880	0.3640	0.2960	0.0949	0.0058
0.75	0.2280	0.3260	0.3210	0.1430	0.0149
1.0	0.1870	0.2890	0.3110	0.1810	0.0279

Scattered energy transmitted, T_E

Cos θ_0	B (g/cm^2)				
	3.75	7.5	15	30	60
0	0.1960	0.1250	0.0617	0.0126	0.0004
0.25	0.2480	0.2210	0.1190	0.0254	0.0011
0.50	0.1990	0.2290	0.1660	0.0471	0.0028
0.75	0.1640	0.2170	0.1980	0.0786	0.0073
1.0	0.1410	0.2020	0.2040	0.1080	0.0162

Table 2. *Transmission after scatterings by concrete (effective* $Z = 13.4$, *composition by weight as given in Ref.* 17)
Based on 5000 photon histories per source energy of 0.66 MeV, cut-off energy = 0.025 MeV.

Scattered number transmitted, T_n

Cos θ_0	B (g/cm^2)				
	3.75	7.5	15	30	60
0	0.3430	0.2600	0.1660	0.0535	0.0026
0.25	0.3570	0.4010	0.2960	0.1090	0.0100
0.50	0.2520	0.3660	0.3630	0.1710	0.0221
0.75	0.2030	0.3180	0.3680	0.2270	0.0376
1.0	0.1690	0.2770	0.3440	0.2710	0.0643

Scattered energy transmitted, T_E

Cos θ_0	B (g/cm^2)				
	3.75	7.5	15	30	60
0	0.1750	0.1150	0.0631	0.0170	0.0006
0.25	0.2050	0.1990	0.1260	0.0391	0.0034
0.50	0.1590	0.2040	0.1780	0.0728	0.0086
0.75	0.1340	0.1900	0.2030	0.1130	0.0161
1.0	0.1150	0.1730	0.2030	0.1490	0.0325

Table 3. *Transmission after scatterings by concrete* (*effective* $Z = 13.4$, *composition by weight as given in Ref.* 17)
Based on 5000 photon histories per source energy of 1.25 MeV, cut-off energy = 0.025 MeV.
Scattered number transmitted, T_n

Cos θ_0	B (g/cm^2)				
	3.75	7.5	15	30	60
0	0.3480	0.3010	0.1810	0.0732	0.0065
0.25	0.3200	0.4260	0.3620	0.1550	0.0178
0.50	0.2160	0.3370	0.3930	0.2380	0.0503
0.75	0.1600	0.2850	0.3810	0.2950	0.0850
1.0	0.1240	0.2460	0.3420	0.3190	0.1330

Scattered energy transmitted, T_E

Cos θ_0	B (g/cm^2)				
	3.75	7.5	15	30	60
0	0.1460	0.1080	0.0534	0.0177	0.0011
0.25	0.1570	0.1870	0.1280	0.0450	0.0039
0.50	0.1150	0.1690	0.1700	0.0895	0.0159
0.75	0.0891	0.1510	0.1880	0.1300	0.0341
1.0	0.0716	0.1370	0.1820	0.1570	0.0604

Table 4. *Transmission after scatterings by concrete* (*effective* $Z = 13.4$, *composition by weight as given in Ref.* 17)
Based on 5000 photon histories per source energy of the γ-ray spectrum produced by the products of U^{235} fission at 1.12 hr after fission, cut-off energy = 0.025 MeV.
Scattered number transmitted, $\overline{T}_n$

Cos θ_0	B (g/cm^2)				
	3.75	7.5	15	30	60
0	0.3200	0.2460	0.1400	0.0472	0.0054
0.25	0.3050	0.3650	0.2690	0.1080	0.0145
0.50	0.2220	0.3150	0.3130	0.1690	0.0313
0.75	0.1700	0.2740	0.3120	0.2130	0.0609
1.00	0.1440	0.2420	0.2950	0.2390	0.0937

Scattered energy transmitted, $\overline{T}_E$

Cos θ_0	B (g/cm^2)				
	3.75	7.5	15	30	60
0	0.1520	0.1000	0.0505	0.0145	0.0018
0.25	0.1580	0.1770	0.1200	0.0460	0.0049
0.50	0.1170	0.1640	0.1630	0.0905	0.0157
0.75	0.0925	0.1520	0.1680	0.1270	0.0386
1.00	0.0809	0.1360	0.1690	0.1430	0.0667

Table 5. *Transmission after scatterings by concrete* (*effective* $Z = 13.4$, *composition by weight as given in Ref.* 17)
Based on 5000 photon histories per source energy of the γ-ray spectrum produced by the products of U^{235} fission at 23.8 hr after fission, cut-off energy = 0.025 MeV.

Scattered number transmitted, $\overline{T}_n$

Cos θ_0	B (g/cm^2)				
	3.75	7.5	15	30	60
0	0.2990	0.2230	0.1310	0.0402	0.0042
0.25	0.3120	0.3450	0.2500	0.0834	0.0098
0.50	0.2260	0.3040	0.2970	0.1450	0.0205
0.75	0.1750	0.2730	0.3010	0.1900	0.0364
1.00	0.1450	0.2360	0.2860	0.2260	0.0569

Scattered energy transmitted, $\overline{T}_E$

Cos θ_0	B (g/cm^2)				
	3.75	7.5	15	30	60
0	0.1660	0.1140	0.0555	0.0152	0.0015
0.25	0.1870	0.1970	0.1240	0.0365	0.0042
0.50	0.1450	0.1870	0.1680	0.0765	0.0108
0.75	0.1150	0.1800	0.1850	0.1110	0.0246
1.00	0.0991	0.1640	0.1880	0.1440	0.0417

Table 6. *Transmission after scatterings by iron* ($Z = 26$)
Based on 5000 photon histories per source energy of 0.35 MeV, cut-off energy = 0.050 MeV.

Scattered number transmitted, T_n

Cos θ_0	B (g/cm^2)				
	3.75	7.5	15	30	60
0	0.2560	0.1650	0.0661	0.0104	0.0003
0.25	0.3140	0.2770	0.1290	0.0225	0.0012
0.50	0.2460	0.2820	0.1840	0.0491	0.0023
0.75	0.2040	0.2520	0.2150	0.0828	0.0058
1.0	0.1170	0.2350	0.2400	0.1190	0.0141

Scattered energy transmitted, T_E

Cos θ_0	B (g/cm^2)				
	3.75	7.5	15	30	60
0	0.1650	0.1030	0.0409	0.0062	0.0001
0.25	0.2200	0.1840	0.0844	0.0141	0.0007
0.50	0.1790	0.2000	0.1280	0.0335	0.0016
0.75	0.1550	0.1860	0.1580	0.0597	0.0041
1.0	0.1380	0.1800	0.1850	0.0908	0.0102

Table 7. Transmission after scatterings by iron ($Z = 26$)
Based on 5000 photon histories per source energy of 0.66 MeV,
cut-off energy = 0.050 MeV.
Scattered number transmitted, T_n

Cos θ_0	B (g/cm^2)				
	3.75	7.5	15	30	60
0	0.3130	0.2190	0.1170	0.0338	0.0028
0.25	0.3300	0.3430	0.2330	0.0711	0.0066
0.50	0.2370	0.3080	0.2950	0.1260	0.0163
0.75	0.1820	0.2710	0.3000	0.1820	0.0307
1.00	0.1530	0.2380	0.2910	0.2210	0.0522

Scattered energy transmitted, T_E

Cos θ_0	B (g/cm^2)				
	3.75	7.5	15	30	60
0	0.1660	0.1080	0.0544	0.0154	0.0011
0.25	0.1930	0.1920	0.1220	0.0359	0.0032
0.50	0.1510	0.1890	0.1720	0.0698	0.0089
0.75	0.1240	0.1770	0.1890	0.1120	0.0177
1.00	0.1060	0.1600	0.1930	0.1460	0.0319

Table 8. Transmission after scatterings by iron ($Z = 26$)
Based on 5000 photon histories per source energy of 1.25 MeV,
cut-off energy = 0.050 MeV.
Scattered number transmitted, T_n

Cos θ_0	B (g/cm^2)					
	3.75	7.5	15	18.77	30	60
0	0.3430	0.2640	0.1480	0.1110	0.0505	0.0045
0.25	0.3020	0.3640	0.2860	0.2390	0.1180	0.0152
0.50	0.2050	0.3020	0.3270	0.3110	0.1980	0.0410
0.75	0.1580	0.2440	0.3100	0.3180	0.2490	0.0830
1.00	0.1310	0.2120	0.2850	0.3050	0.2710	0.1250

Scattered energy transmitted, T_E

Cos θ_0	B (g/cm^2)					
	3.75	7.5	15	18.77	30	60
0	0.1490	0.1040	0.0539	0.0375	0.0156	0.0014
0.25	0.1560	0.1740	0.1240	0.0948	0.0454	0.0052
0.50	0.1150	0.1600	0.1650	0.1520	0.0926	0.0163
0.75	0.0926	0.1400	0.1740	0.1710	0.1330	0.0403
1.00	0.0786	0.1250	0.1700	0.1740	0.1560	0.0675

Table 9. *Transmission after scatterings by iron* ($Z = 26$)
Based on 5000 photon histories per source energy of the γ-spectrum produced by the products of U^{235} fission at 1.12 hr after fission, cut-off energy = 0.050 MeV.

Scattered number transmitted, $\overline{T}_n$

Cos θ_0	B (g/cm^2)				
	3.75	7.5	15	30	60
0	0.2810	0.1990	0.1030	0.0349	0.0047
0.25	0.2630	0.2830	0.2120	0.0824	0.0103
0.50	0.1890	0.2580	0.2520	0.1320	0.0270
0.75	0.1450	0.2230	0.2460	0.1690	0.0498
1.00	0.1220	0.2020	0.2300	0.1920	0.0809

Scattered energy transmitted, $\overline{T}_E$

Cos θ_0	B (g/cm^2)				
	3.75	7.5	15	30	60
0	0.1480	0.0987	0.0485	0.0162	0.0025
0.25	0.1460	0.1620	0.1200	0.0478	0.0059
0.50	0.1060	0.1520	0.1610	0.0845	0.0193
0.75	0.0863	0.1370	0.1620	0.1210	0.0419
1.00	0.0716	0.1250	0.1520	0.1400	0.0691

Table 10. *Transmission after scatterings by iron* ($Z = 26$)
Based on 5000 photon histories per source energy of the γ-spectrum produced by the products of U^{235} fission at 23.8 hr after fission, cut-off energy = 0.050 MeV.

Scattered number transmitted, $\overline{T}_n$

Cos θ_0	B (g/cm^2)				
	3.75	7.5	15	30	60
0	0.2590	0.1800	0.0970	0.0258	0.0023
0.25	0.2600	0.2740	0.1870	0.0572	0.0073
0.50	0.1930	0.2420	0.2310	0.1010	0.0173
0.75	0.1500	0.2120	0.2340	0.1430	0.0342
1.00	0.1240	0.1900	0.2310	0.1690	0.0598

Scattered energy transmitted, $\overline{T}_E$

Cos θ_0	B (g/cm^2)				
	3.75	7.5	15	30	60
0	0.1550	0.1050	0.0543	0.0135	0.0009
0.25	0.1710	0.1800	0.1190	0.0351	0.0042
0.50	0.1320	0.1690	0.1640	0.0693	0.0127
0.75	0.1070	0.1580	0.1780	0.1100	0.0278
1.00	0.0916	0.1420	0.1820	0.1370	0.0503

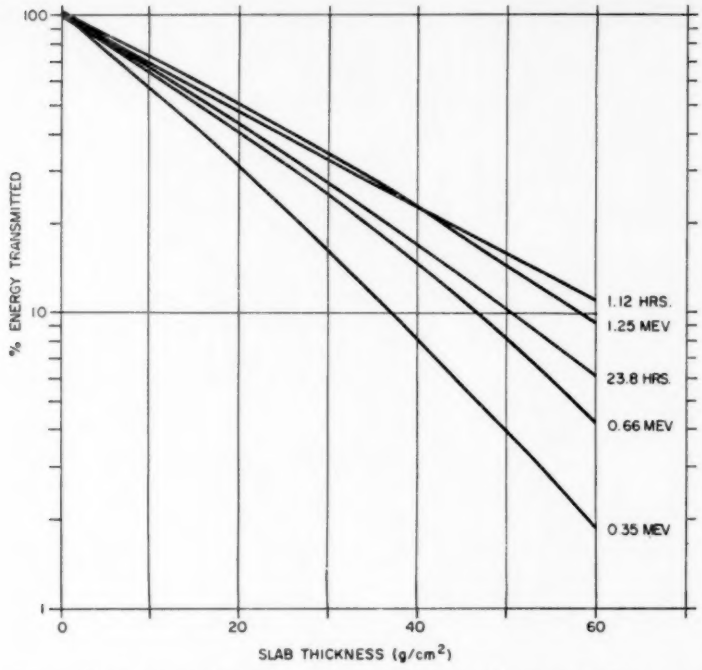

FIG. 2. Attenuation of γ-rays for various source energies incident normally on concrete slabs.

to one incident photon per source energy. From the data in the tables it is evident that a poor approximation may result if one calculates the transmission of scattered photons merely by using normal incidence data. This is especially true for large angles of incidence. It is also noted that for normal incidence, $\cos\theta_0 = 1.0$, on thin slabs the transmission of scattered photons is low. As $\cos\theta_0$ decreases the photons will undergo more interactions because of the greater apparent thickness; the probability of back-scattering, increasing with θ_0, causes the transmission to go through a maximum. [In the limiting case of grazing incidence ($\cos\theta_0 = 0$) the probability of back-scattering at the first collision is approximately 0.5 for the incident energies considered.] For larger slabs the transmission decreases with decreasing $\cos\theta_0$.

Illustrative results

Total energy transmitted. In Figs. 2 and 3 the total energy transmitted for concrete and iron are plotted respectively for various source energy at normal obliquity. The most interesting feature in these figures is the close similarity of the total transmission for a 1.25 MeV source and γ-ray spectrum produced by the products of U^{235} fission at 1.12 hr after fission. (This does not necessarily mean that the differential transmissions for these sources are comparable.) The total energy transmitted for the γ-ray spectrum at 23.8 hr after fission is closer to that for a 0.66 MeV source than for a 1.25 MeV source.

Energy spectrum. In Figs. 4 and 5 are plotted illustrative examples of the energy spectra for various source obliquities, energies and barrier thicknesses for concrete and iron, respectively. It is noted from these figures that in all cases the high energy regions of the spectra are similar for iron and concrete; whereas at lower energies large peaks due to multiple scatterings are observed for concrete. The reason for this effect is that in the low energy region photo-electric absorption is not predominant in the low-Z materials. Single-scattered peaks are

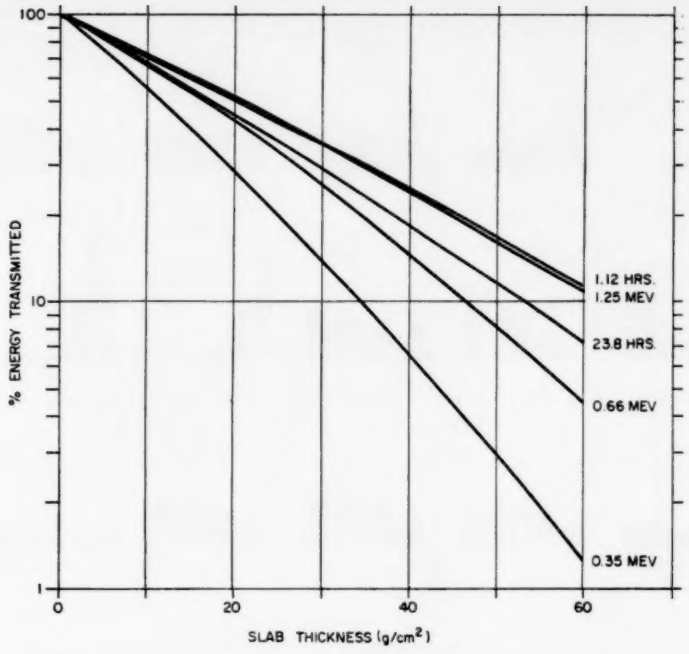

FIG. 3. Attenuation of γ-rays for various source energies incident normally on iron slabs.

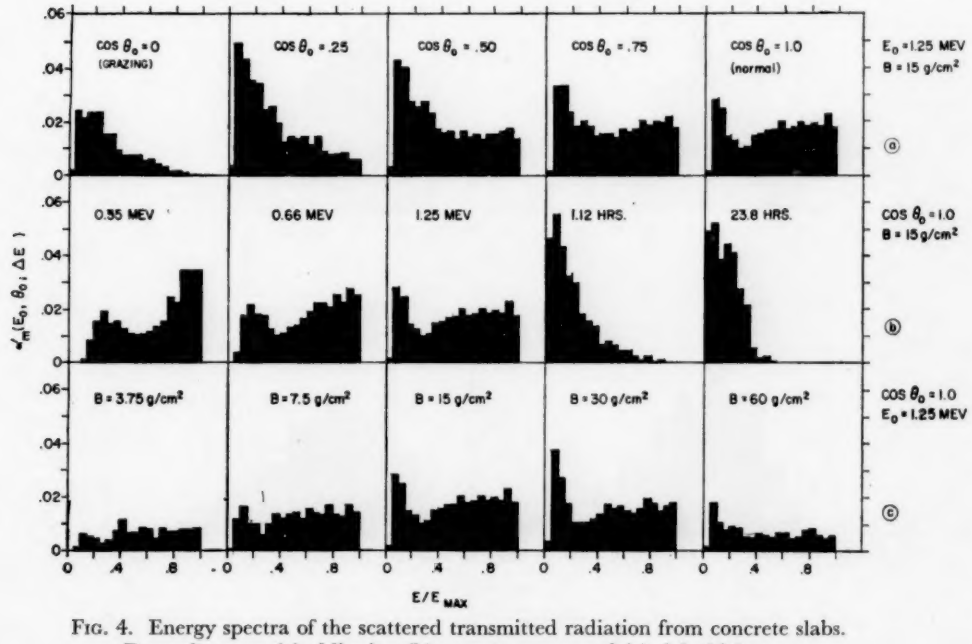

FIG. 4. Energy spectra of the scattered transmitted radiation from concrete slabs. Dependence on (a) obliquity, (b) source energy, and (c) slab thickness.

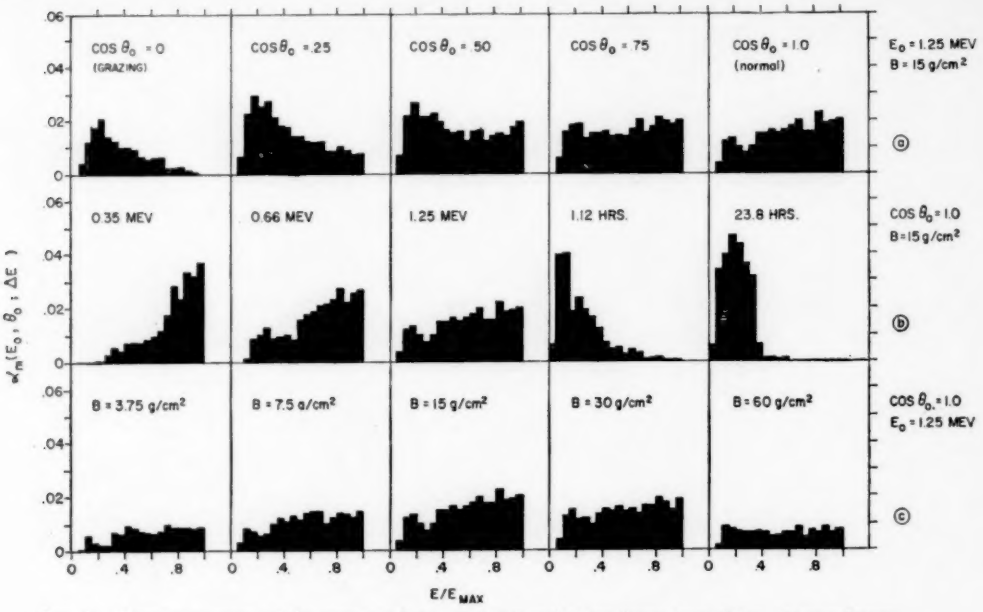

FIG. 5. Energy spectra of the scattered transmitted radiation from iron slabs. Dependence on (a) obliquity, (b) source energy, and (c) slab thickness.

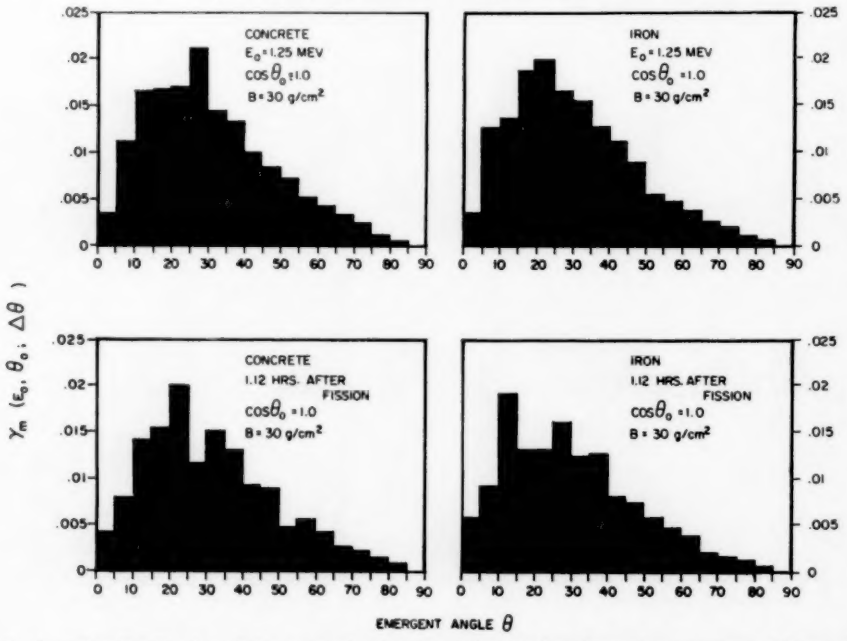

FIG. 6. Angular distribution of the transmitted scattered radiation through concrete and iron. Source energy of 1.25 MeV and 1.12 hr after U^{235} fission normally incident on a slab of 30 g/cm².

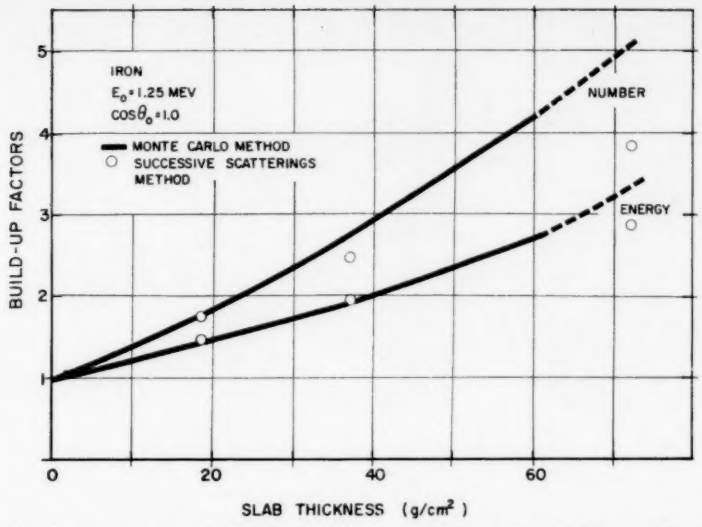

FIG. 7. Number and energy build-up factors for a source of 1.25 MeV normally incident on iron slabs. Points represent the values obtained by PEEBLES.

observed for monoenergetic sources in the region where the energy is nearly equal to the incident energy. These single scattered peaks are especially noticeable for the cases where the source obliquity is normal or close to it. The energy spectra for the gamma rays produced by the products of U^{235} fission at 1.12 and 23.8 hr after fission, are considerably different from those of monoenergetic sources.

Angular distribution of the transmitted energy. The angular distribution of the transmitted energy for sources of 1.25 MeV and 1.12 hr after fission normally incident on concrete and iron of 30 g/cm² thickness is shown in Fig. 6. It is seen that most of the energy is transmitted at small emergent angles which could be attributed to one of the following factors: (1) the change in energy is low for small angles of scatterings; and (2) the greater the angle of scattering the greater thickness the photon traverses, thereby increasing the probability of another interaction before it emerges.

Comparison with the successive scatterings method. The number and energy build-up factors (defined as the total transmission divided by the unscattered transmission) for the case of 1.25 MeV source incident normally on iron are plotted in Fig. 7. The points are the values obtained by PEEBLES[5]. The two methods give similar results (within the combined estimates of error) for relatively thin slabs. As the slab thickness increases, the results diverge, probably because of the few orders of scatterings used by the successive scattering method.

Comparison with the moment method. In Fig. 8 the dose build-up factors for 1.25 and 0.66 MeV normally incident on iron are plotted. The method for determining physical dose is given in Ref. 10. The points in the figure are interpolated from values obtained by GOLDSTEIN and WILKINS[4]. These results are higher than the Monte Carlo method because a photon can pass the boundary more than once in an infinite medium.

SPENCER[12] has determined, with the use of the moment method, the amount of protection one receives in various structures from fallout (1.12 hr after fission) and various isotropic monoenergetic sources (1.25 and 0.66 MeV) on the ground and on the roof. His results are given in terms of reduction factors which are defined as the ratio of the detector response (from the sources on the ground and/or the sources on the roof) in a protected position to the detector response 3 ft above an infinite plane contaminated with the same source

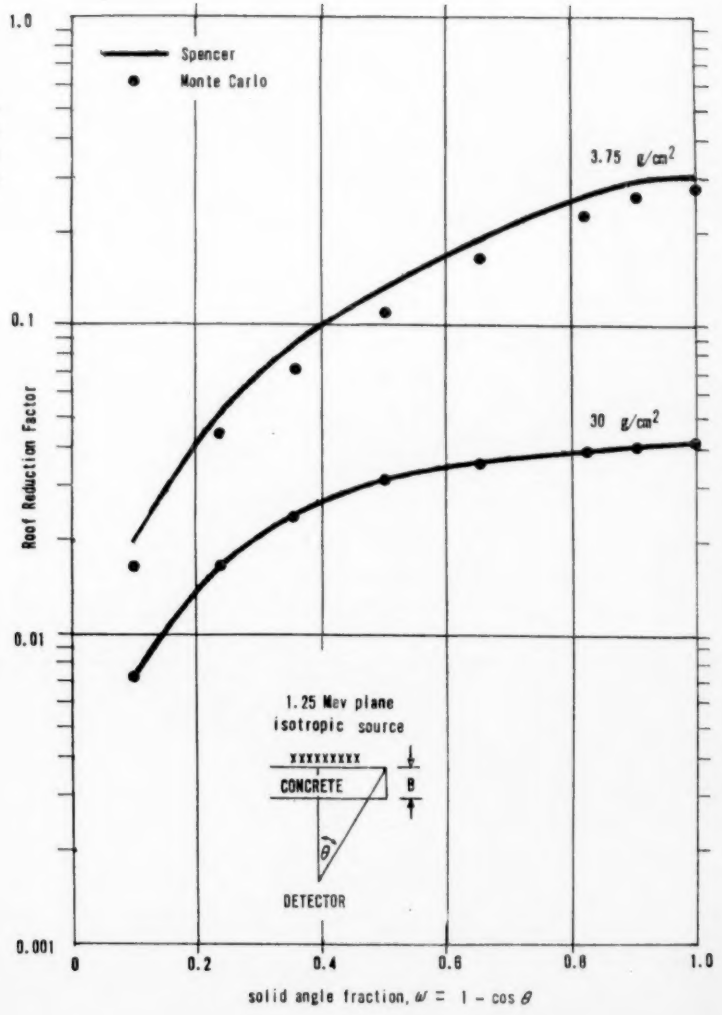

FIG. 9. Roof reduction factor as a function of solid angle fraction and slab thickness obtained by the Monte Carlo method and the moment method.[12]

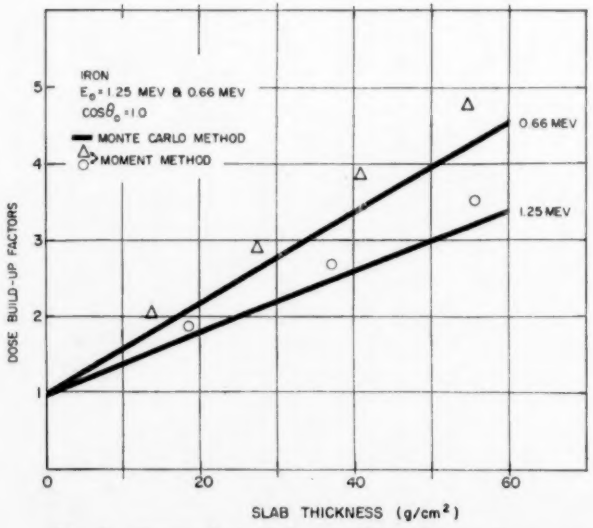

FIG. 8. Comparison of dose build-up factors for γ-rays normally incident on iron slabs obtained by Monte Carlo and moment methods.

density. By way of comparison, the roof reduction factors for a Co^{60} plane isotropic source and barrier thicknesses of 3.75 and 30 g/cm² of concrete are shown in Fig. 9. The abscissa is in units of solid angle fraction, $\omega = 1 - \cos\theta$. As is seen for the thinner barrier, the moment method gives slightly higher results than the Monte Carlo method. For the thicker barrier, the two methods are in agreement.

Comparisons with experiment performed at NRDL. Scofield *et al.*[13] determined experimentally the transmitted angular and energy distributions of scattered γ-rays for plane sources, Co^{60} and Cs^{137}, incident on various slabs of aluminum and iron. The measurements were taken at detection angles of 5°, 10°, 20°, 30°, 45°, 60°, with respect to the normal. Although Ref. 13 provides pulse height distributions rather than γ-ray energy spectra, the authors have provided values for the transmitted scattered angular distribution of number[14] from their transformation of the results given in Ref. 13 into γ-ray energy spectra.[15] Since the effective Z of concrete is 13.4, the experimental results for aluminum ($Z = 13$) were compared to the Monte Carlo results for concrete. The Co^{60}, emitting photons of 1.17 and 1.33 MeV, data were compared with 1.25 MeV source used in the Monte Carlo calculations and the Cs^{137} to that of 0.66 MeV source. The results for the transmitted scattered angular distribution of number due to normally incident γ-rays on concrete and iron of various slabs, and energies for the two methods, are given in Figs. 10 and 11. As is seen, except for the case of Co^{60} incident on iron at a thickness of 1.00 m.f.p. the slab thicknesses are not exactly the same for

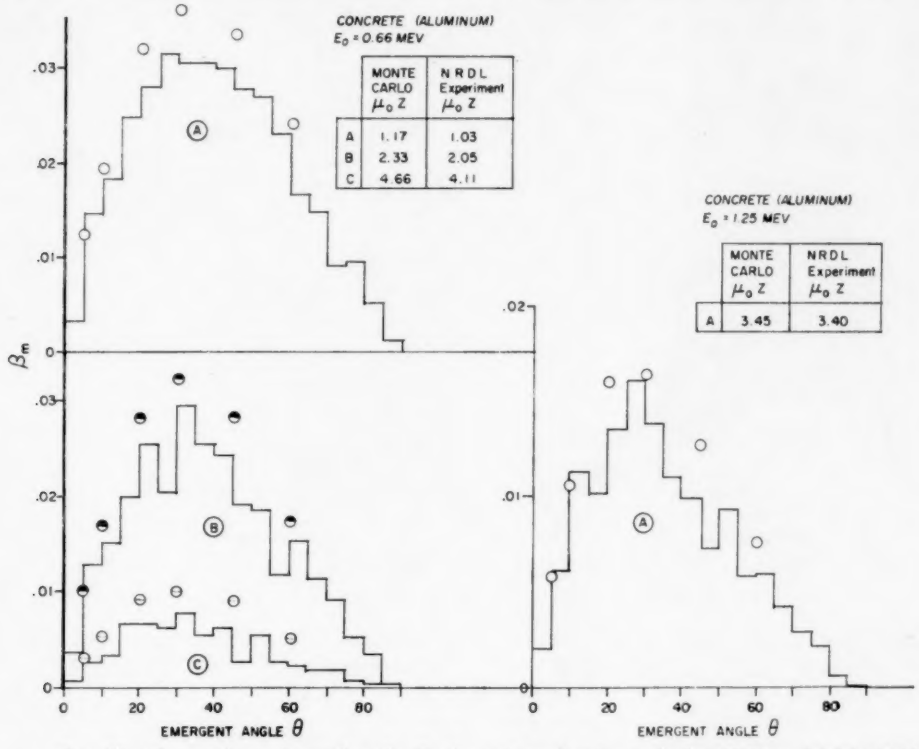

FIG. 10. Comparison of angular distribution of number for radiation (0.66 and 1.25 MeV) normally incident on various slabs of concrete.

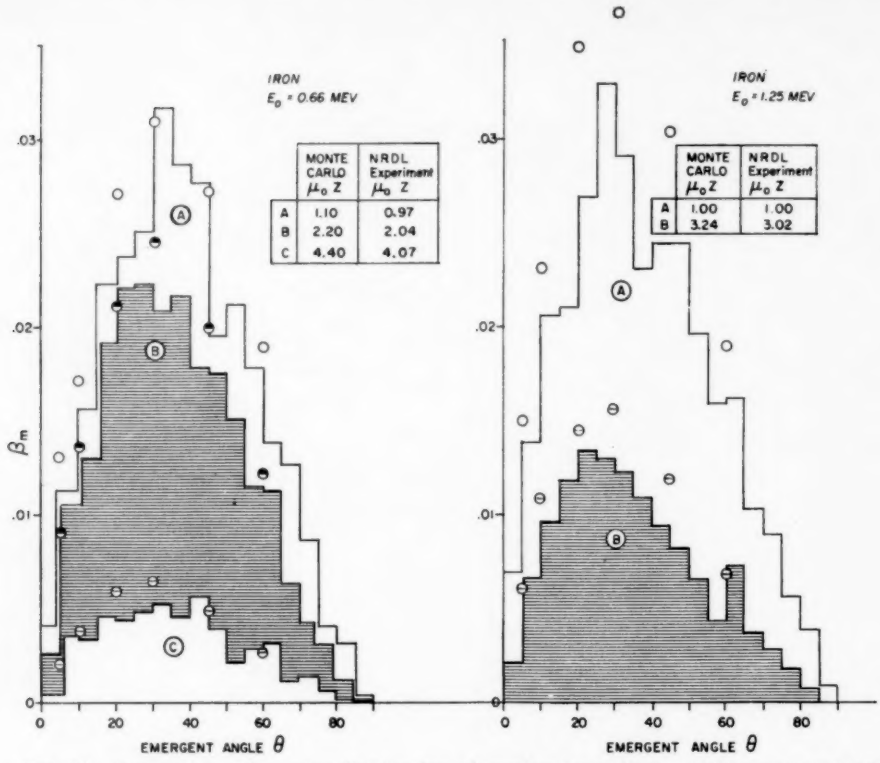

FIG. 11. Comparison of angular distribution of number for radiation (0.66 and 1.25 MeV) normally incident on various slabs of iron.

the various cases. Agreement of the results, which are within the statistical accuracy of the two methods, is satisfactory. The experimental data follow the general trend of the histogram showing peaks around 30° for the various cases. Also, it can be noted here that the angular distributions depend very little on the thickness (from 1 to 4 m.f.p.), incident energy (0.66 to 1.25 MeV), and material (concrete and iron). This was also observed in an experiment performed by KAZANSKI *et al.*[16] with various isotropic point sources.

Acknowledgments—The author is grateful for the technical and scientific assistance in the preparation of the report from Dr. M. J. BERGER, Radiation Theory Section, National Bureau of Standards, Washington, D.C., and Dr. E. T. CLARKE, Technical Operations, Inc., Burlington, Massachusetts. Also the author wishes to thank J. LAMKIN, Radiation Theory Section, National Bureau of Standards, Washington, D.C., for assistance with the coding for the IBM 704.

REFERENCES

1. A. T. NELMS and J. W. COOPER, *Health Phys.* **1,** 427 (1959).
2. C. M. DAVISSON and R. D. EVANS, *Rev. Mod. Phys.* **24,** 79 (1952).
3. L. V. SPENCER and U. FANO, *J. Res. Nat. Bur. Stand.* **46,** 446 (1951).
4. H. GOLDSTEIN and J. E. WILKINS, JR., AEC Report NYO 3075 (1954).
5. G. H. PEEBLES, Rand Report R-240 (1952).
6. M. J. BERGER and J. DOGGETT, *J. Res. Nat. Bur. Stand.* **56,** 89 (1956).
7. C. D. ZERBY, ORNL-224 (1956).
8. D. J. RASO. Thesis, Boston College (1959).
9. J. F. PERKINS, *J. Appl. Phys.* **26,** 1372 (1955).
10. D. J. RASO, TO-B 59-13 (1959).

11. M. J. Berger and D. J. Raso, *Rad. Res.* **12,** 20 (1960).
12. L. V. Spencer, Private communication.
13. N. E. Scofield, R. L. Lynn and W. E. Kreger, Research and Development Technical Report USNRDL-TR-272 (1958).
14. W. E. Kreger. Private communication.
15. N. E. Scofield and L. G. Haggmark, Research and Development Technical Report USNRDL-TR-475 (1960).
16. Yu. A. Kazansky, S. P. Belov and Ye. S. Matusevich, *Atomnaya Energiya* **5,** 457 (1958).

Health Physics Pergamon Press 1961. Vol. 5, pp. 142–148. Printed in Northern Ireland

THE DETERMINATION OF LOCALIZED CONCENTRATION OF Pu^{239} IN BONE*†

J. A. TWENTE and W. S. S. JEE
Division of Radiobiology and Department of Anatomy, College of Medicine
University of Utah, Salt Lake City, Utah

(*Received* 2 *May* 1960)

Abstract—A microdensitometric technique of measuring *localized* concentrations of α-emitting radionuclides was used to determine the Pu^{239} in bone.

The data obtained by microdensitometric scanning of quantitative autoradiograms shows close agreement with data obtained by the previously used technique of the visual counting of α-tracks. The accuracy of the microdensitometric technique was verified by a comparison of the Pu^{239} content of a thoracic vertebral centrum determined microdensitometrically with the Pu^{239} content of an adjacent centrum measured radiochemically. The amount of Pu^{239} found microdensitometrically was 76 per cent of that determined radiochemically.

The average Pu^{239} concentration associated with haversian systems, periosteal surfaces, and endosteal surfaces of trabecular bone in a lumbar vertebra (from a beagle hound injected with 2.85 μc of Pu^{239}/kg 92 days prior to sacrifice) was, respectively, 0.30×10^{-5}, 0.54×10^{-5} and 1.6×10^{-5} $\mu\mu$c per μ^2 of surface.

The calculated average localized dose rate delivered to bone tissue and marrow cells on the endosteal surface deposit is 40 and 60 rads per day. These rates are ten times the previously calculated average skeletal dose rate.

INTRODUCTION

THE chronic effects of plutonium (Pu^{239}), radium (Ra^{226}), mesothorium (Ra^{228}), radiothorium (Th^{228}) and strontium (Sr^{90}) on adult beagle hounds are being studied in this laboratory. The project includes the measurement of localized concentrations of these radionuclides in bone tissue and the calculation of localized dosages of radiation. We expect to be able to relate some of the changes in bone including bone tumors with the localized dose rate and the localized cumulative dose. Such measurements are important in understanding the differences in biological response, in the calculation of relative biological effectiveness (RBE) and in establishing the maximum permissible concentrations (MPC) for these different radionuclides.

This paper presents a microdensitometric technique for determining localized concentrations of α-emitting radionuclides in tissues. The accuracy of the microdensitometric technique is confirmed by comparison of results obtained by it with those obtained by visually counting α-tracks and with results obtained by radiochemical methods.

The Pu^{239} concentrations associated with three types of bone surfaces are measured and the localized dosage of radiation delivered by the endosteal surfaces of trabecular bone is calculated.

METHODS

All previous techniques used to measure localized dosage of radiation utilize quantitative autoradiography. The localized dosage delivered by β-emitters has been measured directly[1–7] while with α-emitters, the localized radionuclide content has been measured by counting α-tracks and the localized dose subsequently calculated.[8–12]

* This work was done under Supplement B to AEC Contract AT(11-1)-119.

† Presented in part before the Radiation Research Society, Pittsburgh (May 1959) *Rad. Res.* **11,** 121.

The determination of the radionuclide content of tissue by visually counting α-tracks in autoradiograms is tedious and time consuming. For this reason, we decided to measure the degree of light absorption of autoradiograms by a photoelectric densitometer and correlate these data with the number of tracks present in these areas.

The beagle hounds used in this study were injected when from 16 to 22 months old with 2.74–2.85 μc of Pu^{239} per kg and sacrificed at time intervals varying from 2 weeks to 3 months after injection. The plutonium was administered as a single intravenous injection of plus 4 plutonium complexed with citrate; the details of the preparation of the injection solutions have been previously reported.[13]

A comparison of the microdensitometric and the visual counting techniques of measuring localized radionuclide concentration was made using quantitative autoradiograms produced by a lumbar vertebral centrum of a beagle hound injected with 2.85 μc of Pu^{239} per kg 3 months before being sacrificed. Three thoracic vertebral centra (ninth, eleventh and twelfth) from a dog injected with 2.74 μc of Pu^{239} per kg 4 weeks prior to sacrifice were used to compare the radionuclide content of a vertebral centrum as determined densitometrically and by routine radiochemical analysis.[13] One half of the centrum of the twelfth thoracic vertebra was used to produce quantitative autoradiograms for the microdensitometric measurements; the other half was serially sectioned and used to measure the amount of bone surface area in the centrum. The centra of the ninth and eleventh thoracic vertebrae were used for radiochemical analysis. The variation of the Pu^{239} content between bones was determined by radiochemical analyses of thoracic vertebral centra taken from another dog sacrificed at 4 weeks and from two other dogs sacrificed at 2 weeks after injection of Pu^{239}.

A. *Quantitative autoradiograms*

The bone specimens were embedded with Scotch Cast Resin no. 2 according to techniques previously described[14] and a cross-sectional surface exposed and ground to smoothness with increasingly fine carborundum papers. Quantitative autoradiograms were produced by clamping the bone on Ilford C-2 nuclear track emulsion on flexible acetate backing.* The range of the plutonium α-particle has been calculated to be 24.1 μ in bone and 29.5 μ in Scotch Cast Resin no. 2.[15] Thus the smallest field in which complete tracks can be measured has a diameter of 53.6 μ. A field diameter of 70 μ was selected to allow for possible differences in the thickness (less than 10 μ) of the Pu^{239} layer on bone surfaces and also for slight errors in apposition of the bone to the nuclear emulsion during the exposure.

The autoradiograms in which α-tracks are counted visually must have an emulsion thick enough to completely stop all α-particles. The range of the plutonium α-particle in Ilford C-2 emulsion has been calculated to be 20.5 μ[15]; the emulsion which we selected for producing autoradiograms of plutonium was 25 μ thick.

The problem of latent image fading during long exposures[16] was eliminated for periods up to 6 months by making the exposure in the presence of a desiccant (calcium chloride) at a temperature of −20°C.

In order to have the densitometer readings proportional to the number of developed grains present in a field, the grains must absorb equal quantities of light. This means that the grains must be the same size in all autoradiograms as well as in different areas of one autoradiogram. All of the autoradiograms were developed in Eastman Kodak D-19 for 10 min at 18°C and fixed in Eastman Kodak acid fixer for 30 min. The autoradiograms were then mounted on standard microscope slides.

B. *Instruments*

The basic instruments used were a Leitz Panphot microscope with the prefocused coil filament tungsten light source, a MacBeth–Ansco densitometer and a Brown recorder. The details of the assembled parts and their operation have been previously described.[17,18] The photoelectric cell of the MacBeth–Ansco densitometer, mounted at the level of the film cassette of the Panphot, detects the slight reduction in the amount of light transmitted in areas of the emulsion of autoradiograms containing α-tracks. For maximum sensitivity, the image of the developed grains in the entire depth of the emulsion must be focused simultaneously on the cathode of the photoelectric cell. This was accomplished by the use of a 6× objective which has a depth of focus greater than 25 μ. The desired magnification of a 70-μ field was obtained by the use of an 8× ocular and proper extension of the bellows of the Leitz Panphot.

C. *Calibration of the instruments*

The MacBeth–Ansco densitometer response (recorded by a Brown potentiometer) was calibrated with a Pu^{239} source of known activity deposited on a flat surface in approximately the same pattern as it is deposited on the surfaces of the suitable bone specimens. In the standards used to calibrate the instrument, Pu^{239} was deposited in uniform thin layers on

* Obtained from Ilford Inc., 2/4 Clements Road, Ilford Essex, England.

the surface of aluminum disks either by electrodeposition* or vaporization.† The α-emitting activity of these disks was determined by routine α-counting techniques by the supplier. The stated activities were checked in this laboratory using a conventional proportional counter standardized with a USNBS U_3O_8 standard. The uniformity of the Pu^{239} deposition was verified by contact autoradiography. The disks were embedded in plastic and quantitative autoradiograms of the edge of the disk were produced using the same procedures as for the bone specimens. The light absorption of 70-μ diameter circles of these autoradiograms was measured. A calibration curve was constructed by plotting activity (tracks per unit time) against the deflation of the Brown recorder (degree of light absorption).

D. *Experiment I*

Comparison of microdensitometric and track counting techniques. An autoradiogram of a cross-section of the lumbar vertebral centrum of a beagle hound, which had been injected with Pu^{239} 3 months prior to sacrifice, is shown in Fig. 1. Visual inspection of Fig. 2 shows that the number of tracks produced by the radionuclide associated with the periosteal bone surface (e), haversian systems of cortical bone (h), and the endosteal surfaces of trabecular bone (p) are grossly different.

An autoradiogram, exposed to the bone for 7 days, was used for the microdensitometric measurement of the Pu^{239} activity associated with all three bone surfaces.

The tracks produced by the Pu^{239} associated with the periosteal surfaces and the haversian systems were counted visually in different areas of the same autoradiogram. However, the number of tracks produced by the Pu^{239} at the endosteal surface was generally too great for accurate visual counting in this autoradiogram, and these data were obtained from an autoradiogram exposed for only 1 day.

Calculation of radionuclide concentration. The Pu^{239} deposition pattern observed in bone tissue shortly after injection is that of a sheet or a thin slab of the radionuclide surrounding all calcified surfaces.[20,21]

A formula relating the number of tracks measured in a specific length of an autoradiogram to the number of disintegrations (per area of bone surface perpendicular to the emulsion) has been reported for this type of deposition pattern.[15] The formula is as follows:

$$D = \frac{4T}{L\,R_{av}} \tag{1}$$

where D is the disintegration rate per area of α-emitting source
T is the number of tracks formed per unit time
L is the length of source measured
R_{av} is the average range of the plutonium α-particle in the media on either side of the source

This formula assumes that the radionuclide is deposited uniformly over the small surface area measured. The radionuclide concentration per area is easily calculated when the disintegration rate per area is known.

Calculation of localized dose rate. A formula for calculating the average dose rate delivered throughout a specified distance from an α-emitting plane source has been previously reported.[15] This formula is as follows:

$$\text{average dose rate} = \frac{DE}{2R\rho}\left(1 + \ln\frac{R}{X}\right) \tag{2}$$

where D is the disintegration rate per unit area of the source
E is the energy of the emitted α-particle
R is the range of the α-particle in the medium considered
ρ is the density of the medium
X is the specified distance from the source

E. *Experiment II*

Accuracy of microdensitometric technique. The reliability and accuracy of the microdensitometric method was established by comparing the Pu^{239} content of a large bone determined microdensitometrically with comparable samples measured by the routine radiochemical technique.[13]

The estimation of the amount of radionuclide in a large bone sample by microdensitometric measurements involves: (1) the measurement of the localized concentration of the radionuclide deposited on bony surfaces in different anatomical regions; and (2) the measurement of the total area of the bone surfaces which contain the radionuclide. One half of the centrum of the twelfth thoracic vertebra was embedded in Scotch Cast Resin no. 2 and used to produce quantitative autoradiograms for microdensitometric scanning. The other half of the twelfth centrum was embedded in ethyl and butyl methacrylate, and serially sectioned at 18 μ thickness using techniques previously described.[14] Approximately

* These disks, obtained from the General Electric Hanford Atomic Products Operation, were prepared according to the technique of Ko[19].

† These disks were obtained from Los Alamos Scientific Laboratory through the courtesy of WRIGHT H. LANGHAM and M. A. VAN DILLA.

FIG. 1. A macrophotograph of quantitative autoradiogram (exposed 30 days) of a cross-section of lumbar vertebra taken from a dog injected with 2.85 μc of Pu^{239}/kg and sacrificed 92 days after injection. ($\times 3$)

FIG. 2. An enlargement of the area of Fig. 1 showing the Pu^{239} deposition associated with the periosteal surface (e), haversian systems of cortical bone (h) and the endosteal surface of trabecular bone (p). ($\times 300$)

BLANK
PAGE

every twentieth section was projected onto a large piece of paper and the outlines of the bone surfaces traced. The length of the trabecular endosteum in these sections was measured. The following formula was used to calculate the total endosteal surface area of the twelfth thoracic vertebral centrum.

$$\text{area} = 2NTL \tag{3}$$

where N is the number of sections in one half of the centrum
T is the thickness of the section
L is the average endosteal length per section

RESULTS AND DISCUSSION

Experiment I

Comparison of microdensitometric and track counting techniques. The results of the microdensitometric method of analyzing autoradiograms and the technique of visually counting tracks in autoradiograms are presented in Table 1. These data show that the average concentration of Pu^{239} on endosteal surfaces of trabecular bone is about five times greater than the radionuclide concentration on haversian systems of cortical bone and three times greater than the deposit on the periosteal surface of cortical bone. A comparison of the minimum and maximum number of tracks detected in a field, as well as the calculated averages, shows that there is very close agreement between the two techniques.

The most apparent advantages in the use of the microdensitometric method as opposed to visual counting techniques for the determination of radionuclide concentration are: (1) that the time and labor involved in obtaining sufficient data for analysis are greatly reduced; (2) that the magnitudes of radionuclide concentration which can be measured microdensitometrically in adjacent areas of an autoradiogram greatly exceed the narrow concentration range which can be counted visually; and (3) the ease of identifying different histological structures and the radionuclide associated with them. In tissues with an exceedingly low radionuclide content the visual counting of tracks may be the more expedient procedure, since the exposure time required to produce a sufficient quantity of tracks in an autoradiogram for microdensitometric measurements may be months or perhaps years.

Although data expressed as the number of tracks per area can be used for quantitative comparison of radionuclide concentration between areas, they give no information regarding the actual concentration of the radionuclide in any given area. However, the average Pu^{239} concentration on the endosteal surface from the the data given in Table 1 may be calculated as follows: The average number of tracks (T) produced by endosteal surfaces is 165–175 per week or about 24 per day per 70 μ length. The length of the surface source measured (L) is the diameter of the field or 70 μ. R_{av} is the average of the ranges of the plutonium α-particle in bone (24.1) and in the plastic (29.5) filling the marrow spaces, or 26.8 μ. Using these values, and equation (1), we find that the average disintegration rate (D) is 96 per day of measured endosteal surface (1876 μ^2) or 0.0511/day per μ^2. As 1 $\mu\mu$c of a radionuclide produces 2.22 dis/min, the average Pu^{239} concentration of the endosteal surface is 1.6×10^{-5} $\mu\mu c/\mu^2$. By similar calculations the average Pu^{239} concentration on the periosteal surfaces and haversian systems is found to be 0.54×10^{-5} and 0.30×10^{-5} $\mu\mu c/\mu^2$, respectively.

Experiment II

Accuracy of microdensitometric technique. The results of the radiochemical determination of Pu^{239} content presented in Table 2 show that there was a ± 3 to ± 10 per cent variation in the radionuclide content of two thoracic vertebral centra taken from the same dog. In addition it is apparent that considerable variation in the Pu^{239} content of thoracic vertebral centra existed between dogs, which was not related to slight differences in the injected dose of Pu^{239}.

The amount of Pu^{239} on the endosteal surface of the twelfth thoracic centrum was determined from microdensitometric measurements made randomly at distances of 0.5 mm throughout the autoradiogram. The average amount of Pu^{239} on 1 μ^2 of endosteal surface was 1.37×10^{-5} $\mu\mu$c. (The standard deviation of the sample was 0.714×10^{-5} $\mu\mu$c.) The number of sections in one-half of this centrum was 380 and the section thickness was 18 μ. The average endosteal length per section was 300 mm. Using equation

Table 1. *Comparison of the densitometric* (D) *and visual track counting* (VTC) *analysis of an autoradiogram of the fourth lumbar centrum of beagle* T16P5* (*exposure time, 7 days*)

	Number of circles measured		Minimum no. tracks/circle		Maximum no. tracks/circle		Average no. tracks/circle	
	D	VTC	D	VTC	D	VTC	D	VTC
Periosteal surface	25	20	27	33	100	84	57	56
Cortical haversian systems	14	26	15	9	78	86	32	36
Endosteal surfaces	140	45	40	35†	330	399†	165	175†

* Injected with 2.85 μc Pu^{239} per kg 3 months prior to sacrifice.
† Track counts made on 1-day exposure autoradiogram. Figures adjusted for comparison with 7-day autoradiograms.

(3), the total endosteal surface area for this bone was calculated to be about 4100 mm^2.

The total amount of Pu^{239} located on the endosteal surfaces of the twelfth thoracic centrum as calculated from the microdensitometric measurements and area is therefore:

$$\frac{1.37 \times 10^{-11}\ \mu c}{\mu^2} \times 4.1 \times 10^9\ \mu^2 = 0.056\ \mu c$$

Thus, the Pu^{239} content of the endosteal surface of the twelfth thoracic vertebral centrum as determined microdensitometrically is about 76 per cent of the amount found radiochemically in the whole eleventh thoracic vertebral centrum of the same dog.

This estimate of Pu^{239} content of the twelfth thoracic centrum by the microdensitometric method is probably low, since measurements of the radionuclide content in cortical bone and marrow were not included in this figure. Further, slight errors, either in estimating the thickness of the section or in measuring the endosteal surface length, are magnified in the final calculation of gross radionuclide content.

Although the microdensitometric technique is impractical for rapid estimation of radionuclide content of large samples of tissue, we feel

Table 2. *Radiochemical determinations of the* Pu^{239} *content of thoracic vertebral centra of adult beagle dogs*

Dog	Time of sacrifice (days)	Injected dose Pu^{239} (μc/kg)	Vertebral centrum	Pu^{239} content (μc)
T9P5	15	2.80	9th thoracic	0.092
			10th thoracic	0.097
T10P5	15	2.74	9th thoracic	0.083
			11th thoracic	0.102
T11P5	28	2.76	9th thoracic	0.091
			11th thoracic	0.075
T12P5	28	2.74	9th thoracic	0.086
			11th thoracic	0.074
			12th thoracic	0.056*

* Calculated from densitometric measurements.

that the results obtained by this technique are close enough to those obtained by the routine radiochemical method to validate the accuracy of microdensitometric measurements of localized radionuclide content in bone tissue.

Calculation of localized dose rate. If it is assumed that Pu^{239} is distributed uniformly throughout the skeleton, the average skeletal dose received by the beagle hounds studied in this laboratory with a Pu^{239} burden of about 30.0 μc of Pu^{239} has been calculated to be 5.4 rads per day at 1 month after injection.[13] However, it is well known that plutonium is not deposited uniformly throughout the skeleton and that the vertebrae contain a relatively higher proportion of the radionuclide than other bones.[22] Furthermore, the cells which actually absorb a dosage of radiation must be within one α-particle range of the Pu^{239} deposit.

The range of the Pu^{239} α-particle has been calculated to be 24.1 μ in bone tissue and 34.1 in marrow, the bone tissue receiving a dosage from endosteal Pu^{239} must lie within 24 μ and the marrow cells within 34 μ of the surface of a trabecula. The average dose rate to these cells can be calculated using equation (2).

If we consider the average dose rate delivered to cells lying within the range of the Pu^{239} α-particle, the specified distance (X) is equal to the α-range (R) and the term $\ln \frac{R}{X}$ is zero. The energy (E) of the Pu^{239} α-particle is 5.15 MeV per disintegration. The range (R) of the alpha particle in bone is 24.1 μ and the density (ρ) of bone is 2.0.[17] The average disintegration rate (D) of the radionuclide on the endosteal surface of the lumbar centrum (Table 1) was calculated to be 0.0511 per day per μ^2 of surface area. Using equation (2) and appropriate conversions, the average dose rate to bone tissue is calculated as follows:

$$\text{average dose rate} = \frac{1}{2 \times 24\mu} \frac{5.15 \text{ MeV}}{\text{dis}} \times \frac{1.6 \times 10^{-6} \text{ erg}}{\text{MeV}} \frac{10^{12}\ \mu^3}{\text{cm}^3} \frac{1 \text{ cm}^3}{2 \text{ g}} \times \frac{1 \text{ rad}}{100 \text{ ergs/g}} \frac{0.0511 \text{ dis}}{\mu^2 \text{ day}}$$

$$\text{average dose rate} = 41 \text{ rads per day}$$

For marrow, the range (R) is 34 μ and the density (ρ) is 1.0. By a similar calculation the average dose rate to the marrow cells, including the endosteal cells, is 62 rads per day. Thus, the localized dose rates to bone and marrow cells are approximately ten times the average skeletal dose rate previously calculated. These figures are of particular interest since about 35 per cent of the osteogenic sarcomas observed in dogs with a Pu^{239} burden have originated in the centra of the vertebral column.[21] It seems reasonable to assume from this data that cells giving rise to osteogenic sarcomas probably receive a much higher dosage of radiation than previously suspected.

Since measurements of the localized radionuclide can be made both rapidly and accurately by the microdensitometric technique, the accumulation of such data should permit additional calculations of localized dosage of radiation to tissues which may eventually be related to other histopathological changes occurring.

Acknowledgments—We wish to acknowledge Miss E. G. BUTLER and Mrs. O. FREUDENBERGER for their technical assistance in this study, and many other members of the Division of Radiobiology for their helpful suggestions and continued encouragement during this work. We especially wish to thank the members of the Chemistry Group for their full co-operation in doing the radiochemical analyses, and the members of the Physics Group for their prompt derivation of the formulae necessary for the calculation of localized dosage of radiation.

REFERENCES

1. R. A. DUDLEY and B. M. DOBYNS, *Science* **109,** 327 (1949).
2. R. A. DUDLEY and S. R. PELC, *Nature, Lond.* **172,** 992 (1953).
3. D. MAZIA, W. S. PLAUT and G. W. ELLIS, *Exp. Cell. Res.* **9,** 305 (1955).
4. J. S. ARNOLD, W. S. S. JEE and K. JOHNSON, *Amer. J. Anat.* **99,** 291 (1956).
5. L. F. BELANGER, *J. Histochem. Cytochem.* **6,** 146 (1958).
6. N. M. BLACKETT, N. F. KEMBER and L. F. LAMERTON, *Lab. Invest.* **8,** 171 (1959).
7. J. S. ARNOLD and W. S. S. JEE, *Lab. Invest.* **8,** 194 (1959).
8. F. E. HOECKER and P. G. ROOFE, *Radiology* **52,** 856 (1949).

9. F. E. Hoecker and P. G. Roofe, *Radiology* **56,** 89 (1951).
10. R. E. Rowland, J. Jowsey and J. H. Marshall, Argonne Nat. Lab. 5829, p. 109 (1957).
11. M. Hindmarsh, M. Owen and J. Vaughan, *Brit. J. Radiol.* **32,** 183 (1959).
12. R. E. Rowland and J. H. Marshall, *Rad. Res.* **11,** 299 (1959).
13. B. J. Stover, D. R. Atherton and N. Keller, *Rad. Res.* **10,** 130 (1959).
14. L. A. Woodruff and W. P. Norris, *Stain Tech.* **30,** 179 (1955).
15. C. W. Mays, Radiobiology Lab. Report, COO-217, p. 161 (1958).
16. S. Deutsch and E. Picciotto, *Nuovo Cim.* **6,** 953 (1957).
17. J. A. Twente, J. S. Arnold, C. W. Mays, D. H. Taysum and W. S. S. Jee, Radiobiology Lab. Report, COO-215, p. 98 (1958).
18. J. A. Twente and W. S. S. Jee, Radiobiology Lab. Report, COO-217, p. 147 (1958).
19. R. Ko, *Nucleonics* **15,** 72 (1957).
20. J. S. Arnold, Radiobiology Lab. Report. *Second Annual Conference on Plutonium, Radium and Mesothorium*, p. 112 (June 1954).
21. W. S. S. Jee, Ph.D. Thesis, University of Utah (1959).
22. D. R. Atherton, C. W. Mays and B. J. Stover, Radiobiology Lab. Report COO-217, p. 118 (1958).

Health Physics Pergamon Press 1961. Vol. 5, pp. 149–154. Printed in Northern Ireland

IMPROVING CESIUM SELECTIVITY OF BENTONITES BY HEAT TREATMENT

T. TAMURA and D. G. JACOBS
Health Physics Division, Oak Ridge National Laboratory*, Oak Ridge, Tennessee

(*Received* 18 *May* 1960)

Abstract—Selectivity for cesium was improved by heating montmorillonites to temperatures in the range of from 600 to 700°C. The optimum temperature depends on the saturating cation and bentonite type. For montmorillonites heated in this temperature range and at higher temperatures, clay–solution contact time was an important consideration. Sorption characteristics over a wide range of cesium concentration were investigated; the results suggested a multifunctional exchange reaction for the 600°C calcium–montmorillonite and a simple mass action reaction for the oven-dried calcium–montmorillonite. The study of the influence of heating periods at 600°C for calcium–montmorillonite showed that longer heating periods resulted in a decreasing degree of initial sorption; however, cesium sorption gradually increased with solution–clay contact time and eventually exceeded the cesium sorption of oven-dried samples.

These findings are significant for the understanding of clay mineral genesis and for applications in ground disposal of radioactive waste.

INTRODUCTION

An earlier paper emphasized the role of clay mineral structure in selective cesium sorption from radioactive waste solutions.[1] Following tests on synthetic micas, which verified the importance of the 10-Å *c*-axis spacing of the minerals, vermiculite was treated with neutral KCl to convert the 14-Å *c*-axis spacing to 10 Å. This treatment resulted in a higher specific affinity for cesium by the mineral, verifying again the importance of the 10-Å spacing.

Although montmorillonite showed some improvement in its ability to sorb cesium after treatment with KCl, it was felt that greater improvements could be demonstrated if the *c*-axis spacing were reduced to 10 Å. The KCl treatment reduced the spacing of montmorillonite from 15 to 12 Å, which is circumspect evidence of a loss of one layer of water and the retention of one layer of water between the silicate sheets (the water layers contribute to the *c*-axis dimension). Though the remaining monolayer of water can be removed by oven drying at 100°C, montmorillonites exhibit a strong tendency to rehydrate. Therefore, any benefit that might be derived from heating would be nullified if the clay were brought into contact with the waste solution.

To overcome rehydration, montmorillonites could be heated to some temperature that would result in irreversible collapse of the silicate sheets. Though it is known that high temperatures reduce the ion-exchange capacity of the clays, earlier studies with synthetic micas and vermiculite had shown that exchange capacity was not the dominant factor in this type of sorption. In addition to reporting the sorption of cesium by montmorillonites which had been heated, measurements of the *c*-axis spacing, ion-exchange capacity, and weight loss of the clays are included.

SAMPLE DESCRIPTION AND PREPARATION

The montmorillonites used for this study were obtained from Ward's Natural Science Establishment and were collected at the same localities from which the original samples were obtained for American

* Operated by Union Carbide Corporation for the U.S. Atomic Energy Commission.

Table 1. *Sorption of cesium from* 6 M $NaNO_3$ *solution by* Ca-, Na- *and* K-*Wyoming bentonite*
(Samples heated for 3 hr at designated temperature; sorption determined at different times and expressed as per cent sorption with 100 per cent = 0.5 mg Cs/g of clay.)

Temperature (°C)	Ca				Na				K			
	Contact time (hr)											
	1	18	115	696	1	18	115	696	1	18	115	696
100	17.3	24.3	23.0	27.7	29.6	32.0	30.1	32.1	35.6	51.6	51.4	49.9
300	25.9	29.5	27.6	29.2	28.8	31.0	31.6	32.4	42.2	51.5	51.1	51.5
500	23.2	32.4	30.9	28.1	29.1	32.6	32.0	30.2	37.6	47.6	47.9	47.6
600	27.3	44.8	51.1	54.4	51.7	48.5	45.8	42.9	40.4	48.7	50.3	47.6
700	21.6	33.4	39.2	47.3	29.4	50.9	58.3	63.5	29.6	51.6	64.8	82.6
800	1.86	3.92	4.79	7.39	0.49	5.64	7.20	15.5	14.9	34.8	51.4	62.3

Petroleum Institute's Project no. 49[2]. The samples were catalogued as montmorillonite no. 26, Clay Spur, Wyoming; metabentonite no. 41, Tazewell, Virginia; montmorillonite no. 23, Chambers, Arizona; and Hectorite no. 34, Hector, California.

Most of the data reported were obtained using montmorillonite no. 26 from Clay Spur, Wyoming. The samples of montmorillonite, containing sodium, calcium or potassium as the saturating cation, were heated to different temperatures up to 800°C. Unless otherwise specified, the duration of heating at a given temperature was 3 hr. Samples equivalent to 1 g of oven-dried material were weighed and placed in contact with 5 ml of 6 M $NaNO_3$ solution containing 0·5 mg of cesium. The amount sorbed at any given time during the contact period was determined by counting the Cs^{137} activity in the supernate.

Ion-exchange capacities were determined using the calcium saturation–versene titration technique described by JACKSON[3]. X-ray diffraction patterns were developed using the oriented specimen technique on a Norelco X-ray diffractometer.

RESULTS

The influence on the sorption of cesium by heating bentonite is shown in Table 1. The nature of the response may be visualized more easily by the plot of the potassium montmorillonite (henceforth referred to as K-montmorillonite) data in Fig. 1. The shape of the curves for sodium and calcium montmorillonites (Na- and Ca-montmorillonite) is similar to the curves shown in Fig. 1.

One of the most striking features of the curves in Fig. 1 and the data in Table 1 is that maximum sorption occurs after heating the sample to from 600 to 700°C. For both Na- and K-montmorillonites, the maximum sorption is achieved after 696 hr contact time by heating to 700°C; with Ca-montmorillonite this maximum occurs at 600°C, though the 700°C sample is still higher than those heated to lower temperatures. The marked decrease of sorption by the 600°C Na-montmorillonite sample with time is not understood.

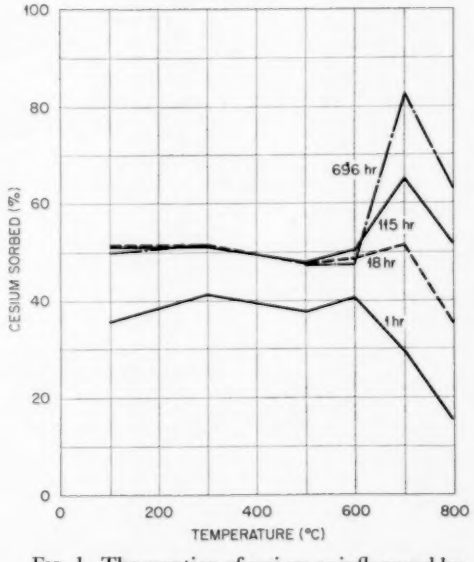

FIG. 1. The sorption of cesium as influenced by heating of K-montmorillonite and by solution–clay contact time.

Of the three saturating cations, potassium appears to be the best ion for cesium sorption. The K-montmorillonite shows good sorption characteristics even after 800°C heating. The Ca- and K-montmorillonite samples are not at equilibrium after 1-hr contact time, even for the oven-dried samples. A strong time dependence is shown by the samples heated to higher temperatures.

In Table 2 the weight loss and ion-exchange capacities of heat-treated clays are shown. The largest single increment of loss in weight occurred after heating the clays to 700°C. For the Na- and K-montmorillonites this is also the temperature at which cesium sorption is at a maximum after 696-hr contact time. Although the 700°C heating of Ca-montmorillonite is beneficial, 600°C heating results in an equal or even higher attraction for cesium. The ion-exchange capacity data are indeed interesting. In all three cases the high cesium affinity is associated with drastic reductions in exchange capacity from the original value; for Na- and K-montmorillonites the reduction is observed at 700°C; and for Ca-montmorillonite it is at 600°C.

Table 2. *The loss in weight and ion-exchange capacity of* Ca- Na- *and* K-*Wyoming bentonite after heating*

Temperature (°C)	Loss in weight (%)			Ion-exchange capacity (mEquiv/100 g)		
	Ca	Na	K	Ca	Na	K
100	0	0	0	83.0	96.2	79.7
300	1.80	0.55	0.40	83.9	94.9	83.4
500	2.40	1.10	0.67	83.7	89.9	83.8
600	2.90	2.00	1.84	49.5	86.7	80.1
700	6.04	5.16	4.21	15.6	33.1	46.1
800	6.29	5.30	4.30	7.96	13.7	15.5

The data in Tables 1 and 2 were obtained after heating the samples for 3 hr at the designated temperature, except the 100°C sample which was oven dried for 18 hr. In order to test the possible influence of heating time on sorption behavior, samples of Ca-montmorillonite were heated for different periods at 600°C. The results are shown in Table 3. A short period of heating gives sorption values equivalent to the oven-dried samples after 1 hr of contact. Then, with longer contact time, more cesium is sorbed by the 600°C sample, and a higher equilibrium value is noted. However, with longer heating periods, the initial rate of the sorption reaction is reduced; with increasing contact time, the material sorbs even more cesium and reaches an even higher equilibrium value.

Included in Table 3 are data taken from the X-ray diffraction patterns. The *c*-axis is reduced from approximately 12.6 Å to 11.5 Å at longer heating intervals. The broad maxima of samples heated for longer periods suggest a greater degree of interstratification. The X-ray diffraction tests were made with samples collected

Table 3. *The influence of heating duration on cesium sorption,* 001 *spacing and weight loss of Wyoming bentonite*

Heating		Sorption (hr)					001 maxima (Å)	X-ray diffraction data		Weight loss (%)
Temperature (°C)	Duration (min)	1	21	75	167	237		Intensity	Peak shape	
100		34.5	32.4	31.4	31.5	29.9	12.6	V. Strong	Sharp	0
600	15	35.5	47.3	51.1	48.8	49.1	12.6	V. Strong	Sharp	4.32
600	30	31.4	46.0	50.4	48.6	50.1	12.6	Strong	Sharp	5.12
600	60	26.6	43.5	51.0	50.6	51.4	12.3	Medium	Sharp	9.78
600	180	24.8	41.1	50.6	52.4	53.8	12.3	Weak	Broad	9.81
600	360	22.6	40.4	49.2	52.6	54.1	11.5	Weak	Broad	10.51
700	60	13.1	27.7	37.5	43.5	45.9	9.93	Weak	Broad	13.58

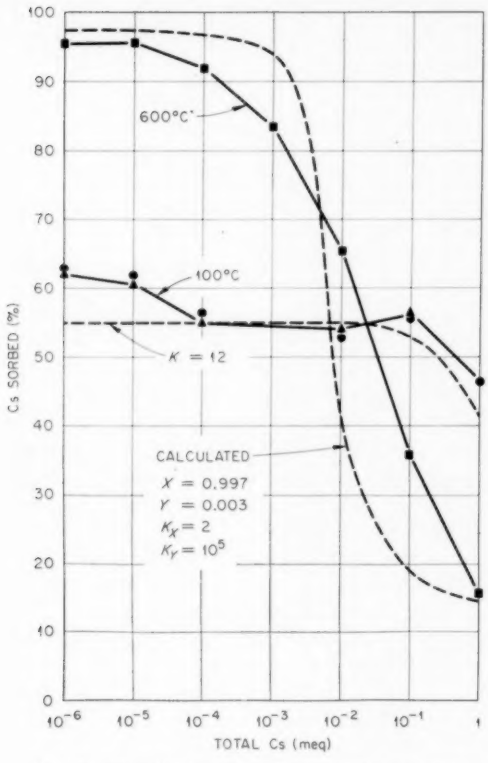

FIG. 2. Description of cesium sorption by Ca-montmorillonite from 0.1 M NaCl based on mass action.

on a glass slide from a water suspension after heating. Weight loss is gradually reduced with heating time; this suggests that the clay was not dehydroxylated during any given heating period. Possibly even 1 hr of heating at 700°C is not sufficient to completely dehydroxylate the clay. Note too that the total weight loss is much greater than that reported in Table 1. The difference is attributable to the fact that the Ca-montmorillonite had been oven-dried previously and exposed to air, thus permitting rehydration. The sorption values in Table 3, however, are not suspect, since the test was conducted on the same batch of material.

Samples of 600°C heated and oven-dried Ca-montmorillonite were contacted with 0.1 M NaCl solutions containing different concentrations of cesium. The cesium concentrations ranged from 10^{-6} to 1 mEquiv per mEquiv of clay.* The sorption data are plotted in Fig. 2. The experimental points correspond to 73 hr of contact time. Calculated curves are also included; in one case an "equilibrium constant" (K) of 12 was assumed for the entire exchange capacity; in the other case the exchange sites were divided into two types for which K's of 2 and 10^5 were assumed. The data agree reasonably well with the two types of response assumed for the system under investigation. It is evident that further "curve fitting" could be accomplished by assuming more than two "equilibrium constants" and by changing the relative distribution of the exchange sites; however, this would not increase the significance of the data.

Further evidence of the effect of heat treatment on other bentonites is shown in Table 4. These data re-emphasize the importance of the saturating cation as well as the heat treatment. It is interesting to note that both dioctahedral and trioctahedral montmorillonites show improvement with heating. The Wyoming and Arizona bentonites are dioctahedral minerals; the hectorite sample is trioctahedral. The metabentonite is actually an interstratified illite–montmorillonite clay.[2]

DISCUSSION

From the data presented there is no question that heating bentonites to some higher temperature will enhance their sorptive capacity for cesium in waste solutions. Questions may be raised regarding the changes which occur in bentonites heated at 600 or 700°C. At these temperatures montmorillonites lose weight attributable to the lattice hydroxyls (Table 2). It might be suspected, therefore, that a new crystal phase or compound is formed which gives rise to the increased specificity. GRIM and BRADLEY[4] report that the layer structure of montmorillonites persists to temperatures of the order of from 800 to 900°C; and above these temperatures, the mineral spinel appears in the samples. The results in Table 1 show that Na- and Ca-montmorillonite sorption is greatly

* The assumption was made that no change in cation-exchange capacity occurred with the 600°C sample; if the reduced capacity had been used the shape of the curve in Fig. 2 would not be affected.

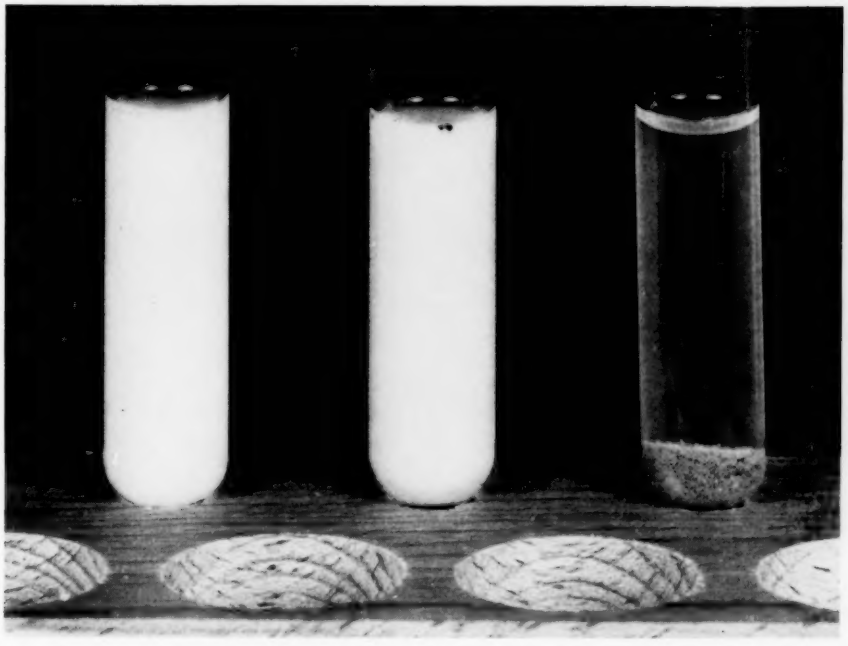

FIG. 3. Physical characteristics of montmorillonite after heat treatment. From left to right: natural montmorillonite, K-montmorillonite, and K-montmorillonite heated to 700° C.

BLANK
PAGE

Table 4. *Influence of heating on the sorption of cesium from* 6 M $NaNO_3$ *by several bentonites*
(Samples heated for 1 hr at designated temperature; sorption determined at different times and expressed as per cent sorption with 100 per cent = 1.0 mg Cs/g of clay.)

Contact Time (hr)	Metabentonite Tazewell, Virginia			Bentonite Chambers, Arizona					Hectorite Hector, California	
	Heating temperature (°C)									
	22	600	700	22	700	K-22*	K-600*	K-700*	22	700
1	21.03	24.78	28.11	31.58	18.63	69.10	80.34	84.61	19.36	26.95
24	26.59	35.71	44.06	31.08	29.11	69.84	78.44	85.21	21.28	35.69
74	25.81	42.51	46.05	30.73	33.60	69.73	78.20	83.99	21.82	35.69
145	27.09	42.75	47.06	30.09	34.89	69.73	77.31	83.24	21.21	36.66
241	25.66	42.69	46.25	30.27	35.10	69.19	77.05	82.36	19.19	35.25

* K refers to potassium saturated Arizona bentonite; all other samples were tested in their natural state of cation saturation.

reduced at 800°C rather than increased as one might suspect if new phases or compounds were formed.

The time-sensitive reaction at 600 to 700°C also suggests that caution be exercised in the use of ion-exchange data to interpret the phenomenon. Exchange capacity is not determined with any particular attention to time. Hence, it is possible that the exchange values may vary with different contact or desorption times, just as the cesium sorption reaction changes with time.

A particularly strong argument in favor of the concept that increased cesium sorption is caused by lattice collapse is evident in the curves of Fig. 2. The curve obtained for the 600°C treated Ca-montmorillonite strongly resembles the sorption curve obtained for illite—a 10-Å *c*-axis mineral.[5] It is interesting to note that cesium sorption by illite, K-vermiculite and the phlogopites, all with 10-Å *c*-axis spacing, is influenced by clay–solution contact time.[1]

From the mineralogical viewpoint there are several interesting speculations. If the increase in cesium selectivity is a function of lattice collapse to 10 Å of the *c*-axis, this technique might be used to differentiate the bentonites. Compare, for example, the 600°C treated K-montmorillonites from Wyoming and Arizona. The plates of Wyoming bentonite must be rehydratable at this temperature, whereas the plates of Arizona bentonite tend to remain closed.

GRIM[6] reports that montmorillonite is generally absent in sediments older than the Mesozoic. He writes:

> It seems likely that metamorphic processes would cause the alteration of montmorillonite to a mica type of mineral, and, therefore, the mineral would tend to disappear in more ancient sediments. When the structure of montmorillonite is completely collapsed so that all the water is removed from between the unit layers, rehydration of the mineral is difficult, and the mineral has many of the attributes of mica.

With the data reported here, it is shown that when the structure is collapsed, the mineral has a much higher specificity for cesium (and potassium). This behavior implies that the collapsed montmorillonite can more effectively "scavenge" for cesium (and potassium) and hasten its transformation to a micaceous mineral.

Heat-treated bentonite may also find applications in waste disposal. Though bentonites are noted for their swelling characteristics, the heated material loses much of this characteristic (Fig. 3). The aggregate material not only settles reasonably fast, but is easy to wet. This property means that the material could be used in a liquid system without the formation of clumps which are difficult to disperse. At Oak Ridge National Laboratory, illite is used to remove cesium from process waste water;[7,8] in regions or countries where illite is not available

in sufficient quantity or purity, the heat-treated bentonite might serve as a substitute. Furthermore, there is reason to believe that further research on the heat treatment should lead to the discovery of materials greatly superior to illite.

Acknowledgments—We are grateful to Mr. E. G. STRUXNESS for his encouragement and assistance during the course of this study. We also thank Mr. F. S. BRINKLEY and Mr. D. G. CATRON for technical assistance.

REFERENCES

1. T. TAMURA and D. G. JACOBS, *Health Phys.* **2,** 391 (1960).
2. P. F. KERR, J. L. KULP and P. K. HAMILTON, *Differential Thermal Analysis of Reference Clay Mineral Specimen.* American Petroleum Institute Project 49, Preliminary Report No. 3, Columbia University, New York, 1949.
3. M. L. JACKSON, *Soil Chemical Analysis.* Prentice-Hall, Englewood Cliffs, New Jersey (1958).
4. R. E. GRIM and W. F. BRADLEY, *J. Amer. Ceram. Soc.* **23,** 242 (1940).
5. K. Z. MORGAN, Health Physics Annual Progress Report, ORNL-2806, pp. 54-66 (1959).
6. R. E. GRIM, *Clay Mineralogy.* McGraw-Hill, New York (1953).
7. K. E. COWSER and R. J. MORTON, *J. Sanit. Engng. Div., Proc. Amer. Soc. Civil Engrs.* **3,** 55 (1959).
8. K. Z. MORGAN, Health Physics Annual Progress Report, ORNL-2806, pp. 1–6 (1959).

Health Physics Pergamon Press 1961. Vol. 5, pp. 155–159. Printed in Northern Ireland

SIGNIFICANCE OF HEALTH PHYSICS EVIDENCE IN THE TRIAL OF A CASE OF RADIATION PERSONAL INJURY*

H. K. SHAPAR
Chief Counsel, Idaho Operations Office, U.S. Atomic Energy Commission, Idaho Falls, Idaho

(*Received* 17 *October* 1960)

Abstract—There has been considerable speculation concerning the evidentiary value of film badge and dosimetry readings and air monitor charts in the trial of personal injury action based on alleged radiation injury. Once health physics data has been introduced into evidence, the interpretation of the data becomes the subject of expert testimony—that of the medical and health physics witnesses. The role of the health physics expert witness in conclusions drawn from the data is discussed. Unless the terminology of the trade can be meaningfully translated into clear and understandable equivalents, the value of the health physics data and records may be attenuated or lost.

THERE has been considerable speculation concerning the evidentiary value of film badge readings and other health physics data in the trial of a personal injury action based on alleged radiation injury. While there is, of course, no such thing as a "typical radiation case", there is the strong probability that extensive use will be made of the available health physics data in any case involving radiation injury. Because of this the lawyer, with the health physicist, has a legitimate concern in assuring that the records system is adequate for litigation purposes. The salient interests of the two disciplines must be accommodated—and within the limitations imposed by the usual economic practicalities.

At the present time the "law of radiation" is far from settled. Under certain circumstances some jurisdictions may adopt a theory of strict or absolute liability and hold that the party who is responsible for radiation-caused injury must pay compensation for the injury—irrespective of whether there was any fault or negligence on his part. On the other hand, courts may apply the traditional negligence concepts so that, insofar as the doctrinal law is concerned, a "radiation case" may go to the jury in much the same manner as the garden variety of automobile injury case. Between or around those two concepts lie various related doctrinal possibilities such as the concepts of nuisance, "ultra-hazardous activities", and "*res ipsa loquitur*".

With respect to the traditional negligence case, it may be said that the four principal elements of such a case are:

(1) Duty of the defendant to use reasonable care.
(2) A breach of that duty.
(3) Causation.
(4) Resulting loss or damage.

Health physics data may be germane to each of those four elements.

However, perhaps the more perplexing difficulties that will arise in the trial of a "radiation case" are those of proof and evidence rather than those of doctrine and concept. The latter, at least, have received considerable comment; the former, unfortunately, have gone largely unnoticed and represent an area where some original thinking is needed on the part of both the health physicist and the lawyer.

These difficulties stem in part from the fact that ionizing radiation from a source outside the human body leaves no evidence other than the injury it inflicts or its effects upon certain instruments and devices. In the past the products and readings of instruments like the camera and X-ray have been successfully introduced into evidence in the law courts. However, many of the physical phenomena

* The opinions expressed are personal and are not necessarily those of the Atomic Energy Commission.

associated with radiation can be proven or disproven *only* with the aid of instruments. Thus, it becomes not a question of using such instruments as the Geiger–Mueller counter or ionization chamber to confirm what is otherwise capable of being perceived by the senses, but rather a question of using the only existent means and methods.

Of prime importance is the necessity for a standard operating procedure for the *systematic* generation of admissible evidence—covering the entire period of possible exposure to persons in the vicinity of the source. The kind of evidence needed depends, of course, on such considerations as the chemical nature of the emitter and the energy characteristics of the radiations. It goes without saying that, in the tailoring of the health physics records system to the individual characteristics peculiar to the operation, the records will be more valuable if, beyond accomplishing their intended health physics functions, they are developed in such a way as to be admissible in evidence. However, in the same sense that there is no way by which total protection against radiation can be achieved, no amount or types of records can guarantee complete immunity from a suit. A reasonable balance must be sought and struck.

The lawyer, in attempting to resolve questions pertaining to the admissibility of particular health physics data, needs to be familiarized by the health physicist with the performance characteristics and limitations of the instruments generating the data, as well as the underlying scientific principles on which the operation of the instruments and the detection and measurement of radiation phenomena are predicated. The trial of a "radiation case" may well involve what might be called a "vacuum of proof". That is, the theory of the plaintiff's case may, in essence, be that unexplained injury and the possibility of exposure to radiation add up to compensable injury. Sufficient admissible health physics data will have to be assembled to fill that vacuum. Furthermore, since, as a practical matter, only the defendant–user has the means of generating the records, the courts may rationalize "negligence" out of a failure to maintain adequate records.

One of the principal factors affecting the admissibility of health physics data is the reliability of the instruments which produce those data. As far as the courts are concerned, the worth of each new device, like the camera or a police radar instrument, has had to be demonstrated. Consequently, one would be ill-advised to assume that a health physics instrument which has demonstrated its utility in the laboratory has concomitantly gained the acceptance of the law courts. As one court has stated:

> Just when a scientific principle or discovery crosses the line between the experimental and demonstrable stages is difficult to define. Somewhere in this twilight zone the evidential force of the principle must be recognized, and while courts will go a long way in admitting expert testimony deduced from a well-recognized scientific principle or discovery, the thing from which the deduction is made must be sufficiently established to have gained general acceptance in the particular field in which it belongs.*

The general rule with respect to any evidence is that the party offering the evidence must show that it is generally trustworthy in giving at least a reasonable approximation of the "truth". If objections are to be made against the admissibility of data obtained from health physics instruments and devices, one may reasonably expect that the objections will be based on the argument that the instrument or device is not a practical application of scientific facts that are generally known or ought to be known or that the instrument has not yet received general scientific recognition for reliability and accuracy. If the instrument has not yet gained such general acceptance, expert testimony will be required to show the scientific principles underlying the application and to convince the court of the reliability of the data. Once the reliability of the instrument has come to be recognized or noticed by the courts, expert testimony as to the *general* nature and trustworthiness of the instrument may be dispensed with. However, there will still be evidentiary requirements for foundational or preliminary proof that *a particular* instrument was properly set up, tested and calibrated and that the persons operating

* *Frye v. United States*, 293 Fed. 1013, 1014 (D.C. Cir. 1923).

the instrument and taking the readings are sufficiently qualified to perform those tasks.

Once the health physics data have been placed into evidence, the interpretation of those data may also require the use of expert testimony. For the layman, who is unfamiliar with the concepts and jargon of radiation measurements, the value of the health physics data, so carefully recorded and laboriously assembled, may be attenuated or lost unless the terminology of the trade is meaningfully translated into clear and understandable equivalents. The complexities of radiation phenomena will remain just complexities for the jury unless terms like "rems", "rads", "inverse square law", etc., can be intelligently simplified and unpatronizingly presented.

Because of the peculiar skills and knowledge which are required to explain the physical theories and applications of radiation monitoring, the role of the expert witness will be a vital one at trial. And the effectiveness of the expert witness, whether health physicist or physician, in reaching admissible conclusions will depend to a large extent on the measurement data which have been successfully introduced and explained and from which the conclusions will in large part be drawn.

The duty to use reasonable care—the first element of a negligence case—will now be considered in connection with the health physics instruments themselves, particularly, scanning instruments used for rapid, qualitative surveys to locate and establish the extent of the radiation source rather than measuring instruments used for quantitative determinations of the kind and amount of the radiation. A failure to use the most modern and up-to-date scanning equipment may in itself be held to be a breach of the required standard of reasonable care—especially if there is the possibility that injury might have been avoided had a known instrument, in use elsewhere, been available at the site of the injury. Courts will expect, at the very least, that the known risks of radiation be minimized and, even when following negligence rather than strict liability doctrines, may insist on a high degree of care. A high degree of care simply means the use of greater precautions under the circumstances and, while sophistically different from strict liability, edges, practically, close to that doctrine. An interesting case on this point, decided in 1932, involved the sinking of two tugs, whose radio receiving sets were not in working order, at a time when bad weather had been predicted in radio reports. The court had these observations to make:

> It is not fair to say that there was a general custom among coastwise carriers so to equip their tugs. One line alone did it; as for the rest, they relied upon their crews, so far as they can be said to have relied at all. . . .
>
> Is it then a final answer that the business had not yet generally adopted receiving sets? There are, no doubt, cases where courts seem to make the general practice of the calling the standard of proper diligence. . . . Indeed in most cases reasonable prudence is in fact common prudence; but strictly it is never its measure; a whole calling may have unduly lagged in the adoption of new and available devices. It never may set its own tests, however persuasive be its usages. Courts must in the end say what is required; there are precautions so imperative that even their universal disregard will not excuse their omission. . . . But here there was no custom at all as to receiving sets; some had them, some did not; the most that can be urged is that they had not yet become general. Certainly in such a case we need not pause; when some have thought a device necessary, at least we may say that they were right, and the others too slack.*

Thus, compliance with customary practices may not meet the required standard of reasonable care and the importance of keeping abreast of current developments is not to be underestimated. The monitory function of health physics instruments, in the context of that standard, is significant not only with respect to preventing personnel from receiving any appreciable exposure but also with respect to *reducing* the hazards of the exposure once an "incident" has occurred.

One of the advantages of adopting and adhering to a clearly defined standard operating procedure for the use of health physics instruments is that it may facilitate a showing of compliance with the applicable health and safety regulations. Lack of such compliance may in itself be held tantamount to negligence or may

* *The T. J. Hooper*, 60 F.2d 737, 739-740 (2nd Cir. 1932).

be damaging evidence of a failure to observe the standard of reasonable care. However, mere compliance with the regulations should not be interpreted as providing immunity from negligence liability any more than compliance with the speed limit and other rules of the road should be interpreted to immunize the automobile driver who is involved in a collision. There is obviously a wide interstitial area marked out for the exercise of discretion and judgment. Also, the possible requirement for the exercise of a high degree of care points up the unwisdom of viewing compliance with the regulations as a serviceable bar to liability for radiation injury.

One of the most troublesome issues—from the point of view of problems of proof—is that of causation: the showing that a specific injury is attributable to a certain exposure to radiation or, for that matter, to radiation at all. This issue will be present not only in a negligence case but also in a case tried under a strict liability doctrine—including workmen's compensation cases where the injury or disease must generally be shown to be one "arising out of and in the course of employment". Aside from the traditional philosophical difficulties inherent in the basic laws of cause and effect and their reflections in such legal theories as the "but for" rule, the "substantial factor" rule and the "more probable than not " rule, there are some special practical problems which are somewhat unique to the "radiation case". For example, there is the situation where radiation is being emitted simultaneously from two or more reactors in the same locality and the radiation from each facility contributes causatively to some physical injury. While similar problems have arisen in the past in cases dealing with stream pollution, converging fires, etc., their resolution by the courts has often proved to be a painful process and with sharp disagreements in the various jurisdictions. Furthermore, their complexity is heightened in the "radiation case" by the absence of an expert consensus on such basic etiological points as the "linear" and "threshold" theories of injury. A consequence of this is that the "radiation case" presents tempting opportunities to both plaintiff and defendant to muddy the waters. And while the example of simultaneous emission from two reactors may be conceded to be a rather remote possibility, it is readily apparent that there are analogous trouble spots in the situation of a workman who has been employed at the site of two or more reactors and develops a cataract during the period of his current employment, as well as in the situation where there are, within a specified period of time, a series of "incidents" at the site of a reactor, only one of which can be attributed to negligence on the part of the owner.

With respect to the various injuries that may some day be alleged in a "radiation case", such as sterility, cataracts, cancer, etc., there can be seen at once an evidentiary problem in the fact that some of the effects from radiation cannot be differentiated pathologically from the normal incidence of the same diseases. The symptoms of the acute radiation syndrome itself, however, appear to have a recognizable temporal sequence which may have great significance in the litigation. For if symptoms like nausea and epilation which usually follow certain overexposures do not appear or appear in a grossly unorthodox manner, the diagnosis of the long-developing injury may be affected. Needless to say, a precise record of those symptoms should be kept.

The role of the expert—this time, the medical witness—again needs to be stressed in connection with the question of damages. The more difficult issues here are those of the diagnosis and prognosis of the long-developing injuries sought to be ascribed to radiation. The effectiveness of conflicting conclusions that are likely to be reached by opposing expert medical witnesses will depend to a large extent on the specific measurements and other health physics data that have been introduced into evidence. It is one thing for a witness to be able to conclude that an exposure to radiation probably caused leukemia or cancer. It may be quite another matter, however, when the same witness is asked whether a dose of 50 rems would probably cause those afflictions. The use of the word "probably" is emphasized since the rule followed by the majority of the courts in this country is that medical expert testimony to be sufficient to take the case to the jury must be to the effect that the accident probably caused the injury and not that the accident "might have"

or "may have" or "could have" caused the injury.* While this last statement is an oversimplification of a greatly complex area, the point remains that there are spectacular opportunities for speculation on the damage question in a "radiation case" and that the reasonable probabilities induced from specific health physics measurements may offer the only promising ties to reality.

The use of a variety of devices, where feasible, offers distinct evidentiary advantages in that the data from one device may be used to corroborate the data from another. The benefit would be apparent with respect to instruments that have not yet gained general recognition.

No matter how smoothly the procedure may appear to be functioning, there is always the human factor to be considered; employees may, at the time of litigation, fail to remember important facts or may have terminated their employment and be unavailable to testify. In deciding upon the degree of documentation which should be required for the various steps and facets of the procedure, it is easy to lose sight of the fact that the records may be needed for litigation which will transpire many years in the future. Depending on the circumstances, it may be desirable for the procedure to provide for particularly detailed job descriptions for certain health physics and other personnel. Also, how well documented are the pre-employment physical examinations? Are records kept on the repair, maintenance, calibration and testing of the instruments? Is there a clearly defined assignment of responsibilities to the employees who are keeping the records? How and when will statements and photographs be taken in the event of an "incident"? Is a record kept of the dates of attendance of employees at health physics lectures? What disposition is made of suggestions from employees with respect to the improvement of facilities, instruments or procedures? Are the records well stored and safeguarded in a manner commensurate with their importance? What record is kept of the precise working locations of employees in the larger reactors and facilities? What documentation is available to aid in refuting an allegation that a film badge or pocket dosimeter was simply not worn at the time of an "incident"? What records are kept with respect to persons who visit the plant on guided tours or on a more or less casual basis? To what extent are the record entries developed solely from observational data rather than the judgment, opinions and conclusions of the technicians? These are but a few illustrative points that deserve consideration, and the implementation is likely to vary according to the type of the operation or plant.

The carefully planned and systematic generation of the proper health physics records and data in the regular course of business will facilitate the admission of those records and data into evidence in future litigation. The health physicist and the laywer have a common interest in achieving that goal, and, as one court has said: ". . . courts are not presumed to be more ignorant than other people".†

* *Bearman v. Prudential Ins. Co. of America*, 186 F.2d 662 (10th Cir. 1951).

† *Theo. B. Robertson Products Co. v. Nudelman*, 389 Ill. 281, 59 N.E. 2d 655, 157 A.L.R. 553 (1945).

Health Physics Pergamon Press 1961. Vol. 5, pp. 160–168. Printed in Northern Ireland

MICROWAVE RADIATION HAZARDS*

M. M. WEISS and W. W. MUMFORD
Bell Telephone Laboratories Incorporated, Whippany, New Jersey

(*Received* 10 *October* 1960)

Abstract—A review of the published literature on the exposure of animals to microwave radiation indicates that the principal hazard results from the heating effect as the energy in the microwave radiation is absorbed in the body. The interpretation of extensive experimental data on small fur-bearing animals has led to the establishment of recommended exposure limits. These limits are discussed from the standpoint of the probable safety factor involved for total immersion of the human being in the microwave radiation field and for localized exposure confined to particular portions of the anatomy. Precautionary measures are discussed and a method for estimating the distance from a radiating antenna is presented. Some presently available microwave radiation intensity measuring devices are described.

INTRODUCTION

THE problems of biological damage from microwave radiation have been receiving more attention as the ability to generate higher powers has improved. An increasing number of investigators have interested themselves in the effects of electromagnetic radiation on living organisms, especially human.

The heating effect of electromagnetic radiation on humans was first demonstrated in 1890 by D'ARSONVAL. Since then, the medical profession has been using higher and higher frequencies to heat living tissue for therapeutic purposes. By 1935 frequencies up to 10 Mc/s were being used. The development of improved techniques for generating higher frequencies and higher power levels, accelerated by military requirements during World War II, made available frequencies from several hundred megacycles to 30,000 Mc/s.[1] The microwave region, the subject of this discussion, is considered to extend from approximately 200 Mc/s up to about 5×10^{11} c/s.

Since the war, progress in developing higher powered microwave systems has continued. Fig. 1 shows a high-power White Alice Communications transmitting and receiving station. Recent interest in space exploration has stimulated further development of higher powered systems. At present, klystrons are available capable of delivering 10.0 kW of average power; and it is predicted that in the next five years the capabilities for power generation will increase by a factor of 100.

The medical profession, the designers and the users of microwave generating systems soon developed an awareness of the possibility of potential damage to humans exposed to radiation from these devices. The principal damaging effect was realized at an early date to be due to the heating of the tissue exposed. Several meetings or symposia have been held in recent years to discuss this problem and to bring together the people who have been studying various aspects of microwave radiation hazards.

A meeting was held at Schenectady, New York, on 1 June 1954 of General Electric personnel to discuss microwave radiation hazards and safety measures. At that time pertinent data was meager but what was available indicated that damage to living tissue when exposed to microwave radiation did occur and was a function of wavelength, the time of exposure, and the field intensity. The most serious hazard was considered to be injury to the eye by cataract formation due to heating of the lens tissue. Other organs

* The material contained in this article is incorporated in a book entitled *Radiation Hazard Management* by J. HANNOCK and M. M. WEISS, to be published by Van Nostrand, Princeton, New Jersey.

FIG. 1. White Alice communications system.

FIG. 3. Microwave field intensity measurements at a White Alice site.

BLANK
PAGE

such as the kidney, brain, sex organs and certain muscle tissue also seemed to indicate change and injury. A tentative set of safety practices was established for use until further evidence became available upon which to base a more realistic approach to the problem.

Another meeting was held on 23 and 24 September 1955 in Rochester, Minnesota, sponsored by the Mayo Clinic, on the Physiologic and Pathologic Effects of Microwaves. The papers presented at this symposium were subsequently published in the I.R.E. Transactions of the Professional Group on Medical Electronics.[1] The data presented yielded sufficient evidence for establishing tolerance levels for experimental animals as a function of exposure time. However, the extrapolation to humans was still subject to considerable uncertainty. The consensus at that time and the apparently conservative approach was to assume that humans are just as susceptible as other animals.

The first Annual Tri-Service Conference sponsored by the Air Research and Development Command was held on 15 and 16 July 1957.[2] At this meeting the military responsibility for research on the biomedical aspects of microwave radiation (assumed by the Air Research and Development Command on 1 July 1957) was outlined. The work to date was described and the program for the future discussed. It was planned to hold periodic meetings to maintain close liaison among the investigators in the field, to expand research programs to include a sampling of frequencies from 200 through 35,000 Mc/s, to investigate the effects of microwaves combined with X-rays, to further study of methods of microwave field measurement, and to study testicular and ocular damage as a function of frequency and cumulative dosages.

The second Annual Tri-Service Conference on Biological Effects of Microwave Energy was held on 8, 9 and 10 July 1958.[3] At this meeting progress in various experiments to advance the available information concerning the effects of microwave energy on living tissue was reported. These experiments indicate a general verification of previous findings; however, more refined methods of measuring microwave radiation field intensities imply that this aspect of these studies represents one of the important sources of uncertainties. More sensitive methods of measuring the effects indicate that lower thresholds of damage are being detected. Also these advances in detection ability make it possible to explore more carefully the subthreshold cumulative effects of low-level microwave radiation exposures.

EFFECTS OF MICROWAVE RADIATION ON LIVING TISSUE

A. *Localized exposure*

Experiments and accidental evidence have established that various organs of the body are particularly sensitive to microwave radiation; this sensitivity leading to injury, is frequently serious, upon exposure.

In 1952 HIRSCH[4] reported cataract formation in a laboratory technician whose eyes were exposed, in his daily work, for approximately 1 year to a power density of 0.1 W/cm^2. Further studies on the effects of localized exposure to the eyes indicated that the hazard to the eye was one of the most serious aspects of exposure to microwave radiation, especially within the critical wavelengths ranging from 3 to 30 cm.

Subsequent studies at 10 cm on animals by ELY and GOLDMAN[5] in which a comparison of the heating effects on the whole body, the eye and the testes were compared, indicated that the testes were the most sensitive. Evidence indicates that moderate testicular damage is probably reversible with a possible temporarily induced sterility. Damage to the eye is probably cumulative and nonreversible. However, further study of these aspects is necessary for more positive substantiation.

Conclusions based upon extrapolation from animals to man can prove misleading. However, until further evidence is available, the more conservative use of the available data is warranted, and the present threshold in animals should be considered dangerous for human eyes.[6]

B. *Cumulative effects*

Several investigators have found indications of cumulative effects.[6–8] In one experiment, ten exposures of 30 min each at a level of 0.15 W/cm^2 produced opacities in two of six rabbits. Thus

there is a possibility that opacities may be produced as a cumulative radiation effect. This is of considerable importance with respect to its connotations in human exposure to low power levels of radiation over long periods of time. BARRON *et al.*[9] conducted a comprehensive case study of personnel exposed to microwave radiation over a number of years. Although there were some indications of physiologic changes in these cases in excess of the control group, they were not considered serious and in all but one case the change was determined to be entirely unrelated to radar exposure.

The results of these studies led to the tentative estimate that localized exposure of the eye to levels exceeding 0.12 W/cm² should be considered as potentially dangerous.[6,10]

C. *Total immersion effects*

Investigations were made by ELY and GOLDMAN[11] using 10-cm microwave radiation to determine the effects and hazards of total immersion. With a maximum available power density of no more than 0.100 W/cm² fatal fevers were induced in rats, rabbits and dogs. No animal survived a treatment which raised the body temperature to 44°C (111.2°F). Continued exposure to 0.025 W/cm² maintained a body temperature rise of 1°C, and 0.050 W/cm² was lethal to rabbits and dogs.*

It was estimated that about 40 per cent of the incident energy was absorbed by the animals, placing the potentially lethal density at 0.020 W/cm² for 100 per cent absorption.

SCHWAN and LI[12] have studied the absorption of microwave radiation by the human body as a function of frequency for various skin thicknesses, accounting for the propagation constants of skin, fat and muscle. At frequencies lower than 400 Mc/s and higher than 3000 Mc/s, the human body absorbs about 40 to 50 per cent of the radiation. Between 1000 and 3000 Mc/s, the percentage absorbed fluctuates between 20 and 100 per cent, depending on frequency, and thickness of skin and subcutaneous fat.

Based on these studies it appears that total immersion of an animal body in fields of 0.01 W/cm² could possibly sustain a body temperature rise of 1.0°C, and continued long exposure to 0.02 W/cm² could possibly be fatal (assuming 100 per cent absorption).

However, ELY and GOLDMAN deduce that the human animal can tolerate more power than fur-bearing animals. They estimate that 100 mW/cm² is required to maintain a human body temperature rise of 2°C.

D. *Basis for establishing working tolerance levels*

Considering the various effects outlined above and in lieu of additional data, considerable conservatism in establishing safe exposure levels is called for. Since a good deal of evidence is presently available to indicate that whole-body exposure is the more critical of the effects leading to permanent damage, recommended safe levels should be based on whole-body exposure criteria. These could be modified, as in the case of ionizing radiation, for instances of known localized exposure. A further caution is suggested in instances of simultaneous exposure to ionizing as well as microwave radiation. Conservative tolerance levels with adequate safety factors included should be used until acceptable results become available to warrant reconsideration of these levels.

An examination of the available local, cumulative and total immersion data has led to general agreement among the groups interested in setting up safe tolerance levels.†

An exposure limit of 10 mW/cm² has been adopted generally in industry and by the armed forces.[13,14] The Bell Laboratories qualifies this limit thus:

(1) Power levels in excess of 10 mW/cm² are potentially hazardous, and personnel must not be permitted to enter areas where major parts of the body may be exposed to such levels.

(2) Power levels between 1 and 10 mW/cm² are to be considered safe only for incidental,

* These measurements were made by exposing the animal to an average field intensity sufficient to maintain a pre-chosen steady-state body temperature. On and off cycling of the field was employed to maintain this condition. This procedure was repeated for body-temperature increments of ½ or 1°C. The transmitter was then shut off entirely and the animal's cooling-temperature record was obtained.

† As of this writing no clear-cut evidence of dose vs. dose-rate effects are available, thus the recommended exposure levels specified in this section.

occasional or casual exposure, but are not permissible for extended exposure.

(3) Power levels under 1 mW/cm² are safe for indefinitely prolonged exposure.

Based upon the possible formation of cataracts at a level of 100 mW/cm², it might seem a factor of 10, namely a safe upper limit of 10 mW/cm², would be adequate. However, the work of ELY and GOLDMAN[11] showed that the lethal level for dogs, rabbits and rats totally immersed in the field was only 50 mW/cm². Thus the safety factor of the above limit is only a factor of 5. Now in these experiments it was determined that only 40 per cent of the incident energy was absorbed by the animal. For total absorption, shown by SCHWAN and LI[12] to be possible under certain conditions, the lethal level becomes only about 20 mW/cm². This reduces the safety factor of the above limit to a factor of 2. This, however, is based upon experiments with fur-bearing animals and, since humans evidently can tolerate more, the safety factor would be higher.

The establishment of an occupational occasional exposure area between 1 and 10 mW/cm² thus appears to be a realistic approach.

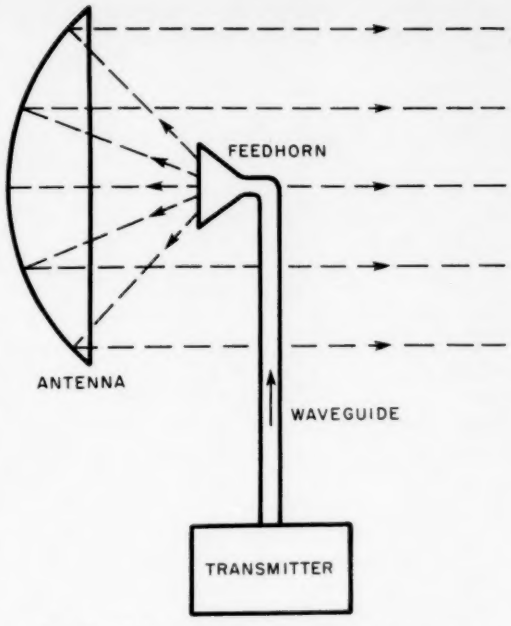

FIG. 2. Schematic of a typical microwave system.

POWER LEVELS IN MICROWAVE SYSTEMS AND SYSTEM COMPONENTS

Microwave systems are generally used for radar, and communications. Generally, the radar systems use pulse operation and scanning antenna beams. Communication systems are commonly continuous-wave and fixed-antenna beam systems. However, these characteristics are not necessarily exclusive to either function and future systems for both radar and communications may employ combinations of the above-mentioned techniques.

A microwave system consists of several subdivisions with significantly different levels of radiation existing in each area (Fig. 2).

A. *Waveguides*

Waveguides are hollow metal tubes usually of either circular or rectangular cross-section used to transmit microwave energy between the high-frequency components of the system such as the transmitter, receiver and antenna. The open end of a waveguide could be a source of localized exposure, especially to the eye, in typical experimental or maintenance activities. A power level of more than 100 mW/cm² should be considered as hazardous.

It is relatively simple to determine the power level at the open end of a waveguide. The power density within a uniformly illuminated area is given by

$$W = \frac{P}{A} \tag{1}$$

where W is the power density (W/cm²)
P is the power in watts being transmitted
A is the cross-section area of the waveguide (cm²)

(For a feedhorn the cross-section area at the mouth for the feedhorn should be substituted for this value.)

Within a rectangular waveguide operating in a customary dominant mode, the greatest power density occurs at the center of the waveguide. Since the electric field is a cosine function, and the power is proportional to the square of the

electric field, the maximum power density will be twice the average power density, or

$$W_{\max} = \frac{2P}{A} \tag{2}$$

From this formula the power levels in the waveguide can be calculated for the 100 mW/cm² (dangerous level), 10 mW/cm² (upper tolerance level for occasional exposure), and 1 mW/cm² for uncontrolled exposure.

B. *Antenna beams*

The problem of evaluating the hazards in the vicinity of a radiating antenna is complicated by a number of factors. The immediate environment of the antenna will influence the radiation pattern by means of reflections and refractions of the beam. The radiation pattern, its side-lobes and general configuration will also enter into this consideration. These too will vary for the same antenna depending on location. However, by simplifying the consideration to a simple antenna radiation pattern, namely a round uniformly illuminated antenna aperture in free space (or above a perfectly reflecting ground) and examining the field intensity along the axis of the main beam, one can arrive at some definite figures. These may then be used as a basis for an evaluation of the need for a more complete solution for the actual and usually more complex situation under consideration.

For an isotropic radiator in free space, the power density at a given distance will be the same as the average power density

$$W = \frac{P}{4\pi r^2} \tag{3}$$

where r is the distance from the radiator.

For an antenna having a power gain G, the power density on the axis of the major lobe (at a great distance where the field falls off inversely as the square of the distance) will be

$$W = \frac{PG}{4\pi r^2} \tag{4}$$

The power density may be expressed in terms of the effective area of the antenna A, and the wavelength λ, by substituting $G = 4\pi A/\lambda^2$ in equation (4) thus:

$$W = \frac{PA}{\lambda^2 r^2} \tag{5}$$

It is often convenient to express the power density in terms of the power density W_0 at the antenna aperture. Since $W_0 = P/A$, equation (5) becomes

$$W = W_0 \frac{A^2}{\lambda^2 r^2} \tag{6}$$

The nearby field will depend upon the antenna design features which affect the illumination of the antenna aperture by the radiation from the feedhorn. Assuming a round aperture with uniform illumination both in amplitude and phase, the power density on the axis of the antenna can be expressed thus:

$$W = 4W_0 \sin^2 \frac{A}{2\lambda r} \tag{7}$$

Equation (7) implies that the power density varies as a function of distance with maxima = $4W_0$. These maxima occur near the antenna and extend out to the furthest distance where

$$\sin \frac{A}{2\lambda r} = 1, \quad \text{i.e. where } \frac{A}{2\lambda r} = \frac{\pi}{2}$$

Beyond this distance this power density falls off and approaches the inverse square relation of equation (6) asymptotically as the distance increases.

Thus we recognize two well-defined zones in front of the antenna, the near region and the far region. In the near region (Fresnel region) the power density maxima $4W_0$ are encountered. In the far region (Fraunhaufer region) the inverse square relation holds. Between the near region and the far region there is a transition region. The central part of this transition region occurs at the distance where the far field formula (6) predicts a power density equal to the maxima in the near field, i.e. it occurs where the distance is defined by the relation

$$W_0 \left(\frac{A}{\lambda r}\right)^2 = 4W_0$$

or

$$r \text{ (boundary)} = \frac{A}{2\lambda} \tag{8}$$

At this boundary distance, the difference between the far field formula (6) and the exact formula (7) amounts to only 1.5 db. In the limited number of cases where this difference is

significant, the general equation (7) may be used. Generally, however, it will be adequate to utilize the approximate formula thus:

$$W = 4W_0 \quad \text{for} \quad r < \frac{A}{2\lambda}$$
$$\text{and} \qquad W = W_0\left(\frac{A}{\lambda r}\right)^2 \quad \text{for} \quad r \geq \frac{A}{2\lambda} \tag{9}$$

These two expressions were derived for a circular antenna aperture uniformly illuminated. In practice, the illumination is usually tapered across the aperture smoothly from the center where the energy is a maximum to the aperture extremities where it may be only one-tenth of the maximum. It can be shown that this tapering of the amplitude of the illumination does not alter the maxima of the power density in the near field appreciably, and has little effect in the far field on the beam axis. The expressions in equation (9) also apply conservatively to square apertures.

For long and narrow rectangular apertures, uniformly illuminated, the following expressions apply approximately and conservatively:

$$W = W_0 \frac{2d_2^2}{\lambda r} \quad \text{for} \quad r < \frac{d_1^2}{2\lambda}$$
$$\text{and} \qquad W = W_0 \left(\frac{A}{\lambda r}\right)^2 \quad \text{for} \quad r \geq \frac{d_1^2}{2\lambda} \tag{10}$$

where d_1 = wide dimension of antenna, and d_2 = narrow dimension of antenna.

The near field formula for rectangular apertures was derived from a more complete analysis for distances such that

$$\frac{d_1}{r} \leq 1 \text{ and } \frac{d_2^2}{\lambda r} \leq 1$$

C. *Hazardous distance and power concept*

These observations can be used to calculate the hazardous power for the antenna, and, if the actual transmitter power exceeds this value, a hazardous distance can be evaluated from the far field formula.

The near field maxima are

$$W_{\max} = 4\frac{P}{A} \tag{11}$$

setting

$$W_{\max} = 0.01 \text{ W/cm}^2$$

then

$$P_{\text{haz}} = 2.5\, A \text{ mW} \tag{12}$$

where A is expressed in cm^2; or, for a circular antenna,

$$P_{\text{haz}} = 1.8\, D^2 \text{ W} \tag{13}$$

where D is in feet.

Thus the beam of a 10-ft dish should be considered hazardous if fed with more than 180 W average power.

It is frequently more convenient to use the antenna gain instead of its diameter to compute the safe power. The gain of the antenna is given approximately by

$$G = \frac{4\pi A}{\lambda^2} \tag{14}$$

Substituting this in equation (12) gives the approximate relation

$$P_{\text{haz}} \simeq \frac{G\lambda^2}{5.0} \text{ mW} \tag{15}$$

Thus the hazardous power feeding a 35 db* gain antenna would be 51 W for $\lambda = 9$ cm (S-band).

With other than round, square or rectangular apertures, the near field pattern will be other than that assumed above. Equations (9) and (10) would then not apply exactly, but can still be used as a guide to evaluate the necessity for detailed analysis of the particular situation at hand.

In cases where a hazardous power level is being fed into a radiating system and hazardous levels are suspected nearby it is essential to determine the maximum hazardous distance, beyond which the power density level is less than 0.01 W cm^2.

If suspect density levels exist near the antenna then they are likely to exist to about the midpoint of the transition region or $r \simeq A/2\lambda$ [equation (8)]. Beyond this distance the far field formula, equation (4), applies. However, this expression is for free space conditions and must be modified to account for the possibility of reinforcement due to reflection from the ground.

* The unit db is a commonly used engineering term to express ratios of power. It is defined by the relation db = 10 log (P_2/P_1). In this case if the antenna gain is 35 db, this is equivalent to a gain of 3162, or $P_2 = 3162P_1$.

The reflection coefficient of the ground may approach unity, thereby doubling the field strength and increasing the power density by a factor of 4. Including this and using the value of 10 mW/cm² for W, as above, the following is obtained:

$$2.5 \text{ mW} = \frac{P_{\text{mW}}}{4\pi r^2} G \tag{16}$$

Solving this for r, the hazardous distance is

$$r_{\text{haz}} = \left(\frac{P_{\text{mW}} G}{10\pi}\right)^{1/2} \text{cm} \simeq \left(\frac{P_{\text{W}} G}{30}\right)^{1/2} \text{ft} \tag{17}$$

Now, from equation (14) defining G in terms of the antenna parameters and the wavelength, an alternate form of equation (17) is

$$r_{\text{haz}} = 2\sqrt{\left(\frac{PA}{\lambda}\right)} \text{cm} \simeq 0.63\sqrt{\left(\frac{P_{\text{mW}} A}{\lambda}\right)} \text{cm} \tag{18}$$

or in terms of the antenna diameter this becomes

$$r_{\text{haz}} = \frac{D}{\lambda}\sqrt{\left(\frac{\pi P}{10}\right)} \text{cm} \tag{19}$$

Therefore using the same example as above where G was assumed to be 35 db, and $P = 1$ kW, average power, the hazardous distance is determined as about 325 ft.

D. *Effect of scanning*

The data on the hazards of microwaves have been based upon average power. In the case of the scanning antenna, the average power absorbed by a fixed subject will be reduced by the ratio of the effective beam width to the scanned angle. Accordingly the hazardous power level is increased by this ratio and the hazardous distance is reduced by the square root of this ratio.

The effective beam width in the far field will, in general, be somewhat greater than the 3-db beam width* and somewhat less than the width to the first null. The exact value depends, of course, upon the form factor of the radiation pattern.

* The 3-db beam width is defined as the angular width of the beam between the two points of the beam which are down by a factor of 2 from the maximum usually at the beam centre.

In the near field the effective beam angle will vary with distance since the field is collimated. Here the average power density of the scanning antenna is given approximately by the relation:

$$W \simeq W_0 \frac{D}{2\pi r} \times \frac{360}{\theta} \tag{20}$$

for $\theta \geq D/2\pi r \times 360$, where θ is the scanned angle in degrees. For $\theta < D/2\pi r \times 360°$

$$W \simeq W_0 \tag{20a}$$

Since $W_0 = \dfrac{4P}{\pi D^2}$ (circular aperture),

$$W \simeq \frac{4P}{\pi D^2} \times \frac{D}{2\pi r} \times \frac{360}{\theta} \quad \text{for} \quad \theta \geq \frac{D}{2\pi r} \times 360 \tag{21}$$

and

$$W = \frac{4P}{\pi D^2} \quad \text{for} \quad \theta < \frac{D}{2\pi r} \times 360 \tag{21a}$$

Setting $W = 0.01$ W/cm², the hazardous distance in the near field is

$$r_{\text{haz}} \simeq \frac{1}{5\pi^2} \frac{P}{D} \times \frac{360}{\theta} \text{ cm} \tag{22}$$

$$\text{for} \quad \theta \geq \frac{D}{2\pi r} \times 360 \quad \text{and} \quad r \leqq \frac{D^2}{4\lambda}$$

where P is in milliwatts, D is in centimeters.

For $\theta < D/2\pi r \times 360$ the discussion in Section C above is applicable.

For example, in the case of a 10-ft circular antenna scanning 360° with an average power of 10,000 W, the hazardous distance would be about 22 ft.

This example neglects reflection from the ground which can sometimes alter the average power density. Hence, a consideration of particular environmental conditions may sometimes be necessary.

Also, it has been assumed that the subject is located in the path through which the main beam sweeps. For positions off the main beam, of course, the average power density will be less. Here again a consideration of the particular environment is indicated.

E. *Peak power vs. average power*

The hazardous level of 0.01 W/cm² was based on average power measurements. In fact many

Table 1. *Power levels in rectangular waveguides*

Band	Waveguide	A (cm^2)	Power levels (W) for:		
			$W_{max} = 100$ (mW/cm^2)	$W_{max} = 10$ (mW/cm^2)	$W_{max} = 1$ (mW/cm^2)
S (10 cm)	Rg 48/U	24.58	1.23	123×10^{-3}	12.3×10^{-3}
X (3 cm)	Rg 52/U	2.32	0.116	11.6×10^{-3}	1.16×10^{-3}
Ka (1 cm)	Rg 96/U	0.258	0.0129	1.29×10^{-3}	0.129×10^{-3}

of the experiments on animals were made with continuous wave oscillators and the deleterious effects appeared to be due solely to the production of heat and the accompanying rise in temperature. If the duty cycle of the radar is 0.001*, the peak power density associated with the hazardous level would be 10 W/cm^2. It may be reasonable to assume that this peak power density may not cause damage by breaking down tissues. However, if the radar duty cycle were, say, 10^{-7}, the peak power density would be 100 kW/cm^2, approaching the level which causes breakdown in air. At this level it would be reasonable to assume that there might be a possibility of breakdown of tissue. Some place between the two examples just cited, danger due to breakdown of tissue from effects other than heating may be possible. A similar situation exists for very narrow-beamed sweeping antennas, whose exposure cycle is very small. The observations of HELLER and PINTO[15] suggest effects other than thermal and, if in fact these athermal effects are due to peak power, rather than average power, a more elaborate specification of safe and hazardous levels will be necessary.

MEASUREMENT OF MICROWAVE POWER DENSITY

The four basic methods of measuring power are calorimetry, bolometry, voltage measurements and radiation pressure measurements on reflecting surfaces. Calorimetric methods involve the transfer of electromagnetic energy into heat. Power is then determined by a measurement of temperature and time. Bolometric measurements are based upon the absorption of power in a temperature-sensitive resistive element. The change in resistance then indicates the power. This method is the most widely used, and the thermistor is generally employed as the sensing element. Although many thermistor bridges are available, many are susceptible to spurious pickup when exposed to pulsed microwave power. However, some commercially available bridges are designed specifically to work in an environment of pulsed microwave power. When used with a calibrated antenna and a matched thermistor in an r.f. head, these can measure power densities in the region of interest relative to the personnel hazard problem. For continuously radiated power, a simple diode rectifier, a d.c. meter and a calibrated antenna are adequate; however, these are entirely unsuited to measure pulsed microwave radiation.

There are several commercially available microwave power density measuring devices. These devices rely upon antenna pickup probes and all have the same limitations. They are frequency sensitive, directive, and respond to only one sense of polarization. For specific surveys these limitations are not serious, however, as a general survey device in situations where the surveyor is unaware of the specifications of the radiation, these devices are of limited value. Fig. 3 shows a survey in progress.

The Model 1200 Densiometer manufactured by Radar Measurements Corporation, Hicksville, N.Y., is designed to cover the frequency

* Duty cycle is the ratio of the time on to the total time per cycle.

range from 200 to 10,000 Mc/s. Measurement in any desired band is accomplished by simply changing to the appropriate antenna, supplied with the instrument. Fig. 4(a) and (b) shows the densiometer equipped with a *c*-band and u.h.f. antenna, respectively. The unit is battery operated and measures average power levels in terms of decibels above and below 10 mW/cm².

Another power density meter presently available is the Model NF-157 manufactured by Empire Devices, Amsterdam, N.Y. This unit covers the frequency range from 200 to 10,000 Mc/s with three different antennas, and responds with an average power indication to pulsed or continuous power. Fig. 5(a) and (b) shows the density meter and the various probe attachments respectively. The mid-scale reading of the meter covers the power density range from 1 mW/cm² to 1000 mW/cm².

These devices and other similar devices only partially supply the requirements for suitable microwave dosimeters. A device not limited by frequency, orientation and polarization is needed. Such a device might be based on either the calorimetric method or the radiation pressure principle. Until a more suitable microwave radiation survey device is made available, a careful survey and evaluation procedure should be employed wherever there are high-power microwave generators. Computations and estimates based on the type of analysis suggested above, coupled with measurements with available power density meters, can yield reasonably safe criteria for the operation of the high-powered systems. A prudent adherence to the suggestions of maximum permissible exposure levels outlined above should go a long way toward avoiding any unfortunate accidents until the problem is more clearly understood and measurement and evaluation techniques have been considerably improved.

REFERENCES

1. Mayo Clinic and Mayo Foundation, Symposium on Physiologic and Pathologic Effects of Microwaves. *I.R.E. Trans. Med. Electron.* **ME-4** (1956).
2. E. G. Pattishall, *Proceedings of Tri-Service Conference on Biological Hazards of Microwave Radiation.* University of Virginia (1957).
3. E. G. Pattishall and F. W. Banghart, *Proceedings of Second Tri-Service Conference on Biological Effects of Microwave Energy.* University of Virginia, ASTIA Document no. AD131477 (1958).
4. F. G. Hirsch, *Microwave Cataracts.* Presented at NSAE Conference on Industrial Health, Cincinnati, Ohio, 25 April (1952).
5. T. S. Ely and D. E. Goldman, Heating characteristics of laboratory animals exposed to 10-cm microwaves. *Proceedings of Tri-Service Conference on Biological Hazards of Microwave Radiation* University of Virginia (1957).
6. D. B. Williams *et al.*, Biologic Effects Studies on Microwave Radiation. Time and Power Thresholds for the Production of Lens Opacities by 12·3-c.m. Microwaves. *I.R.E. Trans. Med. Electron.* **ME-4** (1956).
7. A. W. Richardson *et al.*, *Arch. Phys. Med.* **29,** 765 (1948).
8. L. Daily, Jr. *et al.*, *Amer. J. Ophthalmol.* **35,** 1001 (1952).
9. C. I. Barron *et al.*, Physical Evaluation of Personnel Exposed to Microwave Emanations. *I.R.E. Trans. Med. Electron.* **ME-4**.
10. S. E. Brody, *I.R.E. Trans. Med. Electron.* **ME-4,** 8 (1956).
11. T. S. Ely and D. E. Goldman, Heat Exchange Characteristics of Animals Exposed to 10-cm Microwaves. *I.R.E. Trans. Med. Electron.* **ME-4**.
12. H. P. Schwan and K. Li, *Proc. Inst. Radio Engrs., N.Y.* **44,** No. 11 (1956).
13. *Radio Frequency Hazards*, Bureau Air or USAFTO 31-1-80, Handbook.
14. *Hazards to Health from Microwave Energy,* Army Regulations No. 40–583.
15. J. H. Heller and A. A. Teixevia-Pinto, *Nature, Lond.* **183,** 905 (1959).

FIG. 4(a). Model 1200 densiometer with C-band antenna (5000–5900 Mc/s).

FIG. 4(b). Model 1200 densiometer with u.h.f. antenna (400–450 Mc/s).

FIG. 5(a). Model NF-157 broadband power density meter.

FIG. 5(b). Model NF-157 r.f. probe attachments.

Health Physics Pergamon Press 1961. Vol. 5, pp. 169–172. Printed in Northern Ireland

TEN-CHANNEL RADIATION MONITOR FOR PULSED ACCELERATORS*

W. HIGINBOTHAM, E. RAINEY and J. CHESTER
Brookhaven National Laboratory, Upton, L.I., New York

(*Received* 28 *September* 1960)

Abstract—A monitoring system utilizing 5-l. polyethylene ionization chambers has been installed at ten locations in the Cosmotron building. The current which flows in an ionization chamber during an accelerator pulse is integrated by an electrometer circuit. The resulting signal is displayed locally, at the accelerator console, and is recorded on a strip chart. A timing circuit controls the recorders and resets the integrators just before each accelerator pulse. The total dose over an arbitrary period of time is displayed digitally on a scaler for each detector. Full scale corresponds to 70 μr on a single Cosmotron pulse, or to an average rate of 500 mrems/hr. The circuits are sensitive to 0.1 per cent of the full-scale value.

INTRODUCTION

THE Cosmotron is a 2.5 BeV accelerator which normally is pulsed every 5 sec or 720 times per hr. The duration of each pulse varies from a few μsec to 0.1 sec. It is desirable for a single pulse to produce a reading on the monitor meters which are calibrated in mrem/hr so that one may immediately estimate the dose if exposed to a series of pulses of the same intensity. One would like to have a permanent record of the individual intensities at each station and circuits to sum the successive readings to give an integrated dose over any selected period of time.

The dynamic range of the circuits is from 0.5 to 500 mrems/hr. An RBE of 10 is used, which includes a safety factor of 2, so that this is 0.05 to 50 mrads/hr. The full-scale reading per pulse is

$$\frac{50 \text{ mrad/hrs}}{720 \text{ pulses/hr}} = 70 \ \mu\text{rads/pulse}$$

For a 5000-cm^3 chamber, this gives

$$\frac{7 \times 10^{-5} \text{ e.s.u./cm}^3 \times 5 \times 10^3 \text{ cm}^3}{3 \times 10^9 \text{ e.s.u./C}} = 1.17 \times 10^{-10} \text{ C/pulse}$$

if this is integrated on 11.7 $\mu\mu$F, one obtains 10 V full scale. The circuits are stable to about 10 mV or 0.1 per cent of full scale which is only slightly higher than natural background.

A block diagram of the various circuits is shown in Fig. 1. All elements are repeated ten times except for the timing unit which controls them all in parallel. A start signal, t_0, is obtained from the Cosmotron at the start of the acceleration cycle. The local integrating capacitor is shorted for 0.25 sec following t_0. The recorder prints the baseline at $t_0 + 0.5$ sec and the pulse intensity at $t_0 + 2.35$. The intensity is sampled by the digitizer at $t_0 + 2.0$ sec. The function and operation of the different units are explained below.

IONIZATION CHAMBER AND INTEGRATING AMPLIFIER

The ionization chamber is made from a polyethylene container. Polyethylene is a reasonable approximation to tissue and has good electrical and mechanical properties. The center electrode is a polyethylene rod, 1 in. in diameter, and all electrodes are painted with colloidal graphite. A collection potential of 300 V is sufficient to produce saturation with the pulses encountered. The center electrode is provided with a guard ring.

The amplifier has two electrometer tubes and two transistors, as shown in Fig. 2. It is designed

* Work performed under the auspices of the U.S. Atomic Energy Commission.

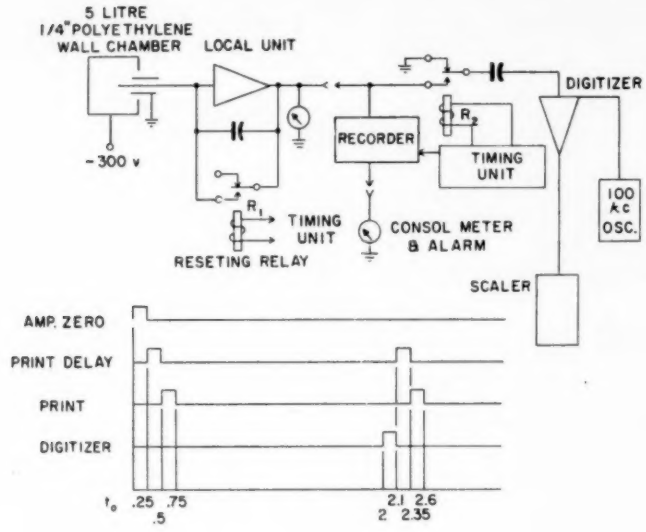

FIG. 1. Cosmotron monitoring system, block diagram.

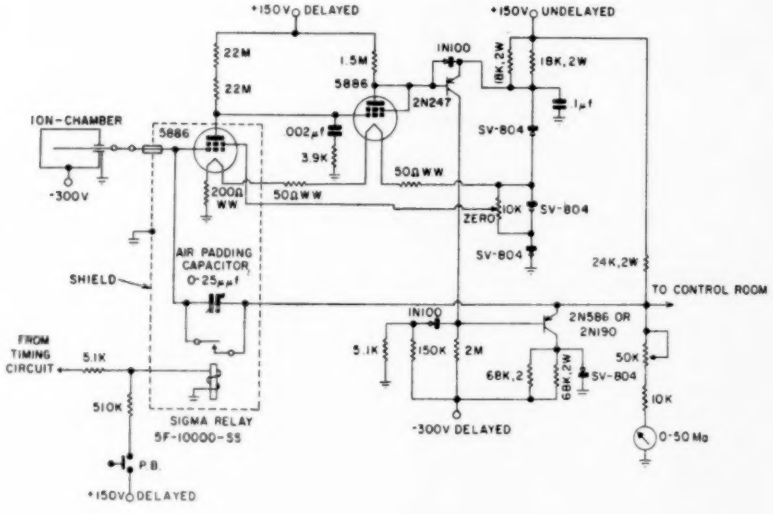

FIG. 2. Electrometer integrating amplifier.

to drive 1000 or more feet of cable. Integration is achieved by negative feedback through the padding capacitor. A variety of relays were examined for switching noise in a high-impedance circuit, and the relay used was selected for low noise upon opening and closing. The contacts have been remounted on Teflon insulation to maintain the high input impedance. The relay is closed for 0.25 sec at the start of the acceleration cycle. The amplifier output rises during the pulse and holds its value during the time between pulses. The local meter is normally set to 2 V full scale so that it reads 100 mrems max. Each chamber–amplifier unit is exposed to a known flux and calibrated by adjusting the feedback capacitor. To keep grid current low, the electrometer filaments are turned on before plate potentials are applied.

CONTROL ROOM RECORDERS AND METERS

Each amplifier is connected directly to a small strip chart recorder*, and to a meter† on the Cosmotron console. The recorders have a sensitivity of 1 mA full scale, a chart speed of 2 in/hr and normally print a dot every 2 sec. The printing mechanism was modified and a solenoid added so that one dot may be printed when the integrator is shorted and another between Cosmotron pulses, while the maximum reading is displayed. The recorders are adjusted to read 100 mrems/hr full scale. The console meters may be set to read 100 or 500 mrems/hr. They are provided with a sensing circuit which trips an alarm if the meter exceeds the selected level.

INTEGRATED DOSE CIRCUIT

So far we have described meters which indicate the dose at each chamber associated with individual Cosmotron pulses. There is also provision for integrating over an arbitrary length of time the dose measured at each chamber. It did not seem practical to integrate over a period of hours by electronic means the relatively small signals available, so the individual pulse intensities are converted to digital values and summed in a scaler. The analog-to-digital conversion is achieved by converting each pulse height to a proportional time "gate" which permits pulses from a stable oscillator to enter a scaler. The scaler reading is, thus, proportional to the total dose received since it was reset to zero.

The height-to-time converter is shown in Fig. 3. Two pentodes are connected as a d.c. amplifier. By virtue of the "bootstrap" capacitor from the cathode of the second pentode to its screen and to a tap in the plate load resistor of the first pentode, both tubes have high voltage gains. A VR-tube in the output cathode circuit permits negative feedback to the input grid. This feedback is through a diode which conducts in only one direction. Normally a current flows through the high resistor, R, and through the diode; the feedback circuit is closed and the input grid is at about -1.5 V; the left-hand lead of capacitor, C, is connected to ground through a relay. Some time after the charge from the the accelerator pulse has been collected, the relay switches the input lead to the output of the electrometer amplifier. Since this is a positive potential, capacitor C charges through the feedback diode. One-tenth second later the relay returns the input lead to ground. Since the C cannot discharge through the diode, the amplifier input is suddenly cut off and its output goes positive until caught by the second diode. C now discharges through R until the first pentode is turned on to almost exactly its former operating point when the output falls and the feedback circuit recloses. The 6AL5 cutoff characteristic is sharpened by the gain of the feedback amplifier so that the circuit is sensitive and stable to a few millivolts. The output pulse is positive. Its duration is proportional to the

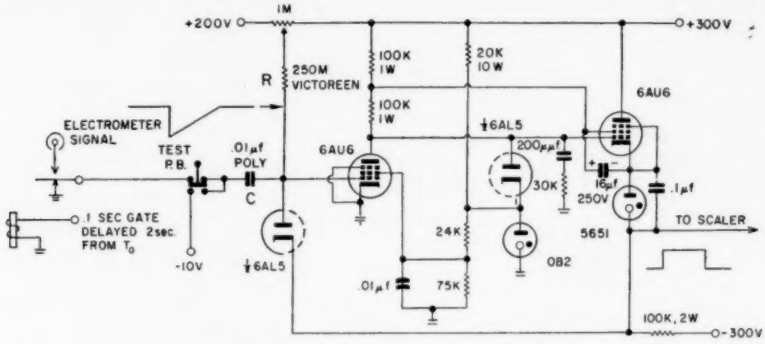

FIG. 3. Amplitude-to-time converter.

* "Rustrak", Rust Industrial Co.

† Mod. 2545, International Instruments, Inc.

input voltage amplitude and inversely proportional to *RC*.

The output square wave passes clock pulses into a scaler. The clock pulses are derived from a 100-kc/s crystal oscillator divided by a scale-of-eight. The scaler has four decatron stages and a four-digit register. The clock frequency, *RC* and scaling factors are chosen so that the scalers read directly in mrems and fine adjustment is made by means of the pot to which *R* is connected.

CENTRAL UNIT

The digitizing circuits described above, the scalers, strip chart recorders and the power supplies are mounted together in one rack in the back of the Cosmotron control room. A timing chassis is also mounted in the cabinet which contains the crystal oscillator, the scale-of-eight and a series of electronic delay circuits to operate the relays at the electrometer units, the strip chart recorders and the analog–digital converter.

Health Physics Pergamon Press 1961. Vol. 5, pp. 173–178. Printed in Northern Ireland

THE HEALTH PHYSICIST IN NUCLEAR WARFARE

H. C. KINNE, Jr.
Chemical Corps, Seventh U.S. Army Training Center, Combined Arms School
APO 114, U.S. Forces

(*Received* 1 *August* 1960)

Abstract—Radiation sources presented by fallout or by neutron-induced activity from nuclear weapons may present a hazard different from that considered in industrial health physics. In order to be of maximum assistance under emergency conditions, the health physicist must be familiar with large area, mixed isotope sources and be ready to consider the acute somatic dose with survival as the primary objective. This paper considers the problem of radiation protection under the conditions of nuclear warfare, discusses fallout, induced activity, the β-hazard and summarizes some "rules of thumb" and calculation techniques designed to assist the health physicist in preparing himself for this eventuality.

As LONG as the potential of a nuclear attack on the United States exists, it is the duty of every health physicist to be prepared to assist his fellow men in their problem of survival under nuclear conditions. The radiological environment in nuclear war may be so different from that of everyday health physics that prior consideration of the problems involved is essential if his potential value is to be realized.

It is the intent of this article to point out some of the parameters of nuclear radiation under the conditions of nuclear war and to discuss some practical "rules of thumb" which can assist the health physicist in his evaluation of this new problem. It must be remembered that the problem, in its simplest terms, is that of survival itself. The sources involved are large, infinite plane, β–γ-sources consisting of mixed isotopes and exhibiting a complex decay scheme. The health physicist must "shift gears" in his thinking from the mr to r, from the long-term hazard to the acute somatic dose if he is to be of maximum assistance.

The "rules of thumb" discussed are in common usage and many have previously appeared in the open literature. They are very broad and general in scope and are not intended to replace either continual monitoring or adequate dosimetry but are merely to furnish rough guide lines that can be simply applied by relatively untrained disaster control workers.

THE FALLOUT FIELD

Since the major radiation source of interest under the conditions of nuclear warfare may well be the fallout field, let us look first at some of the parameters involved here.

Fallout of significance to survival consists largely of particles of the target itself which have been pulverized or vaporized by the interaction of the fireball with the target. Fallout will only occur when the fireball touches the ground, i.e. a surface, low air, or shallow underground burst. Other types of detonations can contribute to the induced activity, but they do not produce significant fallout and will not be considered at this time. Fallout particles have been intimately mixed with fission products and have been bombarded by the intense neutron fluxes associated with the detonation. They exhibit a wide range of particle sizes, but, since the heavy particles fall within the primary range of heat and blast effects and the very small particles are associated with very low intensities, we may assume that the particle size of interest for significant fallout is in the 100–500 μ range.

It is a matter of some interest that, in every instance where a potentially lethal fallout field has been produced by test detonations, the fallout has been visible during delivery. It had the appearance of dust or ashes in the air, as though a neighbor were burning newspaper or a small "dust devil" had passed by and the sand

thrown into the air was returning to earth. Thus, it is probable that the condition of fallout will be apparent to the individuals receiving it and that the visible signs of its arrival may well be the first warning that exposed personnel will have. The science of fallout prediction is not too far advanced and the operational problems involved in disseminating warnings to large numbers of people may well prove insoluble.

A word of caution is advisable here on the use of the standard Geiger–Muller instrument for the identification of fallout. This type of radiac instrument, although widespread in industrial applications, is susceptible to saturation (with an accompanying lack of visible or aural indication of radiation) by fields of comparatively few roentgens per hour. This can be most misleading and could cause grave danger to individuals if they did not realize the fact of fallout and take advantage of existing shelter.

The visibility of significant fallout led to calculations by the United States Naval Radiological Defense Laboratory (USNRDL) in San Francisco which developed a measure of fallout quantity associated with radiation intensity;[1] studies of nuclear tests suggest that about 25 mg of fallout material per ft^2 correspond to a normalized $H + 1$ intensity of 1r/hr. It is easily seen that nearly 1 oz of fallout material is delivered per square foot for an $H + 1$ intensity of 1000 r/hr, an intensity which may cover hundreds of square miles from a megaton yield surface burst.

Fallout presents a β–γ-field of average γ-energy in the 0.6–0.7 MeV range. The decay scheme has been found to approximate $It^n = k$ in its decay with $n = 1.2$. The widespread use of $H + 1$ hr as the time of normalization undoubtedly results from this equation (sometimes referred to as Kaufmann's equation) as k is seen to equal the intensity at this time. The assumption of this decay equation seems valid as a general rule regardless of target composition. Deviations have been seen in the test program, but these would become apparent from actual intensity readings under nuclear warfare conditions and appropriate corrections could be made at that time.

This equation allows the development of our first rule of thumb. It is noted that doubling the time from the burst results in an intensity reduction to approximately one-half the original value. A further refinement is possible as the new value is found to be 10 per cent too high. Thus, an area reading 100 r/hr at $H + 2$ will read 45 r/hr at $H + 4$ (100/2 = 50, 50–10 per cent = 45), and should read 20 r/hr at $H + 8$ hr (45/2 = 22, 22 − 10 per cent = 20).

Total dosage calculations based on this equation reveal another rule of thumb useful in estimating the maximum dose that could be received by an unshielded individual remaining in the radiation field. The infinite dose or dose to infinity is determined as:

$$\int_{t_E}^{\infty} I\,dt$$

$I_0 = I$ at $H + 1$,

t_E = time of entry.

$$I_0 = It^{1.2}$$

then,

$$\text{Dose to } \infty = I_0 \int_{t_E}^{\infty} t^{-1.2}\,dt$$

$$= 5\, I_0 t_E^{-0.2}$$

Since $$I_0 = I_E t_E^{1.2}$$

Therefore $$\text{Dose to } \infty = 5\, I_E t_E$$

Therefore, the dose to infinity from any time is seen to be five times the intensity times the time from the burst. (Time from the burst and intensity must be expressed in the same units: normally hours and r/hr are used.) This rule can also be used for estimating dosage for any time period by calculating the infinite dose from entry and the infinite dose from exit time and taking their difference.

As a mnemonic device, this rule has been termed the FIT Forever rule; FIT being *F*ive *I*ntensity *T*ime and the Forever referring to dose-to-infinity. When this rule is coupled with the 2,4,6 rule for acute effects,

200 r = 50% sick, 0% death

400 r = 100% sick, 50% death

600 r = 100% sick, 100% death

rough hazard calculations can be made by relatively untrained personnel.

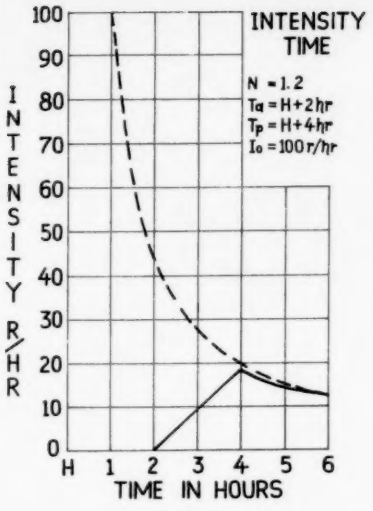

FIG. 2.

The integration technique for dosage calculations, when based on an extrapolated or predicted $H + 1$ intensity for the area of interest, can also be used to determine the total dose received in any given interval of time and, with a little ingenuity, can be used to solve simple time of entry, time of stay problems based on a permissible dose concept. This technique is beyond the capability of the average radiation monitor, however, and several techniques have been developed to help him with this type of problem.

One of the most useful has been developed by the Chemical Section[2] of our Seventh United States Army in Europe and is shown in Fig. 1. This device, called the Commander's Radiation Guide, is a modification of a circular slide rule specifically for fallout calculations. The outer scales relate the intensity to the time since the burst according to Kaufmann's equation for times from $H + 15$ min to H + 120 days; the inner wheel and the color bands leading to the outer scale are an integrator for total dosages, stay time and time of entry problems. Additionally, two intensity readings with the time interval between readings can be used to match a nonstandard (other than $n = 1.2$) decay rate for reasonable accurate short-range predictions or to find an "effective burst time" for overlapping fallout fields from two or more contaminating bursts. The Commander's Radiation Guide has been widely disseminated in Europe, both in our forces and in the military and civil defense organizations of other NATO nations.

Another interesting empirical rule of thumb for fallout has been developed at USNRDL relating the time of arrival of fallout to the time of peak intensity on the ground.[3] Over a wide range of yields, it has been noted that the time of peak intensity is just double the time of arrival of fallout expressed in units of time since the burst itself. An area that starts to receive fallout at $H + 2$ hr will reach peak intensity at $H + 4$; one that starts receiving fallout at $H + 3\frac{1}{2}$ will reach peak at $H + 7$, etc. This implies an actual intensity vs. time curve of the sort shown in Fig. 2, with the dotted line representing the intensity of the "packet" of fallout while it was still airborne. The dotted curve is based on the predicted $H + 1$ intensity for the area of interest; the time of arrival may either be actual or predicted, as most fallout prediction schemes furnish this information.

Obviously, neither the Commander's Radiation Guide nor the integration technique will give total dose received under these conditions, as both are based on the dotted curve. A simplifying assumption, shown in Fig. 3, that the

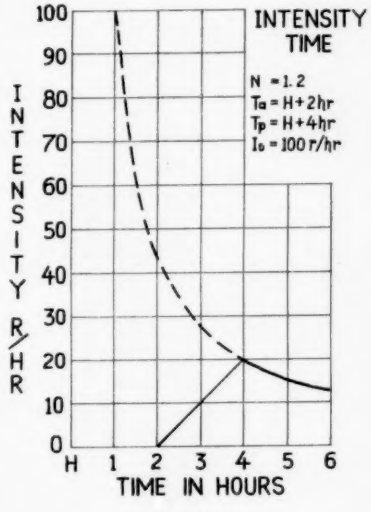

FIG. 3.

actual curves coincide at the time of peak intensity and thereafter allows a good estimate of dose received. Dose during the period t_a to t_p can be calculated either by determining an average dose rate during the period or by assuming one-half of the dose calculated from the theoretical curve. The assumption of one-half the calculated dose introduces a safety factor which may help overcome variations in the shape of the $t_a - t_p$ curve and the 4π character of the radiation field during the delivery of fallout. It must be remembered that these results are merely predictions, they must always be verified by actual instrument readings and should merely serve as "best guesses" as to the expected radiological situation. The state of the art of fallout prediction is not sufficiently advanced to allow complete reliance on prediction.

NEUTRON-INDUCED γ-ACTIVITY

The next most probable large area source of radiation under the conditions of nuclear warfare is that of Neutron Induced Gamma Activity (NIGA). It is well known that the neutron flux of a low air burst (too high for significant fallout production) can irradiate the target area and induce significant γ-activity in the target itself. This can result in a circular area exhibiting intensities in the hundreds of r/hr at $H + 1$. This area is usually from $\frac{1}{4}$ to $\frac{1}{2}$ mile in diameter and is always far smaller than the area which would have been covered by fallout if the same yield weapon had been used as a surface burst.

Decay rates may vary widely with soil composition, but a simplifying assumption based on the widespread occurrence of sodium as a soil constituent as well as the short half-lives associated with other soil elements allows the selection of a single half-life for representative calculations which maintain a fair degree of accuracy in the prediction of future dose rates.

The reverse side of the Commander's Radiation Guide (Fig. 4) has been based on this activity and assumes a 14-hr half-life. No dosage calculation wheel has been included, as the assumption of an average dose rate is satisfactory for short time periods, up to 48 hr, and a rule of thumb regarding infinite dose suffices for longer periods. The rule of thumb results from infinite dose calculations as follows:

Since

$$\frac{dN}{dt} = kN, \quad N = N_0 e^{-kt} \text{ or } I = I_0 e^{-kt}$$

and

$$\text{Dose to } \infty = I_0 \int_{t_E}^{\infty} e^{-kt} dt$$

$$= -I_0 k^{-1} [e^{-\infty} - e^{-kt_E}]$$

$$I_0 = I_E e^{kt_E}$$

Therefore $\quad \text{Dose to } \infty = I_E k^{-1}$

For a 14-hr half-life, $k = 0.0495$ or the infinite dose equals approximately twenty times the intensity at time of entry.

Further investigation reveals that 90 per cent of this infinite dose is received in the first 43 hr, therefore assumption of this dose for time periods of 48 hr or more is certainly justified. Again, deviations from this decay rate will become apparent through monitoring, and modification of predictions can be performed as the situation develops.

THE β-HAZARD

Finally, consideration must be given to the β-hazard presented by these large area radiation sources. This hazard is of two types: Contact hazard and the so-called "β-bath" hazard.

The contact hazard results from β-emitters deposited on the skin and allowed to remain there. These can produce severe local exposures with their associated skin effects. Ordinary hygenic procedures, normal personal cleanliness, will usually prevent these skin effects and thorough cleaning of the person should be routine on leaving a contaminated area. In an emergency, it is unlikely that the capability for mass monitoring will exist, and "preventive maintenance" of the human body must be accomplished by meticulous attention to personal cleanliness if these effects are to be avoided.

The β-bath hazard results from beta emitters within 5 or 10 yd of the individual acting as an area source. Acute effects of this type of radiation have been estimated by ALPEN[4] (see Table 1).

The β-hazard is normally subordinate to the γ-hazard for two reasons: first, it is normally not a lethal problem; and second, the range of

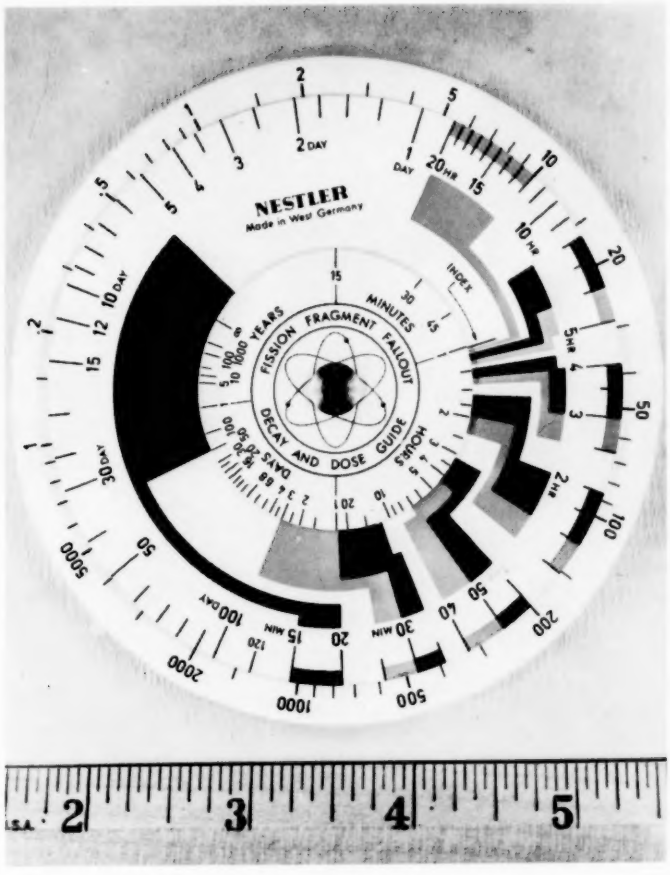
NESTLER
Made in West Germany
FISSION FRAGMENT FALLOUT
DECAY AND DOSE GUIDE
MINUTES
HOURS
DAYS
YEARS
INDEX
2 DAY
1 DAY
20 HR
10 HR
5 HR
2 HR
100 DAY
30 DAY
20 MIN
15 MIN
30 MIN
U.S.A.

FIG. 1.

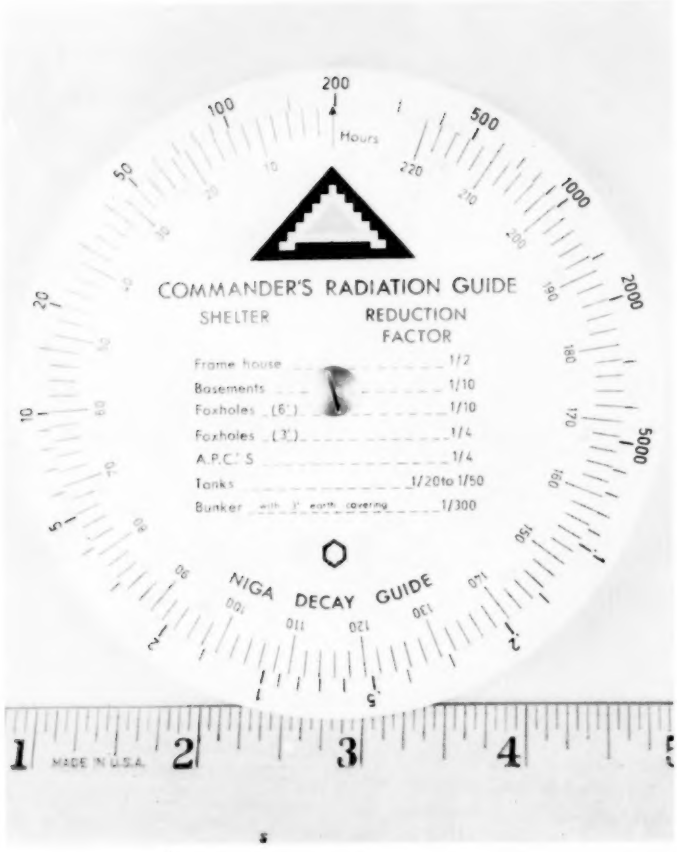
COMMANDER'S RADIATION GUIDE
SHELTER
REDUCTION FACTOR
Frame house 1/2
Basements 1/10
Foxholes (6') 1/10
Foxholes (3') 1/4
A.P.C.'S 1/4
Tanks 1/20 to 1/50
Bunker with 3' earth covering 1/300
NIGA DECAY GUIDE
Hours
MADE IN U.S.A.

FIG. 4.

Table 1

Estimated dose required in less than 1 week (rad)	Effect
00–600	No acute effects
600–2000	Moderate early erythema
2000–4000	Early erythema (under 24 hr)
4000–10,000	Severe erythema (under 24 hr)
10,000–30,000	Severe erythema (under 4 hr)
30,000–100,000	Immediate skin blistering

β-rays is short compared to that of γ-rays, so a much smaller effective source is involved.

Certain situations can exist, however, where the β-hazard could be considered significant. These occur when the geometry of the situation removes a large part of the γ-source without affecting the β-source. Since instruments found in the field are not normally calibrated for β-rays but merely give an indication of its presence through a β-window, the reduced γ-reading found in these conditions could lead to the false assumption of a correspondingly low β-intensity. These situations could include:

(1) A city street, the high vertical building walls effectively removing the γ-field.

(2) A shipboard, or seaside, situation with dilution of the γ-sources beyond the effective β-range.

(3) A truck or large piece of equipment removed from the contaminated zone. This situation could result in a β-hazard for maintenance and repair personnel.

Shielding against the γ-and β-components of fallout is no different than the normal shielding problems of everyday health physics so no particular discussion will be made of this facet of protection. A rule of thumb exists for the γ-energies found in fallout which states: 1 in. of steel is as good as 4 in. of concrete or 5 in. of dirt. This is called the 1,4,5 rule for γ-shielding and is of some help in the training of monitor personnel.

It is immediately apparent from a consideration of the geometries associated with infinite plane sources that a below ground position affords the best natural shielding. A simple shelter in the basement, stocked with food and water for 3 or 4 days occupancy, may well be all that is required for survival and, at any rate, will greatly increase the survival potential of the occupants. Food and water are essential as the complex mechanisms of food delivery to major centers of population may well break down under emergency conditions and severe food shortages could result until the disaster control organization becomes fully effective.

SUMMARY

The problem of health physics in nuclear warfare requires work with mixed isotope sources at survival levels of exposure. The health physicist must shift his thinking to this type of situation if he is to be of maximum value in an emergency period.

Several rules of thumb have been discussed:

For fallout

(1) Double the time is half the intensity, 10 per cent too high.
(2) FIT Forever.
(3) Time peak intensity is twice time of arrival.

For NIGA

(1) Infinite dose is twenty times intensity at entry.

For both sources

(1) 2,4,6 rule for acute effects.
(2) 1,4,5 rule for shielding.

Additional guide lines

(1) No fallout prediction system is sufficiently accurate to warrant movement to or from a specific area based on the prediction alone.

(2) Passive defense is the best course of action during the delivery of fallout. Usually, it will be the best action until after the completion of the initial rapid decay of intensity, i.e. 2 or 3 days.

(3) Panic must be avoided at all costs. Your own home shelter is your safest location.

REFERENCES

1. J. D. SARTOR *et al.*, *Cost and Effectiveness of Decontamination Procedures for Land Targets.* USNRDL TR-196 (1957).
2. Colonel S. EFNOR, JR, Chief; Captain J. A. BRYAN, Nuclear Effects Engineer.
3. P. D. LARIVIERE, *The Relationship of Time of Peak Activity from Fallout to Time of Arrival.* USNRDL (1957).
4. E. L. ALPEN, *Radiological Hazard Evaluation—A Critical Review of Present Concepts and a New Approach Thereto.* USNRDL (1957).

Health Physics Pergamon Press 1961. Vol. 5, pp. 179–202. Printed in Northern Ireland

DOSIMETRIC INVESTIGATION OF THE YUGOSLAV RADIATION ACCIDENT*

G. S. HURST, R. H. RITCHIE, F. W. SANDERS, P. W. REINHARDT, J. A. AUXIER, E. B. WAGNER, A. D. CALLIHAN and K. Z. MORGAN
Health Physics Division, Oak Ridge National Laboratory, Oak Ridge, Tennessee†

(*Received* 3 *November* 1960)

Abstract—A complete investigation of the radiation doses received by individuals exposed to radiation in the Yugoslav accident on 15 October, 1958, has been completed, using modern techniques of dosimetry. The zero power reactor was operated at low power levels to determine the ratio of γ-ray to neutron dose at various locations near the reactor. These measurements were made with special counting methods, one of which measured the neutron dose in the presence of γ-rays, and the other measured the γ-dose in the presence of neutrons. The reactor was operated at a higher power level for a short time to determine (a) the neutron dose by means of threshold detectors and (b) the relationship between neutron dose and Na^{24} activation in man-shaped phantoms. A computational program gave theoretical results for the same three quantities, i.e. the neutron spectrum, the γ–neutron ratio, and Na^{24} activation. The results of theory and experiment are in good agreement.

Final results for the individual doses are shown in Table 7. In this table the charged particle dose refers to the first collision dose due to recoils from fast neutrons and includes the dose delivered by the nitrogen n–p reaction. The second dose column gives the maximum dose obtained for the hydrogen capture γ-radiation produced in the phantoms. The external gamma dose based on the measured γ–neutron ratio is shown in the third column, and the total doses are given in the last column. Of the seven persons investigated, the highest dose received (individual V) was 436 rads and the lowest dose was 207 rads. The doses previously estimated were reported in rem units, showing for individual V an estimated value of 210 rems for the neutron dose and 630 rems for the γ-dose, or a total exposure of 840 rems.

1. DESCRIPTION OF THE ACCIDENT

THE radiation accident[1] which occurred at the Boris Kidrič Institute on 15 October, 1958 resulted in heavy exposure of six young scientists to a mixture of neutrons and γ-radiation during the course of a subcritical experiment with a zero power reactor. The reactor[2] was constructed with natural uranium rods suspended in a large tank which could be filled to various depths with heavy water, and was primarily intended as a combined training and criticality research facility. Further details of the circumstances leading to the incident and of the reactor itself are described in the publications[1,2] from the Boris Kidrič Institute.

Following a brief period of hospitalization in Belgrade, the six patients were transferred to the Foundation Curie in Paris, and placed under the care of Dr. H. JAMMET. A summary of clinical observations, patient management, and dose estimates is described by JAMMET *et al.*[3] These dose estimates, from 1000 to 1200 rems for the highest exposure and from 300 to 500 rems for the lowest, placed five of the six individuals into a range of exposures which is considered to be above the lethal (LD-50) level. It is reported[4] that the hematological observations tended to confirm the physical dose estimates. Following these observations the

* Appendix E is by J. W. SMITH, United Kingdom Atomic Energy Authority, Harwell, England.

† Operated by Union Carbide Corporation for the U.S. Atomic Energy Commission.

highest exposed individual (V) was given fetal bone marrow on 11 November, and the four patients having the next highest exposures were given bone marrow from adult donors at various times between 11 November and 20 November. All of the patients except V recovered.

2. METHODS OF DOSIMETRY

The methods of dosimetry used to investigate the doses received by the individuals exposed in the Yugoslav accident were essentially those used in connection with the Oak Ridge Y-12 accident.[5,6] An outline of the general scheme is as follows. When fast neutrons enter the human body most of these are moderated to thermal energy and a small fraction of these are captured by a (n, γ) process in the Na^{23} in the body giving rise to Na^{24} which, by virtue of its emission of high-energy γ-rays with a radioactive half life of 14.8 hr, is easily detected. It has been shown (HURST *et al.*[6], Fig. 1) that the probability of neutron capture to make Na^{24} is not a strong function of the energy of the fast neutrons and that the probability of capture for neutrons in the fast region is higher than the probability of capture in the thermal region. Thus the uniform distribution of Na^{23} in the human body provides an excellent means of normalizing the neutron exposure of an individual. In particular, for a given neutron energy spectrum the fast neutron dose is proportional to the ratio Na^{24}/Na^{23} in the body or in the blood system. This method of normalization is quite important in the dosimetry of radiation accidents since no assumptions need be made about the exact location of an individual at the time of the energy release. The importance of this fact can be made clear by reference to the Y-12 accident[5] where it was shown, by calculating the neutron dose based on the known number of fissions and the stated location of the individual, that one of the surviving individuals would have received a dose several times the lethal value. Thus little credence can be placed in calculations requiring such assumptions.

More specifically, the determination of the neutron dose, D_n, and the γ-dose, D_γ, may be obtained from three quantities, $(D_n/a)_c$, $(D_\gamma/D_n)_c$, and a, which are related as follows:

$$D_n = (D_n/a)_c \times a$$
$$D_\gamma = (D_\gamma/D_n)_c \times D_n$$

where the quantity $(D_n/a)_c$ is the neutron dose per unit sodium activation which is characteristic of the type of source and the exposure conditions, a is the measured amount of sodium activation within the individual, and $(D_\gamma/D_n)_c$ is the ratio of γ-dose to neutron dose which is characteristic of a given source and set of exposure conditions. In both the Y-12 and Vinča accident investigations the quantity $(D_n/a)_c$ was determined by two methods, experiment and theory. The experimental method at Vinča consisted of measuring the neutron dose (with a Radsan fast neutron dosimeter[7]) required to produce a given amount of activation in a plastic man-shaped phantom filled with an aqueous solution of NaCl. The ratio $(D_\gamma/D_n)_c$ was determined with two types of γ-dosimeters,[8,9] and the Radsan neutron dosimeter. The quantity a was based on the Na^{24} analysis reported by JAMMET *et al.*[3] As a supplement and check on the experimental procedure, the quantities $(D_n/a)_c$ and $(D_\gamma/D_n)_c$ were calculated for the zero power reactor. In addition to the quantities D_γ and D_n, it is desirable to determine the neutron spectrum $N(E)$. This was done by calculation and by experiment using the series of threshold detectors[10,11] developed for this purpose.

3. EXPERIMENTAL INVESTIGATIONS

To accomplish the measurements indicated above, the zero power reactor (Fig. 1) was operated in two different ranges of power level which for convenience will be referred to as "low" power and "high" power. Fig. 2(a) shows the general location of the dosimetry equipment for the low- and high-power runs. The LPS stations show locations where most of the dose measurements were made, the V.T. and H.T. represent, respectively, locations where vertical and horizontal traverses were made with Au and S detectors during the high-power runs. Figs. 2(b) and 2(c) show the location of the phantoms for high-power runs at 1 kW and 5 kW, respectively. To facilitate intercomparison of data obtained from the two types

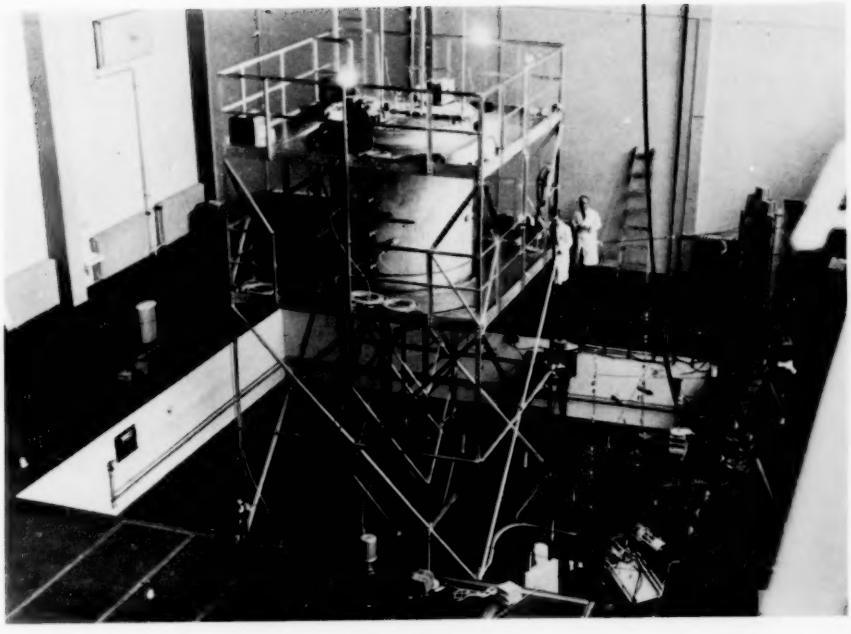

FIG. 1. Zero power reactor.

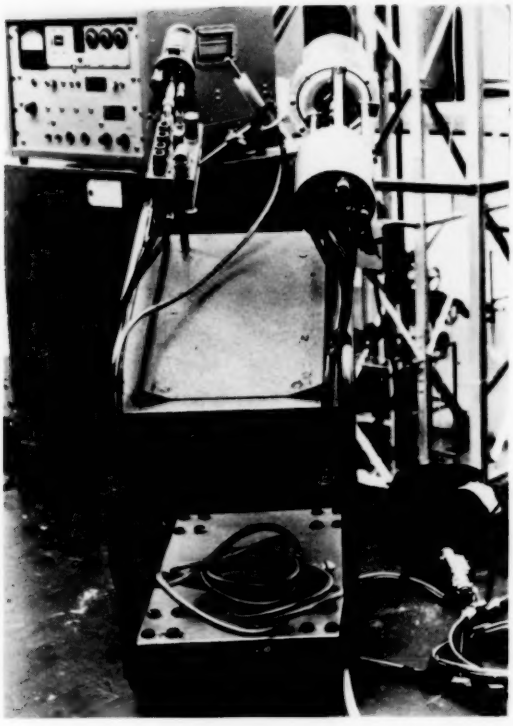

FIG. 3. Mounting arrangement for the low-level dosimeters.

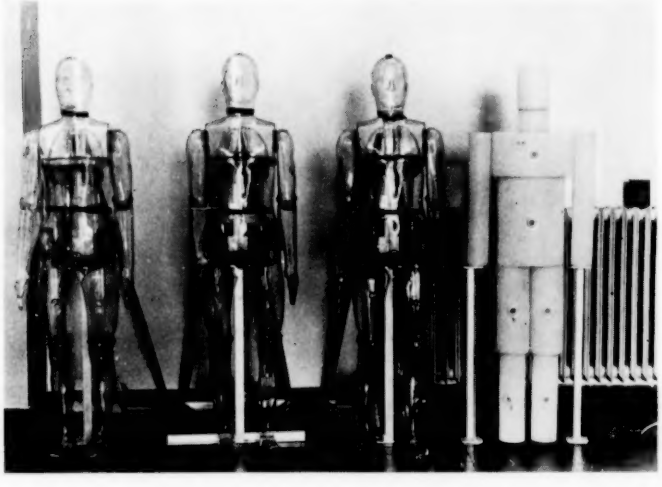

FIG. 4. The four plastic phantoms—Calvin, Remab, Tyrone and Bomab.

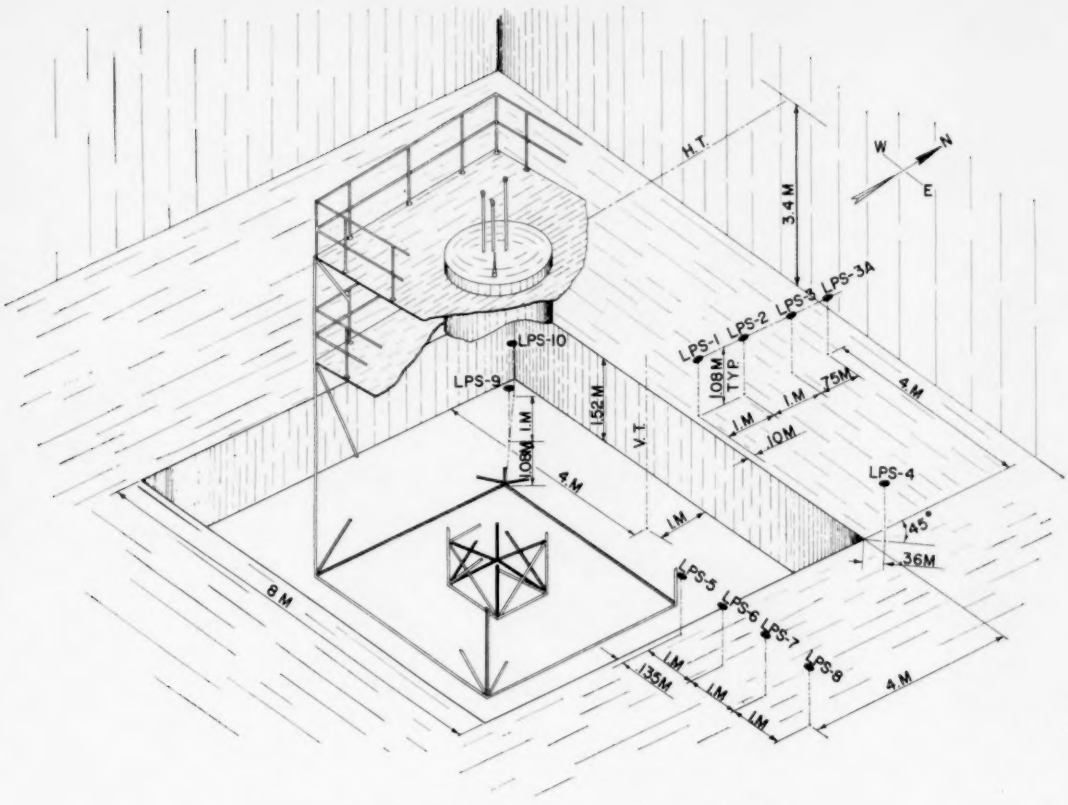

FIG. 2(a). Dosimetry station locations in reactor room.

of operating conditions, a sulfur pellet was placed at a convenient location on the side of the reactor tank before each run.

3.1. *Low-power experiment*

The ratio of γ-dose to fast neutron dose was measured at some of the positions shown in Fig. 2(a), using the equipment mentioned above (mounted as shown in Fig. 3) and with the reactor operating at a power level of approximately 5 W.* The results of the directly measured ratio, D_γ/D_n, are shown in Table 1 which gives also the neutron dose, as measured with Radsan, per unit monitor flux density (i.e. sulfur neutrons/cm^2). The final D_γ/D_n values for the various positions are based on the

Table 1. *Experimental values for D_γ/D_n at various positions*

Position (LPS no.)	Neutron dose per unit monitor (rad/n cm^{-2})	D_γ/D_n
1	1.13×10^{-6}	3.5
2	0.90×10^{-6}	3.6
3	0.75×10^{-6}	3.6
3a	0.66×10^{-6}	3.9
4	0.64×10^{-6}	3.8
8	0.54×10^{-6}	3.5
9	0.86×10^{-6}	4.0
10	0.72×10^{-6}	4.2

* Private communication with D. POPOVIĆ indicated that the power calibration in the initial run yielded a figure approximately 0.56 times the value quoted here. This correction factor applies to all power levels quoted in the remainder of this report.

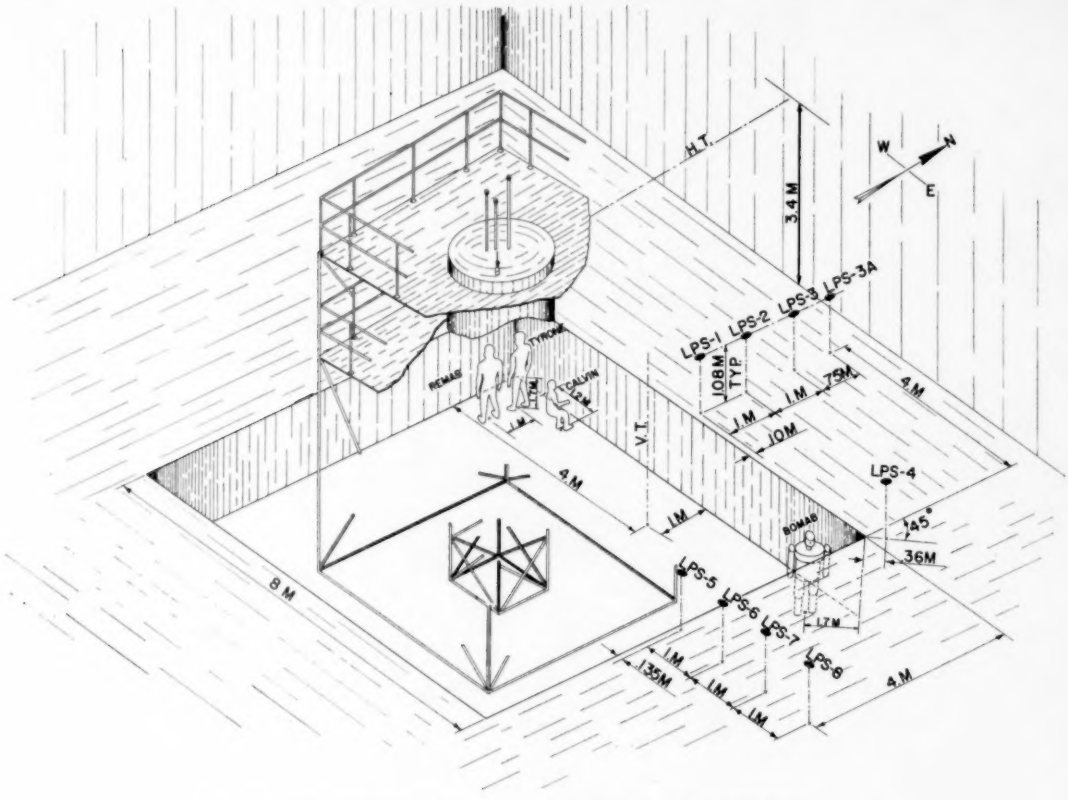

FIG. 2(b). Dosimetry stations and phantom locations in reactor room.

counting method of γ-ray dosimetry described by WAGNER and HURST[8]. The carbon–CO_2 chamber[9] used in this experiment gave results which were 1.3 times the dose values obtained with the counting method, but later studies with the carbon–CO_2 chamber at ORNL showed that it has an appreciable response to thermal neutrons.

3.2. *High-power experiment*

With the reactor operating first at 1 kW, then at 5 kW, two types of measurements were made, neutron spectrum measurements and Na^{24} activation in man-shaped phantoms. The spectral measurements were made with threshold detectors[10,11] located at various positions (stations). The results obtained for Stations 1, 9 and 10 are shown in Table 2, where comparison is made with the spectral data obtained for the Y-12 excursion with the same type of detectors.

Table 2. Experimental information on neutron spectrum (ratio of flux above threshold of various detectors to total fast flux)

Threshold detector	Boris Kidrič (ZPR) threshold energy			Y-12 excursion
	Sta. 1	Sta. 9	Sta. 10	
Pu	1.00	1.00	1.00	1.00
Np	0.36	0.35	0.35	0.89
U	0.20	0.18	0.19	0.54
S	0.094	0.088	0.090	0.25
Au	3.91	3.63	3.87	0.45

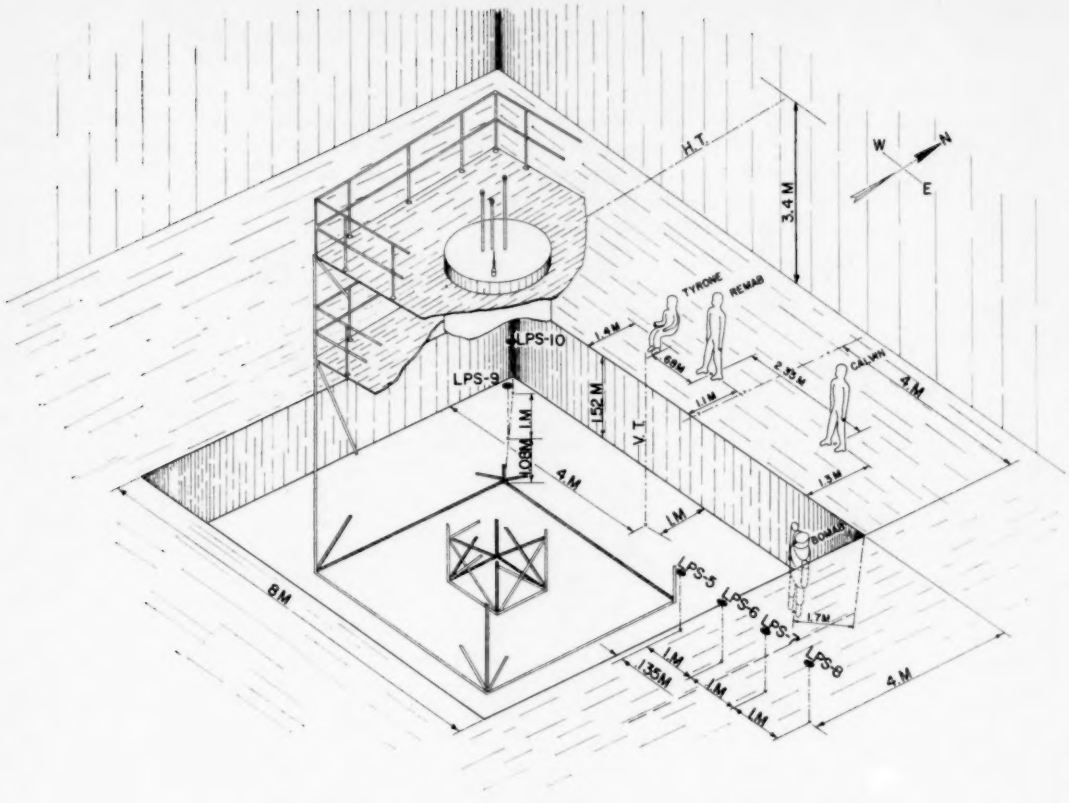

FIG. 2(c). Dosimetry stations and phantom locations in reactor room.

Sodium activation data were obtained by locating phantoms (Fig. 4) at the positions shown in Fig. 2(a). During the 1-kW run the phantoms were located as shown in Fig. 2(b), and during the 5-kW run they were as shown in Fig. 2(c). The phantoms were filled with an aqueous solution of NaCl at a concentration of 15.7 mg Na^{23} per gram of solution. After irradiation the sodium activation, a (in units of μc Na^{24}/mg Na^{23}) was determined according to the technique described in ORNL-2748A.[12] From the data obtained during the low-power experiment, Table 1, and by normalizing the relative exposure in some cases by means of the activation of sulfur pellets placed on the phantoms, the neutron dose received by the phantoms was obtained. The results of $(D_n/a)_c$ are shown in Table 3, where each entry corresponds to the weighted average value of a for all the compartments of the phantom. Further experimental data are given in Appendices A, B, C and D. In particular, Appendix B justifies

Table 3. Neutron dose per unit sodium activation for man-shaped phantoms exposed at the zero power reactor

Phantom	$(D_n/a)_c$ (rad μc^{-1} mg Na)	
	1-kW run	5-kW run
Tyrone	9.12×10^4	7.73×10^4
Remab	8.57×10^4	8.13×10^4
Calvin	9.12×10^4	7.27×10^4
Grand average = 8.65×10^4		

the particular way in which the phantoms were used in this experiment.

4. THEORETICAL INVESTIGATIONS

In this section a description will be given of the methods used in calculating neutron and γ-leakage from the Boris Kidrič zero power reactor in the critical and near-critical state. The methods used are entirely theoretical in the sense that they rely not at all upon measurements which were made at Vinča. Multiple scattering of leakage radiation in walls and structure of the reactor building are neglected and only direct leakage of neutrons and γ-rays from the assembly is considered. As shown below by comparison with experimental data, this approximation is surprisingly good, although the agreement may be fortuitous in some particulars.

The quantities presented are: (1) $N_n(E)$, the neutron leakage spectrum; (2) $D_n(E)$, the neutron first collision dose leakage spectrum; (3) D_n/a, the ratio of the total first collision dose received by an idealized phantom to the Na^{24} activation generated in the phantom by the leakage spectrum incident upon it; and (4) D_γ, the γ-ray first collision dose leaking from the reactor due to the fission process and due to various neutron capture processes occurring in and around the reactor.

The method of computing neutron leakage which has been used in this work is the multigroup-diffusion approach. An existing criticality code written for the IBM-704 which automatically computes neutron leakage in several energy ranges has been employed. The computing time for this code is quite modest for most systems. γ-Ray leakage is treated by special IBM-704 codes. The method uses known γ-ray cross-sections and build-up factors to calculate attenuation kernels for the particular medium under consideration. The radiation field at various points inside or outside the assembly is then computed by summing over source points in the assembly, using best estimates available for the γ-ray spectra of the various sources. The spatial distribution of fissions in the assembly is obtained from the neutron leakage runs and is used in the γ-leakage calculation.

4.1. *Neutron leakage spectrum*

The method which was employed to calculate the neutron leakage spectrum from the Vinča reactor is based primarily upon the use of a multigroup, multiregion reactor analysis code[13] for the IBM-704. The basic equation solved by the code is the multigroup-diffusion approximation to the Boltzmann transport equation. The program approximates the differential equation by a difference equation and allows as many as 250 space points and forty-four energy groups in the solution of the resulting equations.

Since the Boris Kidrič reactor uses a lattice spacing which is quite small (12 cm) compared with the outside dimensions of the reactor, it should be a good approximation to consider an equivalent homogenized reactor.[14] The unit lattice cell was taken to be cylindrical with a fuel rod at its center and containing the same quantity of D_2O as the real unit lattice cell. A preliminary multigroup calculation of the distribution of flux inside this cell was made, using the boundary condition of zero total current at the outer boundary of the equivalent cylindrical cell. Homogenized multigroup cross-sections were computed using the calculated flux distribution as a weighting function. A multigroup calculation of the escape spectrum for the entire reactor was then made with these cross-sections, assuming that a 1-cm layer of aluminum surrounded the volume. Fig. 5 shows a plot of the multiplication factor, k, of the assembly as a function of height. On the same graph is shown the total neutron leakage per fission neutron in the core as a function of height. One sees that this calculation predicts a critical height of approximately 185 cm, compared with the experimental value[2] of 177.6 cm. It is felt that the agreement is sufficiently accurate for our purposes, since the neutron leakage varies by only approximately 4 per cent over the range of heights. It is possible that back-scattering of neutrons from the tank supporting members and from the walls of the room might well account for the difference between experimental and calculated values of the critical height. These results also show that there is negligible difference between neutron leakage per fission neutron in the critical state and in the delayed supercritical state which occurred at the time of the

accident. Estimates of the $k_{ex} = k - 1$ appropriate to the excursion[15] show that $k_{ex} \simeq 10^{-3}$. According to Fig. 5 the neutron leakage per core neutron at this value of k_{ex} is only approximately 2 per cent different from that in the steady state.* Hence, this difference will be neglected in the remainder of this calculation.

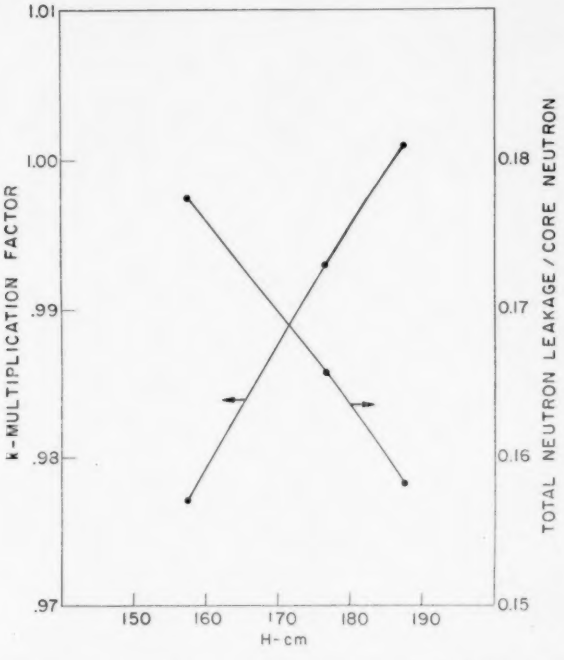

FIG. 5. Multiplication factor and total neutron leakage as a function of height.

Fig. 6 shows the neutron leakage spectrum calculated for the reactor at the critical level.† The quantity plotted in the ordinate is $EN(E)$, and the abscissa gives both the energy E and the lethargy $u = \ln[10/E(\text{MeV})]$. The spectrum is conveniently represented in this way since the number of neutrons escaping between any two energies is just proportional to the area under the portion of the curve between these energies. The total fast leakage in this spectrum is 0.234 neutron per fission while the leakage in the thermal group is 0.157 neutron per fission.

The first collision dose spectrum for neutrons is shown in Fig. 7. The factor $D_0(E)$ is the first collision dose per unit neutron flux.[17] $\int_0^\infty D_0(E)\, N(E)\, dE$ is found to be 4.37×10^{-11} rad cm^2/core neutron.

To make possible a comparison with experimental measurements of D_n, a calculation of $(D_n)_R \equiv \int_0^\infty D_{\text{Radsan}}(E)\, N(E)\, dE$ was carried out. $D_{\text{Radsan}}(E)$ is the dose measured by the Radsan fast neutron dosimeter at energy E and is less than $D_0(E)$ at low energies due to bias losses. Values of $D_{\text{Radsan}}(E)$ were inferred from the work of WAGNER and HURST[18]. The result of this calculation was $(D_n)_R = 3.12 \times 10^{-11}$ rad cm^2 per core neutron.

* A change in the leakage per fission neutron with k would not, by itself, affect the result of this dosimetry study. A radical change in the neutron spectrum, on the other hand, would produce a change in the ratio of D_n/a and would mean that experimental work with a steady operating reactor would not be comparable with conditions obtaining during the accident. However, comparison of the calculations at different values of k indicates negligible change in the spectrum between the two reactor states.

† This spectrum is somewhat different in the low energy range from a preliminary result given elsewhere.[16] Improved values of the homogenized multigroup cross-sections were used in the present calculations.

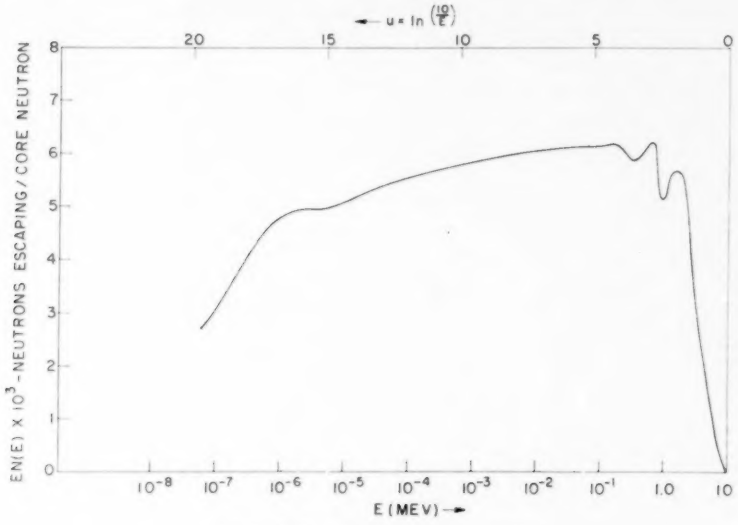

FIG. 6. Escape neutron spectrum.

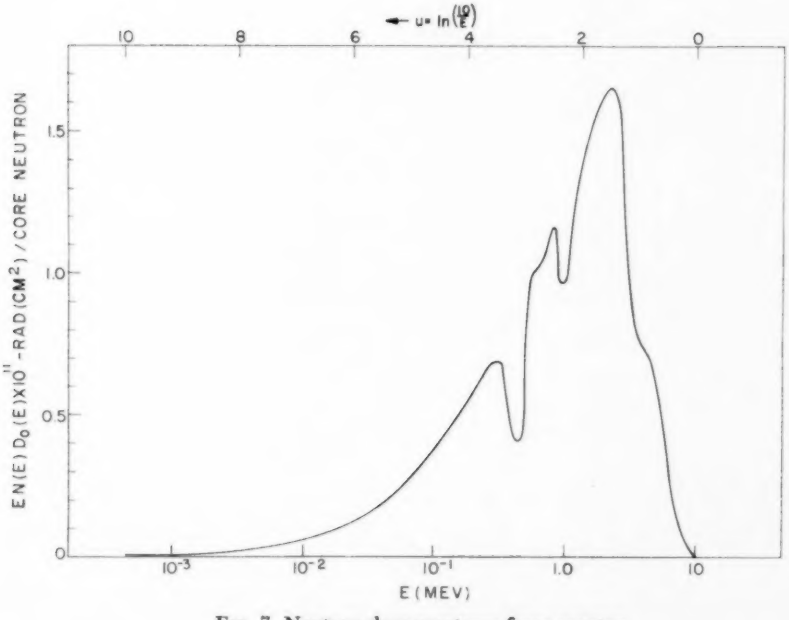

FIG. 7. Neutron dose spectrum from reactor.

In order to calculate a, the Na^{24} activation induced in a man exposed to the calculated spectrum, use was made of approximate results for $\xi(E)$,[6] the capture probability at thermal energy per unit flux of neutrons incident normal to the axis of a circular cylinder of 15 cm radius. Using the function $\xi(E)$, the quantity $(D_n)_R/a$ was calculated from

$$\frac{(D_n)_R}{a} = 1.12 \times 10^{11} \frac{\int_0^\infty D_0(E)\, N(E)\, dE}{\int_0^\infty \xi(E)\, N(E)\, dE} \times \frac{\text{rad}}{\mu\text{c g of Na}^{23}}$$

$$= 7.2 \times 10^4 \text{ rads}/\mu\text{c (mg Na)}^{-1}$$

and compares favorably with the average value of 8.65×10^4 rads/μc (mg Na)$^{-1}$ obtained with the phantoms (see Table 3).

The multigroup computation of the leakage spectrum takes into account the neutron distribution in only one spatial dimension and introduces an artificial absorption to account for leakage transverse to the direction in which computation proceeds. Within the framework of multigroup diffusion theory, one may take into account the dependence of the leakage flux with direction with respect to the reactor axis.[16] This has been done in the comparisons given in Table 4.

Other comparisons can be made between the experimental determination and the calculation of the leakage spectrum by use of the activation of the threshold detectors which were exposed during the work at Vinča. Table 5 shows a comparison of various ratios calculated from the spectrum given above with experimental determinations of these ratios. The experimental values represent station averages. The quantity $\phi_{>E_T}$ represents the neutron flux lying above the effective energy threshold of E_T MeV in the case of various detectors. The quantity $4\pi R^2(D_n)_R/F$ was obtained from the experimental data by employing the Radsan-measured neutron dose rate together with the fission rate, F, occurring inside the assembly. The fission rate was obtained from a power calibration performed by the Yugoslav experimenters.[19] For the purpose of comparison with experiment, the theoretical values have been corrected, approximately, for the non-$1/R^2$ variation of the dose at points in the neighborhood of the reactor.

Table 4. Summary of $4\pi R^2$ × dose due to various sources

γ-Source	$D\gamma \times 10^{10}$(r cm^2/fission)		
	Station 1	Station 9	Station 10
Prompt fission	1.77	1.46	1.63
$U^{238}(n,\gamma)U^{239}$ capture	0.77	0.63	0.69
Moderator capture	0.05	0.05	0.05
Tank 2nd structure capture	~0.30	~0.30	~0.30
Fission products during experiment	1.12	0.92	1.03
Total dose during experiment	4.01	3.36	3.70
Fission products during accident	0.39	0.32	0.36
Total dose during accident	3.28	2.76	3.03
	Dose ratios (r/rad)		
$D\gamma/(D_n)_R$ calculated for experiment	3.52	3.00	3.40
$D\gamma/(D_n)_R$ measured for experiment	3.5	4.0	4.2
$D\gamma/(D_n)_R$ calculated for accident	2.88	2.46	2.78
	$(D_n)_{\text{Radsan}} \times 10^{10}$ (rad cm^2/fission)		
Leakage neutrons	1.14	1.12	1.09

4.2. *γ-Dose leakage*

There are many sources of γ-radiation in and around the reactor which should be considered. It will be seen that reasonably good estimates of the dose from most of them may be made. Although the uncertainties in these estimates are likely to be as much as 20 per cent, it is clearly worthwhile to make such calculations in order to understand better the physics of the accident. Each of the sources of γ-radiation

Table 5. Comparison of calculated and experimental dose and flux ratios

Ratios	Experiment	Theory
$\frac{(D_n)_R}{\phi_{>2.5}} \times 10^8 \left(\frac{\text{rad cm}^2}{\text{neutron}}\right)$	1.6	1.55
$\frac{4\pi R^2 (D_n)_R}{F} \times 10^9 \left(\frac{\text{rad cm}^2}{\text{fission}}\right)$	0.90	0.77
$\frac{\phi_{>1.5}}{\phi_{>2.5}}$	2.1	2.32
$\frac{\phi_{>0.7}}{\phi_{>2.5}}$	3.8	3.84
$\frac{\phi_{>0.01}}{\phi_{>2.5}}$	11.3	15.6
Gold foil—cadmium ratio	3.5–6.5	4.9

have been considered in turn with a detailed description presented in the Appendices.

4.2.1. *Prompt γ-rays from the fission process and capture γ-rays from the U^{238} (n, γ) U^{239} process.* The distribution in energy of prompt fission γ-rays is taken from the work of MAIENSCHEIN *et al.*[20] The energy distribution of γ-rays from the $U^{238}(n, \gamma)U^{239}$ process is taken from the work of BARTHOLOMEW and HIGGS[21]. In order to calculate the escape of these photons from the reactor, one must consider both attenuation in the uranium rods and in the D_2O. Some simplifying assumptions were made in order that leakage from this very inhomogeneous system could be estimated in a reasonably short computing time. For the purpose of calculating leakage the distribution of fissions in a given fuel rod was assumed to be flat in the radial direction and to depend only on position along the length of the rod. The attenuation of γ-rays in the fuel rod in which they originate is accounted for, but their attenuation in other fuel rods is neglected. This approximation should result in little error since the rods are small in diameter compared with the lattice pitch. The computation proceeds by a numerical integration of the product of the source strength and leakage probability for each element in the source. The photon source distribution is obtained from the neutron criticality calculation described above. The attenuation of photons in traveling from a given source point to a field point outside of the reactor is calculated using tabulated photon attenuation coefficients[22] and infinite medium build-up factors for the part of the path lying inside of the reactor. The error involved in using these build-up factors should be small in the cases which we shall consider. A more detailed description of the computational procedure is given in Appendix A.

The leakage probability is a function of the distance from the reactor and the angle which the vector to the field point makes with the axis of the reactor. The results for some of the stations are given in Table 4 and are expressed as $4\pi R^2$ (dose/fission) at the respective stations, where R is the distance from the center of the reactor to the various stations.

4.2.2. *γ-Rays from fission products.* The estimate of this contribution is uncertain owing to the fact that it depends to some extent upon the movement of the exposed persons after the reactor scram. In view of this uncertainty this fraction of the total dose received was approximated. The attenuation kernel of fission product γ-rays in the lattice was taken to be the same as that of prompt fission γ-rays and further it was assumed that the first can be estimated by scaling the second according to the relative energy released in the two processes. Details of this estimate are given in Appendix B, and Table 4 shows the results for Stations 1, 9, and 10 for two different cases: (1) at 15 min after the beginning of a steady power level run (in this case the dose values should be interpreted as r/sec per fission/sec); and (2) 4 min after the beginning of an excursion with a doubling time of 10 sec. The dose values refer to the total fission product γ-dose received during the interval per fission occurring.

4.2.3. *γ-Rays from capture in moderator and fuel cladding.* The thermal utilization, f, for the reactor was calculated by multigroup methods to be 0.9865 for an assumed concentration of 0.16 per cent H_2O in the moderator. Assuming that all of these captures occur in hydrogen nuclei and noting that c, the moderator capture

probability per fission in the critical state, is equal to $(1-f)/b$, where b is the ratio of fission to total capture probability in the fuel, it follows that

$$c = \frac{1-f}{b} = \frac{0.0135}{0.543}$$

$$= 0.0349 \text{ moderator captures/fission}$$

A calculation of the leakage of hydrogen capture γ-rays from the homogenized reactor gave $\sim 0.5 \times 10^{-10}$ rad cm^2/fission for the three stations considered (Table 4). The same multigroup calculation showed the capture probability in the aluminum cladding around the fuel rods to be 0.00642 captures per total capture. The dose due to this source would be expected to be even smaller than that due to captures in the moderator, especially since attenuation of these photons in the fuel rod should make the effective source strength even smaller; thus it has been neglected in Table 4.

4.2.4. *γ-Rays from capture in tank walls and supporting structure.* This source of photons is difficult to estimate accurately because of the very complicated configuration of materials, chiefly aluminum, in the immediate neighborhood of the assembly. A rough estimate, assuming that the structural aluminum may be considered equivalent to a 2-cm layer enveloping the whole reactor, gives 3×10^{-10} r cm^2/fission in the region around the reactor.

4.2.5. *γ-Rays from capture in walls and floor of reactor room.* This contribution is very difficult to estimate with any accuracy and hence was not considered.

4.3. *Discussion*

The chief uncertainties in the estimates given above are: (1) use of infinite medium build-up factors rather than those appropriate to a finite medium; (2) neglect of photon attenuation in rods other than that on which a given photon originates; and (3) neglect of photons from neutron capture in reactor room materials and in air of room. The net uncertainty in the calculation is estimated to be $\sim \pm 20$ per cent. The ratio of the γ-doses during the accident to corresponding doses during the experiment, f, should be more accurate than this and consequently this ratio will be used to correct the experimental data.

Table 4 also shows the neutron dose, $(D_n)_{\text{Radsan}}$ at the three stations considered. These values were estimated by taking into account the angular distribution of radiation leaving the reactor and correcting for the finite size of the reactor by using a radiation center displaced 0.8 m toward a given station from the center of the reactor. Also shown in this table are the values of D_γ/D_n inferred from the above estimates and a comparison of these values with those measured during the experiment.

5. ASSIGNMENT OF INDIVIDUAL DOSES

In previous evaluations of dose received by man, the usual procedure has been to evaluate the first collision dose for both neutrons and γ-radiation. That procedure was followed because of the difficulty of specifying a dose within the body which would have the desired radiobiological significance. This procedure has been justified on the basis that if the first collision doses are determined along with certain additional exposure conditions (i.e. angular and spectral distribution of the incoming radiations) more elaborate correlations of medical effects and exposure doses may be carried out at future times when more detailed biological mechanisms are understood or are being tested. In the case of the Y-12 exposures, the first collision dose for γ-radiation and fast neutrons and the neutron and γ-ray energy distributions are given. In the present case, however, it appears advisable to comment on the γ-radiation which is produced by the capture of low-energy neutrons by the $H(n, \gamma)$ reaction. Based on the neutron spectrum (Section 4) and the calculations by SNYDER,[23] it may be seen that the additional γ-dose near the surface of a 30-cm slab makes an appreciable contribution to the total dose at that point.

We separate the neutron exposure into two dose components, namely (1) the first collision charged particle dose made up of thermal neutron interactions of the type $N^{14}(n, p)C^{14}$ and recoil atoms (H, C, N, O) from fast neutron interactions; and (2) the autointegral γ-dose at the surface of the slab due to the $H(n, \gamma)D$ process.

Data are not presently available which enable one to calculate the H(n, γ)D autointegral dose for a realistic model of a man bombarded with neutrons. However, there are data[23] on the autointegral dose in a slab due to normal irradiation by neutron beams of various energies. These data are conservative in the present connection, i.e. the doses obtained using these values will surely represent overestimates of the autointegral doses to a man and may be too large by a factor of 2.

The surface autointegral doses per unit neutron flux in the slab case were used to calculate the dose for the whole neutron spectrum, shown in Fig. 6. The result was found to be

$$[\mathrm{H}(n,\gamma)\mathrm{D\ autointegral\ dose}]_I = 1.50(\text{charged particle dose})_I$$

It may be seen that

$$(\text{charged particle dose})_I = (\mu\text{c/mg Na})_I (W_I/W_p)^{1/3} \times \left(\frac{\text{charged particle dose to phantom}}{\mu\text{c/mg Na in phantom}}\right)$$

where I refers to the individual case and $(W_I/W_p)^{1/3}$ is a correction factor based on the weight W. From the experimental data obtained on the Na^{24} activation in the phantoms, Section 3, it may be seen that

$$\left(\frac{\text{charged particle dose to phantom}}{\mu\text{c/mg Na in phantom}}\right) = 1.40 \times 8.65 \times 10^4 \text{ rads}/\mu\text{c mg}^{-1}$$

where the factor 1.40 is a correction for the energy lost under the bias of the neutron dosimeter, as derived in Section 4.

The first collision γ-doses (external doses) for the individuals may be expressed as

$$(D_\gamma)_{\mathrm{G,D,B}} = \frac{3.6}{1.4} \times 0.82\ (\text{charged particle dose})_I$$

$$(D_\gamma)_{\mathrm{H,V,M}} = \frac{4.1}{1.4} \times 0.82\ (\text{charged particle dose})_I$$

where we have used the results of Table 1 for the quantities D_γ/D_n most appropriate to the individuals, and the factor 0.82 corrects the D_γ/D_n ratios as measured in the constant power reactor experiment to the values appropriate to the intensity–time relationship for the accident.

Table 6. Individual sodium activation and related data

Individual	Total Na^{24}(μc)	Wt. (kg)	Na^{24} (μc/mg Na)	$(W_I/W_p)^{1/3}$
H	53	65	5.44×10^{-4}	1.00
V	82	80	6.83×10^{-4}	1.08
G	76	70	7.24×10^{-4}	1.03
M	75	72	6.94×10^{-4}	1.04
D	63	52	8.07×10^{-4}	0.93
B	45	90	3.33×10^{-4}	1.12
(Phantom)		65		

Table 6 shows the individual sodium activation as reported by JAMMET *et al.*[3], the weights of the individuals, and the magnitude of the factor $(W_I/W_p)^{1/3}$. The individual doses as determined by the equations above are shown in Table 7.

The main uncertainty in the dose values given in Table 7 is associated with the H(N, γ)D dose component. As already stated, this value may

Table 7. Individual doses (all values are in rad *units)*

Individual	Charged particle dose	H(n, γ)D γ-dose	External γ-dose	Total
H	66	99	158	323
V	89	133	214	436
G	90	135	189	414
M	87	130	209	426
D	91	136	192	419
B	45	67	95	207

be too high by a factor of about 2; however, even in this case, the total doses would be decreased only by about 15 per cent. The uncertainties associated with the other dose components are smaller; the standard deviations for the charged particle doses and for the external γ-doses are estimated to be $\pm$ 12 per cent and $\pm$ 14 per cent, respectively.

Work is now in progress on the study of Na^{24} activation in phantoms of various shapes and sizes and with neutrons of various energies. The question of biological elimination of Na^{24} is being investigated with living animals exposed at various dose levels. When these studies have been completed, it may be desirable to re-evaluate the individual doses received from the various radiation accidents, including the Y-12 (Oak Ridge) accident and the Yugoslavia accident.

APPENDIX A

γ-Dose Leakage Computations

A.1. *Computation of the leakage of γ-rays originating in fuel rods*

The computation proceeds by a numerical evaluation of the following integral:

$$D_\gamma(\mathbf{R}) = \int d\mathbf{r} S(\mathbf{r}) \frac{d_\gamma(|\mathbf{p}|,\vartheta)}{4\pi(|\mathbf{R}-\mathbf{r}|)^2}$$

where $\mathbf{R}$ is a vector from the center of the reactor to the field point where the leakage dose is desired, $\mathbf{r}$ is a vector from the reactor center to the volume element $d\mathbf{r}$ where the γ-source strength is $S(\mathbf{r})$, $\mathbf{p}$ is the part of the vector $\mathbf{R}-\mathbf{r}$ which lies inside the reactor volume, and ϑ is the angle between $\mathbf{R}$ and the cylinder axis. The source distribution function $S(\mathbf{r})$ is obtained from the neutron leakage calculation described above and is equal to the number of photons per fission times the normalized fission probability in the homogenized reactor.

The dose attenuation kernel $d_\gamma(\mathbf{r})$ is calculated by summing over the distribution of energies present in the particular source after weighting each energy component by an attenuation factor which is calculated using known absorption coefficients and build-up factors and a self-absorption factor to account for fuel rod attenuation. More specifically,

$$d_\gamma(r,\vartheta) = \int dE\, n_\gamma(E)\, \mathscr{D}_0(E)\, B[E, r\mu(E)] \times e^{-r\mu(E)}\, \mathscr{S}(E, \mu_r(E)a, \vartheta)$$

where r is the distance from an isotropic point source in an infinite D_2O medium, $\mathscr{D}_0(E)$ is the first collision dose in rads/photon $\times$ cm^{-2} delivered by photons of energy E, $\mu(E)$ is the mass absorption coefficient of the medium for photons of that energy, and $B[(E), r\mu(E)]$ is the build-up factor for photons in the medium. We have chosen to use infinite medium build-up factors even though the systems are bounded.[24] The error incurred in making this approximation should be approximately 10 per cent.

The self-absorption factor $\mathscr{S}(E, \mu_r(E)a_0, \vartheta)$ is calculated by carrying out an integral over the cross-section of the rod at radius a_0, using attenuation coefficients, $\mu_r(E)$, appropriate to natural uranium at the energy E, and taking into account the angle ϑ which the direction of observation makes with the axis of the rod. Build-up factors for the part of the photon path lying inside the rod were taken to be appropriate to the same distance, measured in g/cm^2, in the D_2O medium, as suggested by GOLDSTEIN and WILKINS[25]. As mentioned in Section 4.2.1, rod attenuation of photons not originating in a particular rod is neglected, since the rod radius is small in comparison with the lattice pitch.

Fig. 8 shows a graph of the attenuation kernel for the prompt fission γ-spectrum for the case of no rod absorption and for a natural uranium rod 1 in. in diameter viewed at various angles with respect to the rod axis. Note that the curve labeled $\vartheta = 14.5°$ is probably too small in magnitude since the simple ray path length approach used here will surely break down at grazing angles relative to the rod axis. A "short circuiting" effect will become important, i.e. photons emerging from the rod in directions nearly perpendicular to the axis may make collisions on D_2O molecules which will deflect them into directions nearly parallel with the rod axis. These photons may contribute in larger quantity than those taking longer paths through the rod. However, small values of ϑ are not required for the calculation of doses to any of the stations measured in the experiment.

Table 8 shows values of $4\pi R^2 D_\gamma$ vs. R for three

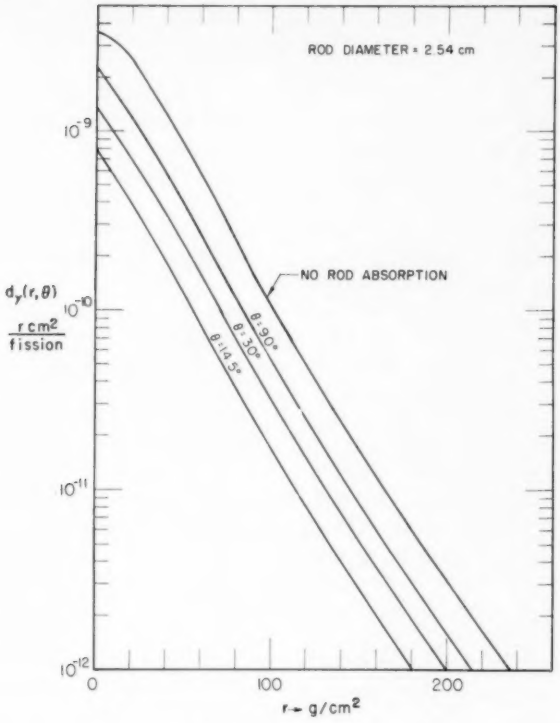

FIG. 8. Attenuation kernel for prompt fission γ-ray spectrum.

Table 8. Dose due to prompt fission γ-rays as a function of distance from reactor

R (cm)	$4\pi R^2 D_\gamma$(r cm²/fission)		
	$\vartheta = 90°$	$\vartheta = 30°$	$\vartheta = 14.5°$
300	2.31×10^{-10}	1.21×10^{-10}	0.795×10^{-10}
400	2.21×10^{-10}	1.19×10^{-10}	0.743×10^{-10}
500	2.16×10^{-10}	1.19×10^{-10}	0.715×10^{-10}
600	2.12×10^{-10}	1.18×10^{-10}	0.697×10^{-10}

different viewing angles, ϑ, and for the prompt fission γ-source distribution.

A.2. *Estimate of fission product γ-contribution to the total dose*

The rate of energy release as photons by fission products may be taken to be the following function of time:[26]

$$E(e) = \frac{0.62}{1+t}\ \text{MeV/sec fission}$$

where t is in seconds and $t \leq 1000$ sec. For comparison, the total photon energy released in prompt fission was taken to be 7.2 MeV.[26]

First, R_s, the ratio of photon energy released per unit time by fission products to the prompt fission rate at the end of approximately 15 min of steady operation is given by

$$R_s = \frac{1}{7.2\ \text{MeV}} \times 0.62 \int_0^{900} \frac{dt}{1+t}\ \text{MeV} \simeq \frac{0.62}{7.2} \ln 900 = 0.586$$

and this ratio should apply at the time measurements of the γ-dose rate were made during the experiment.

Next, R_a, the ratio of total photon energy released by fission products in a time T, during which the reactor is critical on a 10-sec doubling time,* to the prompt fission γ-energy released may be shown to be

$$R_a = \frac{1}{7.2 \text{ MeV}} \times \frac{0.62}{t_0(1 - e^{-T/t_0})} \int_0^T e^{-T/t_0} \ln (1 + t - \tau)\, d\tau$$

where $t_0 = 10 \text{ sec}/0.693$. For an operating time T of 4 min,[27] the above expression is closely equal to

$$R_a = \frac{0.62}{7.2} e^{1/T_0} E_1(1/t_0)$$

Numerical evaluation of these quantities, using values from the data of RITCHIE *et al.*[16] gave the more accurate values of $R_s = 0.632$ and $R_a = 0.219$.

The procedure used in estimating the dose from fission product γ-rays was to assume that the dose attenuation kernel appropriate to this photon distribution is the same as that appropriate to the prompt fission γ-distribution. This should be a good approximation for our purposes.[27] Using this assumption, the leakage calculation for prompt fission γ-rays had only to be scaled by the factors R_s and R_a displayed above in order to obtain the quantities sought.

APPENDIX B

Studies of Na^{24} *Activation in Man-shaped Phantoms*

B.1. *The Los Alamos burro experiment*

An experiment[28] was performed at the Godiva II reactor of Los Alamos Scientific Laboratory to determine whether a phantom composed of a thin shell filled with an aqueous sodium solution could be substituted for a live animal in studies of the relationship between neutron dose and Na^{24} production in the irradiated substance.

A live burro was placed in an aluminum tank which was then filled with NaCl solution and irradiated at 3 m, center to center, from Godiva. Samples of the burro blood serum and of the NaCl solution were prepared and the Na^{24} activities were determined. The burro was removed, the tank refilled with NaCl solution and an exposure made again at the same position. The NaCl solution was sampled and its Na^{24} activity determined. During the second exposure the region in the tank which had previously been filled by the burro was filled by a homogeneous aqueous NaCl solution. The region was, of course, of the same size and shape when filled with NaCl solution as when filled with the burro. If the amount of Na^{24} produced (in the burro and the surrounding NaCl solution) by the first irradiation was, within experimental error, the same as that produced by the second irradiation (when only NaCl solution was present), then the production of Na^{24} in a homogeneous phantom could be considered to be sufficiently quantitatively similar to the production of Na^{24} from the Na^{23} heterogeneously distributed in a live animal that phantoms could be substituted for animals. Concentrations of Na^{24} in the burro and the NaCl solution around it were weighted by the respective volumes and averaged, then compared to the Na^{24} concentration in the full tank of NaCl solution, normalized to the same exposure dose. Relative difference in the amount of Na^{24} produced by the two exposures was 2.9 per cent which is well within the probable experimental error; hence it was concluded that when a man-shaped phantom is filled with a sodium chloride solution, a good approximation to a man is obtained relative to sodium activation.

B.2. *Distribution of* Na^{24} *in phantoms irradiated at Vinča*

Na^{24} concentrations in the phantoms are listed in Tables 9 and 10. All concentrations are corrected to zero time (effective exposure time) and are expressed in μc Na^{24}/mg Na^{23} per rad. Two tables are given because the two

* Private communication with H. D. BROWN and D. NEWBY.

Table 9. Na^{24} *concentrations in molded phantoms*

Segment	Na^{24} Concentration (μc Na^{24}/mg Na^{23}/rad) $\times 10^5$					
	Calvin I	Remab I	Tyrone I	Calvin II	Remab II	Tyrone II
Head and upper torso	1.44	1.44	1.30	1.55	1.38	1.45
Upper left arm	1.16	1.72	1.75	1.54	1.65	1.82
Upper right arm	1.60	1.28	1.13	1.94	1.45	1.68
Lower left arm	1.18	1.57	1.70	1.78	1.77	1.91
Lower right arm	1.54	1.21	1.17	1.89	1.36	1.84
Lower torso	0.848	0.929	0.781	1.10	0.875	1.01
Gonads	0.842	1.04	1.02	2.08	1.85	1.07
Upper left leg	0.914	1.12	1.16	1.34	1.22	1.23
Upper right leg	1.12	1.03	0.879	1.35	1.27	1.26
Lower left leg	1.13	1.40	1.46	1.60	1.39	1.69
Lower right leg	1.34	1.46	1.18	1.68	1.38	1.63
Average	1.09	1.17	1.09	1.38	1.24	1.28

types of phantoms are segmented slightly differently; in both tables the numerals I and II after the name of the phantom indicate first and second high-power exposures, respectively. The molded plastic phantoms, in Table 9, were designated "Calvin", "Remab" and "Tyrone"; the polyethylene bottle phantom, in Table 10, was called "Bomab". The segments labeled "average" were averaged by mixing and sampling the total solution of each phantom.

APPENDIX C

Intercomparison of French and American Na^{24} *Calibration*

C.1. *Summary of the Saclay* Na^{24} *counting method*

The total amount of Na^{24} present in the bodies of the exposed persons was determined by the French group using a scintillation counter. The detector, a 1.5-in. $\times$ 1-in. sodium iodide crystal, was placed at the center of an arc of 1 m radius. The individual to be measured lay on the floor facing the detector and curved so as to fit just inside the arc. A twenty-five-channel analyzer was used in conjunction with this detector. As used, the response peak from Cs^{137} γ-rays was in the ninth channel and that from K^{40} γ-rays was in the twentieth channel. The activity measured in the six persons was known to be Na^{24} from energy and half-life considerations. The equipment was calibrated with a polyethylene bottle containing Na^{24} solution of known activity. This bottle was moved along the inside of the arc to measure the angular dependence of the response of the detector. The size of the bottle (15 cm diameter, 25 cm height) was chosen such that the ratio of counts in channels 1–5 to the counts in channels 16–18 was approximately the same whether the activity in the bottle or the activity in the persons was being measured.

Table 10. Na^{24} *concentrations in bottle phantoms*

Segment	Na^{24} Concentration (μc Na^{24}/mg Na^{23} per rad) $\times 10^5$	
	Bomab I	Bomab II
Head	1.40	1.34
Neck	1.33	1.29
Left arm	1.11	1.46
Right arm	1.62	1.58
Upper torso	0.853	1.00
Lower torso	0.755	0.865
Upper left leg	0.846	1.06
Upper right leg	1.11	1.11
Lower left leg	1.03	1.16
Lower right leg	1.25	2.40
Average	0.991	1.10

C.2. *Studies of the Saclay* Na^{24} *counting geometry*

In order to confirm the method of calibration of the equipment used to measure the Na^{24} activity of the exposed individuals, an experiment was performed at ORNL using a similar crystal, 1.5-in. × 1-in. sodium iodide. A molded plastic phantom (Remab) and the bottle phantom (Bomab) were filled with a homogeneous aqueous solution of Na^{24} of known concentration. The Na^{24} γ-ray activity of the phantoms was measured using the same geometry as had been used to measure the Na^{24} activity of the exposed persons, i.e. the crystal was at the center of an arc of 1 m radius, and the phantom was positioned inside the arc, lying on its side on the floor.

Table 11. *Relative counting efficiency for* Na^{24} *in a bottle and in phantoms*

Energy (MeV)	Relative counting efficiency		
	Bottle	Remab	Bomab
0.366	1.00	0.984	0.997
0.66	1.00	0.969	0.971
1.16	1.00	0.980	1.00
0.366/1.16	2.66	2.66	2.64

The counting efficiency of this geometry was compared to the counting efficiency determined by placing a polyethylene bottle, 15 cm in diameter and 25 cm in height, filled with Na^{24} solution at various positions inside the 1-m arc. The response of the crystal was found to be independent of the position of the bottle along the arc. Integral measurements were made at energies of 0.366, 0.66 and 1.16 MeV. The ratio of the count rate at 0.366 MeV to the count rate at 1.16 MeV was found to be the same for the two phantoms and for the bottle. The results of this experiment, normalized to the counting efficiency for Na^{24} in the bottle, are given in Table 11.

C.3. *Direct intercomparison of Saclay and Oak Ridge* Na^{24} *counting methods*

In order to compare the calibration of the French equipment used to measure the Na^{24} in the bodies of the exposed individuals to the calibration of the ORNL equipment used to determine the Na^{24} concentration in the phantoms, average samples of Calvin II, Remab II and Tyrone II solutions were prepared and sent to Paris for Na^{24} measurements. The results of the French analysis were communicated to us by H. JAMMET and L. JEANMAIRE on 31 May, 1960. An additional solution sample which had been prepared by dissolving irradiated solid NaCl was included in order to obtain a higher disintegration rate. Activity concentrations of the solutions are listed in Table 12.

APPENDIX D

Study of the Neutron Flux Distribution in the Vinča Reactor Room

In order to document neutron data previously given, some of the data from the two high-power runs at Vinča are shown in Figs. 9 through 16. The data presented are from the secondary stations consisting of sulfur, gold and cadmium-shielded gold. Locations of the various stations are shown in Fig. 2.

Table 12. *Cross calibration of French and ORNL equipment for measuring* Na^{24} *concentration*

Solution	ORNL value (μc/ml) × 10^3	French value (μc/ml) × 10^3	ORNL value / French value
Calvin II	1.06	1.03	1.03
Remab II	1.19	1.16	1.03
Tyrone II	1.09	1.05	1.04
Solution from solid NaCl	33.2	33.9	0.98

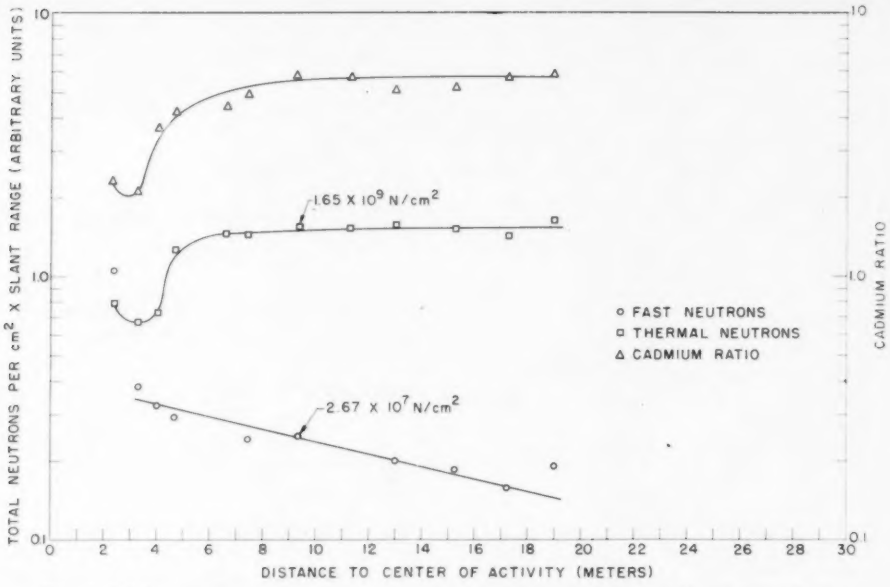

FIG. 9. High-power run no. 1: line running east through LPS-5, 108 cm from floor.

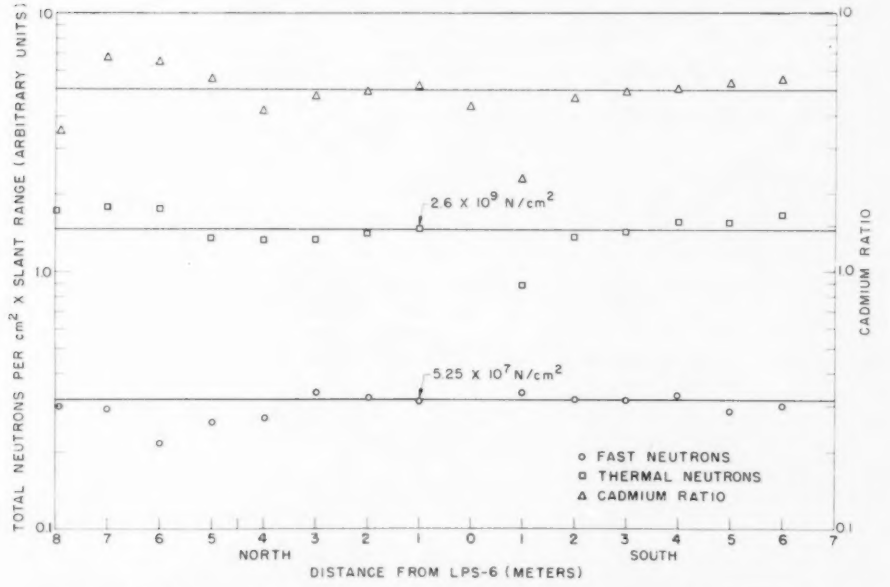

FIG. 10. High-power run no. 1: horizontal traverse 108 cm from floor running north and south through LPS-6.

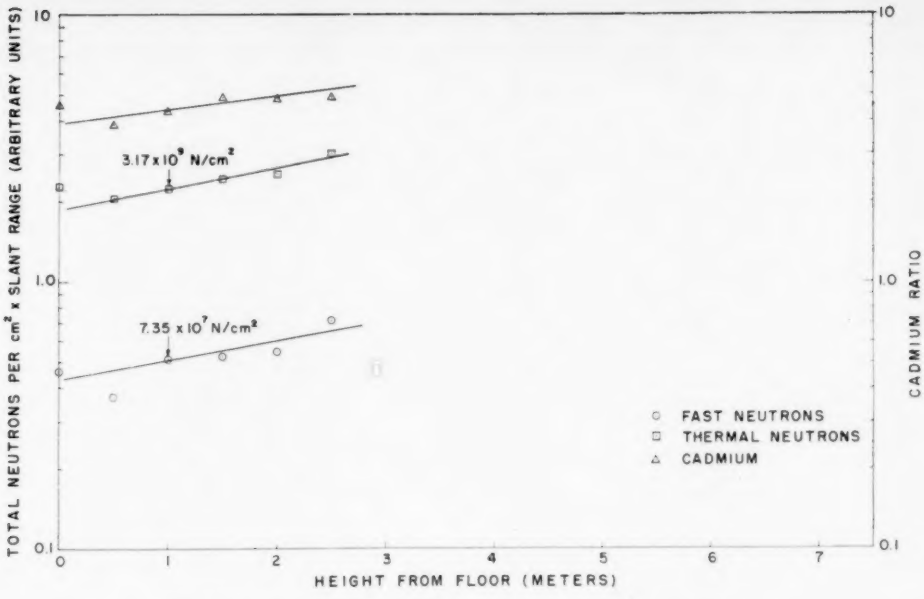

FIG. 11. High-power run no. 1: vertical traverse at LPS-2.

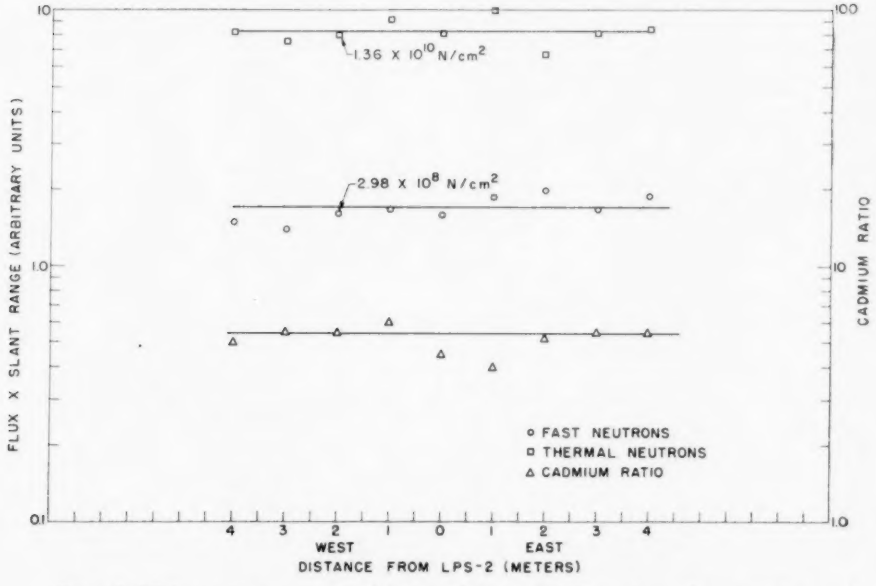

FIG. 12. High-power run no. 2: horizontal traverse 108 cm from floor running east and west through LPS-2.

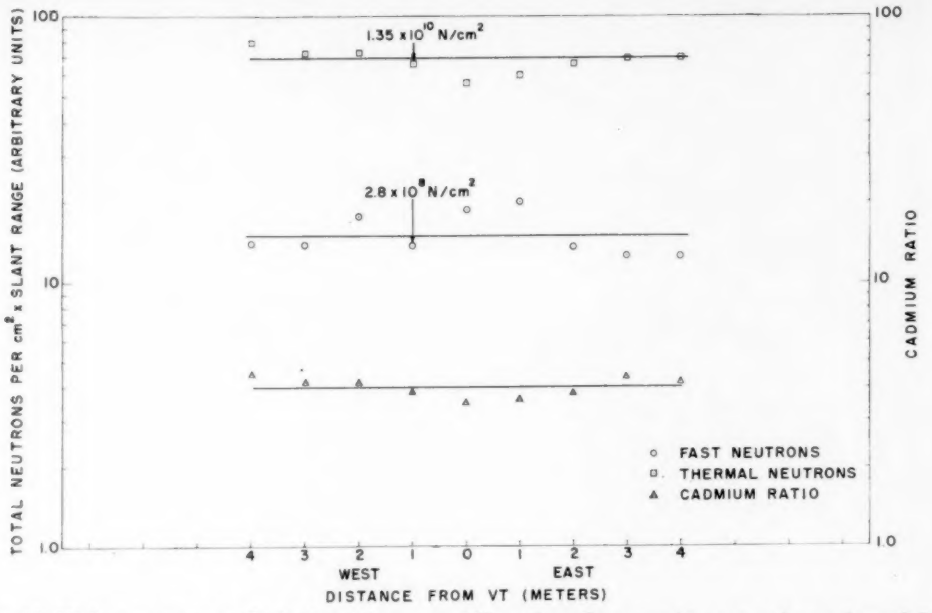

FIG. 13. High-power run no. 2: horizontal traverse 108 cm from floor running east and west through VT.

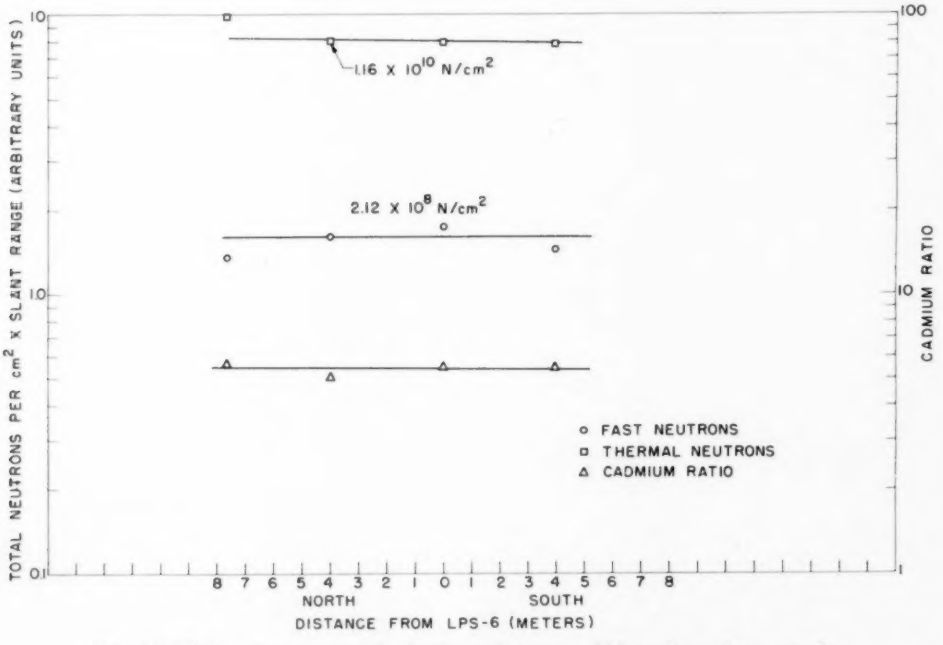

FIG. 14. High-power run no. 2: horizontal traverse 108 cm from floor running north and south through LPS-6.

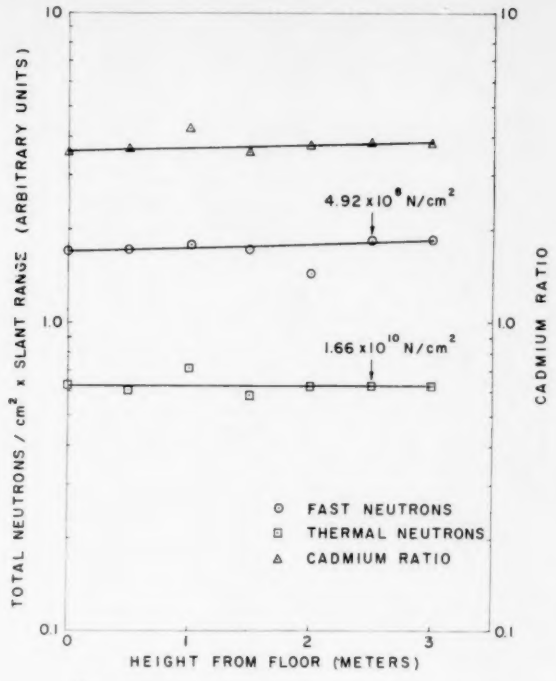

FIG. 15. High-power run no. 2: vertical traverse through VT.

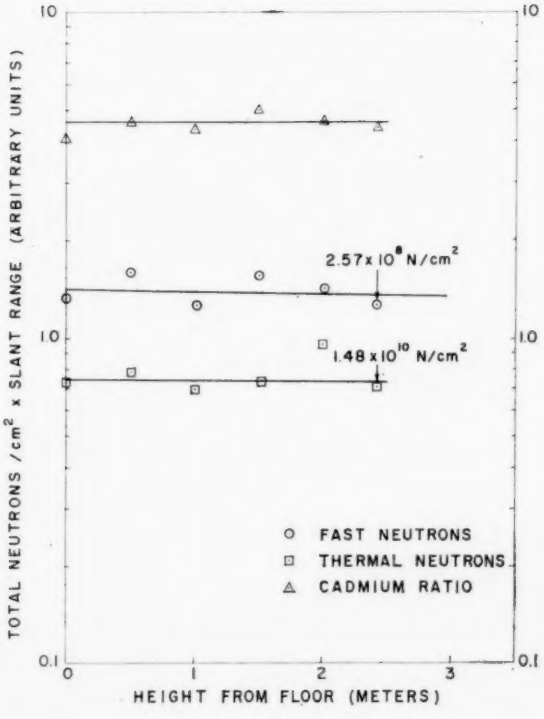

FIG. 16. High-power run no. 2: vertical traverse 3 m west of VT.

APPENDIX E*

Neutron Measurements with a Tissue-equivalent Phantom

Abstract—Measurements were made through a phantom with fast and slow neutron detectors. These measurements are the basis of a method of dose determination at present in its experimental stages. The Vinča results are therefore presented only to indicate the relative contribution from back-scattered neutrons.

E.1. *Apparatus*

The phantom used was a $\frac{1}{4}$-in. thick Polythene container, 60 cm high of elliptical cross-section, with a major axis 36 cm and minor axis 20 cm. This was filled with an approximately tissue-equivalent liquid (6.24×10^{22} atoms/cm^3 H, 0.669×10^{22} atoms/cm^3 C, 0.169×10^{22} atoms/cm^3 N, 3.25×10^{22} atoms/cm^3 O).

A light but rigid internal framework of Perspex supported a series of small detectors through the phantom, on a line at 15° to the normal in both horizontal and vertical directions to minimize the shielding effect of one detector on another.

The detectors used in the first high level run at Vinča, to measure flux above 0.5 MeV, were 0.5-cm wide track plates wrapped in cadmium foil. Each track plate was a sandwich of two Ilford E1 50-μ emulsions, with glass backing, separated by a 250-μ Polythene radiator, and was oriented at an angle of 45° to the front surface of the phantom. Under these conditions the response is constant with neutron energy between 0.5 MeV and 8 MeV at 1.26×10^{-3} tracks/neutron to within $\pm$ 15 per cent.

The detectors used in the second high level run were gold foils (260 mg/cm^2 thick) to determine the slow neutron distribution. Previous experiments using 0.13 MeV, 2.5 MeV, 14 MeV and Po–Be neutrons have shown that the shape of the curve through a phantom obtained from these gold foils is the same as that given by either manganese foils or sodium samples, despite the difference in resonance integrals.

E.2. *Method*

From the relaxation length of the neutron flux in the phantom, as measured by the track

Table 13. *Relaxation length for various neutron energies*

Neutron energy	Relaxation length (cm)
1 MeV (monoenergetic)	4.6
2.5 MeV (monoenergetic)	6.3
Po–Be spectrum (mean 4.5 MeV)	10.0
14 MeV (monoenergetic)	20.0

* This Appendix was written by J. W. Smith, United Kingdom Atomic Energy Authority, Harwell, Berks.

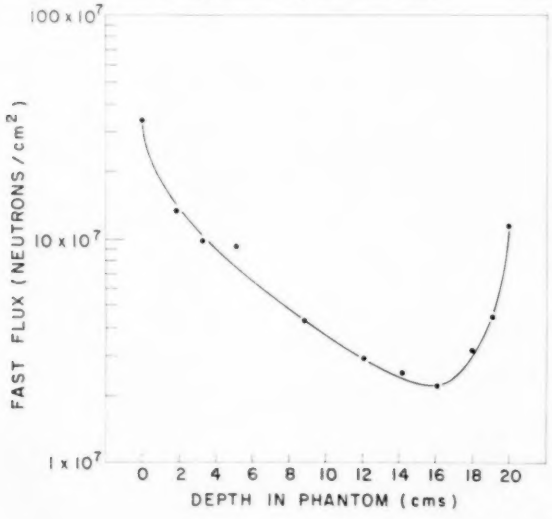

Fig. 17. Flux above 0.5 MeV given by track plates.

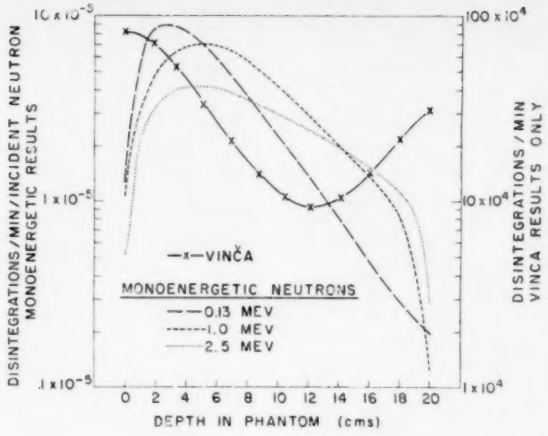

FIG. 18. Distribution of gold foil activity in phantom.

plates, the mean energy of the neutrons with energies greater than 0.5 MeV may be found by comparison with the relaxation lengths obtained by irradiating the phantom with monoenergetic neutrons. The results of these experiments are given in Table 13.

E.3. *Results*

Track plate results from the Vinča experiment are shown in Fig. 17. It can be seen that the back-scattered fast flux is about one-third of the incident fast flux and that the energy indicated by the shape of the curve is considerably lower than the energy of the direct neutrons. It seems possible that the high back-scatter is due to the angle of irradiation; the midline of the phantom was 112 cm above the floor of the reactor hall on the lip of the reactor well so that the angle of elevation to the center of the reactor was about 30°.

Fig. 18 compares the gold foil results from Vinča with previous gold foil curves for neutrons of known energy, all taken with the 20-cm phantom.

Acknowledgments—The authors are pleased to acknowledge the expert services and help given by R. BARKER, G. JENSSEN, G. W. C. TAIT and D. BROWN of the International Atomic Energy Agency in Vienna in making all arrangements for co-operation of the various groups in the experimental investigations; JACKY WEILL, J. FURET, and their associates, the electronics controls group from Centre D'Etudes Nucleaires, Saclay, France, who designed the control equipment and operated the reactor; the Yugoslav Federal Nuclear Energy Commission, expecially S. NAKICENOVIĆ and D. BAUM; V. BABIĆ, Director of the Boris Kidrič Institute, and his scientific staff, particularly D. POPOVIĆ, P. ANASTASIJEVIĆ, and their associates for their full co-operation during the investigation.

We are particularly indebted to H. JAMMET and L. JEANMAIRE, Centre D'Etudes Nucleaires, Saclay, for providing us with Na^{24} data and other information to which the final data are normalized.

Thanks are also due to V. E. ANDERSON of the Oak Ridge Gaseous Diffusion Plant, and H. B. ELDRIDGE, Oak Ridge National Laboratory, for their expert work in performing numerical computations, and to F. J. DAVIS, ORNL, for his advice and assistance in connection with the experimental program.

The authors are most grateful for many valuable suggestions from J. W. SMITH, author of Appendix E, and J. A. DENNIS, United Kingdom Atomic Energy Research Establishment, Harwell, England.

REFERENCES

1. P. P. SAVIĆ, *Bull. Inst. Nucl. Sci. Boris Kidrich* **?**, No. 167 (1959).
2. D. POPOVIĆ, S. TAKAČ, H. MARKOVIĆ, N. RAIŠIĆ, Z. ZDRAVKOVIĆ and LJ. RADANOVIĆ, *Bull. Inst. Nucl. Sci. Boris Kidrich* **9,** No. 168 (1959).
3. H. JAMMET, G. MATHÉ, B. PENDIC, J. F. DUPLAN, B. MAUPIN, R. LATARJET, D. KALIC, L. SCHWARZENBERG, Z. DJUKIC and J. VIGNE, *Rev. Franc. Études Clin. et Biol.* **4,** 210 (1959).
4. G. MATHÉ, H. JAMMET, B. PENDIC, L. SCHWARZENBERG, J. F. DUPLAN, B. MAUPIN, R. LATARJET, M. J. LARRIEU, D. KALIC and Z. DJUKIC, *Rev. Franc. Études Clin. et Biol.* **4,** 226 (1959).

5. *Accidental Radiation Excursion at the Y-12 Plant* Y-1234 (1958).
6. G. S. Hurst, R. H. Ritchie and L. C. Emerson, *Health Phys.* **2,** 121 (1959).
7. E. B. Wagner and G. S. Hurst, *Rev. Sci. Instrum.* **29,** 153 (1958).
8. E. B. Wagner and G. S. Hurst, *Health Phys.* In press.
9. L. H. Ballweg and J. L. Meem, *A Standard Gamma-Ray Ionization Chamber for Shielding Measurements.* ORNL-1028 (1951).
10. G. S. Hurst, J. A. Harter, P. N. Hensley, W. A. Mills, M. Slater and P. W. Reinhardt, *Rev. Sci. Instrum.* **27,** 153 (1956).
11. P. W. Reinhardt and F. J. Davis, *Health Phys.* **1,** 169 (1958).
12. G. S. Hurst and R. H. Ritchie (Editors), *Radiation Accidents: Dosimetric Aspects of Neutron and Gamma-Ray Exposures.* ORNL-2748 (1959).
13. C. L. Daws, J. M. Bookston and R. E. Smith, *GNU-II, A Multigroup One-Dimension Diffusion Equation.* GMR-101 (1957).
14. A. M. Weinberg and E. P. Wigner, *The physical Theory of Neutron Chain Reactors.* The University of Chicago Press, Chicago, Illinois (1958).
15. H. D. Brown and D. Newby, International Atomic Energy Agency, Vienna, Austria. Private communication.
16. R. H. Ritchie, H. B. Eldridge and V. E. Anderson, Calculation of the radiation yield from fission assemblies and comparison with experiments. *Proceedings of the International Symposium on Selected Topics in Radiation Dosimetry, Vienna, Austria, June,* 1960. To be published.
17. G. S. Hurst, *Brit. J. Radiol.* **27,** 353 (1954).
18. E. B. Wagner and G. S. Hurst, *Health Phys.* **2,** 57 (1959).
19. D. Popović, Boris Kidrić Institute, Vinča, Yugoslavia. Private communication.
20. F. C. Maienschein, R. W. Peelle, W. Zobel and T. A. Love, *Second United Nations International Conference on Peaceful Uses of Atomic Energy* Vol. 15, pp 366–372. United Nations, New York (1958).
21. G. A. Bartholomew and L. A. Higgs, *Compilation of Thermal Neutron Capture Gamma Rays.* CRGP-784 (1958).
22. G. W. Grodstein, *X-Ray Attenuation Coefficients from* 10 keV *to* 100 MeV. National Bureau of Standards Circular 583, Washington, D.C. (1957).
23. National Bureau of Standards Handbook 63, *Protection Against Neutron Radiation up to* 30 *Million Electron Volts.* Washington, D.C. (1957).
24. H. Goldstein and J. E. Wilkins, Jr., *Calculations of the Penetration of Gamma Rays.* NYO-3075 (1954).
25. H. Goldstein and J. E. Wilkins, Jr., *Calculations of the Penetration of Gamma Rays* p. 64. NYO-3075 (1954).
26. H. Goldstein, *Fundamental Aspects of Reactor Shielding* p. 63. Addison-Wesley, Cambridge, Massachusetts (1959).
27. H. Goldstein, *Fundamental Aspects of Reactor Shielding* p. 58 *et seq.* Addison-Wesley, Cambridge, Massachusetts (1959).
28. F. W. Sanders and J. A. Auxier, Neutron activation of sodium in anthropomorphous phantoms. *Health Phys.* To be published.

Health Physics Pergamon Press 1961. Vol. 5, pp. 203–211. Printed in Northern Ireland

MEASUREMENT OF ELECTRON FLUX IN MEDIA BOMBARDED BY X-RAYS

D. R. NELSON, R. D. BIRKHOFF, R. H. RITCHIE and H. H. HUBBELL, Jr.
Health Physics Division, Oak Ridge National Laboratory,* Oak Ridge, Tennessee

(*Received* 7 *March* 1960)

Abstract—The energy distribution of the electron flux generated by lightly filtered 250–kV constant potential X-rays has been determined for copper, aluminum and graphite in the form of pairs of parallel plates. The space between the plates was kept at high vacuum and the plate current was recorded as a function of plate voltage. Saturation currents of 0.0063, 0.0011 and 0.00024 e.s.u. $cm^{-2}\ r^{-1}$ for the three chambers, respectively, were obtained at about 30 V plate potential. The energy distributions were calculated from the first and second derivatives of the current–voltage curves. The zero of energy was taken at the bottom of the conduction band. Observations were confined to those electrons able to escape from the material, i.e. those having an energy greater than $(E_F + \phi)$ where E_F is the Fermi energy and ϕ is the work function. The electron flux inside the plates was found to be largest at $E_F + \phi$, and to decline smoothly by an order of magnitude only 2 V higher.

1. INTRODUCTION

ALTHOUGH the ionization per unit volume and energy deposited per unit mass by radiation are useful indices of radiation exposure, a more detailed knowledge of the interaction of the radiation with the absorber is required before biological damage may be quantitatively assessed. In fact, the differences in biological damage found for the same energy deposition from different radiations have led to the introduction of a factor called the relative biological effectiveness which may be different for the various types of radiation and for different biological effects. PLATZMAN[1] has pointed out that a study of the low-energy electrons liberated in a medium by the passage of ionizing radiation may be an important preliminary to a more thorough understanding of the mechanism of biological damage.

A related, but not identical problem has received considerable experimental attention in recent years; namely, the measurement of the energy spectrum of electrons ejected from surfaces by the action of corpuscular radiation. WOLFF[2] has developed a theory of the energy distributions of secondary electrons from surfaces bombarded by electron beams and has obtained approximate agreement with experiments.

GREENING[3] has made a semiquantitative estimate of the low-energy electron distribution emerging from the walls of an irradiated chamber. His calculations are based on secondary emission experiments, and predict that only a small fraction of the electrons will have energy in excess of 100 eV.

Interpretation of secondary emission experiments is complicated by the boundary which is necessarily placed in the irradiated medium. Ideally, the medium should be of effectively infinite extent and bombarded isotropically in order to facilitate theoretical interpretation. Experiments of this type have been carried out by TAYLOR[4] who has investigated the small currents which persist in irradiated ionization chambers even when the chambers are evacuated to a pressure where gaseous ions make a negligible contribution. Analysis of his data to determine energy distribution of the electrons was complicated by his use of a cylindrical chamber. Experiments similar to Taylor's are

* Operated by Union Carbide Corporation for the U.S. Atomic Energy Commission.

described in the present work, utilizing a parallel-plate chamber which is more readily amenable to theoretical analysis.

McKay[5] in his review article on secondary emission has mentioned some of the many experimental difficulties found in the application of conventional electron spectrometers to low-energy spectral measurements. Many of these difficulties may be avoided by applying a stopping potential to the plates for energy analysis as was done in the present work. The electron flux distribution inside the metal plates was calculated from the current–voltage curve of the chamber from a theory based on assumptions of an isotropic distribution of the low-energy electrons inside the plates and a classical model of the barrier penetration.*

2. THEORY

Inside the medium the secondary electrons generated by the high-energy Compton and photoelectrons are assumed to have an isotropic angular distribution. Support for this assumption may be found from the observation that although the primary X-rays strike the plates unidirectionally, equal numbers of electrons having identical energy distributions are found to be emitted from the inner surfaces of the plates. The flux of electrons inside the medium is then defined as the number of electrons crossing a spherical probe having unit cross-sectional area, and this flux is assumed to be independent of both the position of the probe and the angle with which the electrons cross the probe. If E_i is the energy of an electron inside the medium, then the flux or number of electrons in the medium per unit area per roentgen per unit solid angle per unit energy is defined by $N(E_i)$ and the total number crossing the probe within a solid angle $d\Omega_i$ and having energies between E_i and $E_i + dE_i$

$$N(E_i)\, dE_i\, d\Omega_i = 2\pi N(E_i)\, dE_i \sin\theta_i\, d\theta_i \quad (1)$$

where θ_i is the angle with the normal to the surface.

In the Sommerfeld free electron model of a metal, an electron emerging from the metal surface gains a potential energy and loses a kinetic energy in the amount $E_w = E_F + \phi$ where E_F is the Fermi energy and ϕ is the work function. The energy an electron has outside the plates E_0 is then

$$E_0 = E_i - E_w \quad (2)$$

The velocity component parallel to the spectrometer plates is the same for a given electron inside and outside the medium, and it is easily shown that

$$E_i \cos^2\theta_i = E_w + E_0 \cos^2\theta_0 \quad (3)$$

Equation (3) may be solved for $\cos\theta_i$, and this quantity when differentiated yields the differential solid angle inside the medium in terms of the electron energy and angle in the vacuum space.

$$2\pi \sin\theta_i\, d\theta_i = \frac{2\pi E_0 \cos\theta_0 \sin\theta_0\, d\theta_0}{\sqrt{(E_0 + E_w)}\sqrt{(E_w + E_0\cos^2\theta_0)}} \quad (4)$$

The flux of electrons inside the medium having energies between E_i and $E_i + dE_i$ and directed into the solid angle $d\Omega_i$ is then

$$N(E_i)\, dE_i\, d\Omega_i = 2\pi N(E_w + E_0)\, \frac{E_0\, dE_0}{\sqrt{(E_0 + E_w)}} \times \frac{\cos\theta_0 \sin\theta_0\, d\theta_0}{\sqrt{(E_w + E_0\cos^2\theta_0)}} \quad (5)$$

Because no electrons energetically able to cross the boundary will be lost, the above expression is equal to a new distribution $N'(E_0, \theta_0)\, dE_0 d\Omega_0$ outside the medium, and from equation (5) this flux per unit solid angle per unit energy is

$$N'(E_0, \theta_0) = N(E_w + E_0) \times \frac{E_0 \cos\theta_0}{\sqrt{(E_0 + E_w)}\ \sqrt{(E_w + E_0\cos^2\theta_0)}} \quad (6)$$

Three useful results may be obtained from equation (6). If one multiplies both sides by $d\Omega_0 = 2\pi \sin\theta_0\, d\theta_0$ and integrates from $\theta_0 = 0$ to $\theta_0 = \pi/2$, one obtains

$$\int_{\theta_0=0}^{\theta_0=\pi/2} N'(E_0, \theta_0)\, d\Omega_0 = 2\pi N(E_w + E_0) \times \left[1 - \sqrt{\left(\frac{E_w}{E_w + E_0}\right)}\right] \quad (7)$$

* A more complete account of this work appears in Oak Ridge National Laboratory Report 2521 which has the same title as this paper.

Because the integral on the left is the total emission from the surface of the medium, and $2\pi N(E_w + E_0)$ is the emission from any point in the medium into the 2π solid angle toward the surface, the bracket represents the fraction of the total flux per unit energy interval which escapes from the surface.[2]

Secondly, in the case that $E_0 \ll E_w$, it is clear that the angular distribution exhibits a $\cos\theta_0$ dependence in agreement with a considerable body of experimental evidence with surfaces irradiated from the outside with monodirectional

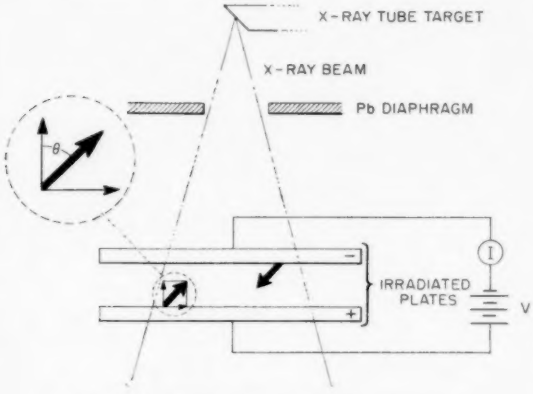

FIG. 1. Simplified schematic of apparatus.

electron beams.[5] For the case that E_0 is of the order of E_w, JONKER[6] has found that the angular distribution still follows the $\cos\theta_0$ dependence, and he interprets this as indicating that the angular distribution inside the medium also follows a cosine law. Since there appear to be no decisive theoretical arguments supporting this angular dependence inside the medium, we feel that this observation is either a peculiarity of the beam geometry or is merely a result of the experimental uncertainty involved in measuring the factor $\sqrt{(E_w + E_0\cos^2\theta_0)}$ which varies relatively slowly with θ_0 when E_0 is not too different from E_w. In any case, for the irradiation geometry employed here, it seems best to utilize the distribution of equation (6) which has the desirable property that, in the limit that $E_0 \gg E_w$, the distributions inside and outside the medium become identical, i.e., $N'(E_0, \theta_0) = N(E_w + E_0)$.

The experimental situation is shown in Fig. 1. It is clear that all electrons emitted from the negative plate will be collected by the positive plate. However, some electrons emitted from the positive plate will be unable to reach the negative plate and their counterparts from the negative plate will constitute a current in the external circuit. Thus all electrons with $E_0 < V$, and those with $E_0 > V$ but emitted at an angle θ_0 such that $\sqrt{(E_0)}\cos\theta_0 < \sqrt{V}$, will indirectly bring about a current. The total current from plates of area $A(\text{cm}^2)$ irradiated at a dose rate R (r/sec) is

$$\begin{aligned} I = eAR\,2\pi &\int_0^V \frac{N(E_w + E_0)}{\sqrt{(E_0 + E_w)}}\,E_0\,dE_0 \\ &\times \int_0^{\pi/2} \frac{\cos\theta_0 \sin\theta_0\,d\theta_0}{\sqrt{(E_w + E_0\cos^2\theta_0)}} \\ &+ eAR\,2\pi \int_V^\infty \frac{N(E_w + E_0)}{\sqrt{(E_0 + E_w)}}\,E_0\,dE_0 \\ &\times \int_{\cos^{-1}\sqrt{(V/E_0)}}^{\pi/2} \frac{\cos\theta_0 \sin\theta_0\,d\theta_0}{\sqrt{(E_w + E_0\cos^2\theta_0)}} \end{aligned} \tag{8}$$

The integrations over angle may be performed immediately and yield,

$$\begin{aligned} I = eAR\,2\pi \Big\{ &[\sqrt{(E_w + V)} - \sqrt{(E_w)}] \\ &\times \int_V^\infty N(E_w + E_0)\,\frac{dE_0}{\sqrt{(E_0 + E_w)}} \\ &+ \int_0^V N(E_w + E_0)[1 - \sqrt{\{E_w/(E_0 + E_w)\}}]\,dE_0 \Big\} \end{aligned} \tag{9}$$

The integral equation (9) may be differentiated twice with respect to the voltage.

$$\left(\frac{dI}{dV}\right)_V = eAR\,2\pi \left[\frac{1}{2\sqrt{(E_w + V)}} \times \int_V^\infty N(E_w + E_0)\,\frac{dE_0}{\sqrt{(E_0 + E_w)}}\right] \tag{10}$$

$$\begin{aligned} \left(\frac{d^2I}{dV^2}\right)_V = eAR\,2\pi \Big[&-\frac{1}{4(E_w + V)^{3/2}} \\ &\times \int_V^\infty N(E_w + E_0)\,\frac{dE_0}{\sqrt{(E_w + E_0)}} \\ &- \frac{1}{2\sqrt{(E_w + V)}}\,\frac{N(E_w + V)}{\sqrt{(E_w + V)}}\Big] \end{aligned} \tag{11}$$

Substitution of the integral in equation (10) into equation (11) yields

$$N(E_w + V) = \frac{1}{eAR\,2\pi} \times \left[-2(E_w + V)\left(\frac{d^2I}{dV^2}\right)_V - \left(\frac{dI}{dV}\right)_V \right] \quad (12)$$

The Fermi energies and photoelectric work functions are given in Table 1.

Table 1. *Fermi energy* E_F *and photoelectric work function* ϕ *for* Cu, Al *and graphite*

	E_F (eV)	ϕ (eV)
Copper	7.00	4.45
Aluminum	11.7	4.20
Graphite	0	4.56

3. EXPERIMENTAL APPARATUS AND PROCEDURE

The current–voltage curve must be measured very accurately in order that the first and second derivative calculated therefrom and the energy distribution shall have any accuracy. A major consideration in obtaining an accurate current–voltage curve was the stability of the X-ray machine or other source of ionizing radiation which might be used. The source of X-rays was a commercial 250-kV constant potential machine with a total of 4.5 mm of Al filtration. The output of the X-ray machine was kept reasonably stable with a Sorenson a.c. voltage regulator, Model 15000-2S. But even with this improved stability, erratic fluctuations having magnitudes of the order of 1 per cent still remained in addition to a 120 cycle ripple component of from 2 to 3 per cent. Of even more importance was a slow decrease in the X-ray output ranging from 1 to 3 per cent during a period of from 4 to 6 hr, the time usually required for a complete set of current–voltage measurements.

The points on the current–voltage curve had to be measured to an accuracy of about 0.02 per cent in order that the accuracy of the calculated second derivative might be of the order of 5 per cent. To achieve this accuracy, a second ion chamber was introduced as a monitor of the X-ray machine's output as shown in Fig. 2. The upper chamber is the test chamber with variable collecting voltage V and the lower chamber is the X-ray beam monitor having a constant saturation voltage V_M. Since both chambers were in the same X-ray beam, both indicated

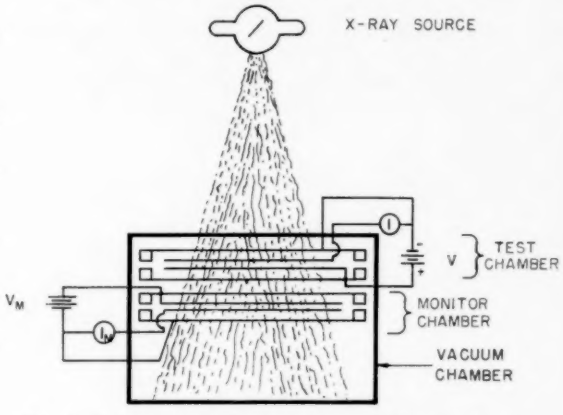

FIG. 2. Schematic of test chamber, monitoring chamber, and guard plates.

the same percentage beam fluctuation. Thus for a given applied voltage V on the test chamber, the ratio I/I_M of the chamber output currents remained constant, independent of any beam fluctuation. The two chamber currents I and I_M were therefore read simultaneously and a very accurate current–voltage curve was obtained from their ratio.

Both the test and monitor chambers consisted of four parallel plates as shown in Fig. 2. The two outer plates of the test and monitor chambers served to support the inner collecting plates and also stopped unwanted electrons generated elsewhere inside the vacuum system from being collected on the inner plates. The inner plates were separated from their supporting plates by eight Fluorothene insulators. The thickness of the plates used in the test chamber was made approximately equal to the range of a 250-keV electron in the medium being studied. Since 250 keV represents the maximum energy which could be produced by the X-ray machine, chamber plates having a greater thickness would not appreciably alter the spectrum of

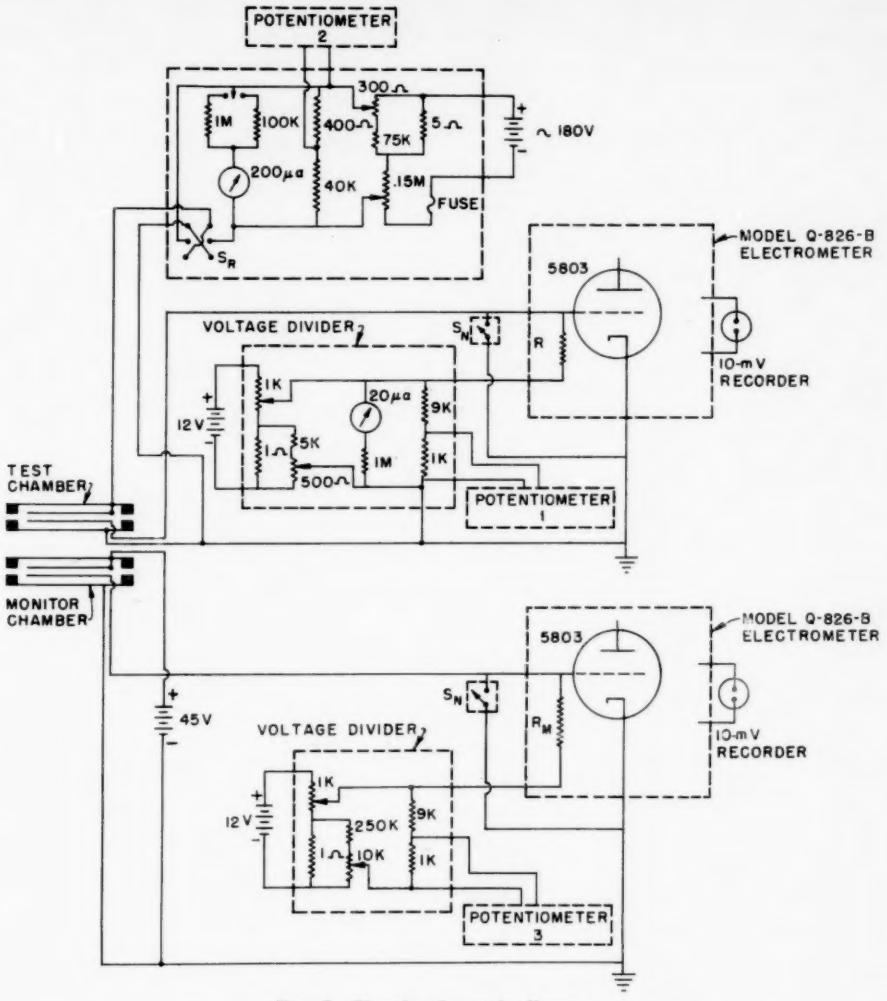

FIG. 3. Circuit schematic diagram.

low-energy electrons, but would attenuate the X-ray beam.

Secondary emission studies have shown that surface oxides and impurities can have a pronounced effect upon electron emission. The copper and aluminum test chamber plates were carefully treated in an effort to remove as much as possible of any such oxide layers and impurities. The copper plates were treated by two cleaning methods. A chemical cleaning process removed approximately half the oxide, and an electropolishing followed by hydrogen annealing left a copper oxide thickness of approximately 20 Å. The aluminum test chamber plates were prepared by mechanical polishing and cleaning with detergent. The graphite plates were not treated since no oxide layer normally exists on a graphite surface.

Measurement of the chamber output currents I and I_M was accomplished simultaneously with two ORNL Q-826-B electrometers using a null voltage method. Fig. 3 is a schematic circuit of

the current–voltage measuring apparatus. The voltages produced by the small chamber currents in the grid resistors R and R_M of the electrometers were bucked out by accurately measured voltages applied in the grid returns. The bucking voltages V_R and V_{RM} were supplied by standard 6- and 12-V wet cells. Rubicon a 10-mV chart recorder. The bucking voltages were adjusted until both electrometers simultaneously gave null readings. Since each electrometer had small erratic drifts in its zero current position, the zero positions were checked with the grounding switches, S_n, shown in Fig. 3. After the bucking voltages had been adjusted to

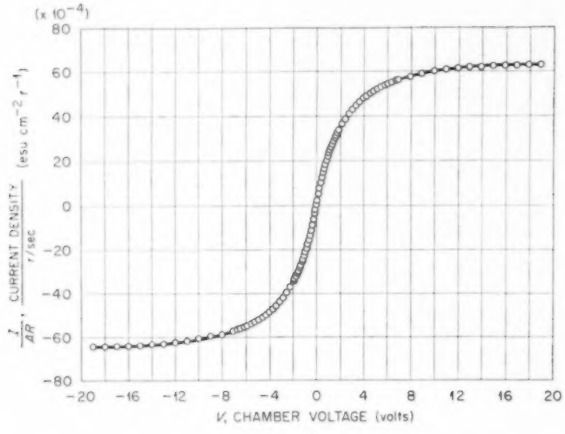

FIG. 4. Current–voltage curve for hydrogen-annealed plates.

High Precision type B and Leeds Northrup type K potentiometers were used to measure one-tenth of the applied bucking voltage with the aid of voltage dividers made from Daven precision wire-wound resistors. The resistors R and R_M of the electrometers were Victoreen precision resistors. Both the Victoreen and Daven resistors fulfilled the necessary requirement of stability such that no significant errors were introduced due to minute resistance changes.

Response times of the electrometers were reduced as much as possible by minimizing capacitance in the grid circuit. When connected to their respective chambers the response times were about 1 sec for the 10^{10} Ω range and 10 sec for the 10^{11} Ω range. Thus all short-term X-ray fluctuations were effectively integrated in the output current readings while the more important longer-term drifts and changes were detected and corrected as described above.

The experimental current–voltage curves were obtained in the following manner. One operator was required to observe the output of each chamber by means of the electrometer and give no deflection on the recorder, both electrometer nulling switches S_n were closed simultaneously. If no deflection occurred in either recorder, then each bucking voltage was assumed to be equal to the potential drop in each grid resistor.

The first derivative of the current–voltage curve was calculated using the expression

$$\left[\frac{d(I/AR)}{dV}\right]_{\left(\frac{V_{i+1}+V_i}{2}\right)} = \frac{y_{i+1}-y_i}{\Delta_x} \qquad (13)$$

The second derivative of the current–voltage curve was calculated at the mid-point among four successive readings, i.e. at $(V_{i+2}+V_{i+1})/2$, using the expression

$$\left[\frac{d^2(I/AR)}{dV^2}\right]_{\left(\frac{V_{i+2}+V_{i+1}}{2}\right)} = \frac{y_{i+3}-y_{i+2}-y_{i+1}+y_i}{2\Delta x^2} \qquad (14)$$

where $\Delta x = (V_{i+1} - V_i)$ represents the voltage mesh, and y_i is the current per unit area per dose rate $(I/AR)_i$ obtained at an applied chamber voltage V_i.

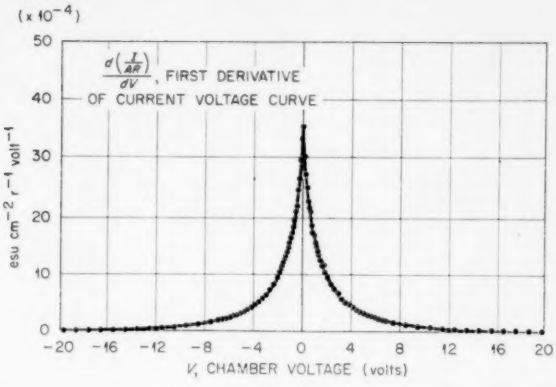

FIG. 5. First derivative of the curve of Fig. 4.

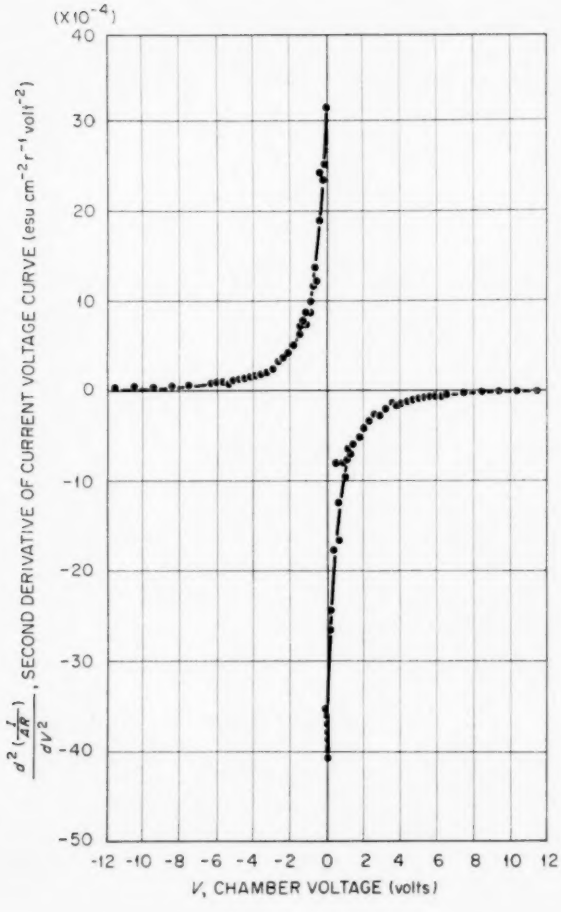

FIG. 6. Second derivative of the curve of Fig. 4.

4. RESULTS

A typical current–voltage curve is shown in Fig. 4 for chemically cleaned, hydrogen-annealed copper plates. The saturation of the curve at relatively low chamber voltages indicates that the flux is predominantly in the low-energy region. The first and second derivative curves for these plates are given in Figs. 5 and 6. The yield, obtained from the saturation portion of the first curve was 0.0063 e.s.u. $cm^{-2}\ r^{-1}$, and for aluminum and graphite plates, 0.0011 and 0.00024, respectively.

The energy distribution of the flux obtained from Figs. 5 and 6 and from equation (12) is shown in Fig. 7. Spectra for aluminum and graphite are shown in Figs. 8 and 9. In all cases the ordinate is the product of the electron flux per unit solid angle inside the medium, the electronic charge, and the 2π steradians subtended by the surface at any point in the medium. That is, the ordinate is total (isotropic) flux in the direction of the surface multiplied by the electronic charge. The abscissae are the electron energies above the bottom of the

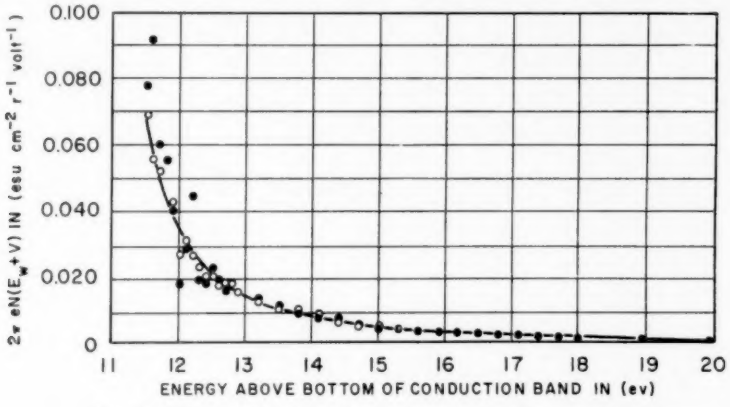

FIG. 7. Energy distribution of electron flux in irradiated copper.

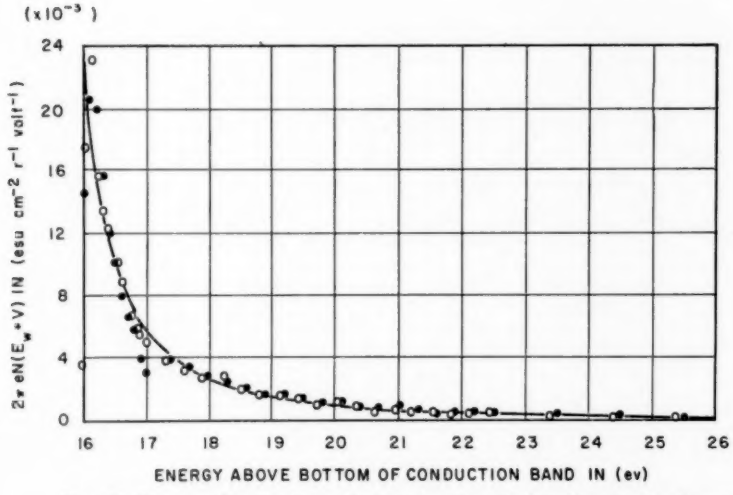

FIG. 8. Energy distribution of electron flux in irradiated aluminum.

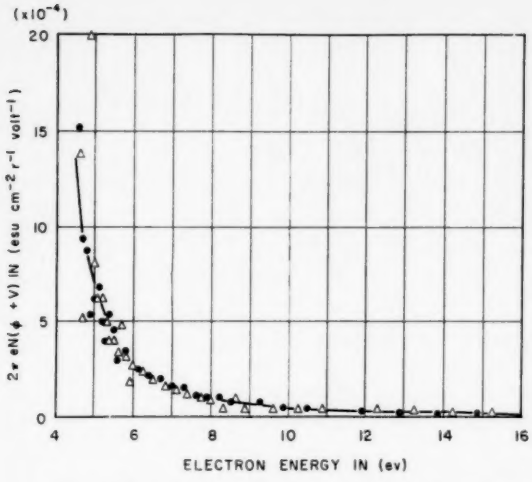

FIG. 9. Energy distribution of electron flux in irradiated graphite.

conduction band. It is probable that the flux continues to increase as the energy decreases below $E_F + \phi$, but this cannot be ascertained in the present investigation which is limited to those electrons having sufficient energy to escape from the material. The open and closed circles represent data taken with the upper plate positive or negative with respect to the lower plate. Within the experimental uncertainty, the two sets of points appear to lie on a single curve.

The electron energy distributions inside the materials determined here are considerably narrower (in terms of the widths of the spectra at half height) than the type of distribution suggested by GREENING as emerging from the surface. Qualitatively, this is because very low energy electrons inside the material are more readily reflected at the surface potential barrier than those having energies several times the work function.[6] The maximum flux is about 0.07, 0.02 and 0.002 e.s.u. cm^{-2} r^{-1} V^{-1} for the annealed copper, aluminum and graphite plates, respectively.

Attempts have been made* to fit simple functions of the energy to the data, but the accuracy of the present data renders such comparisons liable to considerable error. Additional work using a.c. detection methods is in progress and promises to provide the increased accuracy and sensitivity necessary for such curve fitting.

REFERENCES

1. R. L. PLATZMAN, *Rad. Res.* **2,** 1 (1955).
2. P. A. WOLFF, *Phys. Rev.* **95,** 56 (1954).
3. J. R. GREENING, *Brit. J. Radiol* **27,** 163 (1954).
4. L. S. TAYLOR, *Brit. J. Radiol.* **24,** 67 (1951).
5. K. G. MCKAY, *Advanc. Electron.* **1,** 65 (1948).
6. J. L. H. JONKER, *Philips Res. Reps.* **12,** 249 (1957).

* See footnote on p. 204.

Health Physics Pergamon Press 1961. Vol. 5, pp. 212–218. Printed in Northern Ireland

PARTICLE SIZE STUDIES ON PLUTONIUM AEROSOLS

W. D. MOSS, E. C. HYATT and H. F. SCHULTE
Los Alamos Scientific Laboratory, Los Alamos, New Mexico

(*Received* 11 *August* 1960)

Abstract—Particle size is recognized as an important factor in evaluating the health hazard of aerosols and, in addition, has other applications in health physics; however, very little published data is available on plutonium aerosols in plant and laboratory operations. Since the concentration of plutonium in most such aerosols is extremely small relative to the normal dust loading of the atmosphere, direct identification and measurement of plutonium particles is impossible. In these studies, an α-track technique has been used. The sample is collected on a membrane filter and transferred directly to a nuclear emulsion where it is allowed to remain in contact for various time periods. After development of the film, the number of tracks per particle are counted with the microscope. Assuming the particles are spheres of pure plutonium oxide, the particle diameter can be calculated from the number of tracks. Limitations of the technique are discussed.

General air samples and breathing zone samples were collected in a processing plant where plutonium metal is handled in glove boxes. The operations conducted in the rooms included metallurgy and machining of plutonium. Particle sizes measured were mostly less than 0.3 μ with standard deviations of the size distributions being less than 2.0. There was very little variation in these parameters from one operation to another. Reasons for these results are presented. The effect of these data on calculated lung deposition and on sampling efficiency with the annular impactor are discussed.

PARTICLE size is important in evaluating the health significance of an airborne dust and in determining the efficiency of certain types of air samplers and air cleaners. Although the size parameter is not explicitly defined by the ICRP and the NCRP in calculating permissible concentrations, a model has been adopted in which a certain percentage deposition in the lower respiratory tract is assumed.[1] This percentage depends largely on the size, shape, and density of the aerosol particles; in effect, therefore, this defines the limits for the aerosol with the appropriate combination of such properties. Presumably if an aerosol under investigation could be shown to have properties significantly different from those assumed in setting the standards, an appropriate adjustment could be made in the maximum permissible concentration. That such adjustments have not been proposed or requested is at least partly due to the lack of published data on the values of these parameters, particularly those of particle size.

In the case of non-radioactive dust, particularly silica dusts, permissible concentrations have been developed largely from combined clinical and engineering studies in the field. The absence of clinical data in the case of studies on radioactive dusts makes it necessary to calculate permissible concentrations almost wholly from physical measurements. Hence, there is a real need for field data on actual dust properties.

Particle size measurements of uranium aerosols from machining and metallurgy operations have been published.[2] Owing to the extremely low mass concentrations of most radioactive aerosols under field conditions, it is impossible to use ordinary optical sizing methods. Indirect methods, such as the cascade impactor, have given some useful information, but these devices are seriously limited since for highly radioactive dusts it is practically impossible to calibrate the impactor against the test dust. An alternate method, which was used with the impactor on the previous study, was α-track

counting. This technique has been extended and applied to plutonium aerosols with which the cascade impactor is of very limited usefulness. This paper describes the technique and presents some results illustrating its usefulness.

SAMPLING PROCEDURES

The airborne plutonium was collected on 2-in. diameter membrane filters at a flow rate of 1 ft^3/min, using the existing central air sampling system to draw air through the filters, which were counted in an α-scintillation counter. In the central air sampling system, a multiple-stage vacuum pump draws air through sixty 2-in. diameter plastic sampling heads. The heads are installed to collect breathing zone air samples when a man works with his hands in the dry box gloves. In addition, sampling heads, installed near each wall exhaust grill, draw out general room air to check it for airborne plutonium. The system normally draws 2 ft^3/min through a 2-in. diameter HV70 filter paper and operates under from 4 to 5 in. Hg vacuum. With the membrane filter mounted in a 2-in. holder the maximum air flow with the central vacuum pump was 1 ft^3/min.

The major problem in air sampling was collecting sufficient airborne plutonium aerosol for sizing by the α-track method. Eighteen membrane filter samples were collected during each 8-hr day for 2 months and approximately twenty-five samples were obtained with sufficient plutonium aerosol for sizing. The majority of the usable samples were obtained when a minor contaminating incident occurred such as a hole in a dry box glove. During the last 2 months of air sampling the wall exhaust samplers were operated continuously for 1 week, and most of the air samples suitable for particle sizing were collected at these stations. All breathing zone samples would have been preferred, but this was impossible because of insufficient material, under normal operating conditions, at the sampling stations.

SIZING METHOD

The diameters of plutonium dust particles were measured by an autoradiographic method and also optically, where possible. The track method was found useful for determining diameters in the size range of from 0.05 to 2.0 μ. Other workers[3–6] also have reported methods useful for sizing α- and β-emitting dust by autoradiographic techniques. In general, these methods are useful for diameters greater than 1 μ.

If certain assumptions are made, the plutonium dust particle diameters can be calculated from the numbers of tracks produced in the film by the individual particles. If the diameter of the dust particle is greater than 0.5 μ, optical sizing also is possible, the tracks identifying the plutonium. Evidence of attachment of plutonium to non-radioactive dust can be observed and will be discussed later in this paper.

Plutonium lends itself very well to this method of measurement of small diameters because its specific activity is relatively high and because here almost all of it is in relatively pure compounds of Pu^{239}. Information necessary to determine size from track count includes the molecular formula, atomic weight, density, half-life, exposure time, and exposure geometry. The particles are assumed to be spheres of pure plutonium oxide, $Pu^{239}O_2$ with a density of 11.46 and a half-life of 2.43×10^4 years. The exposure geometry was assumed to be 50 per cent in all cases.

Table 1 shows the exposure times necessary to produce ten tracks from various particle sizes using the parameters given above. This table shows that the extent of detection is limited by the long exposure times required for diameters below 0.05 μ; the long exposure times introduce inaccuracies due to fading of the track images in the NTA emulsion.[7] Inaccuracies occur also with particles larger than 2 μ in diameter,

Table 1. Exposure time required to produce ten tracks per particle

Particle diameter (μ)	Exposure time required (min)
2.0	3.4
1.0	27.0
0.5	216.0
0.1	27,000
0.05	216,000
0.01	27,000,000

which produces too many tracks even with short exposures, and from self-absorption within the particle.

EXPOSURE TECHNIQUE

The emulsion is softened before exposure by submerging the 1 in. × 3 in. NTA slide in water for several minutes; the slide is removed from the water and a quarter sector of the membrane filter placed on the slide with the dusty side in contact with the emulsion. A piece of blotting paper is placed over the slide and filter sector, and the blotter and filter paper are pressed against the softened emulsion with a rubber photo squeegee, thus transferring the dust particles from the filter to the emulsion. When excess water is blotted from the slide, the emulsion becomes tacky and the filter then is separated from the emulsion with forceps. The entire time that the filter has been in contact with the emulsion is approximately 10 sec. The slide is then placed in a dark area for the exposure period and then developed for 5 min using D-19 developer. It is then fixed for 40 min, rinsed in water for several minutes, and dried. The development solution was not agitated, and the films were handled carefully to avoid disturbing the particles on the emulsion.

Fig. 1(a) shows the appearance of dust on a section of a membrane filter as viewed under the microscope. Fig. 1(b) shows dust from another section of the same filter after transfer to the nuclear emulsion, exposure and development. These two pictures show that there was little apparent change in the dust distribution as a result of the transfer. Further evidence of quantitative transfer of the dust from the filter to the film is shown in Table 2, which lists the amount of active material transferred from the membrane filter to the NTA emulsion. Note that only a small percentage of the activity remained on the filter paper except in the case of the last sample, and that in all cases more than 90 per cent of the activity can be accounted for. Except for the last sample, the amount transferred was a very high percentage of that on the original filter.

The chief factor affecting the efficiency of transfer to the emulsion is the total amount of material, both active and inactive which is on the filter. The depth the dust penetrates into the filter also may affect the amount transferred, although such penetration is slight with membrane filters.

Table 2. Activity balance of material following transfer

Activity on filter (dis/min)		Activity on emulsion (dis/min)	Per cent transferred
Before transfer	After transfer		
410	2.8	430	100
159	21.6	124	78
303	10.8	292	96
97	3.8	84	87
16.2	1.0	16.2	100
408	19.4	386	95
1830	111	1610	88
1750	910	802	46

To check on these factors the sector of filter paper from which the dust has been transferred was placed at the end of the slide to which the transfer has been made, and kept there during exposure and development. On some films the developer penetrated the filter and permitted development of the emulsion under the filter. Fig. 2 shows a developed image obtained when the filter was left in contact with film during exposure and development. Close examination shows evidence of tracks arising from plutonium particles not in direct contact with the emulsion, although the relative number of such tracks is quite small. To identify positively a single particle not in close contact with the emulsion, there must be a large number of tracks which can be traced back to a common center. If several such particles are closely associated, it is difficult to identify each particle individually.

Filters which contain a relatively small mass of collected material bond themselves tightly to the emulsion and prevent satisfactory development of the emulsion under the filter. The filter can be removed just prior to development but again, where there is little collected material, it is very difficult to separate the filter, even after soaking it in water for several minutes.

In our work, 24 hr is the most suitable initial

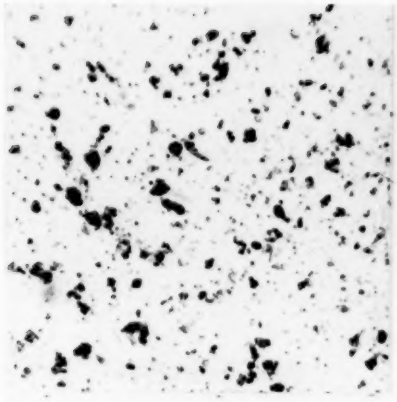

a. ON FILTER PAPER BEFORE TRANSFER

10 μ

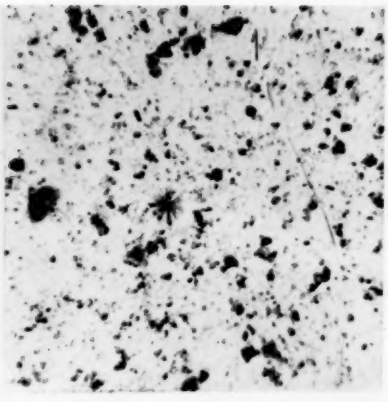

b. ON NTA FILM AFTER TRANSFER

FIG. 1.(a) Photomicrograph of room dust collected on membrane filter and cleared with immersion oil.

FIG. 1.(b) Photomicrograph of room dust from another section of same membrane filter as (a) after transfer to a nuclear emulison, exposure, and development. Comparison of the two pictures shows the quality of the transfer of the dust from the membrane filter to the nuclear emulsion. ×150.

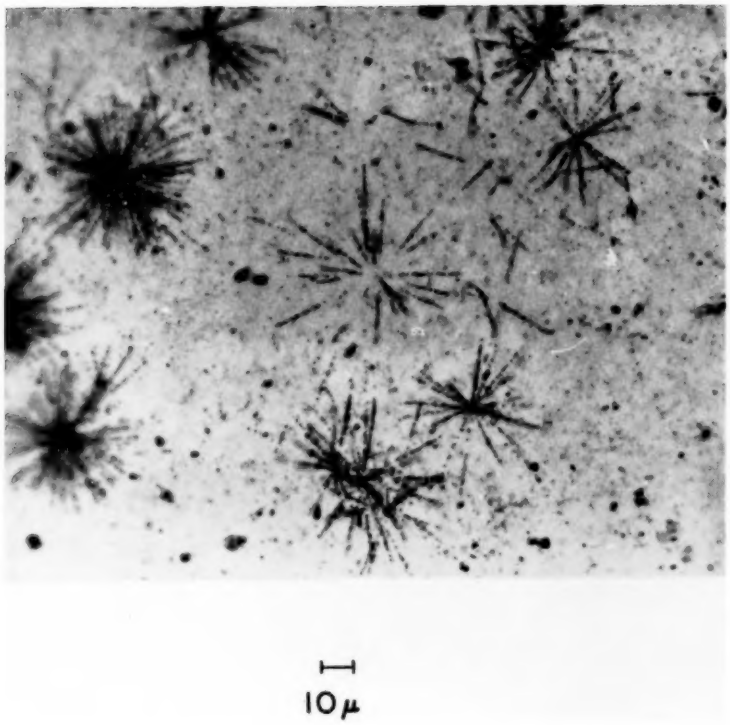

FIG. 2. Photomicrograph of a section of a membrane filter left in contact with a nuclear emulsion during exposure (24 hr) and subsequent development.

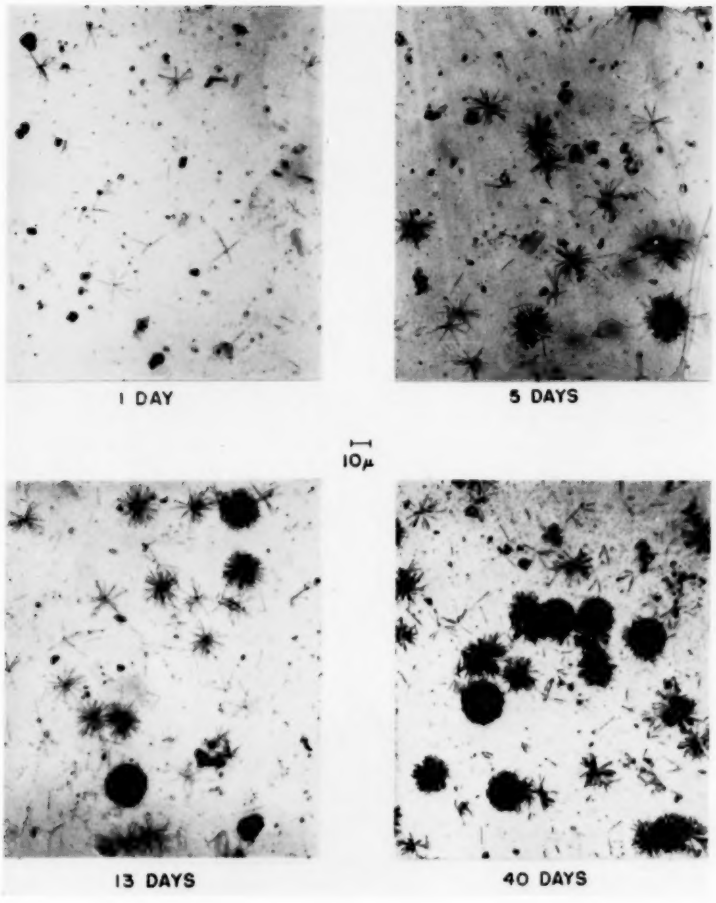

FIG. 3. Photomicrographs of four different sections of the same membrane filter after transfer to a nuclear emulsion, exposure for the times indicated, and development.

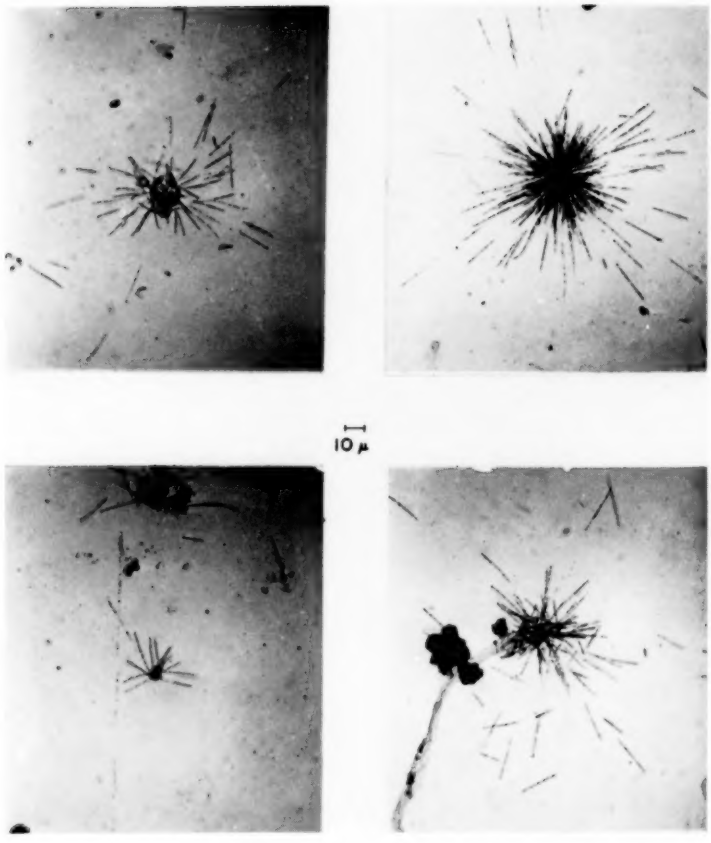

FIG. 4. Photomicrographs of room dust collected on a membrane filter, transferred to a nuclear emulsion and exposed for 24 hr.

exposure time for evaluation of the number and size of the plutonium particles. Additional exposures can be made using other segments of the filter based on results from the 24-hr exposure. Fig. 3 shows a series of exposures on sections of the same membrane filter.

RESULTS

At concentrations below the NCRP permissible levels, the mass of material collected (even during 8-hr sampling) is so small and the number of active particles are so few that only a relatively small percentage of the many samples collected can yield useful data. If sampling is prolonged, the conditions sampled may vary widely and the results obtained are inapplicable to specific situations. Thus, the small number of samples reported here actually represent the collection of hundreds of air samples.

These samples cover two major plant areas: preparation of plutonium from nitrate, and fabrication of plutonium metal. These operations are carried out in two large rooms. Hence, a sample collected in any position in one of these rooms may contain plutonium from any of the several operations in the room. However, the source usually is the operation closest to the sample point because of the air flow pattern in the rooms. A summary of the sampling results is given in Tables 3, 4 and 5. The operation specified for each sample is the one carried out nearest the sampling point.

Since a full day's sampling at the maximum permissible concentration did not collect enough plutonium for sizing, the above samples represent conditions occurring when there had been a failure of the containment, as for example, a leak in a dry box glove. All the operations being performed were routine.

There are several points of interest in these data: (1) all the mass median diameters are very small; (2) the standard deviations or dispersions are very low; and (3) the size characteristics vary little from one sampling point to another or from one operation to another. This is quite different from experience with other industrial aerosols such as uranium and silica. A possible explanation for all three of the above observations lies in the tight containment of plutonium operations. When the containment plus ventilation are working properly, there is essentially no plutonium present in the air. The escape of plutonium as represented by these samples is still very minute on a mass basis, as compared with that encountered in dusty operations. Hence, the operation really being sampled in all cases is that of the minute leakage of airborne dust from the containment. The leakage is itself a size selective process, so that the sizes represented in these tables probably are more representative of this leakage process than of the dust generating operations of loading, fluorination or machining.

Another observation not apparent in these data is that there were practically no agglomerates among the plutonium dust examined optically nor do the track patterns indicate the presence of multiparticle groups. This may be a result of the extremely low mass concentrations encountered or because of the high specific radioactivity weakening the electrostatic forces. In any case, the absence of agglomerates tends to reduce the average particle size and also reduces the standard deviation.

RELATIONSHIP OF PLUTONIUM PARTICLE SIZE TO LUNG RETENTION

Much scattered data on lung retention as a function of particle size have been published and were reviewed by HULTQVIST in 1957.[8] After studying these articles, we feel that the data of BROWN *et al.*[9] probably are the best and the most useful for calculating retention. Their work was done on china clay particles having a density of 2.6 g/cm³. If the primary methods of deposition in the lower respiratory tract are sedimentation, or impaction, then the sizes used by BROWN must be multiplied by $\sqrt{(\rho_p/\rho_c)}$ to obtain the deposition curve for plutonium aerosol, where

ρ_p = density of plutonium aerosol particle

ρ_c = density of china clay = 2.6 g/cm³

On the other hand, if deposition is from only diffusion or Brownian motion, then no correction is needed for density. Since the particle size here is extremely small, it seems likely that deposition is principally by diffusion and a density correction is unnecessary. Then, for a

Table 3. Data on samples collected in metal preparation area—1st half

Operation in area	Air conc. (dis/min m^3)	Count median (μ)	σg	Mass median (MMD) (μ)
Loading nitrate and fluorination WE	9.0	0.14	1.8	0.36
Loading nitrate and fluorination WE	17.0	0.32	1.5	0.50
Loading nitrate and fluorination WE	28.2	0.13	1.7	0.28
Loading nitrate and fluorination WE	20.4	0.32	1.5	0.51
Loading nitrate and fluorination WE	7.7	0.35	1.4	0.50
Loading nitrate and fluorination WE	1.3	0.17	1.8	0.46
Loading nitrate and fluorination WE	103.0	0.35	1.4	0.51
Loading nitrate and fluorination WE	32.0	0.29	1.5	0.46
Loading nitrate and fluorination WE	12.0	0.32	1.4	0.45

WE = sampler near wall exhaust.

Table 4. Data on samples collected in metal preparation area—2nd half

Operation in Area	Air conc. (dis/min m^3)	Count median (μ)	σg	Mass median (MMD) (μ)
Sampling box—plutonium nitrate WE	8.0	0.17	1.6	0.31
Sampling box—plutonium nitrate WE	6.5	0.13	1.9	0.46
Sampling box—plutonium nitrate WE	3.6	0.31	1.7	0.65
Processing contaminated alcohol WE	7.0	0.12	1.6	0.21
Reduction of fluoride to metal WE	9.0	0.12	1.5	0.19
Reduction of fluoride to metal WE	22.4	0.11	1.9	0.51
Reduction of fluoride to metal WE	5.8	0.38	1.4	0.19
Reduction of fluoride to metal BZ	12.8	0.11	1.5	0.19
Reduction of fluoride to metal BZ	15.5	0.11	1.5	0.19

WE = sampler near wall exhaust.
BZ = sampler at breathing level in working area. Operator not necessarily present.

Table 5. Data on samples collected in metal fabrication area

Operation in area		Air Conc. (dis/min m^3)	Count median (μ)	σg	Mass median (MMD) (μ)
Lathe operation no. 1	WE	546.0	0.13	1.6	0.25
Lathe operation	WE	3.9	0.25	1.5	0.41
Lathe operation	BZ	1030.0	0.18	1.3	0.16
Lathe operation	BZ	1185.0	0.21	1.3	0.25
Lathe operation no 2.	WE	8.4	0.24	1.4	0.34
Lathe operation	WE	344.0	0.14	1.5	0.22
Lathe operation	WE	21.2	0.25	1.4	0.35
Lathe operation	BZ	974.0	0.14	1.6	0.25
Contaminated thrash removal	WE	456.0	0.10	1.4	0.14

WE = sampler near wall exhaust.
BZ = sampler at breathing level in working area. Operator not necessarily present.

typical case such as the third sample in Table 3 (MMD = 0.28 μ, $\sigma g = 1.7$), the amount deposited in the lower respiratory tract can be calculated and is found to be 33 per cent. If the full correction for density is applied (deposition by sedimentation or inertia), the deposition is 43 per cent.

For another sample (MMD = 0.50 μ, $\sigma g = 1.4$), the calculated lower respiratory deposition, assuming only diffusion effects, is 42 per cent. A density correction would raise this to 49 per cent. Using the sample of largest size (MMD = 0.65μ, $\sigma g = 1.7$), the calculated deposition is 47 per cent with no density correction. It is interesting to note that MORROW and CASARETT[10], in their experiments on dogs, used a plutonium dioxide aerosol very similar to the last sample above (MMD = 0.68 μ, $\sigma g = 1.8$). They found a total deposition of 56 per cent. Since the particle size is small, only a small fraction of this should be upper respiratory deposition.

In general, these results show that the calculated initial deposition of this material in the lower respiratory tract is somewhat larger than the 25 per cent used in the calculations of the ICRP.

COLLECTION OF SAMPLES BY THE ANNULAR IMPACTOR

The annular impactor has been used extensively for collecting plutonium aerosols,[11,12] and it is interesting to use these particle size data to predict collection efficiencies with this impactor. Since collection is affected by inertial forces, a density correction is necessary. Applying the density corrected data of TAIT to the particle size data on the three samples of the previous section, the following results were obtained.

Table 6. Calculated collection efficiency of the annular impactor

Sample no.	MMD (μ)	σg	Collection efficiency (%)
1	0.28	1.7	51
2	0.50	1.4	70
3	0.65	1.7	73

These results (Table 6) indicate that collection efficiencies for this instrument may be considerably lower than usually assumed for this particular type of plutonium dust. In fact, there may not even be a sharp distinction between such dusts and randon decay products.

RESUSPENSION OF PLUTONIUM DUST

During the sampling for this work, there was a spill in another part of the plant. As a result, it was necessary to clean up and decontaminate the room. Several samples for particle size analysis were collected during this clean-up operation. One sample was sized by the nuclear track method and apparently had a mass median diameter of 1.90 μ and a standard deviation of 1.8; however, microscopic examination revealed that the particles were much larger than predicted from the track counts. Also, it was apparent from the pattern of the tracks that the particles were not pure plutonium. Typical particles with their accompanying tracks are shown in Fig. 4, which should be compared with Fig. 3. Thus, this aerosol, resuspended in the air during clean-up, consisted of relatively large particles of inactive material with small amounts of plutonium incorporated in the particles. An optical size determination was made, and the mass median diameter was 6.8 μ with a geometric standard deviation of 2.2 μ. Such material has a much lower percentage deposition in the lower respiratory tract and would be collected with high efficiency by the annular impactor.

SUMMARY

A technique for measuring the particle size of plutonium aerosols has been described. Using this technique, air samples collected in areas where plutonium metal is prepared and fabricated revealed lower average sizes and greater uniformity of size than anticipated. This may be expected to result in higher deposition rates in the lungs than predicted and would result in low collection efficiency in impactor type sampling devices. There is some evidence that when plutonium dust settles on surfaces and is resuspended during cleaning, the resuspended particles are much larger and are only partly composed of plutonium.

REFERENCES

1. *Recommendations of the International Commission on Radiological Protection*, Suppl. 6, *Brit. J. Radiol.* (1954).
2. E. C. Hyatt, W. D. Moss and H. F. Schulte, *J. Amer. Industr. Hyg. Ass.* **30,** 99 (1959).
3. J. A. Leary, *Analyt. Chem.* **23,** 850 (1951).
4. G. M. Wells, *Further Studies on the Rapid Detection of Plutonium Dust in Air.* Windscale Report R and DB (W) TN-146 (1954).
5. J. J. Fitzgerald and C. G. Detwiler, *A.M.A. Arch. Industr. Health* **15,** 3 (1957).
6. J. Sisefsky, *Brit. J. Appl. Phys.* **10,** 526 (1959).
7. H. Yagoda, *Radioactive Measurements with Nuclear Emulsions* pp. 103-105. John Wiley, New York (1949).
8. B. Hultqvist, *Kgl. Svenska Vetenskapsakad. Handl. Fjarde Serien,* **6,** 1 (1956).
9. J. H. Brown, K. M. Cook, F. C. Ney and T. Hatch, *Amer. J. Publ. Hlth.* **40,** 450 (1950).
10. P. E. Morrow and L. J. Casarett, *Inhaled Particles and Vapours* (Edited by C. N. Davies) p. 167. Pergamon Press, Oxford (1961).
11. G. W. C. Tait, *The Annular Impactor.* Chalk River (Canada) Report CR-HP-577 (1955).
12. J. E. May and J. J. Croley, Jr., *Amer. Industr. Hyg. Ass. Quart.* **18,** 312 (1957).

Health Physics Pergamon Press 1961. Vol. 5, pp. 219–224. Printed in Northern Ireland

HIGH SENSITIVITY SILVER-ACTIVATED PHOSPHATE GLASS FOR THE SIMULTANEOUS MEASUREMENT OF THERMAL NEUTRONS, γ- AND/OR β-RAYS

RYOSUKE YOKOTA*, SABURO NAKAJIMA* and EIJI SAKAI†

(*Received* 16 *November* 1960)

Abstract—A new silver-activated phosphate glass which contains a large amount of Li and a small amount of B was prepared. This glass has greater sensitivity for thermal neutrons, is less energy-dependent, and can be prepared to have lower predose reading than the Al–Ba–K–Ag metaphosphate glass. By exposing three pieces of glass which are covered by brass plate, cadmium plate, and Al foil, respectively, any mixed radiation dose of thermal neutrons, γ-rays and β-rays can be measured separately and simultaneously.

An integrated dose of 50 mr for γ-rays and 8×10^6 n_t/cm^2 can be measured with an accuracy of ± 5 per cent, and 0.1 r or 1.6×10^7 n_t/cm^2 with an accuracy of ± 3 per cent.

1. INTRODUCTION

SCHULMAN *et al.*[1] have developed silver-activated phosphate glass for X- and γ-ray dosimetry. The composition of their optimum mix is KPO_3, 23.14; $Ba(PO_3)_2$, 23.14; $Al(PO_3)_3$, 46.28; and $AgPO_3$, 7.44 weight per cent.

This silver-activated phosphate glass exposed to X- or γ-rays fluoresces when excited by ultra-violet rays. The intensity of fluorescence is linearly proportional to the exposure dose. KONDO[2] has reported that SCHULMAN's glass is sensitive to thermal neutrons.

GINTHER and SCHULMAN[3] have also reported the energy dependence of a silver-activated phosphate glass plate ($\frac{3}{4}$in. $\times$ $\frac{3}{4}$in. $\times$ $\frac{1}{4}$in.) containing Li and Mg but not K and F . THORNTON and AUXIER[4] have reported the response of rods of this glass (1 mm diameter $\times$ 6 mm long) to thermal neutrons.

A new silver-activated phosphate glass which contains a large amount of Li and a small amount of B has been developed. This glass is as sensitive to γ-rays as SCHULMAN's glass.

If appreciable reduction of "predose" reading is made in the measuring system of this glass and fluorometer, lower γ-ray and thermal neutron doses can be measured by the use of a stable and sensitive amplifier in the fluorometer.

The fading and dose-rate dependence is very small, and the response is linear from 50 mr up to 5000 r for Co^{60} γ-rays.

Therefore, this measuring system seems to be ideal for personnel monitoring if the sensitivity is enhanced for thermal neutrons and the predose reading is reduced.

2. PREPARATION OF SILVER-ACTIVATED PHOSPHATE GLASS

High purity metaphosphates of Al, Li, Ag, Mg, K, Ba and Cd were prepared and used. These ingredients were analysed both chemically and spectrophotometrically, as was the boric acid. The composition of the prepared glass is given in Table 1.

The melting crucible used is of pure alumina, while the melting furnace is of the globar type.

Each piece of glass was annealed and then polished to the size of $10 \times 10 \times (3 \pm 0.03)$ mm. Four opposite faces of each piece are polished so as to be transparent, and the other two side planes are ground by fine carborundum. Glasses nos. 2, 3 and 4 can be easily prepared so as to get low predose readings.

The reproducibility of the response of glass no. 2 to γ-rays is good.

* Matsuda Research Laboratories, Tokyo Shibaura Electric Co., Kawasaki, Japan.

† Japan Atomic Energy Research Institute, Tokai, Ibaragi-ken, Japan.

Table 1. *Composition of the prepared glasses*

No. of glass	Composition (wt. %)	
	Base composition	Added component
1	$LiPO_3$ 50, $Al(PO_3)_3$ 50	$AgPO_3$ 8
2	$LiPO_3$ 50, $Al(PO_3)_3$ 50	$AgPO_3$ 8, B_2O_3 3
3	$LiPO_3$ 50, $Al(PO_3)_3$ 50	$AgPO_3$ 8, B_2O_3 5
4	$LiPO_3$ 50, $Al(PO_3)_3$ 50	$AgPO_3$ 8, B_2O_3 7
5	$LiPO_3$ 35, $Mg(PO_3)_2$ 15, $Al(PO_3)_3$ 50	$AgPO_3$ 8
6	$LiPO_3$ 30, $Cd(PO_3)_2$ 20, $Al(PO_3)_3$ 50	$AgPO_3$ 8
7	KPO_3 25, $Ba(PO_3)_2$ 25, $Al(PO_3)_3$ 50	$AgPO_3$ 8

3. FLUOROMETER

The ultra-violet light source is a 100-W super high pressure mercury lamp which has good stability.*

The photocathode of the photomultiplier is semi-transparent Bi-Ag–Cs. This cathode has greater sensitivity in the spectral region of red than the semi-transparent Sb–Cs photocathode which has been used in the United States. Only near ultra-violet light which passes through three filters is focused on the dosimeter glass with a fused silica lens. In the front of the photomultiplier are placed the ultra-violet filter and a red glass filter with sharp cut off at 590 mμ and very low fluorescence when excited by the scattered ultra-violet light. The photocurrent is measured with a stable and sensitive d.c. amplifier which uses an electrometer tube. Phosphate glass containing Mn which emits red fluorescence when excited by ultra-violet light is used as a standard.

The predose reading of no. 2 glass is 0.9 r as observed with the fluorometer. By the use of glass no. 2 and this fluorometer, 30 mr Co^{60} γ-ray exposure can be detected, and 50 mr can be measured within an accuracy of ± 5 per cent.

4. EXPOSURE TO MIXED RADIATIONS OF γ-RAY AND THERMAL NEUTRONS

The glasses were exposed in the hole no. 7 (thermal column) of the homogeneous reactor JRR-1 at the Japan Atomic Energy Research Institute. Exposures were made with the reactor power level at 400 W, 5 kW and 40 kW. The cadmium ratio of indium was 4×10^2 at the position where the glasses were exposed. Hence, any increase in response produced by neutrons above the cadmium cut-off, which is about 0.45 eV for a 0.4 mm cadmium filter, is negligible. Each glass was covered by Al foil (0.02 mm thickness) brass plate (0.3 mm thickness) or cadmium plate (0.3 mm thickness). Also, glasses no. 2 and no. 3 were covered by pure Bi the thickness of which was 17 mm. Glass no. 2 was covered by pure Li having a thickness of 20 mm.

The ingredients of these specimens all have short-lived neutron-capture produced isotopes, so that there was little persistent radioactivity. Gold foils were exposed simultaneously, and from their activation the thermal neutron dose was obtained. Exposure times were as follows: 1, 4, 8, 12 and 16 min. The fluorometer readings (photocurrent) of the exposed glasses are expressed in roentgens, in equivalent Co^{60} γ-response, and are given in Fig. 1. Glass no. 2 is the most sensitive, while SCHULMAN's glass is the least sensitive. The Li shield of 55 mm in diameter and 50 mm in height absorbs all of the thermal neutrons incident upon it, behaving as a sink of thermal neutrons. Also, the coexisting γ-ray flux decreases. Therefore, the response of glass no. 2 covered by Li must be considered only as a reference.

5. SEPARATION OF THERMAL NEUTRON AND γ-RAY INDUCED RESPONSES

(a) The following method is for the use of glass no. 2 only. At first the glass covered by Al foil is exposed to Co^{60} γ-rays, and the response by unit Co^{60} γ-ray exposure is obtained. Let the fluorescence of the glass exposed in the thermal column be denoted by F, expressed in equivalent Co^{60} γ-exposure, the γ-ray exposure dose by D_γ, the first collision thermal neutron dose by D_n, and the fluorescence of the glass exposed to unit γ-ray or thermal neutron dose expressed in equivalent Co^{60} γ-exposure by f_γ or f_n, respectively.

In the case of the glass covered by brass or Cd

* Made by Matsuda Research Laboratories.

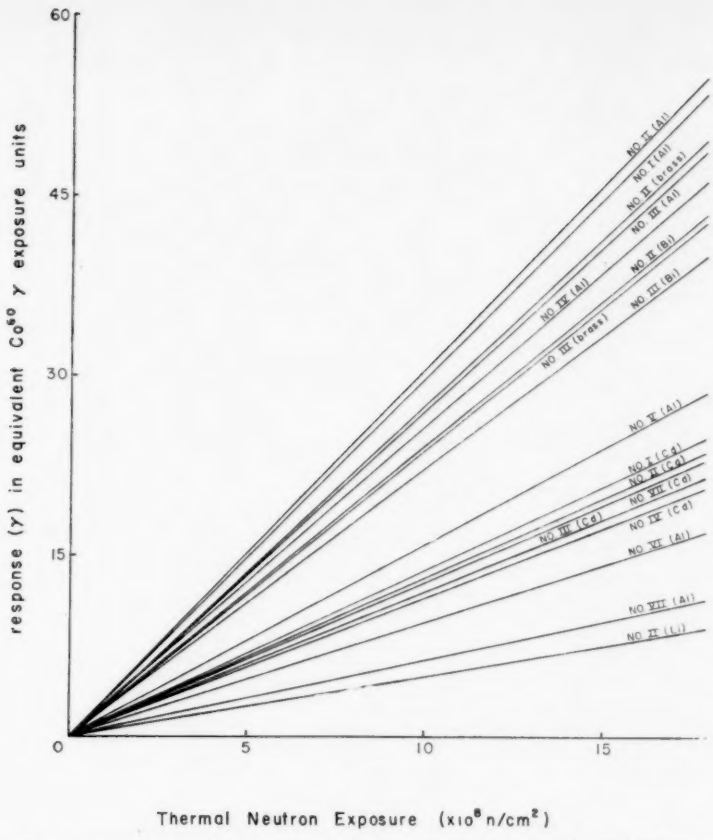

FIG. 1. Response of the prepared glasses exposed in the thermal column. The various kinds of metal used for covering the glass are shown in parentheses.

plate the suffix of br or Cd is added as $f_{\gamma,\mathrm{br}}, f_{\gamma,\mathrm{Cd}}$, etc. Then the following equations are valid:

$$F_{\mathrm{br}} = f_{\gamma,\mathrm{br}} D_\gamma + f_{n,\mathrm{br}} D_n \qquad (1)$$

$$F_{\mathrm{Cd}} = f_{\gamma,\mathrm{Cd}} D + f_{n,\mathrm{Cd}} D_n \qquad (2)$$

$$F_{\mathrm{Bi}} = f_{\gamma,\mathrm{Bi}} D_\gamma + f_{n,\mathrm{Bi}} D_n \qquad (3)$$

and from equations (1) and (3),

$$D_\gamma = \frac{(F_{\mathrm{br}} - F_{\mathrm{Bi}})}{(f_{\gamma,\mathrm{br}} - f_{\gamma,\mathrm{Bi}})} \qquad (4)$$

because $f_{n,\mathrm{br}}$ is equal to $f_{n,\mathrm{Bi}}$.

The values of $f_{\gamma,\mathrm{br}}, f_{\gamma,\mathrm{Bi}}$, and $f_{\gamma,\mathrm{Cd}}$ are 0.733 r, 0.382 r and 0.733 r, respectively. These values were obtained by the exposure to Co^{60} γ-rays.

Therefore, D_γ is obtained from equation (4). Then from equation (1) and (2) $f_{n,\mathrm{br}}$ and $f_{n,\mathrm{Cd}}$ are obtained as 4.99 r/rem and 1.19 r/rem, respectively, because D_n is known from Au foil. Abbreviation used as "rem" is equal to 9.6×10^8 thermal neutrons/cm^2.

Hence, using the two pieces of glass, one covered by brass and the other by cadmium, the exposure dose of any mixed radiation of thermal neutrons and γ-rays is obtained separately from equations (1) and (2) by the measurement of F_{br} and F_{Cd}.

If β-rays exist in the mixed radiation field, the piece of glass covered by Al foil is exposed at the same time. Then we have

$$F_{\mathrm{Al}} = f_{\gamma,\mathrm{Al}} D_\gamma + f_{n,\mathrm{Al}} D_n + f_{\beta,\mathrm{Al}} D_\beta \qquad (5)$$

where $f_{\gamma,\mathrm{Al}}$ is determined by the exposure to

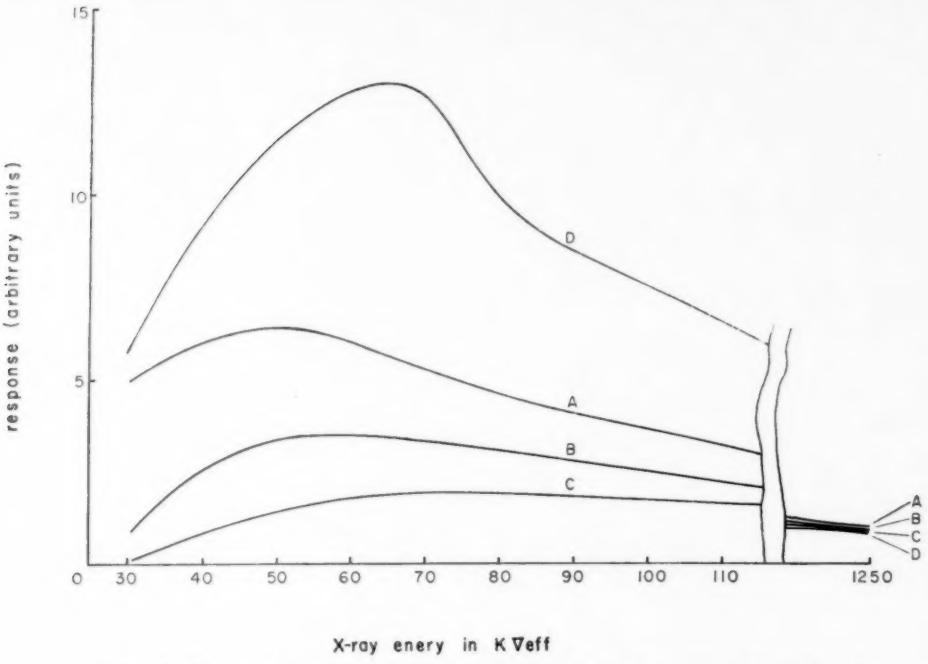

FIG. 2. Energy dependence of no. 2 and no. 7 glass plates (10 × 10 × 3 mm).
A, no. 2 glass plate, bare.
B, no. 2 glass plate, 0.3 mm brass cover.
C, no. 2 glass plate, 0.3 mm cadmium cover.
D, no. 7 glass plate, bare.

Co^{60} γ-rays, and $f_{n,Al}$ is equal to $f_{n,br}$. Thus $f_{\beta,Al}D_\beta$ is obtained. Hole no. 7 (thermal column) has an aluminium cylinder wall with thickness of about 3 mm. This may be the chief source of β-rays.

In our experiment, the following values were obtained:

ϕ_n(thermal neutron flux density)
$= 4.24 \times 10^8\ n_t/\text{cm}^2$ per min
$= 0.442$ rem/min
ϕ_γ(γ-ray flux density) $= 1.05$ r/min
ϕ_β(β-ray flux density) $= 0.08$ rad/min

By making a nomogram, ϕ_γ, ϕ_n and ϕ_β may be obtained immediately.

(b) The following method utilizes glasses no. 2 and no. 3. As the ratio of the sensitivity for Co^{60} γ-ray of glasses no. 2 and no. 3 is 1:0.92, the ratio of that for thermal neutrons is obtained as 1:0.85 from Fig. 1.

Each glass, covered by Al foil, brass plate, or Bi shield is exposed in the thermal column. In glass no. 3, F and f are replaced by F' and f', respectively. Then

$$F'_{Br} = f'_{\gamma,br}D_\gamma + f'_{n,br}D_n \quad (6)$$

$$F'_{Bi} = f'_{\gamma,Bi}D_\gamma + f'_{n,Bi}D_n \quad (7)$$

From equations (6) and (7) $f'_{n,br}$ is obtained as 3.82 r/rem ($f'_{\gamma,br}$ is 0.67 r).

Therefore, the exposure doses of any mixed radiation of thermal neutrons, γ-rays and β-rays are obtained separately by the measurement of F_{Al}, F_{br} and F'_{br}.

In our experiment, $\phi_n = 4.24 \times 10^8\ n_t/\text{cm}^2$ per min (0.442 rem/min), $\phi_\gamma = 1.05$ r/min and $\phi_\beta = 0.08$ rad/min were obtained as before.

6. DEPENDENCE ON ENERGY OF γ-RAYS

Glass no. 2 is a "low-Z" glass, i.e. this glass is composed of low atomic number elements

without containing Ba as SCHULMAN's glass (glass no. 7) does. Therefore, this glass is less energy dependent, as shown in Fig. 2 in the case of $10 \times 10 \times 3$ mm plates. Energy dependence of glass no. 2 is about one-half that of glass no. 7. The energy dependence of glass no. 2 covered by a brass plate (0.3 mm thick) or a cadmium plate (0.3 mm thick) is also shown in Fig. 2. In the case of the glass covered by cadmium plate, the energy dependence is greatly reduced.

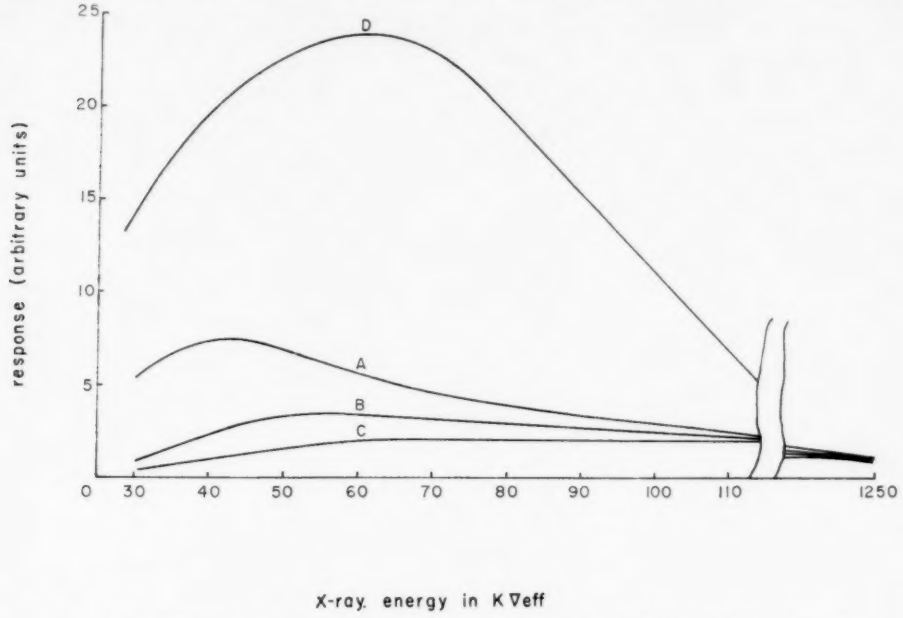

FIG. 3. Energy dependence of no. 2 and no. 7 glass rod (1 mm dia. × 6 mm).
A, no. 2 glass rod, bare.
B, no. 2 glass rod, 0.3 mm brass cover.
C, no. 2 glass rod, 0.3 mm cadmium cover.
D, no. 7 glass rod, bare.

No. 2 glass rods of the size of 1 mm diameter × 6 mm were covered by a brass plate (0.3 mm) or cadmium plate (0.3 mm); the energy dependence is shown in Fig. 3, together with that of glass rod no. 7. In glass rod no. 2 covered by a cadmium plate, the energy dependence is greatly reduced.

7. DISCUSSION

As shown in Fig. 1, the response of glass no. 7 covered by cadmium is larger than that of the bare glass. This is due primarily to the capture γ-rays derived from Cd^{114}, since a 0.3 mm cadmium filter absorbs a large part of the thermal neutrons incident upon it.

The response to thermal neutrons of glass no. 2 is very high compared with that of glass no. 7, although the ratio of the response to γ-rays is 1:0.975.

In no. 2 glass plate ($10 \times 10 \times 3$ mm) covered by brass plate, 1 r Co^{60} γ-ray exposure dose produces the response equivalent to the thermal neutron integrated flux 1.57×10^8 n_{th}/cm^2. In other words, a 1 rem thermal neutron exposure produces the same increase in fluorescence as 6.12 r Co^{60} γ-ray exposure. In DuPont type 502 film covered by a brass plate, according to KALIL[5], a 1 rem thermal neutron exposure produces the same increase in density as a 0.9 r Ra γ-ray exposure.

As the energy dependence between 1 and 3 MeV γ-ray region is small, it may be said that

the no. 2 glass plate is about 6.8 times as sensitive as DuPont 502 film to thermal neutrons when it is assumed that the glass is as sensitive as the film to γ-rays.

In the method of the use of glasses no. 2 covered by brass plate and cadmium plate, there may be an error in the evaluation of the γ-ray exposure, because there is some energy dependence. But it may be emphasized that the evaluation of thermal neutron exposure will still be reliable.

By the method and fluorometer mentioned above we can measure 50 mr for γ-rays and 8×10^6 n_t/cm^2 for thermal neutrons with an accuracy of ± 5 per cent, and 0.1 r and 1.6×10^7 n_t/cm^2 with an accuracy of ± 3 per cent.

REFERENCES

1. J. H. Schulman, R. J. Ginther and C. C. Klick, *J. Appl. Phys.* **22,** 1479 (1951); J. H. Schulman, W. Shurcliff, R. J. Ginther and F. H. Attix, *Nucleonics* **11,** No. 10, 52 (1953).
2. S. Kondo. Private communication.
3. R. J. Ginther and J. H. Schulman, *Nucleonics* **18,** No. 4, 92 (1960).
4. W. T. Thornton and J. A. Auxier, ORNL-2912, 11 August (1960).
5. F. Kalil, *Nucleonics* **13,** No. 11, 91 (1955).

Health Physics Pergamon Press 1961. Vol. 5, pp. 225–230. Printed in Northern Ireland

NOTES

Determination of Radioiodine in Milk

(*Received* 12 *December* 1960)

ATEN *et al.*[1] report the determination of radioiodine in milk after a nuclear accident, by means of a Geiger–Müller γ-counter. They find about 460 counts/min for the maximum permissible concentration of 0.065 μc/l.

A similar emergency counting programme is envisaged in Norway in case of reactor accidents. Nearly all milk produced in Norway is distributed through central dairies, where the individual producers deliver their milk in aluminium containers, mostly holding 50 l. If all individual milk contributions could be checked without loss of time before pooling, economic losses could be kept down to a minimum without jeopardizing the safety.

Tests we have carried out with new compact single-channel scintillation counters, set at the I^{131} energy, have proved most encouraging. Using a preset time of only 10 sec and a net count corresponding to half the background (i.e. 50 per cent increase in reading) as a criterion, a detection level of 0.004 μc/l could be established on the exterior wall of the 50 l. milk container. Measurements of this sensitivity and speed justify in our opinion the relatively high costs of the counting equipment.

When monitoring the walls of containers of other volumes than 50 l., the readings obtained will change. We have found the following ratios:

Milk bottle	1 l.	0.15
Plastic can	5 l.	0.5
Jerry can	20 l.	0.8
Road tank truck		1.5
Rail tank truck		1.7

State Institute of Radiation Hygiene
Oslo

KRISTIAN KOREN
ARNE BULL

Reference

1. A. H. W. ATEN, JR., H. J. L. UMANS and W. M. C. DE JONG, *Health Phys.* **4,** 62 (1960).

Concentration of Uranium in Sea Fish

(*Received* 18 *November* 1960)

IN A recent publication[1] we have referred to a concentration factor for uranium between fish and seawater, which we had undertaken in collaboration with Dr. J. KOOI and Dr. U. HOLLSTEIN*. We have finished the rather restricted series of measurements which we have been able to undertake for the present.

Uranium was determined by ultra-violet fluorescence in the solidified melt of the ash with NaF + 2% LiF. Bones were excluded from the samples as far as possible. As it was our intention to arrive at a reasonably reliable value for the *maximum* permissible concentration of ordinary uranium in seawater, we applied normal precautions to exclude contamination with traces of U, without going to extremes, as such a contamination would only raise the observed uranium concentration, which in turn would lead us to too low a permissible concentration. The fish samples were taken from fish obtained commercially in Amsterdam, so occasionally some contamination may have taken place before the sample reached us. No two samples of the same fish were acquired on the same occasion. The results obtained on fresh fish are collected in Table 1. The probable error of the measurements may be estimated to be around 0.5×10^{-5} or 10^{-5} mg U per g of fish. This shows that most of the figures listed in Table 1 are not significantly different from zero. In some samples, on the other hand, the presence of uranium seems to be definitely established.

Table 1. *Uranium determinations of samples on the flesh of fresh fish*

Fish	Uranium content expressed in 10^{-5} mg/g fish
Gurnard	0.9; 0.25
Mackerel	1.0
Haddock	6 ; 2.5
Whiting	0.4; 9
Plaice	2 ; 0.9
Cod	1.2; 1.0

In the case of herring the situation is more complicated, because this fish is never sold fresh, but always in a more or less preserved, i.e. salted, condition. Occasionally the treatment involved may well introduce uranium contamination. The first two samples we measured showed U contents of 0.8×10^{-5} and 74×10^{-5} mg U/g. As the second value was

* At that time at the Reactor Centrum Nederland.

clearly abnormal we measured another series of ten different herring samples, in which we found an average uranium content of 1.2×10^{-5} mg U/g with a maximum value of 2.3×10^{-5} mg U/g.

From this we conclude that the uranium content of herring is not as a rule higher than that of other fish.

It is a little difficult to choose from our analytical results a reasonable value for the average concentration of uranium in fish. Perhaps 2.1×10^{-5} mg U/g would be acceptable and, if we choose twice this value, we should already be on the safe side.

If we combine the uranium concentration in fish of 2.1×10^{-5} mg U/g with the value of 1.1×10^{-6} mg U/ml determined by Koczy[2] for surface seawater, we find a concentration factor of 20. For natural uranium the maximum permissible concentration in drinking water for occupational exposure[3] is 2×10^{-4} μc/ml, which may be taken to correspond to a MPC of 6.7×10^{-6} μc/ml for the population at large. Combining the concentration factor with the MPC for drinking water for the population at large we calculate a maximum permissible concentration in seawater of 3×10^{-6} μc/ml or 9 μg U/ml. (This figure should, of course, be divided by an extra safety factor, in case one wishes to apply such a factor.)

A. H. W. Aten, Jr.
J. W. Dalenberg
W. C. M. Bakkum

Institute for Nuclear Physics Research
Amsterdam, Netherlands

Acknowledgment—This investigation was performed as part of the programme of the Foundation for Fundamental Research of Matter (FOM) with the financial support of the Organization for pure Research (ZWO).

References

1. A. H. W. Aten, Jr., *Health Phys.* To be published.
2. G. Koczy, *S. B. Akad. Wiss. Wien* II **158,** 113 (1950).
3. Report of ICRP Committee II on Permissible Dose for Internal Radiation (1959). *Health Phys.* **3,** 6 (1960).

A Device for Determining the Orientation of Persons Exposed to Neutron and/or γ-Radiation

(*Received* 3 *February* 1961)

Experience gained in dosimetric experiments necessitated by nuclear accidents[1,2] indicates that a device is needed to determine the orientation of persons at the time of exposure to nuclear accidents. Because the person's orientation and position frequently change between the times he receives the neutron and γ-ray portions of his exposure, detectors for both types of radiation should be provided.

In conjunction with experiments concerning blood sodium activation in man phantoms and live burros, neutron- and γ-radiation measurements were made with several detectors placed around the waist and chest areas of phantoms and burros. Pellets of sulfur, bare gold foils, cadmium-covered gold foils, and metaphosphate glass rods were placed at intervals on belts. The results of a typical exposure are shown in Fig. 1. Gold and sulfur detectors were used to detect thermal and fast neutrons (> 2.5 MeV), respectively,[3,4] and the glass dosimeters were used for measuring γ-radiation.[5]

The data show that the fast-neutron flux above 2.5 MeV is approximately uniform along the front of the phantom, i.e. the side toward the radiation source, and that the flux is decreased by approximately a factor of 10 on the side farthest from the radiation source. The difference in γ-dose and thermal-neutron flux in front of and behind the phantom is approximately a factor of 2. Analysis of the distribution of flux and dose values reveals that four detector stations, properly spaced on a belt worn by the individual, permit the determination of the orientation of the body with respect to the source of neutrons to within $\pm 45°$. These experiments have shown that bare glass may be used in such a detector system rather than Li^6-encapsulated glass. Until the thermal-neutron dose approaches 5 per cent of the γ-dose, the discrepancy is not significant for this application (one tissue rad of thermal neutrons, 3.6×10^{10} n/cm^2, produces a response in glass equivalent to approximately 5 r of Co^{60} γ-rays). Further, if the neutron flux is measured near the glass, as in this case, the thermal-neutron-induced response of the glass can be calculated with sufficient accuracy for this application,[5] and subtracted from the total response. In general, the thermal-neutron flux is a function of the fast-neutron flux. Therefore, in the event the response of the glass induced by thermal neutrons were much greater than that of the γ-radiation, the fast neutron dose would be the critical parameter in most cases.

For female workers, the detector stations can be attached inconspicuously inside laboratory coats by means of "iron-on" patches.

Some prototypes of belt and laboratory coat devices are being tested at ORNL: some of these have been used for months without discomfort or complaint. The plastic-sealed detector station is about 1.5 in. long, 0.5 in. wide and 0.15 in. thick and can be inserted between two existing layers of belt or held to the inner side by a thin added layer. Four detector

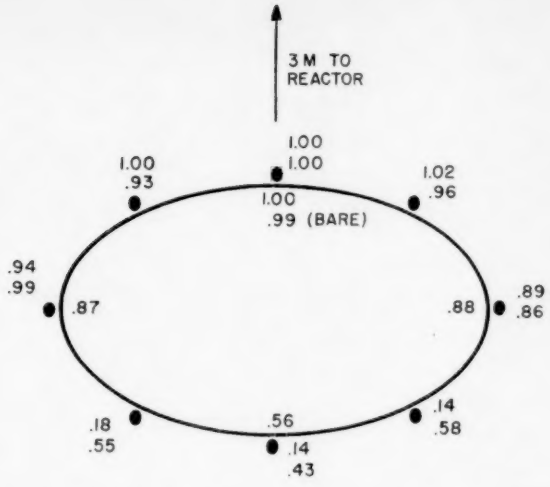

FIG. 1. A typical γ-dose and neutron-flux distribution about the waist of an anthropomorphous phantom exposed to a small critical assembly at a distance of 3 m.

RELATIVE GAMMA DOSES ARE SHOWN INSIDE THE ELLIPSE.
RELATIVE FAST NEUTRON FLUXES ARE SHOWN ABOVE THE
RELATIVE THERMAL NEUTRON FLUXES AT EACH POSITION.

stations and an attractive belt cost less than $10.00. In general, such detectors require no servicing except in the event of an accident. The small plastic envelopes, complete with the detectors, were unscathed after having been put through a complete automatic wash and dry laundering process. In the case of laboratory coats, care should be taken in the ironing process, as extreme heat could damage the plastic or excessive pressure could damage the glass rod.

J. A. AUXIER
F. W. SANDERS
P. N. HENSLEY
Health Physics Division
*Oak Ridge National Laboratory**
Oak Ridge, Tennessee

References

1. G. S. HURST, R. H. RITCHIE and L. C. EMERSON, *Health Phys.* **2,** 121 (1959).
2. G. S. HURST, R. H. RITCHIE, F. W. SANDERS, P. W. REINHARDT, J. A. AUXIER, E. B. WAGNER, A. D. CALLIHAN and K. Z. MORGAN, *Health Phys.* **5,** 179 (1961).
3. G. S. HURST, J. A. HARTER, P. N. HENSLEY, W. A. MILLS, M. SLATER and P. W. REINHARDT, *Rev. Sci. Instrum.* **27,** 153 (1956).
4. P. W. REINHARDT and F. J. DAVIS, *Health Phys.* **1,** 169 (1958).
5. C. H. BERNARD, W. T. THORNTON and J. A. AUXIER, *Health Phys.* **4,** 236 (1961).

* Operated by Union Carbide Corporation for the U.S. Atomic Energy Commission.

Strontium-90 in the Total Diet

(*Received* 23 *December* 1960)

TWENTY-SIX samples of the total diet (each comprised of forty-two meals plus snacks) were prepared by home economics departments of colleges and universities using locally available foods and water at the widely scattered locations noted in Table 1, in mid-November 1959. The composition and method of preparation of these samples is described in Ref. 1. In addition, in eight cities, separate samples of milk, taken from the same bottles used in preparing the total diet samples, were also forwarded to the laboratory.†

Each total-diet sample was twice run through a home-type garbage-disposal unit, in order to grind it to a consistent suspension. The fairly stable slurry was mixed thoroughly with a large electric stirrer, and an aliquot of approximately 2 kg taken for analysis. The aliquot was evaporated to dryness in a stainless-steel beaker; the residue was burned to a red heat and then transferred to a porcelain dish and ashed at 650° for 6 hr. The ash was dissolved in 6 N hydrochloric acid, and tested for strontium-90 by the method described in Ref. 2, with several modifications. Calcium was determined by a combination of the methods described in Refs. 3 and 4.

† The analytical work was performed by Isotopes, Inc., Westwood, N. J., under contract with Consumers Union.

Table 1. Strontium-90 and calcium in total diet and in milk samples, November 1959

Sampling location	No. of days	Total-diet samples						Milk samples			
		Weight (kg)	$\mu\mu$c Sr^{90}/kg	g Ca/kg	S.U.	Daily intake		$\mu\mu$c Sr^{90}		g Ca per kg	S.U.
						$\mu\mu$c Sr^{90}	g Ca	per l.	per kg		
1. Duluth, Minn.	14	50.4	8.1	0·48	16.7	29	1.7				
2. New Orleans, La.	14	52.8	8.6	0.52	16.7	33	2.0	18.7	18.2	1.12	16.2
3. St. Louis, Mo.	14	54.1	7.2	0.45	15.9	28	1.7	13.0	12.6	1.05	12.1
4. Boston, Mass.	14	56.4	7.9	0.51	15.5	32	2.0	10.1	9.8	1.10	8.9
5. Stillwater, Okla.	14	51.8	6.9	0.46	15.0	26	1.7				
6. Pella, Iowa	14	51.4	6.1	0.45	13.4	23	1.7				
7. Pittsburgh, Pa.	14	54.1	5.6	0.43	13.2	22	1.7	13.8	13.4	1.16	11.6
8. NYC (Manhattan)	14	58.7	5.5	0.43	12.6	23	1.8				
9. Hampton, Va.	14	46.4	6.4	0.51	12.5	21	1.7				
10. NYC (Brooklyn)	13	45.5	5.5	0.45	12.2	19	1.6	8.9	8.6	0.80	10.9
11. Atlanta, Ga.	14	47.7	4.9	0.43	11.5	17	1.5	9.5	9.2	1.16	8.0
12. Seattle, Wash.	6	19.3	5.4	0.47	11.4	17	1.5				
13. Glencoe, Ill.	13½	55.5	4.5	0.40	11.3	18	1.6				
14. Grand Forks, N.D.	12	51.8	4.8	0.43	11.2	21	1.8				
15. Washington, D.C.	14	47.3	5.1	0.46	11.2	17	1.6	9.6	9.3	1.00	9.3
16. Memphis, Tenn.	14	50.4	4.9	0.44	11.1	18	1.6				
17. St. Paul, Minn.	14	51.4	5.3	0.48	11.0	19	1.8				
18. Bozeman, Mont.	14	47.7	4.8	0.45	10.7	16	1.5				
19. Boulder, Col.	8	30.0	4.3	0.41	10.5	16	1.5				
20. Louisville, Ky.	14	56.0	4.1	0.44	9.4	16	1.8	10.5	10.2	1.02	10.0
21. Austin, Tex.	13	48.8	3.8	0.42	9.1	14	1.6				
22. Coral Gables, Fla.	14	48.3	4.6	0.51	9.1	16	2.1				
23. Nampa, Idaho	14	52.3	3.7	0.43	8.6	14	1.6				
24. Alameda, N.M.	14	53.6	3.2	0.46	7.1	12	1.8				
25. Los Angeles, Cal.	14	53.2	2.1	0.43	4.9	8	1.6				
26. Quebec, Canada	14	49.6	6.9	0.44	15.8	24	1.6				
Average			5.4	0.45	11.8				11.4	1.05	10·9

Table 2. Strontium-90 and calcium in the milk and the "all other foods" portions of the total diet

Sample	% milk in total-diet sample	Total diet per kg				Strontium units in			Ratios of S.U.'s	
		Milk portion		All other foods		Milk portion	All other foods	Total diet	Total diet to milk	Other foods to milk
		$\mu\mu$c Sr^{90}	g Ca	$\mu\mu$c Sr^{90}	g Ca					
2	29.2	5.3	0.325	3.3	0.195	16.2	16.9	16.7	1.03	1.04
3	28.5	3.6	0.30	3.6	0.15	12.1	24.0	15.9	1.31	1.98
4	27.4	2.7	0.30	5.2	0.21	8.9	24.8	15.5	1.74	2.79
7	28.5	3.8	0.33	1.8	0.10	11.6	18.0	13.2	1.14	1.55
10	34.0	2.9	0.27	2.6	0.18	10.9	14.4	12.2	1.12	1.32
11	32.3	3.0	0.375	1.9	0.055	8.0	34.5	11.5	1.44	4.31
15	32.6	3.0	0.325	2.1	0.135	9.3	15.2	11.2	1.20	1.64
20	27.5	2.8	0.28	1.3	0.16	10.0	8.1	9.4	0.94	0.81
Average	30.0	3.4	0.31	2.7	0.15	10.9	19.5	13.2	1.24	1.93

The analytical data is given in Table 1, in terms of strontium-90 and calcium as well as in strontium units ($\mu\mu$c Sr^{90}/g Ca), for both the total-diet samples and the milk samples.

Table 2 deals only with the data from the eight cities in which both total-diet and milk samples were obtained, and represents the relative contributions of strontium-90 and calcium from the milk and the non-milk ("all other foods") portions of the total diet. These were calculated on the basis of the known proportions of milk in the total-diet samples, and the known strontium-90 and calcium contents of the milk

samples. The ratios of the strontium units in the non-milk portions of the diet to those of the milk portions are given in the last column. These indicate that the strontium unit level of the non-milk part of the diet can be over four times as high as that of the milk, and that in general the milk portion of the diet, because of its high calcium content, lowered the strontium-unit level of the total diet, considerably in some cases.

The variations in the ratios of strontium units in the total diet to that in the milk, ranging from 0.94 to 1.74, indicate that milk is not a reliable index of the strontium-unit level of the total diet, and that only total-diet studies (such as these) will yield good approximation of the strontium-90 ingested by the population in any given locality.

Such total-diet samples can also be useful for determinations of total intake of other radioisotopes in foods, e.g. radium-226. A report on radium-226 content of five of these samples has also been published.[5]

IRVING MICHELSON

Department of Public Service Projects
Consumers Union of U.S., Inc.
Mt. Vernon, New York

References

1. *Consumer Reports* (June), Consumers Union, Mount Vernon (1960).
2. H. L. VOLCHOK, J. L. KULP, W. R. ECKELMANN and J. E. GAETJEN, *Ann. N.Y. Acad. Sci.* **71,** 293 (1957).
3. C. W. GEHRKE, H. E. AFFSPRUNG and Y. C. LEE, *Analyt. Chem.* **26,** 1944 (1954).
4. *Manual of Standard Procedures*, NYO 4700. Health and Safety Laboratory, AEC (1957).
5. I. MICHELSON, *Health Phys.* **5,** 229 (1961).

Radium-226 in the Total Diet

(*Received* 23 *December* 1960)

FIVE samples of the total diet (each a composite containing up to forty-two meals plus snacks) were prepared in November 1959 by home economists in widely separated U.S. cities, using locally available foods and water. The nature of the diets represented and the method of preparation of these samples are described in Ref. 1. After homogenization of the entire sample, 9.1-kg aliquots were dried, ashed at 650°, and the Ra^{226} determined by the radon-emanation method.

The results of the analyses are given in Table 1, in terms of $\mu\mu c$ Ra^{226} per kilogram of total diet, and per gram of calcium; the total daily intake of Ra^{226} is also presented.

This study differs from that of MUTH *et al.*[2] in that each test was made on a *composite* of more than 100 foods plus local water, instead of calculating the total Ra^{226} intake from separate tests on twenty foods and several waters. Nevertheless, the average daily intake found in these tests on U.S. foods agrees closely with the estimate of 3 $\mu\mu c$ average daily intake made by MUTH and his co-workers for a "standard man" eating German foods.

As was to be expected, Ra^{226} content of the total diet varied somewhat from one city to another; the highest differed from the lowest by a factor of 1.8. That it did not vary to a greater extent is due probably, at least in part, to the commingling, in any city, of foods from many areas.

The data from only five cities cannot be expected to yield a reliable average for the country as a whole, nor to furnish a good measure of the variability from area to area. An extension of this study is therefore under consideration.

Table 1

Total-diet samples				$\mu\mu c$ Ra^{226}		g Ca	$\mu\mu c$ Ra^{226}	Daily intake	
Site	Days	Total weight (kg)	Daily intake (kg)	per 9.1-kg aliquot	per kg	per kg	per g Ca	$\mu\mu c$ Ra^{226}	g Ca
Austin, Tex.	13	48.8	3.75	7.93 ± 0.23	0.87	0.42	2.08	3.27	1.58
New York, N.Y.	14	58.7	4.20	9.43 ± 0.23	1.04	0.43	2.40	4.35	1.82
Nampa, Idaho	14	52.3	3.75	5.27 ± 0.23	0.58	0.43	1.35	2.17	1.61
Boulder, Col.	8	30.0	3.75	5.82 ± 0.23	0.64	0.41	1.56	2.50	1.54
Glencoe, Ill.	13¼	55.5	4.10	6.26 ± 0.21	0.69	0.40	1.84	2.82	1.64
				Average	0.76	0.42	1.85	3.02	1.64
				Ratio—low to high:	1:1.8		1:1.8	1:2.0	

Acknowledgment—The analytical work was performed by Isotopes, Inc., Westwood, N. J., under contract with Consumers Union.

IRVING MICHELSON

Department of Public Service Projects
Consumers Union of U.S., Inc.
Mt. Vernon, New York

References

1. *Consumer Reports* (June). Consumers Union, Mount Vernon (1960).
2. H. MUTH, B. RAJEWSKY, H.-J. HANTKE and K. AURAND, *Health Phys.* **2,** 239 (1960).

Health Physics Pergamon Press 1961. Vol. 5, pp. 231–243 Printed in Northern Ireland

NEWS

News Editor: J. J. FITZGERALD

Public Health Service expands courses in radiological health

During the past year over 500 trainees have participated in radiological health courses at the Robert A. Taft Sanitary Engineering Center in Cincinnati, Ohio.

These courses are designed for engineers and scientists engaged in various aspects of radiological health. The major purpose is to provide the trainees with a means to appraise the newest developments in the subject areas and to afford an opportunity for practice and application of the latest techniques. Information acquired at the undergraduate level is usually not included in these courses. A few general courses are offered for those in technical administrative positions who wish to acquire an over-all perspective of radiological health.

The program this year has again been expanded. This expansion is reflected in the increase in both the number and frequency with which courses are being presented. The schedule this spring included:

Radioactive Pollutants in Water—February 13–17, 1961
Radionuclides in Water—February 20–24, 1961
Basic Radiological Health—March 13–24, 1961
Sanitary Engineering Aspects of Nuclear Energy—March 27–April 7, 1961
Reactor Environmental Health Problems—May 1–10, 1961
Radionuclides in Food—June 19–30, 1961

British OHS holds meeting on health physics

The British Occupational Hygiene Society held a meeting in London on January 3 and 4, 1961, to discuss aspects of health physics.

The program for the first day included discussions on: the biological effects of neutrons, the theory of the measurement of dose, instruments for the measurement of dose, and shielding against neutrons.

The program for the second day included discussions on: personnel dosimetry (the use and interpretation of film badges and pocket dosimeters), national film processing and recording service and problems of small-scale processing, and environmental dosimetry.

Health physics research reactor to be built at ORNL

A small research reactor to provide short bursts of radiation for biomedical and health physics research will be built at the Oak Ridge National Laboratory.

The new reactor, designated Fast Burst Reactor, will consist mainly of a core of uranium–molybdenum alloy without shielding or moderator. Radiation exposure will be very small outside the limited access area. It will be located in a hollow enclosed by hills of sufficient height to provide adequate shielding for surrounding areas. The location is about two miles from the central facilities of ORNL and almost directly east of the Tower Shielding Facility.

The Fast Burst Reactor project will include the reactor, a building to house the reactor and accessory equipment, a storage vault and a separate control building. The control building will be located about 800 ft away, behind a ridge, to provide a shielded facility for remote operation of the reactor. The control building will also have laboratory spaces and administrative and service areas for the research groups using the facility. The area surrounding the facility will be fenced to prevent uncontrolled access.

The reactor design provides for a pulse of 40 μsec consisting of fast neutrons as free as possible of thermal neutrons. In addition, the reactor can be operated under constant steady-state conditions at power levels up to 1 kW. The reactor will be operated from a special dolly at various heights up to 30 ft when in use at ORNL. Some experiments will be performed inside the reactor building while others requiring additional unobstructed space for certain measurements will be conducted in the open on a concrete apron. A boom derrick will be provided for outside use to permit operation between heights of 30 and 50 ft.

The research program with the Fast Burst Reactor at ORNL will be concerned principally with radiation dosimetry in connection with instrument development and dose determinations and radiobiology programs involving both large and small animals. In addition, the facility will be available for programs involving medical uses of ionizing radiation and solid-state physics, nuclear chemistry and neutron physics research.

Federal Radiation Council requests comments on questions concerning radiation protection standards for selected radionuclides

The Federal Radiation Council is presently considering the problem of providing radiation protection guides for selected radionuclides to be used in the control of human exposure from environmental sources.

On May 13, 1960, the President approved the recommendations contained in a memorandum from the Federal Radiation Council on *Radiation Protection Guidance for Federal Agencies*. The memorandum was published in the FEDERAL REGISTER, May 18, 1960. There was also released at the same time Staff Report No. 1 of the Federal Radiation Council *Background Material for the Development of Radiation Protection Standards*, dated May 13, 1960. Recommendations of the Council so far approved by the President provide numerical values for Radiation Protection Guides for the whole-body and certain organs of radiation workers and for the whole-body of individuals in the general population as well as an average population gonadal dose.

The Council is currently studying the problem of providing guides to be used in the *control of human exposure from environmental contamination with radioactive materials*. Initially, attention is being directed to iodine-131, radium-226, strontium-89 and strontium-90. The Council and its staff are conferring with scientists from the various disciplines involved in these problems. Foci of the study are the current guides used by the Federal agencies on an interim basis in connection with these radionuclides. These are based on recommendations of the National Committee on Radiation Protection and Measurements.

The Council is currently studying the guides in the light of the biological risk for the benefits derived and the economic burden associated with the implimentation of these recommendations or guides.

Prohibition of nuclear materials on Turnpike

Because of an insurance problem the Massachusetts Turnpike Authority has banned from the Turnpike vehicles carrying nuclear materials. The Authority is concerned that an accident on the Turnpike involving radioactive materials would close the Turnpike and jeopardize the finances of the Authority.

The Authority recognizes that the transportation of nuclear materials on the Turnpike would be less hazardous than the transportation of such materials on other highways. The problem is receiving careful study, and it is hoped that a solution will be forthcoming in the near future.

Wentworth Institute, Boston, Massachusetts, to offer nuclear technician program

Wentworth Institute will offer in September, 1961, the first course in the United States for the training of nuclear engineer technicians. The Institute received a grant from the United States Atomic Energy Commission, the first ever made to a technical institute, to defray the cost of some of the necessary laboratory equipment.

AEC amends regulation on land-burial of low-level radioactive waste

The Atomic Energy Commission is amending its regulation on standards for protection against radiation (Part 20) to reflect its policy on land disposal of low-level packaged radioactive waste materials.

Under the existing Commission regulation, Part 20, licensees are permitted to dispose of very low concentrations of radioactive waste by burial in the soil. The amendment to Section 20.302 of AEC regulations, which became effective February 17, 1961, permits licensees to continue this practice, but states that the Commission will not approve an application for license to receive radioactive waste material from other persons for disposal on land not owned by the Federal or State Governments. A proposed amendment to this effect was published in the Federal Register on February 4, 1960 allowing 30 days for public comment. To date the Commission has issued no licenses to receive waste materials from other persons for burial on non-Government-owned land.

In January of 1960 the Commission announced that it had determined that regional sites for permanent disposal of low-level radioactive waste would be established, as needed, on State or Federal Government-owned land. Placement of the waste materials in Government-owned lands, under long-term Government control, will assure adequate protection of the public health and safety throughout the period of any potential hazard.

Pursuant to this policy, the Commission has made available its land-burial sites at Oak Ridge National Laboratory, Oak Ridge, Tennessee, and at the National Reactor Testing Station near Idaho Falls, Idaho, for the disposal of low-level wastes by AEC licensees.

The types of low-level wastes to which the Commission's policy applies include broken glassware, paper wipes, rags, ashes, animal carcasses, laboratory paraphernalia and other similar things which can no longer be used in experiments.

EURATOM, UKAEA and USAEC to distribute translations of nuclear literature

The European Atomic Energy Community (EURATOM), the United Kingdom Atomic Energy Authority and the United States Atomic Energy Commission have agreed to pool their efforts to collect and disseminate information concerning translations of nuclear literature, especially from such languages unfamiliar to Western readers as Russian and Japanese. A central information office "Transatom" has therefore been established at Euratom's Brussels headquarters. It will function in two ways:

Firstly, by publishing from December 1960, a monthly *Transatom Bulletin*, which will list existing translations recently reported to the Brussels Office, as well as new translations planned by international or national institutions and private firms in the European Community, the United States, the United Kingdom and in other countries.

Secondly, all data relating to translations, including those made before the establishment of "Transatom", are being collected and recorded in a master file system at Brussels. Copies of this card file have been offered to appropriate institutions in countries with great interest in the nuclear field.

Food irradiation committee of AIBS to advise the AEC

At the request of the Atomic Energy Commission, the American Institute of Biological Sciences has established a committee of scientists to consult with the Commission's Division of Biology and Medicine and Office of Isotopes Development on radiation processing of food.

The committee will consider and advise on certain technical phases of the Commission's program aimed at extending the refrigerated shelf-life of selected food products through low-dose radiation processing.

The committee, will also advise the Commission's Office of Isotopes Development and the Division of Biology and Medicine on technical considerations involved in the processing of specific marine, fruit and vegetable products. Particular emphasis will be placed on food technology, nutrition and wholesomeness studies.

AEC publishes four amendments to regulation for radiation protection standards

The Atomic Energy Commission has issued four amendments (to Part 20, Title 10 of the Code of Federal Regulations) designed to clarify and simplify its regulations for the protection of employees in atomic energy industries and the general public against hazards arising from the possession or use of radioactive materials.

Section 20.3 (a) (4) (i) of the regulation is amended to permit three-month calendar quarters to start on any date in January, April, July or October rather than only on the first of the month and to permit calendar quarters which are determined on a weekly basis to consist of alternating 14-week and 12-week periods, rather than only 13-week periods.

Section 20.206 is amended to require posting of Form AEC-3 in such locations as to assure that employees working in or frequenting restricted areas will observe the notice on the way to or from work, rather than to be posted in every establishment where licensed activities are being carried on regardless of whether there are any restricted areas in the establishment which require radiation protection control measures.

Section 20.3 (a) (14) defines "Restricted Area" in part as any area, access to which is controlled by the licensee. Some licensees have requested clarification of the definition since access is controlled to many areas which have no relation to radioactive material. The definition has been changed by adding the phrase "for purposes of protection of individuals from exposure to radiation and radioactive materials". A corresponding change has been made in the definition of an unrestricted area in Section 20.3 (a) (17).

The Appendix "B" Note in the regulation specifies methods of general applicability for determining limits for concentrations of radioactive isotopes in air or water where there is a mixture of more than one radionuclide. Because of the unique physical and chemical state of the mixture of radionuclides in uranium-ore dust, a concentration limit specifically applicable to such a mixture in the dust has been added as paragraph 4 to the Appendix "B" Note.

AEC revises regulation controlling source material

The Atomic Energy Commission has revised its regulation governing the control of source material (thorium and natural and depleted uranium).

Under the revised regulation, possession of up to 15 lb of source material at any one time by a physician, pharmacist or research institution, or by persons receiving such material in medicines or drugs, will be generally licensed; that is, a specific license will not be required. The same 15-lb general license will apply to commercial and industrial firms or medical institutions using source material for educational, developmental or commercial purposes. Receipt of source material by a generally licensed person will be limited to 150 lb a year.

The revised regulation includes a general license to receive title to source material. This will facilitate transactions in which the buyer does not take actual physical possession. There will also be a general license to export quantities of up to 3 lb at any one

time to specified destinations. Specific licenses will be required for export of larger quantities.

Certain finished products containing uranium or thorium will be exempt from domestic licensing requirements. These include incandescent gas mantles, vacuum tubes, and welding rods containing thorium, as well as some types of glazed ceramic tableware containing not more than 10 per cent of source material. Photographic films, negatives and prints containing uranium or thorium will be exempt; as will any finished product made of or containing tungsten–thorium alloys not exceeding 4 per cent thorium by weight, providing no treatment or processing is involved. Exemption from licensing requirements with respect to uranium contained in aircraft counterweights will be continued.

AEC publishes second in series of pamphlets describing biological and medical research

The Atomic Energy Commission has published the second in a series of pamphlets describing its life sciences research program. The purpose is to acquaint scientists, students and interested members of the public with the biomedical program, its objectives and needs. The Commission's biomedical program is directed toward the accumulation of knowledge of the effects of nuclear radiation from any source—natural or man-made—upon living things.

The booklet, titled "Genetics Research", was prepared under the direction of the Commission's Division of Biology and Medicine. It summarizes work in progress at forty-nine institutions through 101 research contracts or projects in the following major areas: (1) cytogenetics; (2) gene action; (3) genetics of populations—population dynamics and effects of mutations; (4) human genetics; (5) mammalian genetics; (6) microbial and biochemical genetics; (7) molecular radiation genetics; (8) mutation-rate analysis; and (9) plant breeding and crop improvement.

The Commission's genetics program involves the study of genetic principles and mechanisms and the effects of radiation on these mechanisms, together with observations on the gross effects in populations or organisms. Projects in the area mentioned above are intended to explore the mechanisms of radiation-induced genetic damage, the expression of this damage in individuals and populations, and the mode and rate of elimination of the damage over many generations; to develop an understanding of the normal chemistry of genetic materials as prerequisite to understanding the way in which radiation acts upon these materials; to and study therapeutic techniques for the prevention or reduction of potential radiation hazards to genetic materials.

Delaware River Port Authority takes out insurance policy against nuclear damage or contamination

The Delaware River Port Authority has taken out a $10,000,000 insurance policy against nuclear damage and contamination, to the Benjamin Franklin or Walt Whitman Bridges or anyone using them.

The policy, the first of this type, protects against injury, sickness, death or loss of property resulting from any nuclear incident, involving any user of the bridges which link Philadelphia and Camden.

Employees have been given a set of regulations that involve actions to be taken in the case of nuclear incidents. The regulations note that since many radioactive elements are now carried by truck there is a "rare" possibility of an incident that would involve the spillage of radioactive materials on the bridges or the approaches to the bridge.

Consumers Union to make dietary radioactivity study

The U.S. Atomic Energy Commission has awarded a research contract to Consumers Union, Mount Vernon, New York, for partial support of studies of radioactivity in sample diets prepared in twenty-five cities in twenty-two states. The AEC will provide $20,000 for the 1961 co-operative study which is a continuation of a 1959 survey made by Consumers Union independent of Government support. It will be directly related to dietary studies carried out by the AEC's Health and Safety Laboratory at New York.

The purpose of the study is to obtain further information on radioactivity in the total diet in the United States. In all of the cities, total diet samples will be analyzed for strontium-90 and naturally occurring calcium and radium-226. Among the twenty-five cities where total diets will be sampled will be New York City, Chicago and San Francisco where the Health and Safety Laboratory is currently analyzing individual food items for radioactivity. The Consumers Union study will also include, in these and possibly several other cities, analyses for man-made radioisotopes cesium-137, cerium-144, plutonium-239 and zinc-65 as well as the naturally occurring radioisotope lead-210. Chemical analyses will be made also for natural isotopes of potassium.

The AEC's program is one of research rather than monitoring foods and diets throughout the United States, and the results obtained from this research program may be useful in estimating regional dietary levels of radioactivity.

The diet samples will consist of three prepared

meals per day for a two-week period or a total of forty-two meals and "snacks of teenagers." In the three metropolitan areas (San Francisco, Chicago and New York), the study will also include diets of several age groups and economic levels. In all twenty-five cities, food will be purchased from local retail markets and prepared locally as for consumption. Then the meals will be packaged in special plastic containers and shipped to Consumers Union's consultant radiochemistry laboratories. In some areas separate samples of milk and whole-wheat products included in the total diet samples will be analyzed in order to estimate their contribution to the radioactivity of the diet.

Special ten-week course in health physics at ORNL

The ORINS Special Training Division and the Health Physics Division of Oak Ridge National Laboratory conducted a special ten-week course in health physics in Oak Ridge in 1961 for the U.S. AEC.

The first four weeks was presented by ORINS, January 9–February 3, 1961, and was repeated March 6–31, 1961. The remaining six weeks, April 3–May 13, 1961, was conducted by ORNL. The ORINS portion of the course was devoted to basic radiation physics and radioisotope techniques, and participants selected either session. The single session in the ORNL Health Physics Division consisted of lectures and discussions on various aspects of health physics and on-the-job training in applied health physics.

Purpose of the course was to provide training in health physics for representatives of state and local governments. The course included academic training and work experience for persons who are concerned with licensing and inspection functions for their states; however, it was not intended that this be purely a course in the "art" of licensing and inspecting.

The course was conducted as another step in encouraging the states to assume control of certain radioactive materials under an amendment to the Atomic Energy Act passed in September 1959.

AEC requires reports from licensees on transfers of special nuclear material

The AEC has issued an amendment to Part 70 of its regulations requiring reports from special nuclear material licensees concerning individual movements of such material.

The amendment prescribes a standard transfer and receipting form (AEC-388) to be used by special nuclear material licensees in initiating and receipting shipments of the specified material. The form is used in conjunction with a standard special nuclear material lease agreement executed with licenses. The receiving licensee's signature on this form, if the transaction involves a transfer of lease responsibility, binds the licensee under his lease agreement for the quantities described on the form.

The amendment was published in the *Federal Register* on August 17, 1960, for comment by interested persons and organizations. The comments submitted were taken into account by the Commission in issuing the effective rule.

Radiation Health and Safety Institute is proposed

The idea of establishing an Institute on Radiation, first conceived in May, 1960, has taken roots. An informal working group assembled at Chicago recently and drafted a statement of proposed objectives, and set out to answer basic questions of organization: status and funds. This group declared its primary objective was: to help the public gain understanding on the meaning and effects of radiation by creating an institution to which the public could turn with complete confidence for radiation information. Still unanswered is the question of status.

The group sought to decide whether to organize independently or attempt to affiliate with a university. On funding the institution, the group sought answers to long-range financial commitments required to support the organization. They did, however, establish the institution's needs for a period of several years at $500,000–$1,000,000. They will ask for grants from foundations interested in supporting such a program. Working papers used during preliminary talks emphasize essentials the group feels imperative to the success of the organization: "The institute must be free from any semblance of subordination to any group identified in the public mind with special interests"; and "in order to attain practical acceptance among those working in the field, the institute must maintain an intimate working relationship with all groups". Those active in the working group include: F. Aley Allan, Mobil International Oil Co.; Joe W. Howland, Univ. of Rochester; Charles F. MacGowan, International Brotherhood of Boilermakers; John H. Rust, Univ. of Chicago; Elwood Swisher, Oil, Chemical and Atomic Workers; G. Edwin Brown, AIF; William A. McAdams, General Electric; C. Rogers McCullough, Nuclear Utilities Service Co.; and Bernard B. Smyth, Dow, Lohnes, & Albertson, Washington, D.C., law firm.

AEC sets up new co-ordination office

AEC grants for nuclear equipment and other types of training assistance in nuclear technology will now be administered from one office. This new co-ordination office is established within that of the Assistant General Manager for Research and Industrial Development under ALFONSO TAMMARO. JOHN C. CERA, previously chief of education and training for the Reactor Development Division, will be the first co-ordinator, reporting directly to TAMMARO. Under CERA's single management will fall AEC grants—domestic, not foreign—for purchases of nuclear equipment; loans of source, by-product and special nuclear materials; special AEC fellowships in nuclear science and engineering, health physics and industrial hygiene; training for prospective nuclear power station operators, and facility training for high school and college teachers in handling radioisotopes.

When AEC announced last August it would discontinue training reactor grants, a major reason was removed for having the Reactor Development Division handle the training grant program. CERA's staff was transferred out of a single division to a higher level. (This move is one of many reflecting AEC's effort to consolidate assistance programs now scattered throughout the divisions of Reactor Development, Biology and Medicine, Research, and the Office of Isotope Development.) To replace training-reactor assistance, AEC plans to provide less-expensive subcritical assemblies and reactor simulators. However, for existing university research reactors AEC will still provide fuel loans, start-up sources, fuel fabrication and reprocessing services. The National Science Foundation will continue to assume primary Federal responsibility for giving construction aid for such reactors.

AEC's isotopic power for space under way

A four-part program on the safe use of isotopic power in space has been authorized by the AEC. Martin Company will manage the entire program. One of the four investigations planned is aimed at confirming theoretical burn-up data on re-entry of isotopic generators by firing simulated or actual cores into space.

The other aims of the study program cover: (1) hazards of landing a radioisotopic generator on the moon (dispersion, length of contamination of different isotopes, etc.); (2) hazards of launching a generator from Cape Canaveral (all previous studies have been based on a West Coast launching—primarily Vandenberg AFB in California); and (3) development of a shielding code for isotopic generators (with a given isotope, what shielding is required? what is best shield shape, weight? how much radiation is self-absorbed?).

Curium-242, polonium-210, cerium-144 and plutonium are the chief nuclides expected to be studied. They are considered the best sources for use in space since they require less shielding than, for example, strontium-90. Generators using strontium, cesium, and mixed fission products are expected to be used in terrestrial and marine applications, where shielding weight and size are not as crucial as in space. Martin and AEC having just begun negotiations, the extent of the space program is not yet defined; financial and other details are still to be worked out.

Tritium cleared for non-licensed use on dials

AEC has issued its first licensing exemption for the use of a radionuclide on luminous watch and other dials. The exemption permits purchasers of watches and other timepieces using tritium to do so without getting a license from the AEC. Those applying the tritium to dials, however, would be subject to fairly strict AEC control.

Under the exemption, not more than 25 mc may be applied per timepiece, and manufacturers must present the timepiece for prelicensing inspection by AEC, to demonstrate that AEC's standards will be met. AEC is also reviewing other nuclides for such clearance.

Stanford Research Institute issues training guides

The Stanford Research Institute has completed work on AEC contracts encompassing research leading to and the development of three thirty-two-hour basic adult education courses covering the following aspects of nuclear technology; (1) radiation safety training; (2) training for radioisotope workers in industry; and (3) training for operating and maintenance personnel in nuclear power generation systems.

The research objectives followed by Stanford in developing these courses were: (1) to assess the scope and magnitude of training needs that now exist or that may be expected to arise as a consequence of the (a) development of nuclear power generation systems and (b) the increasing use of radioisotopes in industry; (2) to design (a) basic survey courses appropriate to the fundamental training needs in each of these areas and (b) general plans for more advanced courses consistent with training needs; (3) to ascertain the effectiveness of these courses in trial presentations conducted in adult vocational educational programs; and (4) to modify the design of these courses as might be indicated by the results

of trial presentations. As a result of these studies, instructor's guides were developed and the effectiveness of these courses evaluated in trial presentations.

The study resulted in the following publications:

(1) Development of Training Programs for Operating and Maintenance Personnel in Nuclear Power Generating Systems
(2) Instructor's Guide: Survey of Nuclear Energy and Power Plant Applications
(3) Trial Presentations of a Nuclear Energy Training Course in Two Adult Vocational Education Programs
(4) Preparation for Nuclear Energy Training in a Trade Union
(5) Development of a Radiation Safety Training Program for Industrial and Public Service Personnel
(6) Instructor's Guide: Radiation Safety
(7) Radiation Safety Training in a Naval Shipyard
(8) Development of a Training Program for Radioisotope Workers in Industry
(9) Instructor's Guide: Survey of Nuclear Fundamentals and Radioisotope Applications in Industry

EEI task force examines radioactive waste problem

The Edison Electric Institute published a report, prepared by Pickard–Warren–Lowe Associates under the guidance and direction of the EEI Technical Appraisal Task Force on Nuclear Power, on "Radioactive Waste Handling in the Nuclear Power Industry". Conclusions were drawn in this report with respect to:

(1) The production of radioactive waste
(2) The cost of handling the waste
(3) The storage capacity or requirements
(4) The magnitude of discharged waste
(5) The radiation levels of the discharged waste
(6) The radiation exposures of personnel

One of the more interesting sections of the EEI report is concerned with an effort to estimate radiation exposures to the general population from nuclear power stations and to compare these estimated exposures with exposures to the same population from other sources. The resulting comparisons, based on genetically significant dose ranges (total gonad dose per person) and excluding doses to occupationally exposed persons, are tabulated below (Table 1). The estimates are made in terms of persons living in the U.S. for the next 30 years and the values indicated are for a 30-year period.

Personnel dosimeter of automatic alarm type developed at ORNL

Oak Ridge National Laboratory recently announced the development of a Personal Radiation Monitor (PRM) which can detect and measure γ-radiation up to 200 r/hr. The transistorized, mercury battery powered device is no larger than a fountain pen and uses a miniature Geiger counter. In a γ-field, the device lights up and emits a warning tone, the signals increasing in intensity as the radiation rises so that the direction of the danger may be quickly determined.

Idaho Chemical Plant criticality

A "low-level criticality" occurred January 25, in a cell at the AEC's Idaho Chemical Processing Plant "when an enriched uranium-235 solution accidentally surged from a geometrically safe container into one that led to momentary occurrence of a chain reaction". The AEC said there were "no significant personnel exposures". The plant was evacuated for five hours after automatic monitoring instruments indicated a radiation rise.

Hazard evaluation branch of AEC issues proposed rules on reactor site criteria

The AEC has published in the Federal Register a proposed regulation stating the criteria which it will consider in determining the suitability of proposed sites for power and testing reactors. Public comments

Table 1

Source of exposure	Minimum dose (rem)	Maximum dose (rem)	Average dose (rem)
Natural radiation	2.0	6.2	4.1
Medical and dental procedures	1.0	5.0	3.0
Fallout from weapons	0.05	0.4	0.22
Luminous dials and television sets	0.01	0.2	0.1
Spent fuel recovery sites	0.003	0.13	0.066
Electric power reactor sites	0.0000001	0.0001	0.00005

are invited through June 10 on the proposed criteria (10 CFR Part 100).

The AEC said the proposed guides were designed to avoid serious injury to persons off-site "if an unlikely but still credible accident should occur", to prevent a catastrophe in the event of a more serious accident "not normally considered credible", and to ensure that "the exposure of large numbers of people in terms of total population dose should be low". The AEC said the problem of total population dose would require further study, and meanwhile "distances to very large cities may have to be greater than those suggested by these guides".

The proposed regulation points out that the criteria "apply primarily to reactors of a general type and design on which experience has been developed". They may also be applied, but more conservatively, to reactors which incorporate design novelties or which are of types unproven by prototypes.

In evaluating a site, the Commission would take into consideration the character and extent of the exclusion area, the surrounding "low population area", the distance from the nearest large population center, physical characteristics of the site—seismology, meteorology, geology and hydrology, and the characteristics of the reactor, including the extent to which it incorporates unusual features having a bearing on accidental releases of radioactive material.

It is pointed out that "where some unfavorable physical characteristics of the site exist, the proposed site may nevertheless be found to be acceptable if the design of the facility includes appropriate and adequate compensating engineering safeguards".

The "exclusion area" surrounding a reactor is defined as one which the operator fully controls and in which residence is normally prohibited. Under certain conditions the area may be traversed by a highway, railroad or waterway. It must be of such a size that an individual located at its boundary for 2 hr following a postulated fission release would not receive more than 25 rems whole body radiation or more than 300 rems in thyroid irradiation from iodine exposure.

The "low population zone" surrounding the exclusion area is defined as an area "which contains residents the total number and density of which is such that appropriate protective measures could be taken in the event of a serious accident". The guides do not specify a permissible population density or total population within the zone, since the possibility of taking "appropriate measures" depends on many factors which will vary from place to place. The extent of the zone is determined in much the same way as for the exclusion area: a person standing on its outer boundary during the entire period of the passage of a radioactive cloud resulting from a postulated release of fission products must not receive more than 25 rems in whole body radiation or more than 300 rems in thyroid irradiation from iodine exposure.

The distance from the nearest population center would be at least $1\frac{1}{3}$ times the distance from the reactor to the outer boundary of the low population zone. However, "where large cities are involved a greater distance may be necessary".

Public Health Service and Department of Interior conduct long range study of activity in Savannah River

The Public Health Service and the Department of Interior are conducting a long-range study of radioactivity in the estuarial waters of the Savannah River, near Savannah, Georgia.

The purpose of the study is to trace the routes of radioactivity in a marine environment from its source to possible human consumption via the "food chain", and to study factors affecting the uptake or reconcentration of radioactivity by various forms of marine life. Measurement of the levels of radioactivity present in the marine environment, including water, fish, mollusks, aquatic plants, silt and suspended solids, will be conducted by the Public Health Service in the estuary and, later, in the upstream waters of the river.

The Savannah River estuary was selected for the study since it represents one of the best of a few river systems in the U.S. suitable for the study of radioactivity in marine waters. The presence of a nuclear reactor plant upstream, between Atlanta, Ga., and Aiken, S.C., 75 miles from the Atlantic, which employs the river for limited disposal of radioactive waste material, makes the Savannah River an ideal location for a survey of this type.

The Public Health Service jointly with the AEC has routinely collected and tested samples of Savannah River water since 1957. According to the Public Health Service the levels of radioactivity reported by this program continue to remain well within the limits recommended as acceptable by scientific advisory groups and the Department of Health, Education, and Welfare.

The initial phase of the new study will consist of monthly and seasonal collections of water and silt samples, shrimp and crabs, oysters, minnows and other types of fish life, together with marine plants. The samples will be examined by the Public Health Service radiological laboratory at Montgomery, Alabama, where an analysis for specific radioactive substances such as strontium-90 will be conducted. The Fish and Wildlife Service of the Department of

the Interior is performing specialized analyses of marine organisms.

The U.S. Coast Guard is providing ships and crew for carrying out the marine sampling program at the Atlantic outlet of the Savannah River.

Draft of site selection formulas prepared by ASA N 6.1

The American Standard Association Sub-Committee on Reactor Site Evaluation, under the chairmanship of R. O. BRITTAN, has written a draft of the mathematical procedure for carrying out the requirements set forth in parts 1 and 2 of the standard. The procedure consists in a determination of the radioactive load on the containment barrier, the driving force acting on the radioactive material to penetrate the barrier and the degree of penetration.

The procedure also requires a determination of the influence of land control on the reduction of radiation injury and the long-range influence of radioactive contamination.

Status of Idaho accident investigation

Motion pictures have provided the first interior views of the SL-1 reactor vessel at the National Reactor Testing Station in Idaho. The SL-1 was the reactor involved in the nuclear criticality accident of January 3, 1961. The motion pictures were taken February 22, 1961, at Idaho and developed there, and were received at Atomic Energy Commission Headquarters on February 27.

Severe damage to the core was disclosed by the motion pictures looking down through five 24-in. long, 6-in. diameter nozzles penetrating the head of the reactor. The motion pictures showed bending, wrenching and expansion of the core. The motion pictures also disclosed the presence of bubbles, evidence that there is water in the core.

The motion pictures showed additionally that four of the five control-rod blades appear to be partially or fully in the core, and that one appears to be entirely out of the core.

Radiation readings taken 2 ft above the reactor vessel from a meter attached to the camera indicate a level of about 650 r/hr. Readings in the reactor room since the accident have ranged from 500 to 1000 r/hr in different parts of the room.

The motion pictures were obtained with a motor-actuated camera suspended from a crane boom and moved back and forth across the top of the reactor vessel within the framework of an "index" template. The crane-operator, at ground level, was directed by telescope-equipped observers peering into the second-story reactor room from a wooden tower 200 ft distant. A photograph interpreter from the Naval Photo Interpretation Center, Suitland, Maryland, was at the test station to assist in planning the photography, and in the interpretation. He will continue to be available in Washington for this work.

The distance and remote manipulation are necessary to shield the workers from the high levels of radioactivity that persist at and near the top of the reactor.

Aerial and ground monitoring indicate that the airborne activity is being confined largely to the reactor building and the immediate vicinity. Direct radiation from the reactor building has shown no increase since the accident. Calculations from the direct radiation readings are as follows: 1.1 r/hr at 1000 ft and 0.002 r/hr at 2000 ft.

Radiologic physics

A one-year course in radiological physics, leading to the degree of Master of Science, is offered under the auspices of the Department of Radiology of the College of Physicians and Surgeons of Columbia University. It is designed to prepare candidates to carry out all the functions of a physicist in a hospital department of radiology; it would also furnish a foundation for those who wish to engage in research or applications in radiologic physics, radiation protection, and dosimetry. The course includes lectures, seminars, conferences and laboratory work. Topics included are elementary and advanced radiologic physics, electronics, radiation standardization and protection, radioactive isotopes, biostatistics, radiobiology, instrument design, and clinical applications of radiation physics. Prerequisite for admission is a bachelor's degree with a major or strong minor in physics, or equivalent scholastic background, and a good academic record. A knowledge of general chemistry and general biology is very desirable.

As part of its national program for the training of radiological health specialists, the Division of Radiological Health, Public Health Service, has awarded a grant to the University enabling financial assistance to qualified candidates. This aid will be in the form of tuition waiver as well as monthly stipend allowances. Applicants must be citizens of the United States or have filed a Declaration of Intent. Preference will be given to candidates who are sponsored by public health agencies for work in their area of responsibility or in closely related fields.

Inquiries should be addressed to Dr. H. H. ROSSI, 630 W. 168th Street, New York 32, New York.

New England Chapter of the HPS

The newly organized New England Chapter of the Health Physics Society boasts of seventy-five members recruited since June 1960. At the first meeting, Officers were elected and the framework of the Chapter outlined.

Elected: JOSEPH FITZGERALD, President
RUSSELL COWING, President-Elect
JOHN D. MURPHY, Secretary–Treasurer

Dr. WALTER D. CLAUS of the Division of Biology and Medicine, U.S. Atomic Energy Commission, spoke at the second meeting. His topic was the "Status for the Health Physicist". With growing recognition of Health Physics as a distinct and important profession, increasing consideration must be given to the establishment and maintenance of professional status.

At the last meeting, Mr. LESTER R. ROGERS of the Division of Licensing and Regulations, discussed Title 10, Code of Federal Regulations, Part 20. Implementation of these revisions has technically and administratively affected the work of all Health Physicists. Mr. ROGERS has assisted us in developing a clearer understanding of these regulations.

News from the United Kingdom—H. J. DUNSTER

Two important reports on radiation hazards have appeared recently in the United Kingdom. The first of these is the second report on Radiological Hazards to Patients, prepared by the committee under the chairmanship of LORD ADRIAN.[1] This report reviews the genetic dose to the population from the medical uses of radiation, and concludes that the genetic dose amounts to 19.3 mr per person per year, of which 14.1 mr per person per year results from diagnostic radiology. The committee considers that these figures do not indicate any need for major restrictions in radiological practice, but makes recommendations which would substantially reduce the doses without any detriment to the examination or treatment.

The other report is the second report on the "Hazards to Man of Nuclear and Allied Radiations", prepared by the committee under the chairmanship of Sir HAROLD HIMSWORTH.[2] The report includes comprehensive reviews of the recent developments in the knowledge of the effects of radiation on the health of the individual and the population, and an assessment of the foreseeable levels of exposure to radiation. Detailed supporting information is included in appendices. The report will be of immense interest and value to everyone working on the problems of radiological health and safety, and the chapter on the assessment of hazards should be read by anyone who has an interest in the implications of the development of nuclear power and the uses of radiation. Some of the major points in this chapter are summarized below:

Information gained since the 1956 report suggests that the severity of early effects of acute dose, the risk of developing leukaemia as a result of radiation exposure, and the number of mutations resulting from low levels of irradiation, may all be somewhat less than was previously estimated. The Committee do not consider, however, that these changes are sufficiently well established to warrant any relaxation in their previous recommendations.

The Committee compare the 1958 and 1959 Recommendations of the ICRP with those which they themselves made in 1956. The differences are not great and the Committee formally advocate the adoption of the ICRP Recommendations subject to certain qualifications. These are discussed in detail in Appendix I. There are three significant departures from the ICRP Recommendations. Persons occupationally exposed below the age of eighteen years should be restricted to 1.5 rems per year compared with the ICRP figure of 5 rems per year. High accidental exposures must be included in full in the accumulated dose, but five years are allowed for working off any excess over the permissible dose. In no case may any part of the dose be ignored for this purpose. Finally, it is suggested that there should be a working limit to the permissible genetic dose to the population as a whole, and that this limit should be based on the sum of the lowest practicable contribution from each source of genetic dose. The working limit should be less than the ICRP figure, which is 5 rems per generation plus the lowest practicable contribution from medical exposure of patients.

After reviewing the possible dangers from the testing of nuclear weapons, the Committee conclude that strontium-90 is the most valuable single indicator of possible total hazard. They derive a maximum permissible concentration in human bone by the direct application of ICRP Recommendations. The values are 67 $\mu\mu$c/g Ca for the average over the whole population, and 200 $\mu\mu$c/g Ca for any individual member of the population. The Committee consider that, because of the need for caution and for making allowances for other sources of radiation, the situation would require re-assessment if the average concentration of strontium-90 in bone in any age group were to rise to 33 $\mu\mu$c/g Ca. The present value for young children (the age group for which the values are highest) is, on the average, about 3 $\mu\mu$c/g Ca, with

a spread of about a factor of 3 in either direction from the mean.

A recent development which can be expected to have a considerable influence in the United Kingdom is the publication by the International Atomic Energy Agency of *Regulations for the Transport of Radioactive Materials*[3]. Considerable progress has already been made in redrafting United Kingdom transport rules and it is to be hoped that all countries will ultimately find it possible to base their own rules on the I.A.E.A. Regulations.

References

1. *Radiological Hazards to Patients*, Second report of the committee. H. M. Stationery Office, London (1960).
2. *The Hazards to Man of Nuclear and Allied Radiations*, Second report to the Medical Research Council. Cmnd 1225. H.M. Stationery Office, London (1960).
3. *Regulations for the Transport of Radioactive Materials*. International Atomic Energy Agency, Vienna (1961).

News from Canada—J. NEIL

Mobile Change Room

The Radiation Hazards Control Branch at the Chalk River Project in Canada has developed, built and operated a mobile change room (Fig. 1). This is one of the many items which have been "tailor-made" to augment the standard radiological health protection equipment.

The change-room trailer was intended for use in those locations where adequate facilities for decontamination of man garbed in plastic clothing, respirators and other protective covering were not available. Such a situation could apply where the use of normal change rooms has been temporarily lost due to heavy contamination or where buildings are inadequately equipped to deal with personnel decontamination.

The trailer is a standard, commercially available, mobile home such as one may see in any trailer park. The inside of the trailer (Fig. 2) has been equipped in a manner which concurs with good change-room practices. The internal walls are so placed that an in-coming man, dressed in plastic suiting and other protective apparel and probably bearing particulate contamination on his outer clothing, is directed through a chain of decontamination processes.

He passes first through a deluge shower cabinet where the particulate contamination is removed from the plastic suit. From this process he moves into an area where his plastic clothing and shoe rubbers are removed by a protectively garbed undresser. Thence he passes through an air-lock to another room where the respirator, coveralls and all the remaining clothing are removed and disposed into chutes which discharge into plastic bags outside the trailer.

Having disrobed, the man passes into one of the two available personal showers. Thereafter, he is monitored and pertinent details of his exposure to radiation are recorded. Provided that the monitoring indicates the absence of personal contamination, the decontamination process is at an end and the man is free to pass into the last area where he may don clean clothing which is stored in cupboards. The man then leaves the trailer.

The ventilation system is of interest. Intake air is passed through absolute filters to ensure the exclusion of particulate activity from the trailer space. The air is tempered in a heater and is passed through ducts into each compartment of the trailer. The air intake, is of course, located at the clean end of the trailer.

The air is exhausted near the entrance through which the man garbed in plastic clothing passes. Again, the air is filtered. By filtering both the intake and exhaust air, it is intended that particulate contamination is neither accepted in the trailer nor freely exhausted from it. To aid the containment of activity, the inside of the trailer is maintained at a slight positive pressure with respect to atmospheric pressure. This tends to preclude the inward flow of possibly contaminated outside air through the small cracks round windows and entrance doors. Efforts were made to ensure the tight fitting of doors and windows.

The trailer was successfully operated for several weeks during the dismantling of some heavily contaminated equipment in a building which was inadequately serviced by suitable change rooms.

News from Ireland—L. COLLERY

An Exhibition of "The Peaceful Uses of Atomic Energy" was held in Dublin on March 8, 9 and 10, 1961, under the auspices of the Royal Dublin Society in co-operation with the United Kingdom Atomic Energy Authority.

This included an exhibition of models of the Calder Hall and Dounreay Reactors and display of radioactive isotopes, etc.

Lectures were given on the use of radioactive isotopes in biological research by Dr. A. R. THOMSON, and on the peaceful uses of atomic energy by J. A. DIXON. Films on related subjects were also shown. The exhibition was of the popular variety and attended by students of the various Science Faculties and members of the public.

News from Japan—TOSHIO AOKI

The problems that are involved in the utilization of atomic energy are somewhat more difficult to solve in Japan than in other countries. The Japanese people are very much concerned with the hazards of radiation. In addition, Japan is a densely populated country. Therefore, it has been necessary to establish an appropriate "climate" among the Japanese people through the assurance that all safety precautions have been and will be taken before proceeding with plans for the utilization of atomic energy.

Laws governing the "Regulation of Nuclear Source Material and Atomic Reactors" have been established. Licenses for the construction of a reactor are issued only after serious deliberation on the potential hazards and safety precautions that will be taken. The Hazard Evaluation Committee of the Japanese Atomic Energy Commission and other governmental agencies are engaged in the analyses of the reactor hazards, of safety precautions and of reactor utilization.

In addition, the Safety Standards Committee is actively engaged in the development of effective reactor safety criteria.

Special studies are presently being pursued to evaluate the effects of reactor accidents on the public, to develop appropriate counter measures to be applied during and following an accident and to estimate the exposures to the population in the environs.

Whole-body counters are being constructed for the Japanese Atomic Research Institute and the National Institute of Radiological Sciences.

AEC participated in radioisotopes for industry conference at Pittsburgh

The Chamber of Commerce of Greater Pittsburgh and the Pittsburgh chapter of the American Nuclear Society cosponsored, in co-operation with the U.S. Atomic Energy Commission, a "Radioisotopes for Industry Conference", February 22 and 23, 1961. The meeting was held in Pittsburgh's Penn–Sheraton Hotel.

The two-day conference was designed to provide information on important industrial applications of radioisotopes. Industry and Atomic Energy Commission speakers reviewed the management, economic and safety considerations in the use of radioisotopes and discussed improvements in production efficiency obtained by their use in industrial tracing, gauging and radiography. A series of brief experience reports by local users on radioisotopes in the chemical, petroleum and steel industries was included.

Management and technical personnel and educators interested in present and future applications of radioisotopes in industry were discussed. Detailed information on the conference may be obtained from PETER STIPANOVICH, Manager, Public Affairs Division, The Chamber of Commerce of Greater Pittsburgh, Chamber of Commerce Building, Pittsburgh 19, Pennsylvania.

IAEA sponsored conference on tritium and nuclear electronics

Two international conferences were sponsored by the International Atomic Energy Agency.

A *Symposium on the Detection and Use of Tritium in the Physical and Biological Sciences* was held in Europe, on April 10–14, and a *Conference on Nuclear Electronics* was scheduled for May 15–20, in Belgrade, Yugoslavia.

The scheduling of a tritium symposium resulted from the International Agency's recognition of the rapid development of tritium as a research tool in the physical and biological sciences, which has led to extensive activity not only in the production and detection of tritium, but also in its application to various problems in chemistry, physics, biology, meteorology and hydrology. The symposium is the first large international meeting in this field and enabled the scientists to present the results of their studies, to exchange information and to formulate plans for future activity.

The conference in Belgrade provided a forum for the exchange of ideas and discussion of recent developments in the rapidly growing nuclear electronics field. The program included such subjects as radiation detectors, pulse technique in classical and fast electronics, and radiation monitoring instruments.

Advance Notice

Tenth International Congress of Radiology

26 *August*–1 *September*, 1962

Montreal, Canada

The Canadian Board of Management announces that members of medical radiological societies, radiobiologists, biophysicists, radiation physicists and scientists in cognate fields are cordially invited to become members or associates of the Tenth International Congress of Radiology and attend its sessions which will convene in Montreal, Canada, 26 August–1 September, 1962.

The scientific programme and scientific exhibits will be arranged in four divisions: Diagnostic Radiology; Therapeutic Radiology; Radiobiology; Radiation Physics. Emphasis will be placed on

FIG. 1. Mobile change room.
[News from Canada, p. 241]

FIG. 2.
[News from Canada, p. 241]

recent advances in knowledge, especially since the last Congress, in the selection of invited and proffered scientific communications and scientific exhibits. Symposia on correlated subjects embracing two or more of the above fields and certain cognate sciences will be included.

Major topics selected for scientific papers and exhibits include:

Recent advances in image amplification, recording and transmission
Roentgendiagnostic assessment of the effect of ionizing radiation
Selective angiography in the investigation of organic disease
Renal disease
Clinical applications of cine-radiography
Neurological and Paediatric radiologic studies
Radiation dose in diagnostic procedures
Effects of ionizing radiation at cellular and subcelullar levels
Radiation protection including employment of medication and hypothermia
Effect of internal emitters on body tissues
Ionizing radiation in relation to carcinogenesis and leukaemogenesis
Total body irradiation, immunity mechanisms and marrow transplantation
Genetic and population effects of ionizing radiation
External localization of pathological processes with radioactive isotopes
Metabolized isotopes in therapeutic radiology
Measurement *in vivo* of absorbed dose in tissues
Advances in external beam therapy
Advances in intracavitary and interstitial radiation therapy
Treatment planning

The Preliminary Announcement containing information pertinent to membership enrolment, proffer of scientific papers and exhibits, hotel reservation, etc. will be sent to all qualified members of national medical radiological societies and other recommended scientists in the late spring of 1961.

For the Board of Management,

ARTHUR C. SINGLETON, M.D., President,
CARLETON B. PEIRCE, M.D., Secretary-General.
Suite 204, 1555 Summerhill, Montreal 25, Canada.

HEALTH PHYSICS SOCIETY
PLACEMENT COLUMN

Orders for ads to be sent prepaid to the Placement Committee at the address below. Ads will appear in the next issue following receipt.

1-Time Charges:

Position wanted: $0.25 per word ($4.00 minimum)
Position offered: $1.00 per word ($15.00 minimum)

Replies to employer or to
Mr. Joseph A. Lenhard,
Chairman Placement Committee H.P. Society,
Research and Development Divison, USAEC
P.O.B. E, Oak Ridge, Tenn.

POSITIONS OFFERED

fee paid positions for
HEALTH PHYSICISTS
Write for Application • No Resume Required • Confidential Handling
We are a national placement service with technical experience, dedicated to people in the nuclear field . . . wherever radioactivity is a factor.
ATOMIC PERSONNEL, INC.
Suite 1207-R, 1518 Walnut Street, Philadelphia 2, Pa.
An Employment Agency for the Nuclear Field

OBITUARY

ELDA ANDERSON,

Pioneer of Health Physics in the Atomic Energy Program, dies at 61

ELDA E. ANDERSON, pioneer in the atomic energy program and in the field of health physics, died of leukemia April 17, 1961 in Oak Ridge, Tennessee, USA.

Miss ANDERSON, a charter member of the Health Physics Society, was elected president of that organization at the national meeting in Gatlinburg in 1959. Following her term as president, she was named chairman of the Society's first committee to establish standards for health physicists. She served as the Society's first secretary-treasurer when it was organized in 1956 and as secretary in 1957. Even in her last year, she was serving that society in a most responsible capacity which is perhaps the best testimony of the high regard of the profession for her scientific standing and character.

She began in health physics work long before many even understood the significance that the field would eventually assume. Her dedication to the need for training was decisive in the prompt establishment of programs that have produced hundreds of health physicists during the past decade—here in the United States and in many countries abroad. The respect and affection of her students alone is testimony to her tremendous worth as both a scientist and a person.

Miss ANDERSON moved rapidly from one job, one joy to another. And yet, she had an intense interest in people and was never too busy or too preoccupied with her many labors and recreations to make a new friend. She was, in both her professional and social life, an example and an inspiration for the many who were fortunate enough to know her well. Possessed of "an incredible zest for life" is the way one of her closest associates describes her.

Miss ANDERSON had known for the past five years that she had leukemia, but she did not slow down, either professionally or personally. Instead, she made a trip around the world involving both work and adventure.

Miss ANDERSON's death results in a tremendous loss to her field, her laboratory, her friends, her community. However, her memorial will be a living, growing one as future advancements in health physics occur in no small part because of the information and inspiration she leaves behind.

Her friends and associates have established a memorial scholarship for training in health physics. Donations may be mailed to J. T. SUTHERLAND, 100 Plymouth Circle, Oak Ridge, Tennessee, treasurer of the East Tennessee Chapter of the Health Physics Society. It is requested that contributions be made out to the Elda E. Anderson Memorial Scholarship Fund.

ELDA E. ANDERSON